

*The role of aluminium content in the control of the morphology of
fly ash based hierarchical zeolite X*

By

Mero-Lee Ursula Cornelius

**A thesis submitted in fulfilment of the requirements of the degree of Magister of
Scientiae in Chemistry in the Chemistry Department, University of the Western Cape.**



Supervisors: Prof. Leslie Petrik

Dr. Olanrewaju Fatoba

November 2015

Abstract

Coal is the main source of electricity in South Africa, the combustion of which produces a large amount of waste (coal fly ash) annually. The large-scale generation of coal fly ash places major strain on landfills and the material is toxic in nature. The high silicon and aluminium content in fly ash makes it a suitable starting material for zeolite synthesis. Utilisation of fly ash as a starting material for zeolite synthesis alleviates an environmental burden by converting a waste product to an industrially applicable material.

In this study, hierarchical zeolite X was synthesised from coal fly ash via the fusion method. The clear fused fly ash (FFA) extract (with molar composition $0.12 \text{ Al} \cdot 14.6 \text{ Na} \cdot 1.00 \text{ Si} \cdot 163 \text{ H}_2\text{O}$) served as the synthesis solution for hydrothermal treatment. The influence of synthesis parameters (such as Si/Al ratio, aluminium source, hydrothermal temperature and stirring) on hierarchical zeolite X formation was studied to determine the cause behind the formation of this material. Synthesised zeolites and starting materials (Arnot coal fly ash and fused fly ash) were characterised by various analytical techniques such as XRD and SEM-EDS to determine the phase purity, morphology and elemental composition (framework Si/Al ratio) of these materials. The synthesis of hierarchical zeolite X under hydrothermal conditions was found to be highly sensitive to the aluminium content of the synthesis solution. The hierarchical morphology of zeolite X was formed preferentially in relatively aluminium-deficient (i.e. high Si/Al ratio) synthesis environments under stirred hydrothermal conditions of 90 °C for 16 hours. In the case of sodium aluminate addition, octahedral shaped zeolite X crystals were formed in relatively low Si/Al ratio synthesis environments, which was attributed to the presence of excess sodium cation content in the synthesis solution.

Selected hierarchical zeolites (D2 and E2) were characterised further to gain more insight into the properties of this material. HR-TEM and FTIR revealed that hierarchical zeolite D2 and E2 exhibited the typical structural features of zeolite X. Zeolite D2 and E2 contained both micropores and mesopores and had a high BET surface area of 338-362 m²/g. These zeolites also exhibited appreciable solid acidity (0.81-1.12 mmol H/g zeolite). These properties make hierarchical zeolite X a favourable material for application in catalysis or adsorption. Overall, the formation of zeolite X with hierarchical morphology was proposed to be linked to the presence of zeolite P1 structural units in the framework of the zeolite.

Keywords: Coal fly ash, zeolite synthesis, hierarchical zeolite X.

Declaration

I declare that “The role of aluminium content in the control of the morphology of fly ash based hierarchical zeolite X.” is my own work, that it has not been submitted for any degree or examination in any other university, and that all the resources I have used or quoted have been indicated and acknowledged by complete references.

Mero-Lee Cornelius

November 2015

Signature:



Acknowledgements

I wish to thank my supervisors, Prof. Leslie Petrik and Dr. Olanrewaju Fatoba, for their support and guidance during my research project. I am truly grateful for the opportunity to have been part of the Environmental Nano Sciences (ENS) research group and for the insight and advice of Prof. Leslie Petrik during my research project. I would like to acknowledge the Environmental Nano Sciences (ENS) research group for their support during the study and a special thank you to Roland Missengue for his mentorship. To the ENS technical and administration staff (Averil Abbott, Vanessa Kellerman, Ilse Wells and Rallston Richards); your support and assistance during the research has been invaluable. I would also like to thank the National Research Foundation (NRF) and Prof. Leslie Petrik for funding the research project.

I would like to thank the staff at the Electron Microscope Unit at the University of the Western Cape (particularly Franscious Cummings and Adrian Josephs) and Nicholas Laidler from Geology Department at the University of Cape Town for their assistance with SEM, TEM and XRD facilities, respectively. Thank you to the various other analytical facilities that assisted me during this project. Thank you to Ebrahim Mohiuddin for his kind assistance with FTIR analysis during the research project.

I thank the Almighty God for his grace and for giving me the strength to carry out and complete this work. Last but not least, my heartfelt thank you and appreciation to my family, friends and partner for their continued love, support and encouragement.

Table of Contents

Abstract.....	ii
Declaration.....	iii
Acknowledgements.....	iv
Table of Contents.....	v
List of Figures.....	ix
List of Tables.....	xii

Chapter 1: Introduction

1 Introduction.....	1
1.1 Background.....	1
1.2 Problem Statement.....	4
1.3 Aim and Objectives of the Study.....	4
1.4 Research Questions.....	5
1.5 Research Approach.....	5
1.6 Scope and delimitations of the study.....	7
1.7 Thesis Outline.....	7

Chapter 2: Literature Review

2 Introduction.....	8
2.1 Classification of zeolites and their characteristic properties.....	10
2.2 Zeolite synthesis techniques.....	16
2.2.1 Pre-synthesis step.....	17
2.2.2 Hydrothermal Synthesis.....	25
2.2.3 Product recovery and post-synthesis treatment.....	30
2.2.4 Alternative methods of zeolite synthesis.....	30
2.3 Coal fly ash utilisation in zeolite synthesis.....	30
2.3.1 Synthesis of zeolites from coal fly ash.....	32

2.4	Hierarchical porous zeolites.....	35
2.4.1	Synthesis of hierarchical zeolites.....	36
2.5	Characterisation of zeolites.....	40
2.5.1	Elemental Analysis	40
2.5.2	Morphological Analysis.....	42
2.5.3	Structural Analysis.....	44
2.5.4	Textural Analysis	49
2.5.5	Acidity of zeolites	51
2.6	Applications of zeolites.....	53
2.6.1	Applications of hierarchically porous zeolites.....	54
2.7	Chapter Summary	56
 Chapter 3: Research Design and Methodology		
3	Introduction.....	58
3.1	Materials and chemical reagents.....	60
3.2	Equipment list	60
3.3	Synthesis of zeolites from coal fly ash	61
3.3.1	Pre-synthesis step.....	61
3.3.2	Hydrothermal synthesis step	64
3.3.3	Post-synthesis step	66
3.4	Characterisation techniques	68
3.4.1	Elemental analysis	68
3.4.2	Mineralogical analysis by X-ray diffraction spectroscopy	70
3.4.3	Morphological analysis by Scanning emission microscopy and Transmission electron microscopy	70
3.4.4	Structural analysis by Fourier transform infrared spectroscopy	71
3.4.5	Textural analysis by Nitrogen physisorption	72
3.4.6	Acidity determination by titrimetric analysis	72

3.5	Chapter Summary	74
Chapter 4: Characterisation of South African fly ash and alkali-activation of fly ash		
4	Introduction.....	75
4.1	Elemental Analysis of Arnot Fly Ash by X-Ray Fluorescence Spectroscopy.....	76
4.2	Textural analysis of Arnot Fly Ash by nitrogen physisorption	79
4.3	Morphological Analysis of Arnot Fly Ash and Fused Fly Ash by Scanning Electron Microscopy	81
4.4	Qualitative Mineralogical Analysis of Arnot Fly Ash and Fused Fly Ash by X-Ray Diffraction Spectroscopy	82
4.5	Structural Analysis of Arnot Fly Ash and Fused Fly Ash by Fourier Transform Infrared Spectroscopy	83
4.6	Chapter Summary	88
Chapter 5: The influence of hydrothermal synthesis parameters on the formation of hierarchical zeolite X		
5	Introduction.....	89
5.1	Hydrothermal synthesis of hierarchical zeolite X.....	89
5.1.1	The effect of hydrothermal temperature on hierarchical zeolite X formation ...	90
5.1.2	The effect of static synthesis on hierarchical zeolite X formation.....	96
5.1.3	The effect of hydrothermal time on hierarchical X crystallisation	100
5.2	Structural study of the transformation of the clear FFA extract to zeolites with time.	106
5.3	Chapter Summary	122
Chapter 6: The influence of molar regime adjustment on the formation of hierarchical zeolite X		
6	Introduction.....	123
6.1	The effect of Si/Al ratio on hierarchical zeolite X formation.....	123
6.2	The effect of aluminium source on hierarchical zeolite X formation.....	132
6.3	Further characterisation of selected hierarchical zeolite X.....	142

6.3.1	Elemental Analysis by XRF and LA-ICP-MS.....	142
6.3.2	Morphological (fine structure) analysis by HR-TEM.....	147
6.3.3	Structural Analysis by FTIR	149
6.3.4	Textural Properties by N ₂ physisorption.....	151
6.3.5	Acidity determination by titrimetric methods.....	154
6.4	Chapter Summary	156
Chapter 7: Conclusions and recommendations		
7	Introduction.....	158
7.1	Main findings of this study	158
7.1.1	The effect of synthesis parameters on hierarchical zeolite X formation	158
7.1.2	Structural study of the transformation of a clear FFA extract to hierarchical zeolite X with time monitored by Fourier transform infrared spectroscopy (FTIR)	159
7.1.3	The effect of molar regime adjustment on the formation of hierarchical zeolite X.....	160
7.1.4	Further characterisation of selected hierarchical zeolite X.....	161
7.2	Recommendations for future work	162
References.....		164
Appendix.....		175

List of Figures

Figure 1.1: Schematic diagram of the research approach for zeolite synthesis from a clear fused fly ash extract.	6
Figure 2.1: The common structural units which occur in zeolite frameworks	11
Figure 2.2: Examples of three framework types; (a) SOD, (b) LTA, (c) FAU with the supercage and (d) GIS.....	12
Figure 2.3: Acidic sites, Brönsted (left) and Lewis (right) sites, of the zeolite framework	14
Figure 2.4: A SEM micrograph of zeolite X showing the typical octahedral morphology of the material.....	43
Figure 2.5: A typical HR-TEM micrograph depicting the lattices fringes in a FAU-type zeolite.....	44
Figure 2.6: A simulated powder XRD diffractogram illustrating the typical reflections for zeolite X.....	45
Figure 2.7: Zeolite X (FAU) framework with D6R structural unit encircled in red.....	47
Figure 2.8: A typical FTIR vibrational spectrum of zeolite Na-X.....	48
Figure 2.9: Classification of adsorption isotherms and the type of hysteresis loops, by IUPAC.....	50
Figure 2.10: A typical nitrogen adsorption-desorption isotherm for zeolite Na-X.....	51
Figure 2.11: A typical ammonia-TPD profile for zeolite X.....	52
Figure 3.1: An overview of the experimental approach for zeolite synthesis from coal fly ash, including the a) pre-synthesis, (b) hydrothermal synthesis and (c) post-synthesis steps.....	59
Figure 3.2: The experimental set-up for the hydrothermal synthesis process.	61
Figure 4.1: Nitrogen adsorption/desorption isotherm for as-received Arnot coal fly ash.	79
Figure 4.2: SEM micrographs of (a) as-received Arnot coal fly ash and (b) fused fly ash (1000 X magnification).....	81
Figure 4.3: XRD diffractograms of as-received Arnot coal fly ash and fused fly ash, where Q denotes Quartz, M-Mullite, H-Hematite, Mag-Magnetite, *-Sodium silicate species and o-Sodium aluminosilicate species.	82
Figure 4.4: FTIR vibrational spectra of as-received Arnot coal fly ash and fused fly ash.	84
Figure 4.5: The depolymerisation and condensation process involving silicate species, including the corresponding wavenumbers for each species.	86

Figure 5.1: SEM micrographs of Na-zeolites synthesised under stirred conditions from a clear FFA extract (without an additional Al source) at hydrothermal temperatures between 70-94 °C and a fixed hydrothermal time of 24 hours. Images were obtained at 10 000 X magnification (left) and 50 000 X magnification (right).	92
Figure 5.2: XRD diffractograms of Na-zeolites synthesised under stirred conditions from a clear FFA extract (without an additional Al source) at hydrothermal temperatures between 70 and 94 °C, at a fixed hydrothermal time of 24 hours.....	94
Figure 5.3: SEM micrographs of Na-zeolites synthesised from a clear FFA extract (without an additional Al source) under (a) static and (b) stirred hydrothermal conditions, at 90 °C for 24 hours. Images were measured at 10 000 X magnification (left) and 50 000 X magnification (right).	97
Figure 5.4: XRD diffractograms of Na-zeolites synthesised from a clear FFA extract (without an additional Al source) under static and stirred hydrothermal conditions, at 90 °C for 24 hours.....	99
Figure 5.5: SEM micrographs (10 000X magnification) of Na-zeolites synthesised from a clear FFA extract (without an additional Al source) for different hydrothermal time periods, at a fixed hydrothermal temperature of 90°C.	101
Figure 5.6: XRD diffractograms of Na-zeolites synthesised from a clear FFA extract (without an additional Al source) for different hydrothermal time periods, at a fixed hydrothermal temperature of 90°C.....	103
Figure 5.7: FTIR spectrum of the freeze-dried clear FFA extract without an additional Al source (molar composition: 0.12 Al·14.6 Na·1.00 Si·163 H ₂ O) used for hydrothermal synthesis of zeolites.	107
Figure 5.8: FTIR spectra of freeze-dried, unwashed Na-zeolites synthesised from a clear FFA extract without an additional Al source (molar composition: 0.12 Al·14.6 Na·1.00 Si·163 H ₂ O) for different time periods, under stirred hydrothermal conditions of 90 °C.....	110
Figure 5.9: FTIR spectra of freeze-dried, washed Na-zeolites synthesised from a clear FFA extract without an additional Al source (molar composition: 0.12 Al·14.6 Na·1.00 Si·163 H ₂ O) for different time periods, under stirred hydrothermal conditions of 90 °C.....	113
Figure 5.10: FTIR spectra (wavenumber range 2000-400 cm ⁻¹) of freeze-dried supernatant samples collected at different hydrothermal time periods.	118
Figure 5.11: FTIR spectra (wavenumber range 800-400 cm ⁻¹) of freeze-dried supernatant samples collected at different hydrothermal time periods.	119

Figure 6.1: SEM micrographs (10 000X magnification) of Na-zeolites synthesised under stirred hydrothermal conditions at a temperature of 90 °C for 16 hours at different Si/Al molar ratios (achieved by addition of aluminium hydroxide to the synthesis mixture).	128
Figure 6.2: XRD diffractograms of Na-zeolites synthesised under stirred hydrothermal conditions at a temperature of 90 °C for 16 hours at different Si/Al molar ratios (achieved by addition of aluminium hydroxide to the synthesis mixture).	130
Figure 6.3: SEM micrographs (10 000X magnification) of Na-zeolites synthesised under stirred hydrothermal conditions at a temperature of 90 °C for 16 hours at different Si/Al molar ratios (achieved by addition of sodium aluminate to the synthesis mixture).	137
Figure 6.4: XRD diffractograms of Na-zeolites synthesised under stirred hydrothermal conditions at a temperature of 90 °C for 16 hours at different Si/Al molar ratios (achieved by addition of sodium aluminate to the synthesis mixture).	139
Figure 6.5: HR-TEM micrograph (a) and SAED diffraction pattern (b) of zeolite D2 (NA-X) synthesised from a clear FFA extract, using aluminium hydroxide as an additional aluminium source.	147
Figure 6.6: HR-TEM micrograph (a) and SAED diffraction pattern (b) of zeolite E2 (NA-X) synthesised from a clear FFA extract, using sodium aluminate as an additional aluminium source.	148
Figure 6.7: FTIR spectra of Na-zeolite D2 and E2 synthesised from a clear FFA extract at 90 °C for 16 hours.	149
Figure 6.8: Nitrogen adsorption/desorption isotherm of Na-X zeolite D2 and E2.	151
Figure 6.9: BJH pore size distribution of Na-X zeolite D2 and E2.	152

List of Tables

Table 3.1: List of chemical reagents used, including the supplier name and batch details.	60
Table 3.2: List of equipment used for the synthesis of zeolites.....	60
Table 3.3: The experimental outline for the investigation on the effect of pre-synthesis parameter variation (Si/Al ratio, Al source) on the formation of hierarchical zeolite X.	63
Table 3.4: The experimental outline for the investigation on the effect of synthesis parameter variation (temperature, static synthesis) on the formation of hierarchical zeolite X.	65
Table 4.1: The elemental composition of as-received Arnot coal fly ash and loss on ignition (L.O.I), determined by XRF (n= 3).....	76
Table 4.2: The elemental composition of as-received Arnot coal fly ash (trace elements), as determined by XRF (n= 3).....	77
Table 4.3: Textural properties of as-received Arnot coal fly ash determined by nitrogen physisorption.....	80
Table 5.1: The average molar composition of a clear FFA extract, determined by ICP-OES (n= 3).....	90
Table 5.2: Summary of properties of Na-zeolites synthesised from a clear FFA extract (without an additional Al source) at different hydrothermal temperatures, for a fixed hydrothermal time period of 24 hours.	93
Table 5.3: Summary of properties of Na-zeolites synthesised from a clear FFA extract (without an additional Al source) under static or stirred hydrothermal conditions, at 90 °C for 24 hours.....	98
Table 5.4: Summary of properties of Na-zeolites synthesised from a clear FFA extract (without additional reagents) for different hydrothermal time periods, at a hydrothermal temperature of 90°C.....	102
Table 5.5: Vibrational band assignments for aluminosilicates present in the clear FFA extract.	108
Table 5.6: Vibrational band assignments for aluminosilicate species present in unwashed Na-zeolites.	111
Table 5.7: Vibrational band assignments for aluminosilicate species present in washed Na-zeolites.	114
Table 5.8: Type of secondary building units observed by FTIR at different time periods during stirred hydrothermal treatment at 90 °C.	116

Table 6.1: Variation of Si/Al molar ratio of synthesis solution by addition of different quantities of aluminium hydroxide to clear FFA extract solutions.....	124
Table 6.2: The calculation of zeolite yield (mass %) from coal fly ash, using aluminium hydroxide as an additional Al source.....	126
Table 6.3: Summary of properties of Na-zeolites synthesised at different Si/Al molar ratios (achieved by addition of aluminium hydroxide to the synthesis mixture), under stirred hydrothermal conditions at 90 °C for 16 hours.....	129
Table 6.4: Variation of Si/Al molar ratio of synthesis solution by addition of sodium aluminate.....	133
Table 6.5: The calculation of zeolite yield (mass %) from coal fly ash, using sodium aluminate as an additional Al source	135
Table 6.6: Summary of properties of Na-zeolites synthesised at different Si/Al molar ratios (achieved by addition of sodium aluminate to the synthesis mixture), under stirred hydrothermal conditions at 90 °C for 16 hours.....	138
Table 6.7: Major elemental composition of zeolites D2 and E2 and loss on ignition (L.O.I), determined by XRF spectroscopy (n= 3).....	142
Table 6.8: Trace elemental composition of zeolites D2 and E2, determined by LA-ICP-MS spectroscopy (n= 3).....	143
Table 6.9: The percentage of fly ash elements transferred to the solid zeolite product	145
Table 6.10: Textural properties of Na-X zeolite D2 and E2 determined by nitrogen physisorption.....	153
Table 6.11: Brönsted acidity of zeolite D2 and E2, determined by titrimetric method.	154

1 Introduction

This chapter will provide brief background information on the research project, including zeolite synthesis and the utilisation of coal fly ash as a starting material for zeolite synthesis. The motivation of the research project highlights the research gaps in literature to date. The aim and objectives of the research as well as research questions will focus on bridging the research gaps identified. The scope and delimitations of the study as well as the thesis structure will also be presented.

1.1 Background

Coal is the primary source used for electricity production in South Africa. Globally, coal-fired power stations produce millions of tonnes of coal combustion products (CCPs) per year as by-products. One such CCP is coal fly ash (Heidrich et al., 2013). The generation of tonnes of coal fly ash places strain on landfills and poses an environmental threat (contamination of soil, surface water and groundwater, and air pollution) due to the toxic elements fly ash contains (Heidrich et al., 2013; Shoumkova and Stoyanova, 2013). Utilisation of coal fly ash has been a major area of research, aiming to alleviate the environmental burden associated with it. Although coal fly ash has been utilised for the production of concrete and other materials (eg. geopolymers), a large percentage of coal fly ash remains unutilised and destined for landfills (Chang and Shih, 2000; Heidrich et al., 2013).

Coal fly ash is composed of minerals such as quartz, mullite, hematite and magnetite as well as toxic elements such as uranium, strontium, zirconium, lead... (Kruger, 1997; Shoumkova and Stoyanova, 2013). Fly ash is a low-value by-product rich in elements such as silicon, aluminium and iron (Blissett and Rowson, 2012; Chang and Shih, 2000; Heidrich et al., 2013; Kruger, 1997). Silicon and aluminium are the main resources required for zeolite synthesis. Conventionally zeolites are synthesised by hydrothermal treatment of a mother liquid containing aluminium and silicon from pure chemical reagents (Feijen et al., 1994; Shigemoto et al., 1995; Yu, 2007). Due to the large quantities of coal fly ash produced annually, coupled with the high silicon and aluminium content, it is a favourable and low-cost starting material for the synthesis of zeolites (Chang and Shih, 2000; Franus, 2012; Shigemoto et al., 1993).

Zeolites are microporous, aluminosilicate materials with a three-dimensional network of pores and channels (Franus, 2012; Yu, 2007). The presence of aluminium in the zeolite

Chapter 1 - Introduction

framework results in a net negative charge which may be counter-balanced by cations; most commonly sodium cations serve as counter-ions in the zeolite framework. This unique property is responsible for the cation-exchange capability of zeolites. Zeolites possess other interesting properties such as thermal stability, shape-selectivity and acidity (Granda Valdes et al., 2006; McCusker and Baerlocher, 2007; Weitkamp, 2000).

Zeolites produced from fly ash may find application in various fields depending on the chemical and physical properties of the zeolitic material (Chang and Shih, 2000; Franus, 2012; Shigemoto et al., 1993). Zeolites have been applied as molecular sieves, ion-exchange materials and catalysts for reactions such as alkylation, hydrocracking and fluid catalytic cracking (Chang and Shih, 2000; Granda Valdes et al., 2006; Tao et al., 2006; Weitkamp, 2000). Zeolites have also been used for gas purification and separation applications, as well as water purification (Franus, 2012). Limitations of catalytic and adsorption applications of zeolites have been extensively reported (Moller and Bein, 2011; Na et al., 2011). These limitations included low activity and rapid deactivation of zeolites with large crystal size. The microporous nature of zeolites also restricts the size of reactant and product molecules which may react in (and exit) zeolitic pores (Liu et al., 2009; Moller and Bein, 2011; Na et al., 2011). These diffusion and mass flow limitations of microporous zeolites may be reduced or eliminated either by synthesising zeolites with reduced particle size or by incorporating larger pores (such as mesopores and/or macropores) into the zeolite framework. Zeolite crystals with reduced size have exhibited improved activity but a loss in shape-selectivity, poor catalyst separation (in liquid phase) and pressure drop (in gas phase) has also been reported (Hsu et al., 2011).

Due to diffusion limitations, the synthesis of hierarchical zeolites is an area of great interest. Hierarchical zeolites are materials which contain micropores (< 2 nm), mesopores (2-50 nm) and/or macropores (> 50 nm) in some cases (Terasaki et al., 2007). Hierarchical zeolites may be produced by synthesising zeolite nano-sheets (Inayat et al., 2012; Moller and Bein, 2011) or by incorporating an additional pore system into the zeolite framework (Moller and Bein, 2011). The incorporation of mesopores (and/or macropores) into the zeolite framework has been achieved by various synthesis techniques. Some of these synthesis methods include the addition of amphiphilic organosilane compounds, polymers and carbon into the synthesis mixture. Post-synthesis treatment such as desilication or dealumination of zeolites has also been reported (Hsu et al., 2011; Inayat et al., 2012; Liu et al., 2009; Na et al., 2011; Tao et al.,

Chapter 1 - Introduction

2006). Although these synthetic methods have been successful in incorporating mesopores (and/or macropores) into the zeolite framework, the preparation procedures are often complex and involve additional reagents (such as organic surfactants) which adds further complexity to the synthesis procedure (Liu et al., 2009; Na et al., 2011; Tao et al., 2006).

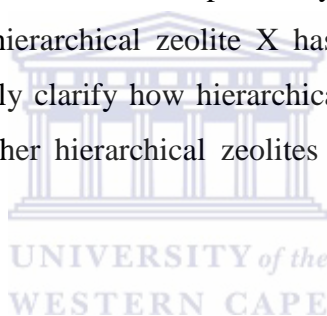
Musyoka, (2012) synthesised hierarchical zeolite X from a clear fused fly ash (FFA) extract, without the addition of organic structure-directing agents. Although mesoporosity was incorporated into the pore system of zeolite X using a relatively simple synthesis procedure, the cause behind the formation of this hierarchical zeolite has not been reported to date. To elucidate the cause behind hierarchical zeolite X formation the influence of synthesis parameters such as hydrothermal temperature and time, agitation, Si/Al ratio and aluminium source was investigated in this study. Although, Musyoka, (2012) investigated the effect of hydrothermal temperature and ageing on hierarchical zeolite X formation, the effect of Si/Al ratio or aluminium source has not been reported to date. Zeolite structure and composition is known to be influenced by the Si/Al ratio of the synthesis solution (Feijen et al., 1994; Yu, 2007), while the source of silicon and aluminium has been reported to influence the morphology and crystal size of zeolites (Shigemoto et al., 1993; Yu, 2007). The control of zeolite crystal size and morphology is of great interest in tailoring zeolites with specific properties for certain applications. The Si/Al ratio of the synthesis solution may be altered by the addition of either a silicon or aluminium source to the synthesis solution. The aluminium content of the synthesis solution was shown to influence the crystallization of zeolite X from fly ash by Chang and Shih, (2000). The effect of Si/Al ratio (by the addition of two different aluminium sources) as well as other synthesis parameters on hierarchical zeolite X formation was therefore investigated in this study to gain insight into the formation of this zeolite.

Hierarchical materials, such as hierarchical zeolite X, may find new application in fields such as catalysis and adsorption due to the ability of these materials to circumvent the well-known diffusion and mass-transfer problems experienced in the application of conventional, microporous zeolites in these fields (Liu et al., 2009; Moller and Bein, 2011; Na et al., 2011). Hierarchical zeolites exhibit enhanced diffusion of large organic reactants and products through the pore system and increased exposure of acid sites in the pore walls of the zeolite. In catalytic applications, loss of shape-selectivity by hierarchical zeolites may be of concern (Xu et al., 2008). Hierarchical zeolites still remain interesting materials for application as “green” heterogeneous, solid-acid catalysts for processing large organic

molecules. A good understanding of the cause responsible for the formation of hierarchical zeolite X from a clear FFA extract is therefore required to tailor other hierarchical zeolites without the addition of complex structure-directing agents. The determination of the cause behind the formation of hierarchical zeolite X was therefore the main focus of this study.

1.2 Problem Statement

Of the tonnes of coal fly ash produced annually, only a small quantity is used in industry for the production of cement and bricks, as well as for backfilling of mine voids. The large production of coal fly ash, which contains toxic and harmful chemicals, has placed massive strain on landfills. This study aims to utilise waste coal fly ash for the synthesis of zeolites which are of much greater value. A novel form of zeolite X with hierarchical morphology was synthesised from a clear FFA extract as reported by other researchers. However, the cause behind the formation of hierarchical zeolite X has not been reported to date. The success of this study will not only clarify how hierarchical zeolite X is formed, but it will establish a way to synthesise other hierarchical zeolites without the addition of complex structure-directing agents.



1.3 Aim and Objectives of the Study

The aim of this study is to investigate the cause behind the formation of hierarchical zeolite X.

The objectives of this study include:

- Investigating the role of chemical parameters (such as Si/Al ratio and aluminium source) on the formation of hierarchical zeolite X.
- Investigating the role of synthesis parameters (such as hydrothermal temperature and static and stirred hydrothermal conditions) on the formation of hierarchical zeolite X.
- Investigating the influence of hydrothermal time on the crystallisation of hierarchical zeolite X from a clear FFA extract, using FTIR spectroscopy.
- Characterisation of synthesised zeolites and starting materials by various analytical techniques to determine the elemental composition (XRF, LA-ICP-MS), morphology (SEM), fine structure (TEM), mineralogy (XRD), structural composition (FTIR), solid acidity (titrimetric acidity determination) and surface area (nitrogen physisorption).

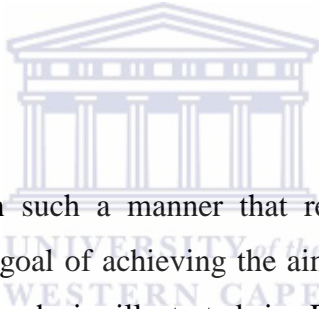
- Determining the cause behind the formation of hierarchical zeolite X.

1.4 Research Questions

This study aims to answer the following research questions:

- What is the influence of chemical parameters (such as Si/Al ratio and aluminium source) on the formation of hierarchical zeolite X?
- What is the influence of synthesis parameters (such as hydrothermal temperature and static and stirred hydrothermal conditions) on formation of hierarchical zeolite X?
- What is the influence of hydrothermal time on the crystallisation of hierarchical zeolite X from a clear FFA extract?
- What is the cause behind the formation of hierarchical zeolite X from a clear FFA extract of fly ash?

1.5 Research Approach



The research was carried out in such a manner that results act as a starting point for successive experiments, with the goal of achieving the aim and objectives of this study. An overview of the research approach is illustrated in Figure 1.1. Firstly, a review of experimental techniques for zeolite synthesis and fly ash-based zeolite synthesis was carried out. Experimental procedures suited to this study were selected for the synthesis and characterisation of fly ash-based hierarchical zeolite X. The main starting material for zeolites synthesised in this study was coal fly ash, received from the Arnot power plant in South Africa. The as-received coal fly ash was characterised to determine the chemical and physical properties thereof such as morphology, surface area, elemental and mineralogical composition. Next, the fly ash was activated by a well-reported alkali fusion process to convert fly ash to more reactive species. The fused fly ash was then characterised to determine whether the alkali-activation process was indeed effective in converting fly ash to more reactive species.

The following step was the hydrothermal synthesis of hierarchical zeolite X from a clear FFA extract of Arnot coal fly ash using the experimental conditions reported by Musyoka, (2012) as a baseline, followed by the characterisation of synthesised products. Next, the effect of

Chapter 1 - Introduction

synthesis parameters such as hydrothermal temperature and time, agitation, Si/Al ratio and aluminium source on the formation of hierarchical zeolite X was investigated, to elucidate the cause behind its formation. Individual synthesis parameters were varied one at a time, keeping all other parameters constant. The synthesised products were characterised to determine the mineralogical (by XRD) and morphology (by SEM-EDS) of the material and the optimal synthesis conditions were used as the basis for subsequent experiments.

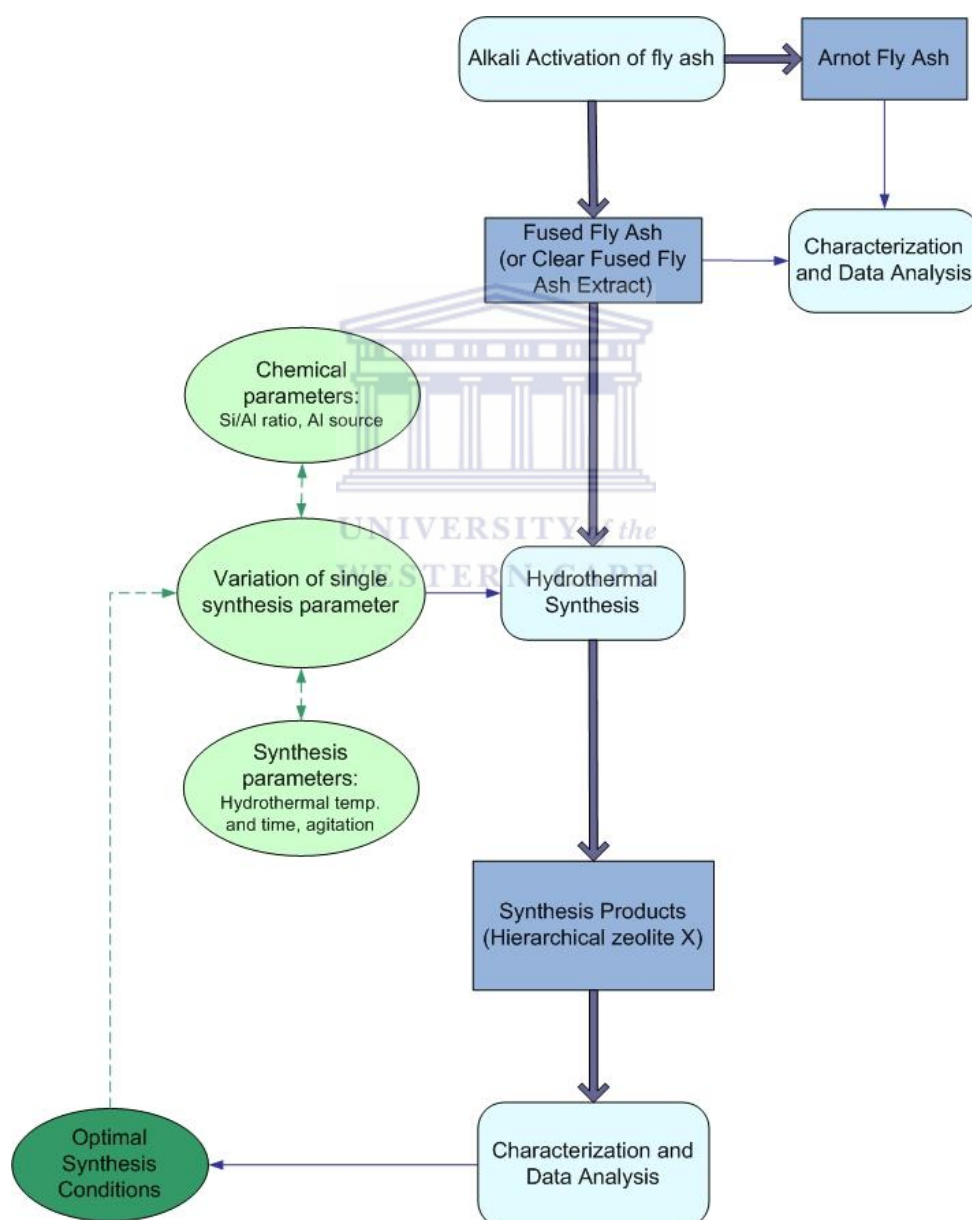


Figure 1.1: Schematic diagram of the research approach for zeolite synthesis from a clear fused fly ash extract.

1.6 Scope and delimitations of the study

Zeolite science covers a broad range of topics including synthesis techniques and various analytical techniques used for zeolite characterisation. The literature review briefly discusses zeolites in terms of classification, structure, characteristic properties, synthesis techniques and applications. The main focus of the literature review was zeolite synthesis from coal fly ash, the synthesis of hierarchical zeolites and relevant characterisation techniques. Particular attention was paid to the characteristics and synthesis of zeolite X since hierarchical zeolite X is the target zeolite in this study. The starting material for zeolite synthesis in this study was coal fly ash received from the Arnot power plant located in Mpumalanga, South Africa. The study focussed on the effect of chemical parameters (such as Si/Al ratio and aluminium source) as well as hydrothermal synthesis parameters (temperature and time, stirring) on the formation and morphology of fly ash based hierarchical zeolite X. The choice of the investigated synthesis parameters was based on the gap analysis carried out during the literature review and other chemical parameters (such as water content, alkalinity, etc.) were not investigated in this study in the interest of time. The main characterisation techniques utilised in this study were therefore mineralogical (XRD) and morphological (SEM) analysis. Selected zeolites were further characterised by various other analytical techniques to gain more insight into the properties of the material.

1.7 Thesis Outline

The contents of this thesis will be structured in the following manner:

- Chapter One: Introduction.
- Chapter Two: Literature review.
- Chapter Three: Research design and methodology.
- Chapter Four: Characterisation of South African fly ash and alkali-activation of fly ash.
- Chapter Five: The influence of hydrothermal synthesis parameters on the formation of hierarchical zeolite X.
- Chapter Six: The influence of molar regime adjustment on the formation of hierarchical zeolite X.
- Chapter Seven: Conclusions and recommendations.

Literature Review

2 *Introduction*

A review of literature relevant to this study will be presented in this chapter. The literature review will cover a brief history of zeolite science, including the principles of green chemistry and how zeolites are related to green chemistry. This will be followed by an outline of how zeolites are classified, characteristic structural features of zeolites as well as the unique properties associated with zeolites. Next, zeolite synthesis will be discussed with emphasis on the synthesis of zeolite X. An alternative starting material, coal fly ash, for zeolite synthesis will be discussed, including a brief description of the origin and properties of coal fly ash. The main focus of the study is the synthesis of zeolite X from coal fly ash, particularly the synthesis of hierarchical zeolite X from coal fly ash. A brief review of synthesis routes for hierarchical zeolites will therefore be discussed. The principles of the characterisation techniques applicable to zeolites will also be summarised briefly.

In recent years, the development of sustainable chemical processes has received much attention in an effort to reduce the environmental impact of chemical processes (Centi and Perathoner, 2003; Gupta and Paul, 2014). Green chemistry has been defined by the United States Environmental Protection Agency as “the use of chemistry for pollution prevention, and design of chemical products and processes that are environmentally benign” (Centi and Perathoner, 2003). A few green principles have been defined to serve as a guideline for the development of green synthetic products or processes. The green principles of chemistry include; the prevention of waste, an efficient atom economy which states that the transformation of reactants to the desired product should be maximised, chemical processes should avoid the use of toxic or harmful chemicals where possible, the use of secondary substances (such as solvents) should be avoided or made as harmless as possible, simple and inherently safe processes should be used, energy consumption should be minimised, renewable raw materials should be used wherever possible and catalytic substances are preferred over stoichiometric reagents (Centi and Perathoner, 2003; Gupta and Paul, 2014). Zeolites are crystalline materials with properties such as shape selectivity, ion-exchangeability and solid acidity which make them suitable ‘green’ materials for application in catalysis and adsorption (Na et al., 2013; Tessonier et al., 2006).

In the past, the word “zeolite” referred to a family of minerals that exhibited properties such as ion-exchangeability and the ability to desorb water reversibly. The latter property was the

Chapter 2 – Literature Review

inspiration for the term “zeolite” which was derived from the Greek words *zeo* (meaning that which boils) and *lithos* (which means stone) (Davis and Lobo, 1992). For years zeolites have been known to occur naturally as hydrated aluminosilicate minerals with examples such as mordenite, faujasite, chinoptilolite, chabazite and erionite (Weitkamp, 2000). These natural zeolites are formed during various geological processes involving the transformation of natural resources such as volcanic ash, quartz and clay (Granda Valdes et al., 2006). Synthetic analogues of natural zeolites were first reported by Richard Barrer and Robert Milton (the pioneers of zeolite synthesis) in the period from 1948 to 1955 (Cundy and Cox, 2005; Weitkamp, 2000).

More recently, zeolites have been described as crystalline aluminosilicates consisting of silica (SiO_4) and alumina (AlO_4) tetrahedra as primary building units. The SiO_4 and AlO_4 tetrahedra are connected by a common oxygen atom resulting in the formation of a three-dimensional framework, which is characteristic of zeolites (Louis et al., 2004). The zeolite framework contains well-defined channels, cages and/or cavities (Huang et al., 2010). In the zeolite framework, the substitution of silicon atoms by aluminium atoms results in an excess negative charge on aluminium atoms in framework tetrahedra. The excess negative charge is compensated by the presence of positively charged counter-ions which are mainly alkaline (for example sodium) and/or alkaline-earth (for example calcium) cations. The substitution of counter-ions by other cations leads to the ion exchange property of zeolites (Granda Valdes et al., 2006; Weitkamp, 2000).

The porous nature of zeolites gives rise to the size and shape selectivity of these materials. Zeolites are therefore suitable materials for application as molecular sieves and have been applied as such for many years. Zeolites have also found great application in the field of catalysis, particularly in the petroleum industry, due to the unique properties of these materials such as shape selectivity, large surface area and solid acidity (Tao et al., 2006; Weitkamp, 2000). Large pore zeolites (synthetic X and Y) have been used industrially as catalysts for the fluid catalytic cracking (FCC) of heavy fractions of petroleum (Hölderich and van Bekkum, 1991; Holm et al., 2011). After its application in FCC, zeolites were used in the petrochemical industry as catalysts for hydrocracking of distillates, the enhancement of gasoline octane number by isomerisation and disproportionation of toluene to form xylenes and benzene (Holm et al., 2011; Hunger, 2010).

2.1 Classification of zeolites and their characteristic properties

The characteristic properties of zeolites are closely related to their structure. It is therefore important to understand the structure of zeolites so as to fully exploit their unique properties. This section will discuss how zeolites are classified, their characteristic structural features and some of the unique properties which arise as a result of these features.

Since 1970, zeolites have been classified according to framework type (Meier and Baerlocher, 1999). Zeolite framework type basically describes how framework tetrahedral atoms are connected to each other. The framework type represents a group of zeolites with characteristic pore dimensions, channel systems and cages, as well as cation sites (McCusker and Baerlocher, 2007; Na et al., 2011). Other factors such as chemical composition, nature of framework species and type of post-synthesis treatment also influences the structural characteristics of zeolites (Franus, 2012; McCusker and Baerlocher, 2007). Zeolite framework types are described by three letter codes, which have been approved by the Structure Commission of the International Zeolite Association in agreement with the rules of the International Union of Pure and Applied Chemistry (IUPAC) Commission on zeolite nomenclature. Some common framework types include GIS, FAU, LTA and MFI; the codes arise from the zeolite or material type which it describes. The code LTA was derived from Linde Type A, while MFI was derived from Zeolite Socony Mobil-five and FAU was derived from the mineral faujasite (Meier and Baerlocher, 1999).

A distinctive feature of zeolitic materials is that they are composed of a three dimensional framework structure which consists of TO_4 tetrahedra, the basic building unit (BBU) of zeolites, where T denotes any tetrahedrally coordinated cation, usually Si and Al (Davis and Lobo, 1992). The framework structure of zeolites is further characterised by cavities and channels which create a relatively open framework structure. Zeolites are therefore described by framework type with regard to the dimensions of pores and channels. The pore openings of zeolites are characterised by the term n-ring (where n is the number of T-atoms in the ring structure), which describes the size of the ring from which the pore is formed. A small pore opening (8-ring) has an effective pore width of 0.41 nm compared to medium pore openings of 0.56 nm (10-ring) and large pore openings of 0.74 nm (12-ring). These values serve only as a guide for the effective pore widths of zeolites since ring distortion may result in variation of pore dimensions (Deutschmann et al., 2009; Hagen, 2006; Hölderich and van Bekkum, 1991).

Framework types are made up of a variety of structural units namely; cages, channels, sheets and/or chains (Meier and Baerlocher, 1999). Channels may intersect to generate three-dimensional (3-D) channel networks; a vital feature for application of zeolites in catalysis and adsorption (Roth and Cejka, 2011). Zeolitic framework types may therefore be classified by different structural features such as pore dimensions, structural subunits and/or channel systems (McCusker and Baerlocher, 2007; Weitkamp, 2000). Some common structural units are depicted in Figure 2.1, namely the α -cavity, β -cage, D4R, D6R and pentasil units.

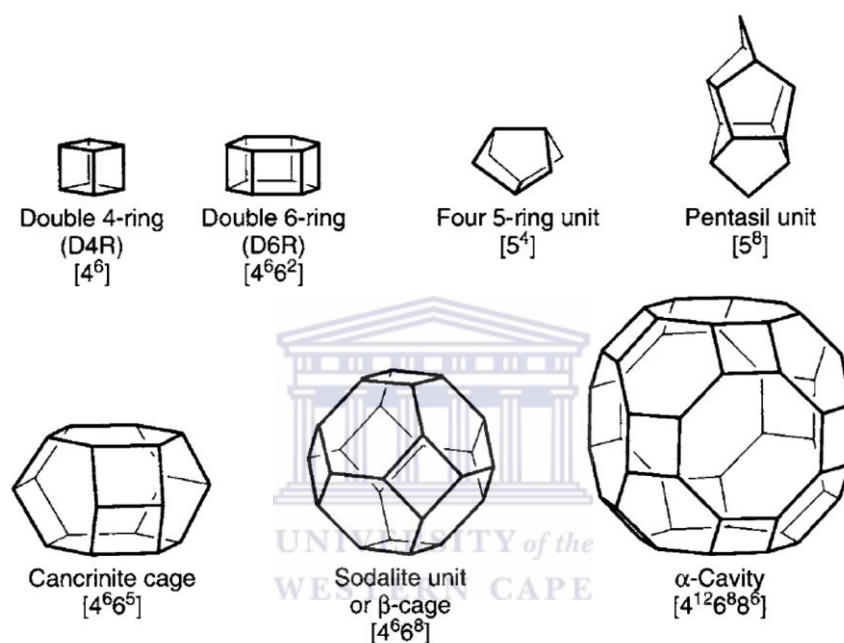


Figure 2.1: The common structural units which occur in zeolite frameworks (McCusker and Baerlocher, 2007).

Of the numerous approved zeolite framework types, a few (namely SOD, LTA and FAU) will be described briefly. SOD is a code used to describe sodalite-type material. SOD is not considered a true zeolite since it only has 6-ring openings. However, the framework density of SOD does fall within the acceptable range for zeolites. The SOD framework type is defined as a body-centred cubic arrangement of sodalite cages (β -cages) joined by shared 4- or 6-rings (Davis and Lobo, 1992; Reyes et al., 2013). Furthermore, the SOD framework may be seen as the stacking of single 6-ring arrangements in the $[111]$ direction. An illustration of the SOD framework type is depicted in Figure 2.2 (a), where T-atoms are represented by nodes and oxygen atoms are represented by lines (Hagen, 2006; McCusker and Baerlocher, 2007).

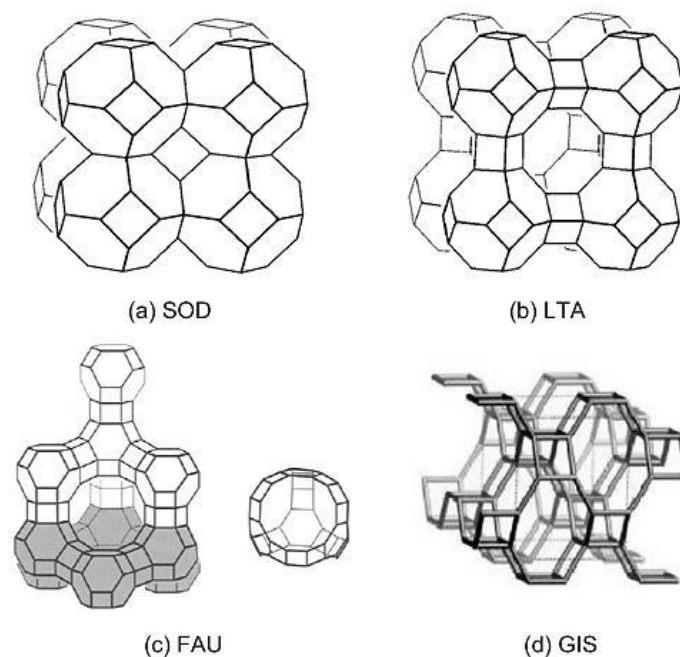


Figure 2.2: Examples of three framework types; (a) SOD, (b) LTA, (c) FAU with the supercage and (d) GIS (Hagen, 2006; McCusker & Baerlocher, 2007).

The LTA framework, depicted in Figure 2.2 (b), is named after the Linde Type A material which is closely related to SOD. The LTA framework consists of a primitive cubic arrangement of sodalite cages joined together by oxygen bridges to form double 4-rings (D4R), unlike the SOD framework in which 4-rings are shared (Corma et al., 2004). The LTA framework contains an α -cavity in the centre of the unit cell and three-dimensional 8-ring channels (Hagen, 2006; Meier and Baerlocher, 1999). The LTA framework is one of the more open zeolite frameworks (McCusker and Baerlocher, 2007). An example of a material with LTA framework structure is zeolite A, which has been widely applied as a laundry detergent due to its ion-exchange capability (Hölderich and van Bekkum, 1991; van Hooff and Roelofsen, 1991).

The framework type FAU, depicted in Figure 2.2 (c), is used to describe faujasite-type materials (Meier and Baerlocher, 1999). FAU-type materials are composed of sodalite cages arranged much like the carbon atoms in a diamond. Sodalite cages in FAU frameworks are joined together by double 6-rings (D6R) forming a “supercage” that consists of four tetrahedrally oriented, 12-ring openings (Eulenberger et al., 1967; McCusker and Baerlocher, 2007). The great void volume in combination with large pore openings and 3-D channel network has made FAU materials suitable for catalytic and adsorption applications (Chang

Chapter 2 – Literature Review

and Shih, 1998). Some examples of faujasite materials are zeolite X and Y. These zeolites exhibit the same diffraction pattern and are typically discerned by the framework Si/Al ratio, which is 1-1.5 for zeolite X and 1.5-3.8 for zeolite Y (Eulenberger et al., 1967; Payra and Dutta, 2003). Faujasite materials, such as zeolite X, are characterised by a large pore diameter of 0.74 nm (Franus, 2012; Inayat et al., 2012).

The GIS framework, depicted in Figure 2.2 (d), is used to describe gismondine-type frameworks. The GIS framework is made up of a two-dimensional array of double crankshaft chains, stacked together to form 8-ring channels (Musyoka et al., 2012). These channels lie parallel to each other in the x- and y-direction but are displaced with respect to each other in the z-direction; this gives rise to the three-dimensional channel network in the GIS framework. Double crankshaft chains are known to be flexible and consequently, so is the GIS framework (McCusker and Baerlocher, 2007; Musyoka et al., 2012). Some examples of materials with GIS framework structure are gismondine, garronite and zeolite Na-P1. The latter is typically used as an ion-exchanger in the laundry industry (McCusker and Baerlocher, 2007).

Although framework type plays an important role in the structural properties of zeolites other factors such as zeolite chemical composition, extra-framework species and defects in the zeolite structure also influence zeolite properties. Most of the properties of zeolites stem from the anionic nature of the zeolite framework and the presence of exchangeable counter-ions in the framework (Davis and Lobo, 1992; McCusker and Baerlocher, 2007). As mentioned previously, an anionic aluminosilicate framework is formed when tetravalent framework silicon atoms are substituted by trivalent aluminium atoms, allowing cations (such as Na^+ and Ca^{2+}) to serve as counter-ions that charge compensate the zeolite framework (Davis and Lobo, 1992; Hunger, 2010; McCusker and Baerlocher, 2007). These extra-framework cations are exchangeable which gives rise to the ion-exchange property of zeolites. Extra-framework cations may originate from the synthesis solution or be incorporated to charge-balance the framework by post-synthesis treatments. The position of extra-framework cations in the cages and channels of zeolites is of interest as it affects the catalytic and adsorption properties of the material (McCusker and Baerlocher, 2007; Payra and Dutta, 2003). In the case of pure silica zeolites, the framework is neutral owing to the absence of trivalent aluminium atoms (Granda Valdes et al., 2006; Weitkamp, 2000).

Chapter 2 – Literature Review

Zeolites may contain Brönsted acid sites or Lewis acid sites, as depicted in Figure 2.3 (Hagen, 2006; van Hooff and Roelofsen, 1991; Xie et al., 1994).

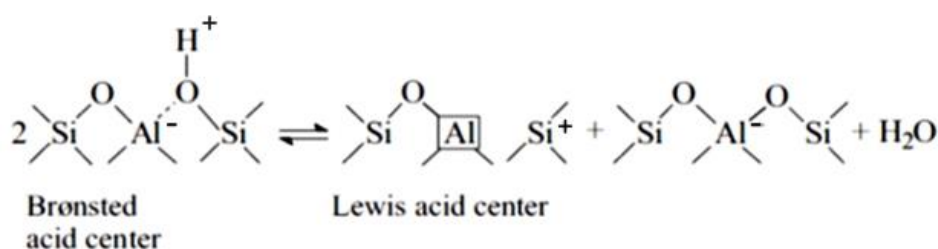


Figure 2.3: Acidic sites, Brönsted (left) and Lewis (right) sites, of the zeolite framework (adapted from Hagen, 2006).

The acidic nature of zeolites also stems from the presence of aluminium atoms and exchangeable counter-ions in the zeolite framework (Hölderich and van Bekkum, 1991; Weitkamp, 2000). Zeolites are typically synthesised in the sodium form, i.e. containing sodium cations as counter-balancing ions. The sodium form of zeolites exhibit Lewis base properties due to framework oxygen atoms (Xie et al., 1994). The amount of aluminium atoms in the zeolite framework is directly proportional to the number of monovalent counter-ions (such as sodium cations) present in the zeolite framework (Hölderich and van Bekkum, 1991). The sodium-form (Na-form) of zeolites may be converted to the acidic proton-form (H-form) by ion-exchange with ammonium salts followed by calcination (Hunger, 2010, Weitkamp, 2000).

Brönsted acid sites in zeolites occur at the bridging hydroxyl group (proton and oxygen) connected to framework aluminium atoms (Weitkamp, 2000; Xie et al., 1994). Lewis acid sites are formed by the dehydroxylation of Brönsted acid sites, as illustrated in Figure 2.3 (Hagen, 2006; van Hooff and Roelofsen, 1991; Weitkamp and Hunger, 2007). Zeolite acidity is dependent on the type of T-atoms incorporated into the zeolite framework (such as aluminium, gallium or iron) and the Si/T ratio of the zeolite framework (Hölderich and van Bekkum, 1991; Louis et al., 2004). Zeolites may therefore serve as solid acid catalysts and replace conventional Brönsted acids in various catalytic applications (Hölderich and van Bekkum, 1991; Weitkamp, 2000). Framework acidity therefore plays an important role in the catalytic application of zeolites.

Chapter 2 – Literature Review

Another important characteristic of zeolites, linked to framework composition, is framework stability. High-silica zeolites such as ZSM-5 are usually characterised by high thermal stability compared to low-silica aluminosilicates, which are in turn thermally more stable than the corresponding aluminophosphate. The chemical composition of zeolites often dictates the characteristic features of a specific framework type. Structural defects may also arise in structurally-related framework types since they are often formed under similar synthesis conditions. Common structural defects include crystal intergrowth or stacking faults. Intergrowth between ZSM-5 (MFI) and ZSM-11 (MEL) zeolites is a common example of a structural defect. Structural similarity between zeolites makes it possible for an occasional fault in sheet stacking to occur. The occurrence of stacking faults may block zeolite channels which affects catalytic and adsorption properties of the material. If stacking faults occur periodically a new framework type will be formed with a novel repeat structure (McCusker and Baerlocher, 2007).

The focus of this study will be on zeolite X which is a large pore FAU-type zeolite with a pore diameter of 0.74 nm and high content of aluminium in the framework, which is usually charge-compensated by sodium cations (Franus, 2012; Shigemoto et al., 1995). Zeolite X is composed of sodalite cages linked by double 6 ring (D6R) units, which is the characteristic secondary building unit (SBU) for FAU-type zeolites (McCusker & Baerlocher, 2007; Shigemoto et al., 1995). Sodalite cages join together through D6R linkages to form the zeolite X framework which consists of 6-ring pore openings (β -cages) and 12-ring pore openings (supercages). Sodium cations are typically present in the zeolite X framework as charge-balancing cations. Charge-balancing sodium cations may be easily exchanged with other cations such as potassium (K^+) and lithium (Li^+) ions. Zeolite X has therefore been applied in ion-exchange applications (Shigemoto et al., 1995). More recently, zeolite X has also found an interesting application as a heterogeneous catalyst in organic synthesis due to the larger pore size of this material compared to other zeolites (Krishnan et al., 2002; Ojha et al., 2003).

The unique properties of zeolites are closely linked to the structural characteristics of these materials. Properties such as shape selectivity, ion-exchangeability, thermal stability and solid acidity are directly related to the structural features of zeolites such as the pore network, cages and channels, zeolite chemical composition and extra-framework species. These unique properties have made zeolites favourable materials for catalytic and adsorption applications

(McCusker & Baerlocher, 2007). An understanding of how these materials are synthesised as well as how synthesis parameters influence material properties is therefore required.

2.2 Zeolite synthesis techniques

This section will deal with synthesis techniques used for the preparation of zeolites including; a brief history of zeolite synthesis, the mechanism of zeolite synthesis and factors which influence the synthesis process.

The first synthetic zeolite (without a natural counterpart) was prepared in 1948 by Richard Barrer; although the first natural zeolite, stilbite, was discovered as far back as 1756 by Axel Fredrik Cronstedt (Feijen et al., 1994; Yu, 2007). Barrer had begun his investigations into zeolite synthesis in the early 1940's by monitoring the conversion of certain mineral phases in high salt environments at relatively high temperatures (170-270 °C). This approach led to the formation of the first synthetic zeolite. At the end of the 1940's Robert Milton and his co-workers went on to synthesise zeolites A, P and X. These zeolites were synthesised by hydrothermal treatment of a reactive aluminosilicate gel in highly alkaline medium, in the presence of metal cations. Hydrothermal treatment was carried out at relatively low temperatures (~100 °C) and autogenous pressure (Cundy and Cox, 2005; Yu, 2007).

By the early 1950's, 20 synthetic zeolites had been synthesised by Milton and his co-workers via the hydrothermal synthesis approach, 14 of which did not have natural analogues (Cundy and Cox, 2005; Yu, 2007). It was, however, Barrer and Denny who discovered that the introduction of organic quaternary ammonium cations into the aluminosilicate gel mixture could increase the Si/Al ratio of the zeolite framework (Yu, 2007). The incorporation of organic compounds into zeolite synthesis played a vital role in advancing zeolite science and led to the synthesis of high-silica zeolites such as zeolite beta and ZSM-5 (Cundy and Cox, 2005; Yu, 2007). Barrer and Milton were therefore thought to be the pioneers of zeolite synthesis technology (Weitkamp, 2000).

In modern day zeolite science, hydrothermal synthesis is still commonly employed as the most typical preparation route for zeolites (Yu, 2007). Hydrothermal synthesis involves the conversion of a supersaturated alkaline solution containing silicon and aluminium precursor species, metal cations, mineralising anions and water (in certain cases, organic templates) into a well-defined crystalline aluminosilicate material (Feijen et al., 1994; Hamilton et al.,

1993). The hydrothermal synthesis technique is not limited to zeolites alone but has also been applied in the preparation of various inorganic, porous materials namely; chemical sensors, ceramics, superionic conductors and magnetic materials. The unique advantages of the hydrothermal synthesis technique (such as low energy consumption, high reactant reactivity, low air pollution and the production of metastable phases) attracted substantial interest to this technology (Yu, 2007). Zeolite synthesis involves a pre-synthesis ageing step, hydrothermal treatment as well as post-synthesis treatment of the hydrothermal product. During the pre-synthesis step, precursors are mixed together to form the synthesis mixture prior to the hydrothermal treatment step. The hydrothermal synthesis step involves elevated temperatures (and often pressure) of the synthesis mixture to yield the zeolite product. The zeolite product may then be subjected to post-synthesis treatments to modify the properties of the material (Davis and Lobo, 1992; Yu, 2007).

2.2.1 Pre-synthesis step

The pre-synthesis step involves the preparation of the synthesis solution by mixing the reactants together in a pre-determined order, prior to the hydrothermal treatment step. During this stage of zeolite synthesis, the synthesis solution may be allowed to age under static or stirred conditions for a given period of time under ambient or elevated temperatures. Zeolite formation involves complicated chemical processes namely; depolymerisation, dissolution, precipitation and polymerisation. The chemistry of zeolite formation is complex and influenced by many factors such as molar composition of the synthesis mixture, sources of reactants, Si/Al ratio, system alkalinity, water content and hydrothermal conditions (Feijen et al., 1994; Yu, 2007). The effect of chemical parameters for zeolite synthesis is therefore considered during this step. The influence of synthesis parameters (such as hydrothermal temperature and time, stirring, Si/Al ratio and aluminium source) on the formation of hierarchical zeolite X will be investigated in this study. Therefore the pre-synthesis parameters which affect zeolite synthesis will be discussed briefly.

2.2.1.1 Molar composition of the synthesis mixture

The initial molar composition of the synthesis solution ($w\text{Na}_2\text{O}-x\text{Al}_2\text{O}_3-y\text{SiO}_2-z\text{H}_2\text{O}$) plays a vital role in the type of zeolite phase which crystallises (Feijen et al., 1994; Yu, 2007). Under the same hydrothermal conditions, different zeolite phases may crystallise by altering the molar composition of the synthesis solution. This may be achieved by altering the Si/Al ratio, alkalinity or water content of the synthesis solution. However, boundary regions exist where

a particular molar composition could give rise to two different phases (Yu, 2007). The effect of these pre-synthesis parameters will be discussed in more detail in the following sections.

2.2.1.2 Sources of reagents

The nature of starting materials used in zeolite synthesis plays a major role in the crystallisation process. The common sources of silicon in zeolite synthesis include sodium silicate, fumed silica, sodium metasilicate hydrate, colloidal silica and tetraethylorthosilicate (TEOS) (Shigemoto et al., 1993; Shigemoto et al., 1995; Yu, 2007). The type of silicon source used for zeolite synthesis plays an important role in determining the type of zeolite phase formed. This is due to different levels of solubility and reactivity between the different sources of silicon. The distribution and nature of polysilicate species differs between silicon sources and therefore significantly influences the processes of nucleation and crystallisation (Hamilton et al., 1993; Yu, 2007). The source of aluminium also affects the crystallisation of zeolites. The aluminium sources commonly used in the zeolite synthesis include aluminium hydroxide, sodium aluminate, aluminium isopropoxide, aluminium sulphate, aluminium nitrate and aluminium metal (Shigemoto et al., 1993; Shigemoto et al., 1995; Yu, 2007).

Shigemoto et al., (1993) investigated the influence of both the aluminium and silicon source on zeolite formation and crystallinity. Silicon sources included α -quartz and fumed silica while aluminium sources included mullite and sodium aluminate, in addition to fly ash (Shigemoto et al., 1993). The starting materials were fused with sodium hydroxide (NaOH) at a temperature of 500 °C for 1 hour, prior to hydrothermal synthesis which was carried out at 100 °C for 6 hours. Zeolite X with a high crystallinity was synthesised when fumed silica and sodium aluminate were used as starting materials for zeolite synthesis; this result was used as a reference for further work by Shigemoto et al., (1993). An even higher zeolite X crystallinity was achieved when α -quartz and sodium aluminate was used. Zeolite X with notably lower crystallinity was synthesised when fumed silica and mullite were used. Shigemoto et al., (1993) proposed that the reactivity of mullite was lower compared to α -quartz due to the partial conversion of mullite to sodium aluminate species by the alkali fusion process compared to the complete conversion of α -quartz to sodium silicate species. The low yield of zeolite X from fly ash was attributed to the low reactivity of mullite, which constituted 40% of the fly ash used by Shigemoto et al., (1993). Shigemoto et al., (1993) therefore illustrated how reactivity of silicon and aluminium sources influences zeolite formation and crystallinity.

Chapter 2 – Literature Review

Hamilton et al., (1993) investigated the effect of silicon source on zeolite Na-X crystallisation by using eleven different sources of silicon, under hydrothermal conditions at 115 °C for set time periods. The source of silicon was reported to affect zeolite Na-X particle size and the length of the crystallisation process. Hamilton et al., (1993) proposed that certain silicon sources reduced the crystallisation period by enhancing the formation of Na-X nuclei during the nucleation phase which resulted in the formation of relatively smaller zeolite crystals. Hamilton et al., (1993) related the difference in Na-X crystallisation to the varying ability of silicon sources to form Na-X nuclei under the hydrothermal conditions investigated as well as the variation in the level of impurities present in the different silicon sources.

The surface area of silicon sources is another factor which plays a vital role in the crystallisation kinetics of zeolites. The surface area of the silicon source influences zeolite crystal size and particle size distribution. A silicon source with higher surface area is dissolved more easily in a basic solution than silicon sources with low surface areas. High surface area silicon sources were reported to promote supersaturation which leads to an increased rate of nucleation in basic media, and consequently resulted in the formation of smaller zeolite A crystals (Meise and Schwochow, 1973). On the contrary, low surface area silicon sources with low solubility were reported to promote the formation of large zeolite crystals. Large zeolite crystals are favourably formed due to the reduced rate of dissolution of silicon sources which results in the generation of fewer nucleation sites (Meise and Schwochow, 1973; Yu, 2007). It is noteworthy that in this study a clear fused fly ash (FFA) extract prepared by a high temperature fusion method, containing dissolved silica and alumina species, will be used as the synthesis solution for the preparation of zeolites. Therefore, the effect of the surface area of silicon sources is not seemed a significant factor to consider in the synthesis of zeolite X from a clear FFA extract in this study.

In a study by Xing-dong et al., (2013), aluminium sulphate and aluminium chloride were used as sources of aluminium to determine the influence of aluminium source on the formation of zeolite A. By using aluminium chloride as the aluminium source, the crystallisation temperature and reaction alkalinity was reported to affect zeolite crystal formation as well as the particle size distribution of zeolite crystals while crystallisation time influenced the crystal morphology. In the case of aluminium sulphate, crystallisation time and temperature as well as reaction alkalinity influenced the type of zeolite phase that crystallised. Highly crystalline zeolite A was formed at a relatively shorter crystallisation

time when aluminium sulphate was used as the aluminium source compared to aluminium chloride (Xing-dong et al., 2013). The aluminium source therefore plays a vital role in zeolite synthesis since it influences factors such as crystallisation time, crystal morphology and particle size distribution.

The control of crystal size and morphology of zeolites is of great interest in tailoring zeolites with specific properties for application in catalysis and adsorption. The type of silicon source has been reported to influence the crystallinity and crystal size of zeolite X while the type of aluminium source has been reported to influence the morphology and crystal size of zeolite A. Various silicon and aluminium sources have been reported as starting materials for zeolite X synthesis. Fumed silica, sodium metasilicate hydrate, sodium silicate solution, sodium aluminate solution and mullite were among the silicon and aluminium sources used (Shigemoto et al., 1993; Shigemoto et al., 1995; Xing-dong et al., 2013). Understanding how these reactants behave under hydrothermal synthesis conditions is important to gain a better understanding of how coal fly ash may be converted to zeolites; particularly how a clear fused fly ash extract is transformed into hierarchical zeolite X. The influence of aluminium source on the morphology and crystal size of zeolite X (more specifically hierarchical zeolite X) has not been reportedly extensively to date. Therefore the effect of two different aluminium sources on hierarchical zeolite X formation will be investigated in this study.

2.2.1.3 Si/Al ratio

Zeolite structure and composition is determined by the Si/Al ratio of the synthesis solution. Zeolites with framework Si/Al ratio less than 5 are usually prepared from synthesis solutions with high alkalinity and low Si/Al ratio. These low Si/Al ratio zeolites include zeolite P, X and A. Zeolites with high Si/Al ratios (greater than 5) are typically prepared from weakly alkaline or neutral fluoride synthesis solutions with relatively higher Si/Al ratios (Feijen et al., 1994; Yu, 2007). These high-silica zeolites include ZSM-5, ZSM-11 and zeolite beta. However, it should be noted that there is no direct quantitative correlation between the Si/Al ratio of the synthesis solution and that of the crystallised zeolite product (Yu, 2007). The typical framework Si/Al ratio of zeolite X is 1-1.5, while the Si/Al ratio of zeolite Y is 1.5-3.8, zeolite A is 1 and zeolite P is 2-8 (Eulenberger et al., 1967; Payra and Dutta, 2003; Yu, 2007). Optimised conditions are therefore required for the formation of crystallised zeolite phases with a specific Si/Al ratio (Yu, 2007).

Chapter 2 – Literature Review

In the synthesis of fly ash-based zeolites, the Si/Al ratio of the synthesis solution was proven to influence the type of zeolite phase formed. Crystalline zeolite X was synthesised by using a mixture of fused fly ash (FFA) and deionised water without the addition of any other chemical reagents (Chang and Shih, 2000; Musyoka, 2012; Shigemoto et al., 1993). In a study by Shigemoto et al., (1993), the addition of sodium aluminate solution to the synthesis solution resulted in the formation of zeolite A and zeolite X as a minor product due to the reduced Si/Al ratio of the initial synthesis solution. Chang and Shih, (2000) synthesised zeolite A by adding aluminium hydroxide hydrate to the fused fly ash slurry to alter the Si/Al ratio of the initial synthesis solution. In both studies, a relatively low Si/Al ratio resulted in an increased yield of zeolite A. However, as the yield of zeolite A increased, the yield of zeolite X decreased since the lower Si/Al ratio of the synthesis solution favoured the formation zeolite A over zeolite X (Chang and Shih, 2000; Shigemoto et al., 1993). The synthesis of either zeolite X or A was thought to be dependent on the Si/Al ratio (and the quantity of dissolved aluminium species) in the FFA slurry that was used as the synthesis solution for the hydrothermal process (Chang and Shih, 2000). The formation of zeolite X from a clear FFA extract is therefore strongly dependent on the initial Si/Al ratio of synthesis solution used for hydrothermal treatment.

Musyoka, (2012) reported the synthesis of hierarchical zeolite X from a clear FFA extract under hydrothermal conditions. The effect of hydrothermal temperature and ageing on the formation of hierarchical zeolite X was investigated by Musyoka, (2012). However, the effect of Si/Al ratio on the formation and morphology of hierarchical zeolite X has not been reported to date. Therefore in this study, the effect of Si/Al ratio on hierarchical zeolite X formation and morphology will be investigated using two different sources of aluminium (aluminium hydroxide and sodium aluminate).

2.2.1.4 Alkalinity

Zeolites are commonly synthesised from alkaline synthesis solutions; generally denoted as a $\text{Na}_2\text{O}-\text{Al}_2\text{O}_3-\text{SiO}_2-\text{H}_2\text{O}$ reaction system. The alkalinity of the reaction system may be defined as the $\text{H}_2\text{O}/\text{Na}_2\text{O}$ or OH/Si ratio (Yu, 2007). Higher alkalinity of the reaction system was reported to improve the solubility of silicon and aluminium sources, thereby enhancing the crystallisation kinetics in the synthesis of zeolite X from coal fly ash (Shigemoto et al., 1993). However, Shigemoto et al., (1993) did not report the effect of alkalinity on the morphology of zeolite X. Zeolite morphology was reportedly also affected by system alkalinity by other

researchers (Koroglu et al., 2002; Meise and Schwochow, 1973). Meise and Schwochow, (1973) reported that the alkalinity of the reaction system influenced the particle size of zeolite A crystals. A decrease in particle size and narrow particle size distribution was observed by Meise and Schwochow, (1973) as the alkalinity of the reaction system was increased. Koroglu et al., (2002) investigated the effect of alkalinity on zeolite Y and reported similar results. The particle size distribution and crystallisation of zeolite Y was influenced by the alkalinity of the reaction system (Koroglu et al., 2002). Furthermore, Koroglu et al., (2002) reported that relatively higher system alkalinity resulted in the formation of smaller zeolite Y crystals due to the generation of a larger amount of zeolite Y nuclei during crystallisation.

2.2.1.5 Water

Water behaves as a solvent in zeolite synthesis and may also take part in the synthesis reaction. The water content of the reaction system may be varied in a specific range for the synthesis of a particular zeolite phase. Variation of the water content alters the concentration of reactants which influences the crystallisation process. Typically, diluting the synthesis solution results in lower supersaturation and the crystal growth process is preferred over the nucleation process. As mentioned before, lower supersaturation yields large zeolite crystals (Yu, 2007). Huang et al., (2010) investigated the effect of water content on the formation of hierarchically structured zeolite Y synthesised using a three step temperature-controlled synthesis method. The particle size and porosity of the synthesised zeolite Y could be controlled by varying the water to silica ($\text{H}_2\text{O}/\text{SiO}_2$) molar ratio of the synthesis solution. The formation of smaller faujasite nanocrystals were favoured by lower water content in the synthesis solution. The BET surface area and micropore volume of synthesised Y zeolites decreased as water content was decreased (Huang et al., 2010). The molar regime of the synthesis mixture used by Huang et al., (2010) was different to that used in this study. Furthermore, although mild hydrothermal temperatures were used by Huang et al., (2010), crystallisation time for Na-Y was at least 4 days. Water also plays an important role in determining the function of structure-directing agents and enables the incorporation of different pore architectures by an individual structure-directing agent (Yu, 2007).

2.2.1.6 Solvents

The synthesis of zeolites is commonly carried out in aqueous solution (Yu, 2007). Zeolite formation in the presence of organic solvents (like alcohols) has been reported previously (Huang et al., 2011; Yu, 2007). The choice of solvent in zeolite synthesis influences the

interaction between reaction species, especially structure-directing agents. An effective solvent has an intermediate level of interaction with the structure-directing agent. A structure-directing agent that strongly interacts with the solvent is incapable of interaction with zeolite framework species, which leads to inhibition of the nucleation stage. A solvent classified as low-medium or high-medium hydrogen bonding is a favourable synthesis medium for zeolite synthesis since interaction between the structure-directing agent and framework species is possible (Yu, 2007). The interaction of framework species, structure-directing agent and the synthesis solvent is a crucial parameter to consider in zeolite synthesis.

2.2.1.7 Inorganic species

The nature of inorganic species in the synthesis solution is an important factor in zeolite crystallisation (Feijen et al., 1994; Yu, 2007). Low Si/Al ratio zeolites are usually prepared with alkali-metal hydroxides under basic conditions. Certain zeolites, for example X, Y, P, A and hydroxysodalite, are prepared from an aluminosilicate gel containing sodium ions, while other zeolites (such as merlinoite and theta-1) are formed in the presence of potassium ions. In certain cases, for example the synthesis of zeolite beta and X, both sodium and potassium ions have been used for zeolite synthesis. Inorganic cations present in the synthesis solution have an important effect on the type of zeolite framework structures formed (Yu, 2007). Cations are thought to have two roles in zeolite synthesis, namely; as a source of hydroxide ions which aid in the dissolution of aluminate and silicate species and as a limited structure-directing agent (Xing-dong et al., 2013; Yu, 2007). Cations are commonly added as a base in the form MOH, where M is either an alkali or alkaline earth metal. Hence, the addition of cations simultaneously controls the hydroxide concentration of the synthesis solution (Yu, 2007). In terms of the structure-directing effect of cations; in aqueous solutions cations are thought to influence the order of water molecules (Feijen et al., 1994; Yu, 2007). The water molecules ordered around metal centres are then displaced by silica and alumina tetrahedra which results in the formation of cage-like structures that may serve as precursor species for zeolites (Wijnen et al., 1990; Xing-dong et al., 2013; Yu, 2007).

2.2.1.8 Organic templating agents

Barrer and Denny used an organic templating agent, tetramethylammonium cation which is a quaternary ammonium cation, in the synthesis solution that allowed the formation of zeolite phases with higher Si/Al ratio (Davis and Lobo, 1992; Yu, 2007). Templating is referred to as the phenomenon of the organisation of oxide tetrahedra into a specific geometry by organic

species, during either the gelation or nucleation process. This organisation of oxide tetrahedra into a specific geometric topology gives rise to the first building blocks for a specific zeolite structure (Feijen et al., 1994; Yu, 2007). The gel chemistry as well as the type of template species plays a role in the formation of specific zeolite structures; the templating effect of organic species is only activated in the optimal synthesis environment. Common organic templates include tetraalkylammonium cations such as tetramethylammonium (TMA), tetraethylammonium (TEA) and tetrapropylammonium (TPA). The templating effect of the TMA cation, for example, is known to result in the formation of sodalite cages (Feijen et al., 1994).

2.2.1.9 Seeding

Seeding refers to the addition of a small quantity of the target zeolite into the synthesis solution, typically before the hydrothermal process commences. The seeding process is used to direct the process of crystallisation towards the formation of a particular zeolite and control the crystal size of zeolites (Feijen et al., 1994; Yu, 2007).

2.2.1.10 Ageing Process

The ageing process refers to the period in which a homogeneous mixture is formed, prior to the hydrothermal synthesis step. The ageing step may be carried out under stirred (or static) conditions at room temperature or at elevated temperatures (Feijen et al., 1994; Robson, 2001). The gel chemistry of the synthesis solution is greatly affected by the ageing process; hence the processes of nucleation and crystal growth are also influenced by this stage. The ageing process is believed to give rise to germ nuclei which are dormant until the crystallisation temperature is increased. The ageing process not only increases the nucleation rate, but reduces the induction and hydrothermal period, thereby enhancing the overall crystallisation process. Furthermore, the ageing process reduces crystal size and increases the overall crystal population (Feijen et al., 1994; Yu, 2007).

2.2.1.11 Equipment

Zeolite synthesis takes place at elevated temperatures and pressures, therefore the reaction vessels used for hydrothermal synthesis are usually sealed containers. Stainless steel autoclaves are commonly employed as reaction vessels due to the safety concerns linked with the generation of high autogenous pressures caused by the vaporisation of organic templates at high temperatures. The autoclaves are usually lined with Teflon which makes it resistant to alkaline or acidic media under hydrothermal conditions (Yu, 2007). This study involves the

synthesis of zeolite X under relatively mild conditions; therefore polypropylene (PP) bottles are suitable reaction vessels.

All of these factors highlight that a specific set of synthesis conditions are required for the crystallisation of a specific zeolite phase and slight variation in these parameters could result in the crystallisation of contaminant zeolite phases or a different zeolite phase altogether. Therefore, careful consideration of these factors is required prior to the hydrothermal synthesis of a particular zeolite.

2.2.2 Hydrothermal Synthesis

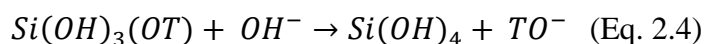
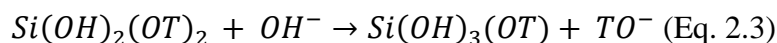
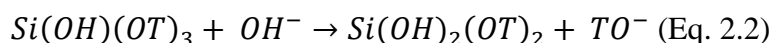
The synthesis formulation, an alkaline solution, is subjected to an elevated temperature (and pressure) and transformed into a well-defined crystalline aluminosilicate material. The conversion of the synthesis solution (which contains silicon and aluminium precursor species, metal cations, a mineralising agent and water as well as organic templates, in certain cases) into a crystalline zeolite occurs via various chemical processes. The mechanism of zeolite synthesis as well as physical parameters which affect zeolite synthesis will be discussed briefly in the following sections.

2.2.2.1 Mechanism of synthesis

Understanding the mechanism of transformation of silicon and aluminium precursors via chemical processes (under hydrothermal conditions) to a crystalline zeolite is important. A good understanding of the mechanism of zeolite synthesis enables the design and tailoring of zeolites with specific morphologies, sizes and other properties (Cundy and Cox, 2005; Huo, 2011; Yu, 2007). The mechanism of zeolite formation may be divided into three stages namely; induction, nucleation and crystal growth (Cundy and Cox, 2005; Feijen et al., 1994). The synthesis mechanism presented will focus on aluminosilicate materials.

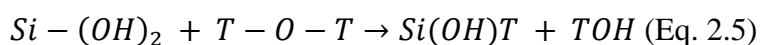
The sol-gel chemistry of zeolites involves a variety of reactions including hydrolysis and condensation. The hydrolysis of metal cations occurs to form precursor species containing metal-hydroxide (T-OH) groups, where T refers to silicon or aluminium atoms in the case of aluminosilicate materials (Lalena et al., 2008; Livage, 1994). In the case of zeolite synthesis, hydrolysis reactions are typically catalysed by hydroxide ions (Feijen et al., 1994). The hydrolysis of silicate species from the most condensed form, $\text{Si}(\text{OT})_4$, to the least condensed form, $\text{Si}(\text{OH})_4$, is illustrated in Equations 2.1-2.4.

Chapter 2 – Literature Review

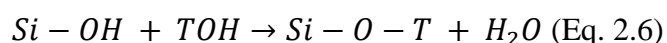


The hydrolysis of a fully condensed silicon centre (bonded to four other T atoms through oxo-bridges) is illustrated in Equation 2.1, adapted from Feijen et al., (1994), which yields a silicon centre bonded to three other T atoms through oxo-bridges and containing one Si-OH bond. Subsequently, the silicon centre coordinated to three other T atoms undergoes hydrolysis to form a silicon centre coordinated to two other T atoms and containing two Si-OH bonds, as illustrated in Equation 2.2. Subsequent hydrolysis reactions of silicon centres results in the formation of the least condensed silicon centre, Si(OH)₄, as illustrated in Equation 2.4. These small, soluble silicate and aluminosilicate species serve as precursors for the synthesis of the zeolite framework through condensations reactions.

The condensation process is divided into two major mechanisms namely; olation and oxolation. In both cases water molecules are eliminated from starting materials, containing at least one metal-hydroxide (T-OH) group, resulting in the formation of poly-nuclear species. Olation involves a condensation reaction which yields a hydroxyl bridge between two metal centres. The process of olation involves the nucleophilic substitution of negatively charged OH⁻ species onto a positively charged hydrated metal centre and the elimination of a water molecule, as illustrated in Equation 2.5 (Lalena et al., 2008; Livage, 1994).



The oxolation process involves the condensation reaction of two metal-hydroxide groups and the elimination of a water molecule to form an oxo-bridge, as illustrated in Equation 2.6. The oxolation process occurs by nucleophilic addition, unlike olation which occurs by nucleophilic substitution (Lalena et al., 2008; Livage, 1994).



The olation reaction occurs in a limited pH range (under acidic conditions) while the oxolation process may take place over a wider pH range. However, the oxolation process is usually slower since it is a two-step process (Lalena et al., 2008; Livage, 1994). These

Chapter 2 – Literature Review

hydrolysis/depolymerisation and condensation reactions occur in the different stages of zeolite crystallisation, which will be described briefly in the following sections.

i Induction

The induction period involves the dissolution of silica and alumina from precursor feedstocks, followed by condensation reactions that yields dissolved aluminosilicate species in the synthesis solution. These dissolved aluminosilicate species serve as precursors for zeolite crystals. During the induction period, the amount of dissolved aluminosilicate species increases with time. This is achieved by hydrolysis (depolymerisation) and dissolution of silica followed by condensation of aluminosilicate species, thereby facilitating the transformation of the synthesis solution into a supersaturated solution (Cundy and Cox, 2005; Feijen et al., 1994).

Zeolite crystallisation is a process that is dependent on a driving force termed supersaturation. Supersaturation refers to a solution in which the concentration of the solute is higher than the equilibrium solute concentration, for a given temperature. These supersaturated solutions are known to be metastable, which means a small finite change is required to change the state of the synthesis system (Cubillas and Anderson, 2010; Myerson, 2002). Supersaturation is typically generated by a change in temperature, change in solvent composition, solvent evaporation or chemical reaction. In a supersaturated solution, precursor species aggregate and form germ nuclei. If these germ nuclei are too small, they undergo depolymerisation and dissolve back into the synthesis solution. On the other hand, germ nuclei may grow in size with time until the critical nuclei size is reached, after which growth will occur spontaneously and result in the formation of stable nuclei (Myerson, 2002).

ii Nucleation

Nucleation occurs during the initial stages of crystallisation, after the induction period, and involves the generation of stable crystal nuclei. The nucleation process may be divided into primary and secondary nucleation. Primary nucleation may be subdivided into two types namely; homogenous and heterogeneous nucleation. Homogeneous nucleation occurs spontaneously while heterogeneous nucleation occurs as a result of impurities present in the synthesis solution. It has been reported that heterogeneous nucleation may be suppressed by filtering the reagents prior to use in the synthesis mixture. Secondary nucleation occurs as result of zeolite seed crystals present in the synthesis solution and is thus linked to the seeding process (Cubillas and Anderson, 2010; Huo, 2011). The nucleation process is

typically thought to occur at the boundary layer of silica sol particles. The concentration of oligomeric species, essential for nucleation, is thought to be largest at the boundary layer due to the dissolution of silica in this region (Cundy and Cox, 2005; Feijen et al., 1994).

iii Crystal growth

The nucleation process is followed by the crystal growth process. The crystal growth process involves nuclei growth by condensation of precursor aluminosilicate species to form fully grown crystals. Experimentally, the crystallisation process exhibits a sigmoidal profile for the formation of crystalline material with time. The crystallisation process is considered self-accelerating due to the autocatalytic nature of the first period in the process. The inflection point of the sigmoidal curve divides the period of autocatalytic growth of crystalline mass and the period of delayed crystal growth (Feijen et al., 1994).

It should be noted that the nucleation process competes with the crystal growth process, since both processes consume precursor aluminosilicate species. The rate of the nucleation process is therefore thought to go through a maximum and decrease with time since precursor species are consumed by the crystal growth process, thereby limiting the concentration available in solution for the formation of new nuclei. Crystal growth occurs in solution at the interface between the growing crystal plane and the solution. It was proposed that the crystal growth process occurs by the condensation of dissolved species onto growing crystal surfaces (Cundy and Cox, 2005; Feijen et al., 1994).

2.2.2.2 Factors influencing hydrothermal treatment

The crystallisation of zeolites during the hydrothermal treatment step is affected by various parameters such as crystallisation temperature and time as well as the agitation of the synthesis solution. The effect of these synthesis parameters on zeolite crystallisation (particularly zeolite X crystallisation) will be discussed briefly.

i Crystallisation time and temperature

The crystallisation (hydrothermal) temperature is a significant factor to consider in the hydrothermal synthesis of zeolites. The majority of research into zeolite synthesis places emphasis on hydrothermal temperature due to the strong effect it has on zeolite formation. A particular zeolite phase crystallises in a specific temperature range. Nucleation and crystal growth processes are greatly affected by hydrothermal temperature. Both the rate of nucleation and crystal growth are enhanced by an increase in hydrothermal temperature,

particularly the crystal growth rate is increased over the nucleation rate (Feijen et al., 1994; Yu, 2007). Increased hydrothermal temperature results in greater growth rates and thereby yields larger zeolite crystals (Yu, 2007). Hydrothermal temperature has been reported to affect crystal morphology of faujasite-type zeolite X; crystal dimensions were reported to increase with an increase in hydrothermal temperature (Musyoka et al., 2014; Yu, 2007). Another example is the increase of the aspect ratio of MFI-type zeolite crystals with hydrothermal temperature. This effect corresponded to the different activation energies required for growth of individual crystal faces (Yu, 2007).

The hydrothermal period (time) is a synthesis parameter which affects the crystallinity of the zeolite phase formed. Typically as time increases, zeolite crystallinity increases (Yu, 2007). It is important to note that zeolites are metastable phases. In the synthesis of zeolites, Ostwald's law of successive transformations is applicable. A metastable phase is formed first which is successively replaced by a more stable phase and so forth. In an alkaline aluminosilicate synthesis environment, the prolonged crystallisation of zeolite X is known to result in the formation of the more stable zeolite P, while zeolite A is transformed into hydroxysodalite with prolonged hydrothermal time (Feijen et al., 1994; Yu, 2007). Therefore both hydrothermal temperature and time are important factors to consider in the synthesis of zeolites.

ii Agitation by stirring

The synthesis of zeolites usually occurs in a static environment. The effect of stirring has been proven to enhance the kinetics of zeolite crystallisation and influence crystal size. The enhancement of crystallisation kinetics by stirring reduces the crystallisation period required to achieve a specific zeolite phase (Yu, 2007). The influence of stirring on the formation of intergrown zeolite Y polymorphs was studied by Hanif et al., (2000). The diffusion of structure-directing agents (SDAs) to the growing zeolite crystal surface was investigated by synthesis under static and stirred conditions. Stirring resulted in the rapid supersaturation of the synthesis solution that led to the formation of smaller zeolite crystals as a result of enhanced mass transfer of reactants (Hanif et al., 2000). Hanif et al., (2000) therefore illustrated that crystal size of zeolite Y polymorphs could be controlled by stirring the synthesis solution. Additionally, stirring may influence the selectivity for various zeolite phases (Yu, 2007). It is noteworthy that the preferential formation of zeolite A rather than zeolite X was reported to occur in a stirred system by Di Renzo et al., (1991). However, the

synthesis of hierarchical zeolite X was achieved in a stirred system by Musyoka et al., (2013). Crystallisation kinetics and crystal size is therefore affected by stirring the synthesis solution (Di Renzo et al., 1991; Hanif et al., 2000; Yu, 2007). It is important to understand the effect of stirring the synthesis solution on the formation of hierarchical zeolite X. Therefore, the effect of a static synthesis environment on the formation of hierarchical zeolite X will be investigated in this study for comparison to the stirred synthesis environment. These physical parameters of hydrothermal synthesis (such as temperature, time and stirring) significantly influence the crystallisation process and the type of zeolite which crystallises and therefore require careful thought for the synthesis of a particular zeolite.

2.2.3 Product recovery and post-synthesis treatment

After the hydrothermal process is complete, the reaction vessel is allowed to cool down to room temperature and the solid product may be recovered by filtration. The solid product is then washed with deionised water until the pH of the filtrate reaches ≤ 9 . The solid product is then allowed to dry in an oven at temperatures of 80-110 °C overnight (Robson, 2001; Yu, 2007). If an organic template was used during the synthesis of the zeolite, the template may be removed by calcination at an appropriate temperature (Deutschmann et al., 2009, Hagen, 2006). Other post-synthesis treatments such as ion-exchange, metal-loading, steaming and demetallation may be used to change the chemical and physical properties of the zeolite material (Deutschmann et al., 2009; Payra and Dutta, 2003).

2.2.4 Alternative methods of zeolite synthesis

Although hydrothermal synthesis is widely used for the preparation of zeolites, various other synthesis techniques have been developed based on the hydrothermal synthesis technique. The demand for tailor-made zeolites with specific properties has arisen from the many applications of zeolites and this demand has led to the development of new synthesis techniques. These new synthesis techniques include; fluoride ion synthesis route, microwave-assisted hydrothermal synthesis, dry-gel conversion synthesis and solvothermal synthesis (Feijen et al., 1994; Yu, 2007).

2.3 Coal fly ash utilisation in zeolite synthesis

A more recent approach to zeolite synthesis will be highlighted in this section, focusing on the use of waste materials (namely coal fly ash) as starting material for zeolite synthesis. Coal

Chapter 2 – Literature Review

fly ash is a by-product of the coal combustion process (Shigemoto et al., 1993). Globally coal remains the main fuel for energy production. In 2012, coal was reported to be responsible for 41 % of electricity production in the world. As the global energy demand increases, the utilisation of coal as an energy source continues to rise (Heidrich et al., 2013). The combustion of coal, by coal-fired power plants, produces coal combustion products (CCPs) which include coal fly ash, boiler slag, bottom ash, fluidised-bed combustion ash and flu gas desulphurisation products. The thermal treatment of coal results in the transformation of mineral phases present in coal to inorganic oxides which are amorphous in nature (Querol et al., 2002).

In 2015, about 34 million tonnes of coal fly ash was produced by coal-fired power plants in South Africa (Eskom, 2015). While in 2012, a survey by the American Coal Ash Association revealed that coal fly ash made up large percentage of the total CCP produced globally (Adams, 2012). Initially, coal fly ash was treated as a waste by-product of coal combustion but negative environmental impacts (such as land-use and pollution) resulted in the beneficiation and utilisation of coal fly ash by other industrial sectors (Chang and Shih, 2000; Querol et al., 2002). Currently, coal fly ash is either stored in landfills or transported for utilisation elsewhere (Molina and Poole, 2004). Storage of coal fly ash in landfills places large strain on land and poses an environmental threat due to leaching of toxic elements into soil and the atmosphere. This pollution results in contamination of soil, ground water, surface water and air (Chang and Shih, 2000; Shoumkova and Stoyanova, 2013). Waste coal fly ash has therefore been used in many applications to reduce land-use and pollution impacts. Coal fly ash has long been utilised by the construction industry for concrete production (Querol et al., 2002). Since then, coal fly ash has been used in the production of other materials such as geo-polymers and zeolites (Molina and Poole, 2004; Musyoka et al., 2013; Musyoka et al., 2014; Shigemoto et al., 1993).

The type of coal fly ash produced by combustion depends on the nature of the combusted coal (Kruger, 1997). Either siliceous or calcareous ashes may be generated by coal combustion, siliceous ashes are predominantly made up of the oxide forms of silicon, aluminium and iron; with lime content limited to less than 10 %. Calcareous fly ash is composed of more than 10 % lime and contains other oxides such as silicon-, aluminium- and iron-oxide (Heidrich et al., 2013). Fly ash consists of glassy spheres, unburned carbon and some crystalline material (Kruger, 1997; Shaheen et al., 2014). Two classes of fly ash (Class

F and Class C) have been classified by the American Society for Testing and Materials in ASTM method C618 (Blissett and Rowson, 2012). The oxide composition of fly ash varies depending on the type of fly ash; class F fly ash contains more than 70 % of SiO₂, Al₂O₃ and Fe₂O₃ combined while class C fly ash contains a minimum of 50 % of these oxides (Blissett and Rowson, 2012; Chang and Shih, 2000; Kruger, 1997). The characteristically high silicon and aluminium content in fly ash makes it a favourable starting material for zeolites (Blissett and Rowson, 2012).

2.3.1 Synthesis of zeolites from coal fly ash

Zeolites are microporous, aluminosilicate materials synthesised by the hydrothermal synthesis technique. Hydrothermal synthesis of zeolites involves an alkaline aluminosilicate mixture subjected to elevated temperatures. The high content of silicon and aluminium in coal fly ash makes it a suitable starting material for zeolite synthesis (Blissett and Rowson, 2012). The synthesis of zeolites from fly ash requires the addition of sodium hydroxide and in some cases, an additional aluminium or silicon source. The role of sodium hydroxide in zeolite synthesis is the delivery of the hydroxide ion which serves as a mineralising agent. The hydroxide ion is also responsible for dissolution of silicon and aluminium species from the mineral phases in coal fly ash such as quartz and mullite (Murayama et al., 2002; Shoumkova and Stoyanova, 2013). Sodium hydroxide (NaOH) is either added to fly ash as an aqueous solution (Franus, 2012) or NaOH is mixed with fly ash and fused at an elevated temperature (Chang and Shih, 2000; Shigemoto et al., 1993). The degree of alkalinity in the synthesis of fly ash-based zeolites is extremely important. The crystalline mineral phases in coal fly ash are transformed to more reactive silicate and aluminate species in the presence of sodium hydroxide (Chang and Shih, 2000). The efficiency of the transformation of quartz and mullite to silicate and aluminate species depends on the concentration of alkali (Shigemoto et al., 1993). The dissolution of silicon and aluminium species is followed by condensation of aluminate and silicate species to form an aluminosilicate gel which, with the aid of sodium cations, undergoes crystallisation to form zeolite crystals (Murayama et al., 2002).

Shigemoto et al., (1993) synthesised zeolite Na-X from fly ash by the fusion method. A mixture of fly ash and NaOH (with an optimised fly ash to NaOH mass ratio of 1:1.2) was milled and then fused at an optimum temperature of 550 °C for an hour. Hydrothermal synthesis of the fused fly ash slurry was carried out at 100 °C for 6 hours which resulted in the formation of zeolite Na-X with crystallinity of 62 % and typical octahedral morphology

Chapter 2 – Literature Review

(Shigemoto et al., 1993). Furthermore, Shigemoto et al., (1993) studied the formation of zeolite Na-A from fly ash under hydrothermal conditions by enriching the starting material with aluminium (in the form of sodium aluminate). Shigemoto et al., (1993) found that an increase in sodium aluminate content led to an increased zeolite Na-A crystallinity and decreased zeolite Na-X formation.

A similar approach was used by Chang and Shih, (2000) to synthesise zeolite A and X from class F fly ash sourced from three different power plants. In this case, hydrothermal synthesis of a fused fly ash slurry was carried out at 60 °C for 20 days. The formation of zeolite A was achieved by adjusting the Si/Al ratio of the fused fly ash slurry by addition of aluminium hydroxide hydrate. Chang and Shih, (2000) reported that the synthesis of either zeolite X or A was dependent on the aluminium content present in the fused fly ash solution (synthesis solution) used in the hydrothermal process; an increased aluminium concentration leading to an increased yield of zeolite A. Chang and Shih, (2000) also reported that the synthesis of zeolite A and X were independent of the chemical composition of the three different fly ash sources (Chang and Shih, 2000). It should be noted that the phase purity of zeolite A was affected by the chemical composition of the fly ash sources, since zeolite X was observed by XRD for zeolite A samples produced from two of the fly ash sources. Therefore the conclusion that zeolite A and X synthesis is independent of the chemical composition of the fly ash source is doubtful. The chemical composition of the starting material (in this case fly ash) affects the chemical composition of the synthesis solution and hence affects the crystallisation of specific zeolite phases (Yu, 2007).

In 2012, the synthesis of hierarchical zeolite X from a clear fused fly ash extract of class F type coal fly ash under hydrothermal conditions of 80-94 °C for 24 hours was reported (Musyoka, 2012). A simple synthesis procedure resulted in the formation of hierarchical zeolite X with enhanced surface area and the hierarchical crystal morphology resembled spherical assemblies of disc-like platelets (Musyoka, 2012). Musyoka, (2012) reported a BET surface area for hierarchical zeolite X ranging from 235 to 282 m²/g. Muriithi, (2012) reported the synthesis of hierarchical zeolite X from a clear FFA extract, using similar synthesis conditions as Musyoka, (2012), under hydrothermal conditions of 94 °C for 9 hours. The BET surface area of hierarchical zeolite X was reported to be 257 m²/g by Muriithi, (2012); which was comparable to the BET surface area of NaX observed by Musyoka, (2012).

Chapter 2 – Literature Review

Franus, (2012) synthesised zeolite X from class F coal fly ash using two synthesis methods namely; hydrothermal and low-temperature synthesis of a fly ash-NaOH solution. Under hydrothermal conditions, Franus, (2012) used a synthesis mixture made up of 20 g of fly ash and 500 mL of 3M NaOH solution which was subjected to a temperature of 75 °C for 24 hours. Zeolite X crystallised together with minor hydroxysodalite peaks and unreacted phases such as mullite and quartz. The morphology of zeolite X formed by hydrothermal synthesis was needle-like and according to Franus, (2012) a ball of wool pattern was formed by the zeolite X crystals, similar to the hierarchical zeolite X morphology reported by Musyoka, (2012). However, zeolite X synthesised by Franus, (2012) contained contaminant mineral phases such as mullite and quartz and crystals were not well defined as was reported by Musyoka, (2012). Energy Dispersive X-ray Spectroscopy (EDS) analysis reported by Franus, (2012) revealed that the sodium cation (Na^+) was the main charge-balancing cation in the zeolite framework. Other cations present in the zeolite structure and detected by EDS were potassium (K^+), calcium (Ca^{2+}) and magnesium (Mg^{2+}) ions (Franus, 2012).

From nitrogen adsorption/desorption isotherms Franus, (2012) concluded that zeolite X synthesised from fly ash exhibited a type I isotherm with adsorption increasing at relatively low pressures which indicated a large number of micropores (Franus, 2012). The isotherm formed by nitrogen physisorption did however exhibit type IV behaviour with an H4 hysteresis loop, which indicated the presence of mesopores in the zeolite structure (Sing, 1982; Thommes, 2007). The specific surface area of the synthesised zeolites and fly ash was determined by the Brunauer-Emmett-Teller (BET) method. Compared to the specific surface area of fly ash, synthesised zeolites exhibited a much larger specific surface area ($333 \text{ m}^2/\text{g}$) than fly ash ($16.2 \text{ m}^2/\text{g}$) due to the microporous nature of zeolites. Furthermore, Barret-Joyner-Halenda (BJH) desorption curves were used to analyse the pore size distribution of fly ash compared to that of fly ash-based zeolites (Franus, 2012). Franus, (2012) observed that the majority of pores in the synthesised zeolites had a diameter of 4 nm. The BJH curves further confirmed the presence of mesopores in the structure of the synthesised zeolites by the presence of pores with diameter ranging from 2 to 50 nm. It was reported that the BJH desorption curves illustrated capillary condensation which occurred in the mesopore range (Franus, 2012). Franus, (2012) was therefore able to synthesise zeolite X with both micro- and meso-porosity from class F type coal fly ash. Both Muriithi, (2012) and Musyoka, (2012) reported similar results for the textural properties of fly ash based zeolite X.

In general, waste fly ash formed by coal combustion has successfully been used as a starting material for the synthesis of various zeolites (Chang and Shih, 2000; Franus, 2012; Musyoka et al., 2012; Musyoka et al., 2013; Shigemoto et al., 1993). What is particularly interesting about fly ash-based zeolites is the presence of hierarchical porous architecture in these materials, which have been synthesised in the absence of additional structure-directing agents (Franus, 2012; Musyoka, 2012). The formation of hierarchical zeolite X will therefore be the focus of this study. The main aim of the study is to elucidate the cause behind the formation of hierarchical zeolite X from a clear fused fly ash extract.

2.4 Hierarchical porous zeolites

Due to the characteristic properties of zeolites, such as thermal stability, acidity, high surface area and ion exchange capacity, zeolites have been applied in fields such as catalysis, adsorption and gas separation (Na et al., 2013). Zeolites serve as solid acid catalysts in the petrochemical, oil refining and fine chemical industries. The application of zeolites, in catalysis and adsorption, has been limited by the microporous nature of the zeolite framework which contains Angstrom-sized pores (Moller and Bein, 2011; Na et al., 2011; Na et al., 2013). In general, pores are classified by internal pore diameter and three categories exist namely; micropores (<2 nm), mesopores (2-50 nm) and macropores (>50 nm) (Liu et al., 2009; Sing, 1982; Thommes, 2007). The microporous nature of the zeolite framework limits the diffusion of reactants and products to and from the active sites (Na et al., 2013). Microporous zeolites are therefore limited to processing molecules smaller than 1 nm in size (Moller and Bein, 2011; Na et al., 2011).

Circumventing the diffusion limitation of conventional, microporous zeolites has been an area of great research (Na et al., 2013). New synthetic approaches have resulted in the hierarchical porous structure of zeolites and other materials (Moller and Bein, 2011; Terasaki et al., 2007). Various approaches have been used to overcome the well-known diffusion limitations of microporous zeolites (Na et al., 2013). These approaches include; the synthesis of zeolites with enlarged micropores which enable improved diffusion, the synthesis of small zeolite crystals which reduces the length of the diffusion pathway and lastly, the incorporation of mesopores into the zeolite framework (Liu et al., 2009; Na et al., 2013). Materials with a combination of interlinked pore structures namely; micropores, mesopores and/or macropores are termed hierarchical nanoporous materials or hierarchical materials

(Terasaki et al., 2007; Na et al., 2013). Hierarchical zeolites consist of a minimum of one additional pore structure other than the typical micropores of zeolitic materials (Holm et al., 2011). Hierarchically porous materials (such as zeolites) have major advantages over their microporous counterparts. Advantages of hierarchical zeolites include the improved diffusion pathway and accessibility of active sites and the ability to process relatively larger molecules (Liu et al., 2009; Na et al., 2013). The synthesis of hierarchically structured porous zeolites aims to improve the accessibility of internal zeolite pores and hence improve the application of these materials in the field of catalysis and adsorption (Liu et al., 2009; Moller and Bein, 2011). However, a major disadvantage of hierarchical zeolites is the loss of shape-selectivity compared to conventional microporous zeolites, which exhibits this attractive catalytic property.

2.4.1 Synthesis of hierarchical zeolites

A variety of synthesis approaches exist for the preparation of mesoporous materials and hierarchically porous materials (Moller and Bein, 2011). Larger pores may be incorporated into zeolite structures by two different synthetic approaches. The first approach includes the incorporation of a second pore system, consisting of mesopores and/or macropores, into the zeolitic material (Moller and Bein, 2011). The presence of larger pores, relative to micropores, improves the accessibility of internal pores to larger molecules through enhanced diffusion (Liu et al., 2009; Moller and Bein, 2011). The second approach involves the synthesis of thin zeolite nano-sheets which improve the exposure of most or all pores for surface adsorption (Inayat et al., 2012; Moller and Bein, 2011). Both of these approaches circumvent the diffusion limitations of microporous zeolites (Liu et al., 2009; Moller and Bein, 2011). The synthesis approaches used to incorporate mesoporosity into zeolites will be reviewed in the next section. Mesopores have been incorporated into the zeolite framework by various techniques namely post-synthesis treatment of synthesised zeolites or direct synthesis by using the templating strategy (Liu et al., 2009; Moller and Bein, 2011; Na et al., 2013).

2.4.1.1 Post-synthesis treatments

Post-synthesis treatment involves the chemical degradation of pre-formed zeolites by elimination of framework atoms (aluminium or silicon) by a base or acid (Na et al., 2013). Chemical degradation of pre-formed zeolites results in a second pore system consisting of mesopores and/or macropores (Na et al., 2013; Tao et al., 2006). In the case of silicon

removal, the chemical degradation process is called desilication while aluminium removal is termed dealumination (Na et al., 2013). Dealumination is commonly applied to low-silica zeolites. Dealumination is most commonly achieved by the repeated steaming of the ammonium-form of zeolites, followed by treatment with a mild acid to remove extra-framework aluminium atoms (Dumitriu and Hulea, 2003; Na et al., 2013; Tao et al., 2006). MOR type zeolites were dealuminated in this manner by Dumitriu and Hulea, (2003). Dealuminated zeolite Mordenite exhibited increased specific surface area and enhanced mesoporosity (Dumitriu and Hulea, 2003). A similar approach was applied by Hurgobin, (1998) for the synthesis of dealuminated zeolite Beta with enhanced total surface area and mesopore area. However, dealumination often negatively influences the acidic properties and crystallinity of zeolites. Removal of framework aluminium atoms reduces the Brønsted acidity of zeolites (Na et al., 2013; Tao et al., 2006).

Desilication is typically applied to high-silica zeolites and carried out in basic solution such as NaOH. Low concentrations of base have been reported to successfully remove silicon from the zeolite framework. The amount of silicon removed from the zeolite framework is closely related to the aluminium content of the framework, due to the high affinity of silicon for aluminium (Na et al., 2013; Tao et al., 2006). Zeolites Beta and Mordenite were desilicated using NaOH, under mild basic conditions. The desilication process increased the specific surface area of zeolites as well as the mesopore volume. Furthermore, the Lewis acidity of the zeolites was enhanced which improved the catalytic activity of these zeolites (Aslam et al., 2014). Although the post-synthesis demetallation technique is a suitable method for the production of mesoporous materials on a large scale, this technique may lead to loss of framework crystallinity or complete framework degradation. Furthermore, demetallation alters the acidic properties of zeolites and mesopores are randomly generated with a wide pore size distribution (Na et al., 2013). Controlled incorporation of mesopores into the zeolite framework is therefore not possible using the post-synthesis demetallation method. Other methods such as direct synthesis using templating agents have therefore been investigated.

2.4.1.2 Direct synthesis by templating

Direct synthesis methods for the incorporation of mesopores into the zeolite framework involve using a templating agent in the initial synthesis solution (Na et al., 2013). Common templating agents include carbon nanoparticles and nanotubes, surfactant molecules such as organosilane compounds and silylated-polymers (Na et al., 2013; Tao et al., 2006). Zeolites

Chapter 2 – Literature Review

are crystallised with template molecules included in the framework. The removal of templating agents is achieved by calcination yielding a zeolite with mesopores as well as the inherent zeolitic micropores (Na et al., 2013).

Typically, zeolites are microporous materials; specific microporous structures may be directed by various quaternary ammonium cations (Na et al., 2011). On the other hand, mesoporous zeolites may be formed by incorporating relatively larger templating agents into the initial synthesis solution of zeolites (Na et al., 2011). Kresge et al., (1992) first reported the synthesis of ordered mesoporous material MCM-41 using surfactants as pore-generating agents. These mesoporous materials were reported to form through a supramolecular mechanism initiated by the organic templating agent (Kresge et al., 1992). Later in an attempt to synthesise a crystalline mesoporous molecular sieve, a two-dimensional zeolite consisting of MFI nanosheets was synthesised using a di-quaternary ammonium cation as a templating agent by Choi et al., (2009). Na et al., (2011) then successfully synthesised an ordered, crystalline mesoporous material by using a poly-quaternary ammonium surfactant such as 18-N₃-18, which incorporated both micropores and mesopores into the zeolite framework. Micropores were generated by quaternary ammonium groups on the interior of the mesoporous walls which were directed by aggregated surfactant molecules (Na et al., 2011).

In more recent years, mesopore-directing templates are often used together with quaternary ammonium cations in a dual manner; this method of mesopore generation is termed dual-templating method. Mesopore-generating organic templates include [3-(trimethoxysilyl) propyl] octadecyldimethylammonium chloride (TPOAC) and 3-(trimethoxysilyl) propyl hexadecyl dimethyl ammonium chloride (TPHAC) (Inayat et al., 2012; Liu et al., 2009). Organic templates aggregate to form micelles which result in the incorporation of larger, meso-scaled pores into the zeolite framework (Na et al., 2011). The dual-templating method has been used to synthesise hierarchical zeolite A using an organosilane surfactant, TPOAC, in methanol medium by Liu et al., (2009).

Much like Choi et al., (2009), Inayat et al., (2012) synthesised assemblies of FAU-type zeolite nanosheets by using an organosilane surfactant, TPHAC, in the initial synthesis solution. The organosilane templates were removed from the zeolite framework by calcination (Inayat et al., 2012). Hierarchical zeolite X synthesised by Inayat et al., (2012) appeared as ball-like assemblies of zeolite nanosheets. The nanosheet balls exhibited an increased crystal diameter compared to conventional zeolite X crystals; however, the

triangular faces of zeolite X crystals were still visible for hierarchical zeolite X (Inayat et al., 2012). Inayat et al., (2012) proposed that the reason for the formation of hierarchical zeolite X was a combination of the surface activity of the TPHAC molecules and the effect of cations in the synthesis mixture. The TPHAC molecules were thought to initiate the formation of micelle-like assemblies as proposed by Na et al., (2011) which resulted in mesoporosity, while the balancing effect of cations directed the crystallisation process into a type of twinned crystal growth (Inayat et al., 2012).

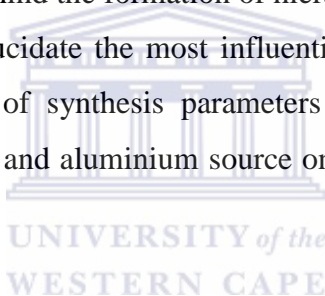
2.4.1.3 Other methods

Other methods of incorporating mesopores into the zeolite framework exist. The use of polymers as templates, ethanol as an organic additive and temperature-controlled methods have been used (Huang et al., 2010; Huang et al., 2011; Tao et al., 2006). Inorganic cations and alkali and alkali-earth metal sources have also influenced zeolite morphology as mentioned before (Deng et al., 2006; Franus, 2012; Katsuki and Hasegawa, 2007). Polymers such as polystyrene spheres have been used as templating agents resulting in the incorporation of new pore systems (mesopores and macropores) in the zeolite framework (Tao et al., 2006). Cationic and silylated polymers are typically used as mesoporous templating agents in zeolite synthesis (Na et al., 2013; Tao et al., 2006).

Hierarchically structured zeolite Y with controlled particle sizes were prepared by Huang et al., (2010) using a three-step temperature controlled crystallisation process, in the absence of any pore-generating agent, organic additives or seeding crystals. Hierarchically structured zeolite Y exhibited a large external surface area (up to 691 m²/g) and total pore volume (0.420 cm³/g) (Huang et al., 2010). Nitrogen physisorption isotherms depicted a type H₄ hysteresis loop which is typical of materials containing uniform, slit-shaped mesopores (Huang et al., 2010; Sing, 1982; Thommes, 2007). Nitrogen uptake at higher partial pressure was also observed which indicated that the material contained macropores as well (Huang et al., 2010). Although hierarchical zeolite Y was synthesised without the use of organic additives or pore-generating agents, an energy-intensive and time-consuming three-step temperature controlled process was required to form the hierarchically structured zeolite (Huang et al., 2010). A more simple synthesis route for hierarchical zeolite X was reported by Musyoka, (2012). Hierarchical zeolite X with similar morphology to the “ball-like house of cards-like” assembly of zeolite X nanosheets reported by Inayat et al., (2012) was

synthesised, in the absence of additives, from a clear fused fly ash (FFA) extract (Musyoka, 2012).

Mesoporosity may therefore be incorporated into zeolitic materials by the porogenic action of organic surfactants and polymers or in some cases by temperature-programmed synthesis (Inayat et al., 2012; Huang et al., 2010; Huang et al., 2011; Liu et al., 2009; Na et al., 2011; Na et al., 2013; Tao et al., 2006). Although these synthesis routes produced mesoporous materials, in some cases these materials suffered from poor crystallinity which resulted in lower acidity and hence, reduced catalytic activity. Furthermore, these synthesis routes involved costly and complex organic surfactants or energy-intensive and time-consuming techniques. Musyoka, (2012) successfully synthesised hierarchical zeolite X from a clear FFA extract, without the addition of organic structure-directing agents. Although mesoporosity was incorporated into the pore system of zeolite X using a relatively simple synthesis procedure, the cause behind the formation of hierarchical zeolite X from fly ash has not been reported to date. To elucidate the most influential parameters behind hierarchical zeolite X formation, the effect of synthesis parameters such as agitation, hydrothermal temperature and time, Si/Al ratio and aluminium source on the formation of this zeolite will be investigated in this study.



2.5 Characterisation of zeolites

The functionality of zeolites is closely related to the structure (Morris and Wheatley, 2007). An understanding of the structural characteristics of zeolites is vital to understand their chemical and physical properties. Understanding the relationship between the structure and function of zeolites allows the design of zeolites which are tailor-made for specific applications (Morris and Wheatley, 2007; van Hooff and Roelofsen, 1991). This section will therefore describe the relevant characterisation techniques used to analyse properties of zeolites such as elemental composition and mineral structure, crystal morphology and surface area.

2.5.1 Elemental Analysis

The elemental composition of zeolites is an important indicator of zeolite type. The silicon/aluminium (Si/Al) atomic ratio or silica/alumina ($\text{SiO}_2/\text{Al}_2\text{O}_3$) molecular ratio and the presence of other framework or extra-framework cations such as alkali, alkali-earth and

transition metal atoms may be determined by analytical techniques such as X-Ray Fluorescence (XRF) spectroscopy, Inductively-Coupled Plasma-Optical Emission spectroscopy (ICP-OES) and Inductively-Coupled Plasma-Mass spectroscopy (ICP-MS). The surface elemental composition of zeolites may be determined by X-Ray Photoelectron spectroscopy (XPS) (van Hooff and Roelofsen, 1991).

2.5.1.1 X-Ray Fluorescence Spectroscopy

The chemical composition of zeolites is typically determined by XRF spectroscopy. XRF spectroscopy is a non-destructive, quantitative analytical technique which utilises X-rays to determine the elemental composition of materials. The XRF technique makes use of X-rays of high energy to irradiate a material. The high-energy X-rays cause electrons from the sample material to be expelled from different atoms. As a result, holes are left behind in low-lying orbitals. An electron from a higher energy level then fills the hole, consequently releasing energy. The liberation of energy results in either the generation of radiation (which is known as X-ray fluorescence) or in the expulsion of a secondary electron (which is known as the Auger effect). The XRF radiation emitted is characteristic of individual atoms and can therefore be used for quantitative elemental analysis of a material (van Hooff and Roelofsen, 1991).

The chemical composition of zeolites is therefore determined using XRF spectroscopy (van Hooff and Roelofsen, 1991). The general composition of aluminosilicate zeolites is given by the formula $M^I M_{0.5}^{II} [(AlO_2)_x \cdot (SiO_2)_y \cdot (H_2O)_z]$. The parameter x denotes the number of aluminium atoms in each unit cell, while the parameter y denotes the number of silicon atoms in each unit cell and z denotes the amount of water molecules required for hydration of the zeolite. The symbols M^I and M^{II} denote framework cations which may be alkali or alkaline earth metals, respectively (Hagen, 2006). More commonly, the Si/Al atomic ratio or SiO_2/Al_2O_3 molecular ratio is used to express zeolite chemical composition. XRF spectroscopy allows the determination of the SiO_2/Al_2O_3 molecular ratio of a zeolite and the content of other elements such as framework and extra-framework cations (van Hooff and Roelofsen, 1991).

2.5.1.2 Inductively-coupled Plasma-Optical Emission Spectroscopy

ICP-OES is an analytical technique used to determine the elemental composition of zeolites and initial synthesis solutions used in the hydrothermal process. ICP-OES is a wet analytical technique which involves the full dissolution of the material with acidic solutions, in case of

solids, and analysis of the resulting solution. Therefore unlike XRF spectroscopy, ICP-OES is a destructive analytical technique (van Hooff and Roelofsen, 1991). In ICP-OES spectroscopy, the sample in solution is ionised by a plasma torch to form free atoms (ionised or excited). The elements are quantified by ICP-OES based on the emission given off by atoms in the excited state (Rouessac and Rouessac, 2007). The Si/Al atomic ratio or the $\text{SiO}_2/\text{Al}_2\text{O}_3$ molecular ratio may be determined by ICP-OES as well as the elemental composition of the zeolite sample. Elemental components of the zeolite sample such as alkali, alkaline earth and transition metal atoms may also be determined using ICP-OES (van Hooff and Roelofsen, 1991).

2.5.1.3 Inductively-coupled Plasma-Mass Spectroscopy

The elemental composition of materials may also be characterised by mass spectroscopy (MS). Mass spectroscopy entails the characterisation of materials based on the atomic or molecular mass of individual species in the material. Although MS is a destructive analytical technique, only a minute quantity of sample is required due to the superior sensitivity of the technique. The versatility and great sensitivity of MS makes it a widely used analytical technique in modern day chemistry (Rouessac and Rouessac, 2007). Mass spectroscopy involves the transformation of sample atoms into ions in the gas phase. In Inductively-coupled Plasma-Mass spectroscopy (ICP-MS), sample atoms are ionised by a plasma torch. Ionisation results in charged species which are subjected to a magnetic and/or electric field under a high vacuum. The type of field applied to the charged species depends on the instrument used for ICP-MS analysis.

The force used to accelerate the charged species in the field is related to the mass-to-charge ratio of the species, which in turn corresponds to the nature of the charged species. A typical mass spectrometer consists of three main components namely; an ionisation source, a mass-selective analyser and a detector. The result of an MS experiment is a graph called a “mass spectrum” which consists of ion abundance plotted against the mass-to-charge ratio in increasing order. Elemental analysis of inorganic materials is commonly carried out by ICP-MS, while mixtures of organic molecules may be analysed by MS coupled to chromatographic techniques such as HPLC-MS and GC-MS (Rouessac and Rouessac, 2007).

2.5.2 Morphological Analysis

The morphology and particle size of zeolite crystals affects the properties of the material. In applications where adsorption kinetics and ion-exchange play a crucial role, the morphology

of the zeolite structure is extremely important (van Hooff and Roelofsen, 1991). The analysis of zeolite morphology by analytical techniques such as Scanning emission microscopy (SEM) and High resolution-Transmission electron microscopy (HRTEM) is therefore a vital tool in zeolite science.

2.5.2.1 Scanning Emission Microscopy

Scanning emission microscopy is commonly used to characterise the morphology (size and shape) and particle size distribution of zeolite crystals (van Hooff and Roelofsen, 1991). In SEM, images of the sample material are generated by the emission of secondary electrons and back-scattered primary electrons which are produced by a focused electron beam. The scattered electrons are focused by an objective lens which results in an image of the sample (Haber et al., 1995; Terasaki et al., 2007). Terasaki et al., (2007) reported that the surface-fine structure may be determined by SEM provided that an uncoated as-synthesised zeolite sample was used. The growth steps of zeolite crystals were also determined by studying the surface morphology of crystals using High-resolution SEM (HRSEM) (Terasaki et al., 2007). The typical octahedral morphology of zeolite X is illustrated in Figure 2.4 (Hamilton et al., 1993).



Figure 2.4: A SEM micrograph of zeolite X showing the typical octahedral morphology of the material (Hamilton et al., 1993).

2.5.2.2 High resolution-Transmission Electron Microscopy

In High resolution-Transmission electron microscopy (HRTEM), electrons and nuclei of constituent atoms of the sample material interact, which results in the scattering of electrons that are focused by an objective lens to produce a highly resolved image of the sample material (Terasaki et al., 2007). The principle of transmission electron microscopy is related to that of SEM, however much higher magnification is achieved by HRTEM. HRTEM is

therefore used to determine the fine structure of zeolites (Haber et al., 1995; Terasaki et al., 2007). The determination of fine structure of zeolites by HRTEM analysis includes the detection of structural defects, surface-fine structures and stacking of sheets (Terasaki et al., 2007). HRTEM also allows the determination of the metal distribution and particle size of metals deposited on zeolitic support materials (Haber et al., 1995; Hagen, 2006). The typical fine structure of FAU-type zeolites (such as X and Y) is illustrated in Figure 2.5 (van Hooff and Roelofsen, 1991).

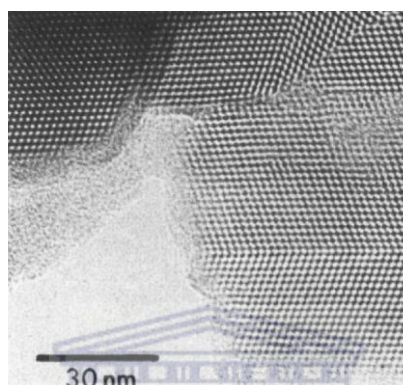


Figure 2.5: A typical HR-TEM micrograph depicting the lattices fringes in a FAU-type zeolite (van Hooff and Roelofsen, 1991).

2.5.3 Structural Analysis

The structure of a zeolite determines the unique properties of the material which in turn determines the type of applications the zeolite may be used for. The application of a particular zeolite is therefore related to the structural properties of the zeolite. An understanding of zeolite structure is vital to understanding the unique properties these materials possess. Improved properties of zeolites for specific applications may be achieved by controlling the structural features of zeolites. Analytical techniques such as X-ray diffraction (XRD) spectroscopy, Fourier transform infrared (FTIR) spectroscopy, Raman spectroscopy and Nuclear Magnetic Resonance (NMR) spectroscopy are used to elucidate the structural properties of zeolites (Morris and Wheatley, 2007; van Hooff and Roelofsen, 1991).

2.5.3.1 X-Ray Diffraction Spectroscopy

The X-ray diffraction technique is used to determine the mineral phase identity of zeolites. The XRD technique may be used for simple phase identification as well as more advanced

Chapter 2 – Literature Review

refinement techniques such as the structural modelling of zeolites (Haber et al., 1995; Morris and Wheatley, 2007; van Hooff and Roelofsen, 1991). Other properties of the zeolite structure such as the position of extra-framework species and average particle size may also be determined by XRD (Haber et al., 1995; Morris and Wheatley, 2007). The determination of the crystalline structure of a particular material makes use of diffracted radiation with wavelength magnitude in the same range as the interatomic distances of the structure of interest. X-ray radiation is therefore commonly used in the determination of zeolite structures, other radiation sources such as electrons and neutrons are also used (Morris and Wheatley, 2007). A typical XRD diffractogram of zeolite X is illustrated in Figure 2.6 (Treacy and Higgins, 2001).

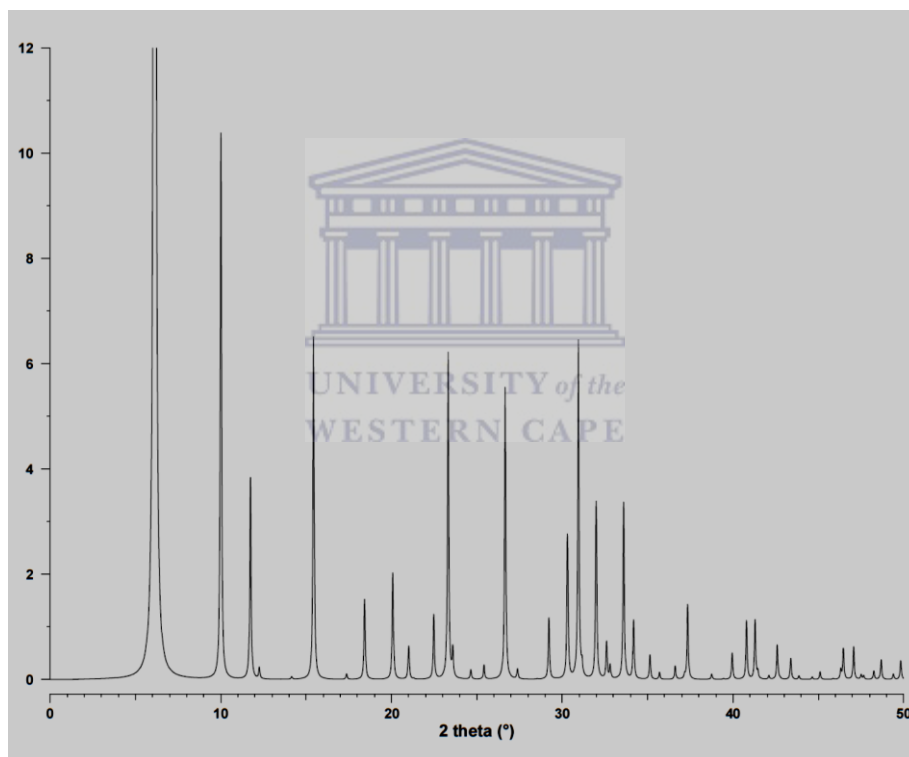


Figure 2.6: A simulated powder XRD diffractogram illustrating the typical reflections for zeolite X (Treacy and Higgins, 2001).

A diffraction pattern for a crystal arises from the interaction of X-ray radiation, of wavelength λ , with a regular collection of points in the crystal lattice of the same order of magnitude as the wavelength of radiation (Morris and Wheatley, 2007; van Hooff and Roelofsen, 1991). Diffraction patterns may be understood by considering the lattice points to lie in different planes. Miller indices (hkl) are used to describe the planes of lattice points.

Chapter 2 – Literature Review

The significance of lattice planes is that the diffraction of a collection of lattice points corresponds to reflection from these lattice planes. A particular set of planes (denoted as hkl), with an interplanar distance of d , results in a diffraction maximum at an angle (θ) described by Bragg's law, as depicted in Equation 2.7 (Morris and Wheatley, 2007).

$$n\lambda = 2d \sin\theta \text{ (Eq. 2.7)}$$

Satisfaction of Bragg's law results in diffraction maxima. The position of these maximum diffraction peaks only relies on the shape and size of the crystal lattice (Morris and Wheatley, 2007). In zeolite science, powder XRD is commonly employed for phase identification and to determine if any impure phases are present in the crystalline sample. The peak positions in the diffractogram are dependent on the crystal lattice and serve as a fingerprint for the identification of a particular zeolite phase (Morris and Wheatley, 2007; van Hooff and Roelofsen, 1991). Powder XRD may also be used to refine and completely determine the structural configuration of zeolites (Morris and Wheatley, 2007). Other properties of the zeolite crystal such as crystallite size may also be determined from diffraction data by making use of the Debye-Scherrer equation; depicted in Equation 2.8, where crystallite size is denoted by t , the full width at half maximum (FWHM) describing the degree of line broadening is defined by B while, as described previously, λ is the wavelength of X-ray radiation and θ is the Bragg angle (Van Hooff and Roelofsen, 1991).

$$t \text{ (in nm)} = \frac{0.9 \lambda \text{ (in nm)}}{B \cos \theta} \text{ (Eq. 2.8)}$$

X-ray diffraction data may also be used to determine the extent of crystallinity of synthesised zeolites. The degree of crystallinity may be determined by comparing the intensity of the diffraction peaks of synthesised zeolites with that of a highly-crystalline zeolite sample, according to Equation (2.9) (van Hooff and Roelofsen, 1991).

$$\% \text{ Crystallinity} = \frac{\text{Intensity of } (hkl)\text{peak}_{\text{sample}}}{\text{Intensity of } (hkl)\text{peak}_{\text{standard}}} \times 100\% \text{ (Eq. 2.9)}$$

Powder X-ray diffraction is therefore an important technique for the characterisation of zeolites. XRD provides important information regarding the zeolite crystals such as the structure of crystals, crystallite size and phase purity (van Hooff and Roelofsen, 1991).

Chapter 2 – Literature Review

2.5.3.2 Fourier Transform Infrared Spectroscopy

Structural information about zeolites may also be determined by FTIR spectroscopy (Lercher and Jentys, 2007). Infrared spectroscopy involves the adsorption or reflection of electromagnetic radiation in the range of 1 to 1000 μm . Infrared radiation is absorbed by the chemical bonds present in molecules. More specifically, if a bond exists between two different atoms, an electric dipole oscillating at a particular frequency is generated. An interaction occurs when this non-symmetrical bond is irradiated by monochromatic light of the same frequency as the electric dipole. The interaction (absorption/reflection) of monochromatic light with bonds in a molecule is measured by a spectrometer and depicted as a spectrum from which structural information may be gathered (Rouessac and Rouessac, 2007). The bending and stretching vibrations of the T-O bonds of zeolites may be observed in FTIR spectra, in the wavenumber range of 200 to 1500 cm^{-1} (Lercher and Jentys, 2007).

Structural information such as the lattice vibrations of the zeolite, hydroxyl groups present in the zeolite framework and the position of framework cations may be analysed by FTIR spectroscopy (Lercher and Jentys, 2007). Typical vibrational modes for the zeolite framework are the symmetric stretching mode (750-820 cm^{-1}), asymmetric stretching mode (1050-1150 cm^{-1}), double ring vibrations (500-650 cm^{-1}) and pore opening vibrations (300-420 cm^{-1}) (Lercher and Jentys, 2007; van Hooff and Roelofsen, 1991). These bands are known as structure-sensitive vibrational bands which have characteristic vibrations for certain zeolite structures, for example the double six ring structures (D6R) in faujasite type zeolite X, as illustrated in Figure 2.7 (Hagen, 2006; Lercher and Jentys, 2007).

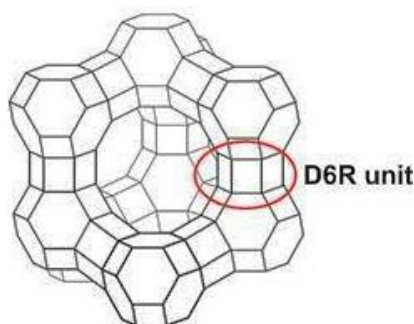


Figure 2.7: Zeolite X (FAU) framework with D6R structural unit encircled in red (Hagen, 2006).

Chapter 2 – Literature Review

The type, content and acidity of hydroxyl groups in the zeolitic framework may be determined by FTIR spectra. In general, a lower wavenumber for the O-H band represents more acidic hydroxyl groups. The wavenumber for the O-H band is influenced by three factors namely; the coordination type of the oxygen atom (bridging or terminal oxygen atom), the steric environment of the oxygen atom (the type of zeolite lattice structures surrounding the oxygen atom) and the interference by framework or extra-framework oxygen atoms with the hydroxyl group. Bridging hydroxyl (SiOHAl) groups serve as Brönsted acid sites in zeolite structures and are observed between 3550 and 3650 cm^{-1} in FTIR spectroscopy. Additionally, two other types of hydroxyl groups are present in the zeolite framework, which are non-acidic. One hydroxyl group is found on the external surface of the zeolite structure as a result of termination of the zeolite crystal, while the other hydroxyl group is present on structural defects due to incomplete condensation reactions or the removal of framework atoms. The hydroxyl groups on the external surface are observed in the wavenumber range from 3740-3745 cm^{-1} and are always present in the IR spectra of zeolites. The relative intensity of the external hydroxyl band is related to the primary particle size of zeolites; low intensity peaks indicating the presence of large particle size zeolites (Lercher and Jentys, 2007). A typical FTIR spectrum of zeolite Na-X (Si/Al ratio = 1.5-2.5) with vibrations of secondary building units and aluminosilicate species marked with a dotted line is illustrated in Figure 2.8 (Thuadaij and Nuntiya, 2012).

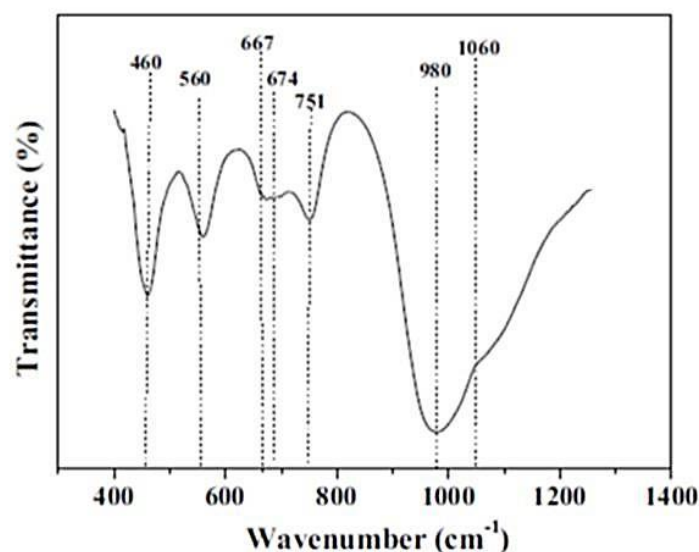


Figure 2.8: A typical FTIR vibrational spectrum of zeolite Na-X (Thuadaij and Nuntiya, 2012).

Complementary spectroscopic techniques may be used together with FTIR to analyse the position of cations in the zeolite framework. These analytical techniques include Raman, UV/Vis and photoelectron spectroscopy. The stretching vibrational mode for counter-ions (in the zeolite framework) is usually observed at wavenumbers below 300 cm^{-1} . Wavenumbers for this vibration depends on the mass, charge and location of the cations in the zeolite framework. FTIR spectroscopy may therefore be used for structural identification and characterisation of zeolites (Lercher and Jentys, 2007).

2.5.4 Textural Analysis

Zeolites typically consist of micropores which are characterised by an internal pore width smaller than 2 nm. The ineffective diffusion of larger molecules through the small pores of zeolites results in low reaction rates which restrict the application of zeolites (Thommes, 2007). The incorporation of mesopores into zeolitic materials is of interest in order to circumvent the diffusion limitations experienced with microporous materials (Liu et al., 2009; Thommes, 2007). The development of hierarchically structured zeolites is employed to enhance the mass transfer properties of zeolites. A good understanding of the textural properties of zeolitic materials is therefore vital for application of these hierarchical materials (Thommes, 2007).

2.5.4.1 Nitrogen Physisorption

Nitrogen physisorption is used to characterise the textural properties of zeolites such as the total surface area, pore size, pore size distribution and pore volume. These textural properties influence the application of a zeolitic material. In particular, the catalytic application of zeolites is affected by the textural properties of the material. The total surface area of a zeolite influences the accessibility of active sites in solid acid catalyst applications (Haber et al., 1995; Thommes, 2007). Pore dimensions influence the transport properties and selectivity of the zeolite in applications such as adsorption and catalysis. The gas adsorption technique is commonly employed to characterise the textural properties of zeolites since a range of pore sizes may be analysed using this technique (0.35-100 nm) (Thommes, 2007). Nitrogen physisorption is a technique which involves adsorption and desorption of gas molecules from a carrier gas stream, which is continuously flowed over the catalyst (Deutschmann et al., 2009; Haber et al., 1995).

Physical adsorption, often termed physisorption, is a process by which a gas molecule (known as the adsorptive) comes into contact with a solid surface (known as the adsorbent).

Chapter 2 – Literature Review

After the gas molecule has been adsorbed onto the adsorbent, it is known as the adsorbate. Non-specific forces such as London dispersion forces and intermolecular repulsion are the interactions involved in the physisorption process. The physisorption process in porous materials is influenced by fluid-fluid and fluid-wall interactions as well as the stability of fluids in confined pore spaces. These interactions are reflected in the type and shape of the adsorption isotherm formed. The sorption properties of micropores and mesopores vary from that of macropores which is why different isotherms are observed (Sing, 1982; Thommes, 2007). Adsorption isotherms have been classified into six types by the International Union of Pure and Applied Chemistry (IUPAC), as illustrated in Figure 2.9.

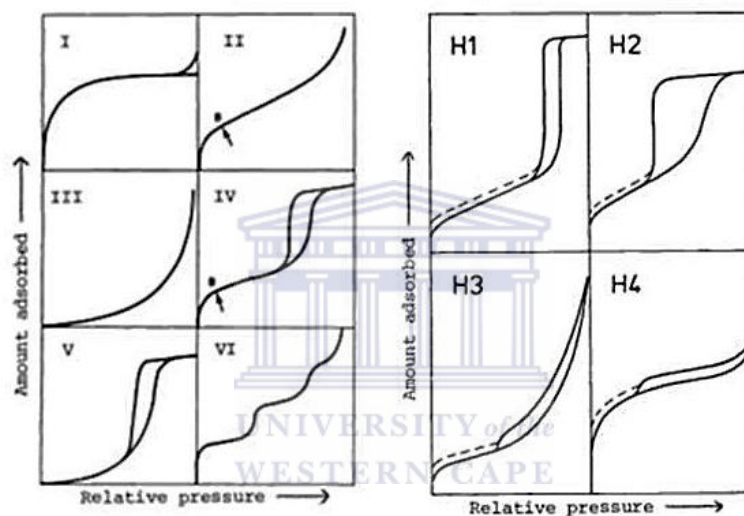


Figure 2.9: Classification of adsorption isotherms and the type of hysteresis loops, by IUPAC (Sing, 1982).

Zeolites typically exhibit type I or type IV isotherms depending on the pore architecture of the material (Sing, 1982). Type I isotherms represent reversible adsorption in microporous materials with relatively low external surface area (Sing, 1982; Thommes, 2007). Type IV isotherms consist of a hysteresis loop which is usually related to capillary condensation in mesopores (Sing, 1982). Hysteresis loops may be classified into four types as illustrated in Figure 2.9. The type and shape of the hysteresis loop is related to the pore structure of the material involved. The type H1 hysteresis loop is related to porous materials with narrow pore size distribution such as materials consisting of compact or agglomerated spherical particles which are uniform or pore channels which are cylindrical in shape (Sing, 1982; Thommes, 2007). The type H2 hysteresis loop has been linked to materials with some degree

of disorder where the shape of pores and pore size distribution is poorly defined. The type H3 hysteresis loop is associated with the presence of aggregated plate-like particles which result in slit-shaped pores. The type H4 hysteresis loop is indicative of materials with narrow slit-shaped pores as well. However, in some H4 hysteresis cases, type 1 isotherm behaviour is observed which indicates that the material possesses micropores as well as mesopores (Sing, 1982; Thommes, 2007).

Textural properties of zeolites such as specific surface area, pore size, pore size distribution and pore volume play important roles in the application of zeolites to catalysis. Therefore nitrogen physisorption is a useful technique for zeolite characterisation. A typical nitrogen adsorption-desorption isotherm for zeolite Na-X is illustrated in Figure 2.10, which is a type I isotherm with type IV characteristics such as the H4 hysteresis loop (Zhang et al., 2013).

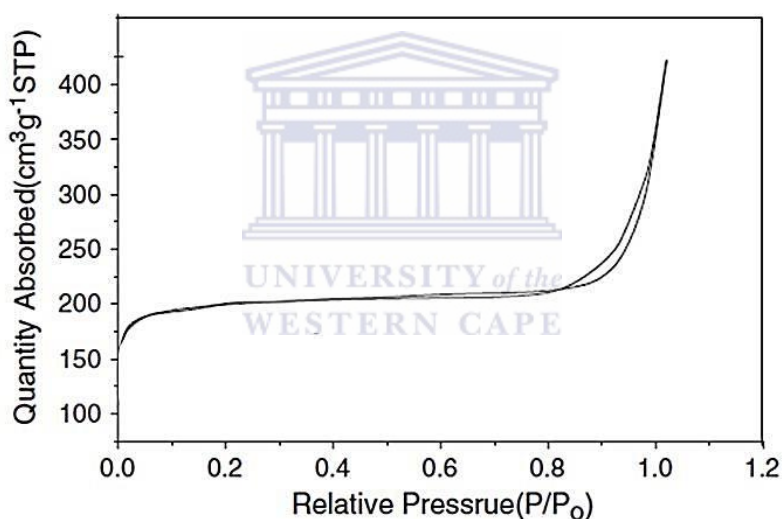


Figure 2.10: A typical nitrogen adsorption-desorption isotherm for zeolite Na-X (adapted from Zhang et al., 2013).

2.5.5 Acidity of zeolites

The acidic properties of zeolites play an important role in the application of zeolites as catalysts. The acid sites of zeolites may catalyse various reactions which are usually catalysed by conventional Brönsted acids (Hölderich and van Bekkum, 1991; Weitkamp, 2000). Therefore zeolite acidity is an important zeolite property to monitor. The acidity of zeolites is typically determined by ammonia-temperature programmed desorption (NH₃-TPD) (Fadoni

and Lucarelli, 1999; van Hooff and Roelofsen, 1991) or titrimetric methods (Louis et al., 2004).

2.5.5.1 Temperature programmed desorption

The determination of zeolite acidity may be carried out by temperature programmed desorption (TPD) of a base; ammonia is commonly used (van Hooff and Roelofsen, 1991). The zeolite is exposed to a base, such as ammonia, to adsorb onto acid sites in the zeolite framework. A temperature programme is then followed, at a constant rate, which allows the base to be desorbed from the acid sites of the zeolite. The amount of base desorbed is recorded by either mass spectrometry or thermal conductivity detectors (Fadoni and Lucarelli, 1999; van Hooff and Roelofsen, 1991). A desorption spectrum is used to characterise the quantity and type of acid sites present in the zeolite framework (van Hooff and Roelofsen, 1991). A typical ammonia-TPD profile for zeolite X is illustrated in Figure 2.11 (Barman, 2010).

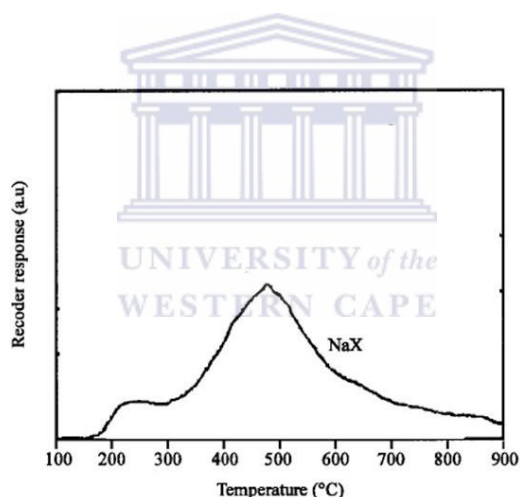


Figure 2.11: A typical ammonia-TPD profile for zeolite X (adapted from Barman, 2010).

The two peaks indicate that this material contains two different types of acid sites, the high temperature peak corresponding to relatively stronger acid sites than the low temperature peak (van Hooff and Roelofsen, 1991).

2.5.5.2 Acidity determination by titrimetric method using H-NMR

A more modern approach to the determination of zeolite acidity is a non-destructive, titrimetric method which involves the exchange of H and D on the hydroxyl groups of the zeolite, achieved by H₂O and D₂O molecules (Louis et al., 2004). Unlike the ammonia-TPD

method described in Section 2.5.5.1 which distinguishes between Brønsted and Lewis acid sites, this method determines only the Brønsted acidity that a particular zeolite sample possesses (Louis et al., 2004; van Hooff and Roelofsen, 1991). This method was reported to be in good agreement with the Brønsted acidity calculated from the framework Si/Al ratio of zeolites (Louis et al., 2004).

2.6 Applications of zeolites

The primary applications of zeolites are in catalysis, adsorption and ion-exchange (Hölderich and van Bekkum, 1991; Payra and Dutta, 2003). The unique properties of zeolites such as ion-exchangeability and microporosity lead to the application of zeolites as ion-exchangers and molecular sieves, respectively. Adsorption applications of zeolites are based on the removal of impurities from mixtures of gas or liquid components. Bulk separation processes which are based on the molecular sieving principle also make use of zeolites. Aluminium-rich zeolites are typically used for the separation of small quantities of polar (or polarisable) molecules. Some adsorption processes include; removal of carbon dioxide from natural gas and flue gas, desulphurisation, organic solvent separation, isomer purification and removal of pollutants such as NO_x, SO_x and mercury (Payra and Dutta, 2003). Another common application of zeolites is in ion-exchange processes. Due to the negatively-charged framework, zeolites have a high affinity for cations. Some of the major ion-exchange applications of zeolites have been in the detergent industry, where zeolites are employed as substitutes for phosphates as water-softeners. Zeolite A and X are common zeolites used in the detergent industry. An important ion-exchange application is the removal of radioactive isotopes of cesium and strontium cations (Molina and Poole, 2004; Payra and Dutta, 2003).

The most important application of zeolites still remains catalysis. The synthesis of faujasite zeolites (X and Y) by Barrer and Milton in the 1950's resulted in the application of zeolites in catalysis. Specifically, these faujasite type zeolites were applied as industrial catalysts for fluid catalytic cracking (FCC) in the petroleum industry. Zeolites replaced amorphous silica-alumina FCC catalysts and exhibited significantly enhanced catalytic activity which stimulated interest in these aluminosilicate materials for various other refining and petrochemical processes (Weitkamp, 2000). Some of the catalytic applications of zeolites include; light gasoline isomerisation, hydrocracking of heavy distillate fractions, xylene isomerisation and ethylbenzene synthesis (Hölderich and van Bekkum, 1991; Payra and

Dutta, 2003; Weitkamp, 2000). The transformation of hydrocarbons over zeolites occurs due to the strong acidity and microporous nature of these materials (Payra and Dutta, 2003). Although zeolites are excellent heterogeneous catalysts, a major drawback experienced in catalytic applications of zeolites is mass transfer limitations. Recently, hierarchical zeolites have been developed by various techniques to circumvent this problem (Liu et al., 2009; Na et al., 2011; Tao et al., 2006).

2.6.1 Applications of hierarchically porous zeolites

The micropore structure of zeolites results in shape-selectivity which has led to great interest in the application of zeolites as heterogeneous catalysts in the past (Holm et al., 2011). The application of zeolites in catalysis has however been limited to small molecules due to the well-known diffusional problems associated with these microporous materials (Moller and Bein, 2011). Hierarchical zeolites are advantageous in two ways namely; its ability to improve existing catalytic and adsorption processes and its application as heterogeneous catalyst for processes involving larger molecules (Holm et al., 2011). Liu et al., (2009) investigated the adsorption capacity of hierarchical zeolite Sr-A for methane and hydrogen gas from coke oven gas. The methane adsorption capacity and CH₄/H₂ ideal separation factor of hierarchical zeolite A was improved compared to conventional zeolite A. Hierarchical zeolite A was therefore reported to be a promising adsorbent for gas adsorption (Liu et al., 2009). Fly ash-based hierarchical zeolite Na-X and K-X were investigated for their activity in transesterification of sunflower oil with methanol by Babajide et al., (2012). Both zeolites were active for the transesterification reaction yielding fatty acid methyl esters (Babajide et al., 2012). Babajide et al., (2012) reported hierarchical zeolite K-X had the greatest catalytic activity in the transesterification reaction due to increased basicity compared to hierarchical zeolite Na-X. Hierarchical zeolite X, synthesised from a waste by-product such as fly ash, was therefore reported to be a useful heterogeneous catalyst for transforming these larger molecules (Babajide et al., 2012).

The hierarchical structure of fly ash-based zeolite X crystals imparts increased external surface area and greater intracrystalline void space due to enhanced mesoporosity in the zeolite structure (Babajide et al., 2012; Musyoka, 2012). This property makes hierarchical zeolite X an attractive material for applications in catalysis and adsorption, since the diffusional constraints associated with microporous zeolite catalysis may be circumvented. The hierarchical pore structure of the zeolite framework has a few interesting effects on the

Chapter 2 – Literature Review

catalytic performance of the material. Firstly, the diffusion of large organic reactants (and/or products) through the pore system is enhanced due to the presence of larger pores. Secondly, acid sites in the pore walls are more accessible to reactants (Xu et al., 2008). These properties of hierarchical zeolites may be especially attractive for the transformation of large organic molecules, which to date has been limited (Xavier et al., 2009; Xu et al., 2008). Hierarchical zeolites, such as fly ash-based hierarchical zeolite X, may serve as green heterogeneous solid acid catalysts for the transformation of large organic molecules.



2.7 Chapter Summary

The literature review aimed to summarise the research reported to date relevant to the current study. Waste coal fly ash formed by coal combustion has successfully been used as a starting material for the synthesis of various zeolites (Chang and Shih, 2000; Franus, 2012; Musyoka, 2012; Shigemoto et al., 1993). What is particularly interesting about fly ash based zeolites is the hierarchical morphology of some of these materials, which have been synthesised in the absence of additional structure-directing agents (Musyoka, 2012). A study on the formation of hierarchical zeolite X and the causes behind its formation is the main focus of this study. In this study, a clear fused fly ash extract will be converted to hierarchical zeolite X under hydrothermal conditions. Literature on the topic of hierarchical zeolite X is limited, to date. However, the following gaps have been identified in terms of the formation of zeolites (such as zeolite X) and their crystal morphology:

1. Musyoka, (2012) reported the synthesis of hierarchical zeolite X from a clear fused fly ash extract, under stirred hydrothermal conditions, without the addition of a templating agent. The cause behind the formation of hierarchical zeolite X from a clear FFA extract has not been reported by Musyoka, (2012). Crystallisation temperature and ageing was investigated by Musyoka, (2012), however the influence of Si/Al ratio on the formation of hierarchical zeolite X was not reported to date. The Si/Al ratio of the synthesis solution has been reported to play a significant role in the crystallisation of a particular zeolite phase (Chang and Shih, 2000; Shigemoto et al., 1993). The influence of Si/Al ratio on the formation and morphology of hierarchical zeolite X will therefore be investigated in this study.
2. The source of aluminium for hydrothermal zeolite synthesis has been reported to influence the morphology and crystal size of zeolite A by Xing-dong et al., (2013), whereas silicon source has been reported to influence the crystal size of zeolite X by Hamilton et al., (1993) and Shigemoto et al., (1993). The influence of aluminium source on the morphology of zeolite X, particularly hierarchical zeolite X, has not been reported to date. Therefore in this study, the influence of two different aluminium sources (aluminium hydroxide and sodium aluminate) on the formation and morphology of hierarchical zeolite X will be investigated.

Chapter 2 – Literature Review

3. The crystal size and porosity of hierarchical zeolite Y was controlled by the water content in the synthesis solution, as reported by Huang et al., (2010). The influence of water content on hierarchical zeolite X formation from a clear FFA extract has not been reported to date.
4. Musyoka, (2012) reported the synthesis of hierarchical zeolite X from a clear FFA extract under stirred synthesis conditions. However, the formation of hierarchical zeolite X under static conditions was not reported. It is important to understand the effect of stirring on the formation of hierarchical zeolite X. Therefore to elucidate whether stirring contributed to the formation of hierarchical zeolite X, the effect of a static synthesis environment on hierarchical zeolite X formation will be investigated in this study for comparison to the stirred synthesis environment.

Although Musyoka, (2012) successfully prepared hierarchical zeolite X from the clear FFA extract, an understanding of the reasons for the formation of hierarchical zeolite X has not been reported to date. Furthermore, the influence of agitation, Si/Al ratio (and aluminium source) on the formation of hierarchical zeolite X has not been reported to date. Therefore, this study aims to investigate the influence of these synthesis parameters on the formation of hierarchical zeolite X.

Research Design and Methodology

3 Introduction

The experimental and analytical procedures employed in the transformation of Arnot coal fly ash to zeolites will be outlined in this chapter. Firstly, the chemical reagents and equipment used in this study will be reported followed by a description of the fusion process of coal fly ash. Next, the synthesis procedure for zeolites from a clear fused fly ash (FFA) extract will be described. The analytical procedures for the characterisation of zeolites, starting materials and other synthesis products by various techniques are also presented in this chapter. An overview of the zeolite synthesis procedure is depicted in Figure 3.1, illustrating the (a) pre-synthesis, (b) hydrothermal synthesis and (c) post-synthesis steps.



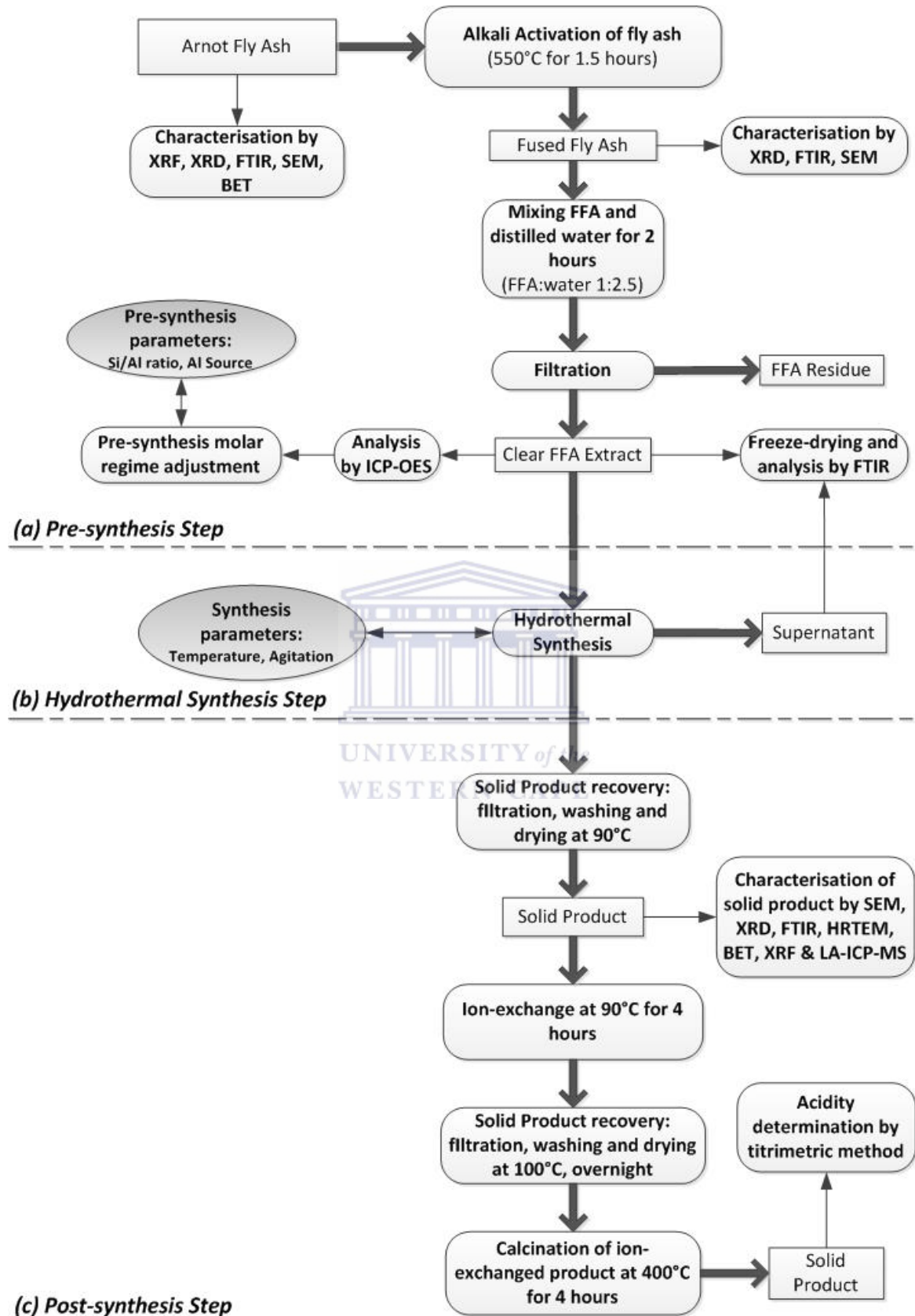


Figure 3.1: An overview of the experimental approach for zeolite synthesis from coal fly ash, including the a) pre-synthesis, (b) hydrothermal synthesis and (c) post-synthesis steps.

3.1 Materials and chemical reagents

The chemical reagents used in this study are summarised in Table 3.1, along with the origin (suppliers) of chemicals and batch details. Coal fly ash was sampled at the Arnot coal-fired power plant situated in Mpumalanga, South Africa. The Arnot coal fly ash was mixed to form a homogeneous sample which was stored in a sealed container, in a cool and dry area away from direct sunlight. One batch of Arnot coal fly ash was used throughout the study to prevent variability in the composition of the fly ash source.

Table 3.1: List of chemical reagents used, including the supplier name and batch details.

Reagent Name	Supplier	% Purity	Batch no.
Coal fly ash	Arnot Power Plant, Mpumalanga, South Africa	-	N/A
Sodium hydroxide pearls	Kimix, Cape Town, South Africa	97	QA-1 K10/0812
Sodium hydroxide pearls	Scienceworld, Cape Town, South Africa	99	20130912
Anhydrous aluminium hydroxide	Sigma Aldrich, Johannesburg, South Africa	≥95	MKBP3033V
Anhydrous sodium aluminate	Sigma Aldrich, Johannesburg, South Africa	99	SZBD2200V

3.2 Equipment list

A list of equipment used for the zeolite synthesis process, as well as the use of the equipment, is listed in Table 3.2.

Table 3.2: List of equipment used for the synthesis of zeolites.

Equipment	Use (s)
Analytical balance	Weighing
Muffle furnace	Fusion of coal fly ash, calcination
Thermo-stated heater/stirrer plate	Mixing step, zeolite synthesis
Oven	Zeolite synthesis, drying

The hydrothermal synthesis step was carried out in a thermo-stated oil bath. A schematic representation of the thermo-stated heater/stirrer plate used for zeolite synthesis is illustrated in Figure 3.2.

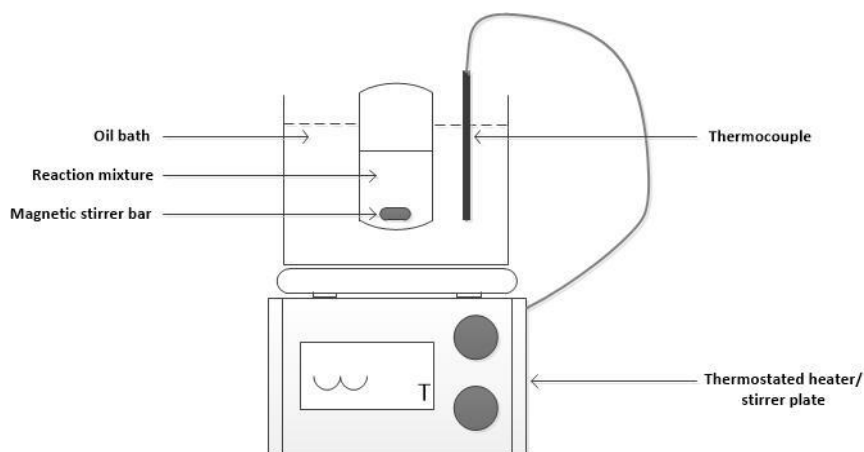


Figure 3.2: The experimental set-up for the hydrothermal synthesis process.

3.3 Synthesis of zeolites from coal fly ash

In this study, zeolite synthesis from Arnot coal fly ash was carried out by the fusion method. The first step in the synthesis procedure for hierarchical zeolite X was the alkali activation of coal fly ash by the fusion method; powdered fused fly ash was then characterised prior to use in zeolite synthesis. The effect of variation of different pre-synthesis parameters (such as Si/Al molar ratio and Al source) and synthesis parameters (such as hydrothermal temperature and static hydrothermal synthesis) on the formation hierarchical zeolite X was studied.

3.3.1 Pre-synthesis step

The pre-synthesis step for zeolite synthesis from coal fly ash involved the alkali-activation of Arnot coal fly ash with sodium hydroxide by the fusion method and the preparation of the synthesis solution (i.e. clear fused fly ash solution) by mixing powdered fused fly ash (FFA) with deionised water followed by filtration. These pre-synthesis procedures will be described in more detail in the following sections.

3.3.1.1 Alkali activation of Arnot coal fly ash

As-received Arnot coal fly ash (FA) was added to anhydrous sodium hydroxide (NaOH) pearls at a mass ratio of 1:1.2, respectively, and the dry FA and NaOH was mixed (~5 minutes) until a homogeneous mixture was formed. The dry, powdered homogeneous

mixture was placed into a crucible which was transferred into a muffle furnace where the mixture was fused at 550°C for 1.5 hours. Once the fusion process was complete, the fused fly ash (FFA) was allowed to cool to room temperature. Alkali fused fly ash was then ground to form a homogeneous powder which was used in zeolite synthesis. The FFA powder was characterised by XRD, FTIR and SEM and compared to as-received Arnot coal fly ash to determine whether the alkali activation process was successful in the transformation of the refractive mineral phases of coal fly ash (such as quartz and mullite) into more suitable precursors for zeolite synthesis.

3.3.1.2 Preparation of synthesis solution

Prior to the hydrothermal synthesis of hierarchical zeolite X, FFA powder was mixed with deionised water at a solid to liquid ratio of 1:2.5, respectively. The FFA-deionised water mixture was stirred at room temperature for 2 hours. The FFA slurry was then filtered and the clear FFA extract was collected and used as the synthesis solution for the hydrothermal synthesis of hierarchical zeolite X. Three different clear FFA extract samples were analysed by ICP-OES to determine the average elemental composition of a clear FFA extract sample.

3.3.1.3 Molar composition adjustment of the synthesis solution

The molar composition of the synthesis solution (clear FFA extract in this case) used for zeolite synthesis plays a vital role in the resultant zeolite phase and its properties. The effect of Si/Al molar ratio of the synthesis solution on the formation of hierarchical zeolite X from a clear FFA extract under hydrothermal conditions was therefore investigated in this study. Variation in Si/Al molar ratio of the synthesis solution was achieved by the addition of different amounts of an additional aluminium (Al) source to the clear FFA extract, as listed in Table 3.3. The molar composition of the clear FFA extract was normalized by setting moles of Si = 1 (0.12 Al·14.6 Na·1.00 Si·163 H₂O) for ease of reading the amount of aluminium added to the clear FFA extract. In this study either anhydrous aluminium hydroxide or anhydrous sodium aluminate was used as an additional source of aluminium; the procedure was similar to that reported by Chang and Shih, (2000).

Chapter 3 - Research Design and Methodology

Table 3.3: The experimental outline for the investigation on the effect of pre-synthesis parameter variation (Si/Al ratio, Al source) on the formation of hierarchical zeolite X.

Code	No. of experiments	Parameter under investigation	Pre-synthesis Conditions					Hydrothermal Conditions
			Preparation of clear FFA extract	Initial Si (mol)	Initial Al (mol)	Additional Al (mol)	Calculated Si/Al molar ratio of synthesis solution	
C6	2	Si/Al molar ratio of synthesis solution (by addition of anhydrous aluminium hydroxide)	Fusion ratio: 1:1.2	1.00	0.116	0	8.6	Hydrothermal temperature: 90 °C Hydrothermal time: 16 hours Hydrothermal agitation: 300 rpm
D1	1					0.006	8.2	
D2	3					0.021	7.3	
D3	1					0.044	6.2	
D4	1					0.070	5.4	
D5	1					0.197	3.2	
C6	2	Aluminium source by addition of anhydrous sodium aluminate (at different Si/Al molar ratios of the synthesis solution)	Extraction solid-to-liquid ratio: 1:2.5	1.00	0.116	0	8.6	
E1	1					0.006	8.2	
E2	3					0.021	7.3	
E3	1					0.044	6.2	
E4	1					0.070	5.4	
E5	1					0.197	3.2	

- i The effect of Si/Al molar ratio (of the synthesis solution) on hierarchical zeolite X formation

The effect of Si/Al molar ratio of the synthesis solution on the formation of hierarchical zeolite X was investigated, as shown in Table 3.3. The initial synthesis solution (clear FFA extract) was generated as described in Section 3.3.1.2. Then the required amount of anhydrous aluminium hydroxide powder was added to the clear FFA extract to vary Si/Al molar ratio, as listed in Table 3.3, and mixed for 30 minutes by stirring at 350 rpm. The resultant solution was subjected to hydrothermal treatment at 90 °C for 16 hours, while stirring using a magnetic stirrer bar at 300 rpm.

- ii The effect of aluminium source on hierarchical zeolite X formation

Similarly, the effect of aluminium source on the formation of hierarchical zeolite X from a clear FFA extract under hydrothermal conditions was investigated. In this case, the source of additional aluminium was anhydrous sodium aluminate, instead of anhydrous aluminium hydroxide, to determine the influence of aluminium source (and counter-ions) on the formation of hierarchical zeolite X. The clear FFA extract was generated as described in Section 3.3.2.2. Then the required amount of anhydrous sodium aluminate powder was added to the clear FFA extract to vary the Si/Al molar ratio, as listed in Table 3.3. The mixture was then stirred for 30 minutes at 350 rpm. The resultant solution was used as the synthesis solution which was subjected to hydrothermal treatment at 90 °C for 16 hours, while stirring at 300 rpm using a magnetic stirrer bar.

3.3.2 Hydrothermal synthesis step

In this study, the influence of various hydrothermal synthesis parameters (hydrothermal temperature and static hydrothermal synthesis) on the formation of hierarchical zeolite X was investigated. The variation of hydrothermal synthesis parameters is outlined in Table 3.4.

Chapter 3 - Research Design and Methodology

Table 3.4: The experimental outline for the investigation on the effect of synthesis parameter variation (temperature, static synthesis) on the formation of hierarchical zeolite X.

Code	Number of experiments	Pre-synthesis Conditions	Hydrothermal Conditions			
		Preparation of clear FFA extract	Constant parameters	Parameter under investigation	Levels	
A1	1	Fusion ratio: 1:1.2 Extraction solid-to-liquid ratio: 1:2.5 Molar composition of clear FFA extract: 0.12 Al·14.6 Na·1.00 Si·163 H ₂ O	Hydrothermal time: 24 hours Hydrothermal agitation: 300 rpm	Hydrothermal temperature (°C)	70	
A2	1				80	
A3	1				85	
A4	1				90	
A5	1				94	
B1	1		Fusion ratio: 1:1.2 Extraction solid-to-liquid ratio: 1:2.5 Molar composition of clear FFA extract: 0.12 Al·14.6 Na·1.00 Si·163 H ₂ O	Hydrothermal temperature: 90 °C Hydrothermal time: 24 hours	Effect of static synthesis	Static
A4	1					Stirred (300 rpm)
C1	2		Fusion ratio: 1:1.2 Extraction solid-to-liquid ratio: 1:2.5 Molar composition of clear FFA extract: 0.12 Al·14.6 Na·1.00 Si·163 H ₂ O	Hydrothermal temperature: 90 °C Hydrothermal agitation: 300 rpm	Hydrothermal time (hours)	6
C2	2					8
C3	2					10
C4	2	12				
C5	2	14				
C6	2	16				
C7	1	20				
C8	1	24				

3.3.2.1 Hydrothermal temperature

The influence of hydrothermal temperature on the formation of hierarchical zeolite X from a clear FFA extract, with molar composition $0.12 \text{ Al} \cdot 14.6 \text{ Na} \cdot 1.00 \text{ Si} \cdot 163 \text{ H}_2\text{O}$, was investigated at different hydrothermal temperatures (70, 80, 85, 90 and 94 °C) for a set hydrothermal period of 24 hours. No additional reagents were used and all other parameters were kept constant, as listed in Table 3.4. Musyoka, (2012) reported the synthesis of hierarchical zeolite X under these conditions at temperatures of 80, 90 and 94 °C. In this study, this set of experiments was therefore used as a baseline study for further investigations.

3.3.2.2 The effect of static hydrothermal synthesis on hierarchical zeolite X formation

The influence of static hydrothermal synthesis on the formation and morphology of zeolite X, from a clear FFA extract (with molar composition $0.12 \text{ Al} \cdot 14.6 \text{ Na} \cdot 1.00 \text{ Si} \cdot 163 \text{ H}_2\text{O}$), was investigated to determine whether zeolite X with hierarchical morphology may be formed under static conditions. The synthesis of hierarchical zeolite X was carried out under static conditions in a hot-air oven at 90 °C for 24 hours for comparison to the stirred synthesis system, as listed in Table 3.4.

3.3.2.3 Effect of hydrothermal time period on zeolite X crystallisation

The transformation of a clear FFA extract (with molar composition $0.12 \text{ Al} \cdot 14.6 \text{ Na} \cdot 1.00 \text{ Si} \cdot 163 \text{ H}_2\text{O}$) to hierarchical zeolite X at different hydrothermal times (6-24 hours) was carried out to investigate the effect of hydrothermal time on the crystallisation of zeolite X, while keeping all other parameters constant, as listed in Table 3.4. Hydrothermal treatment was carried out at a temperature of 90 °C, under stirred conditions (300 rpm) using a magnetic stirrer bar.

3.3.3 Post-synthesis step

The post-synthesis steps in zeolite synthesis (from a clear FFA extract) involved recovery of the solid product and ion-exchange of the solid product to convert the sodium (Na) form of the material to the acidic (H) form. These post-synthesis steps will be described in more detail in the following sections.

3.3.3.1 Product recovery

After hydrothermal synthesis, the reaction mixture was allowed to cool to room temperature. Once cool, the solid product was separated by filtration and washed with deionised water until the pH of the filtrate was in the range of 8-9. The solid product was then dried in an

oven overnight at 90 °C, before characterisation. Solid products were characterised by scanning emission microscopy (SEM)-energy-dispersive X-ray spectroscopy (EDS) and X-ray diffraction (XRD) spectroscopy. For a given set of experiments, the optimum synthesis condition at which zeolite X (with hierarchical morphology) crystallised was selected based on zeolite morphology and crystallinity determined by SEM and XRD, respectively. This optimum set of synthesis conditions was then used in subsequent experiments.

3.3.3.2 Protonation of zeolites by ion-exchange

The selected zeolites (D2 and E2) were replicated for further characterisation by XRF, LA-ICP-MS, HR-TEM, FTIR and nitrogen physisorption. Subsequently, the synthesised Na-zeolites (D2 and E2) were protonated using a modified version of a procedure described in literature (Chang and Shih, 2000), to convert the sodium form (Na-form) of the synthesised zeolites to the acidic form (H-form).

The Na-form of selected zeolites was mixed with 1 M ammonium chloride solution at a solid to liquid ratio of 1:20. The ion-exchange experiment was then carried out at 90 °C for 4 hours, in a thermo-stated oil bath, under stirred conditions. After the ion-exchange experiment, the mixture was filtered and the solid product was washed with deionised water until the filtrate reached the pH range of 7-8. The solid product was then allowed to air-dry overnight and the ion-exchange experiment was repeated three times. The solid product was then separated by filtration and washed with deionised water until the filtrate reached the pH range of 7-8. The solid product was then dried in an oven overnight at 100 °C, followed by calcination in air at 400 °C for 4 hours (to convert the ammonium-form of the solid product to the proton-form). Protonated zeolites were characterised by titrimetric method for Brønsted acidity determination.

3.4 Characterisation techniques

A variety of analytical techniques were used to characterise the synthesised zeolites as well as the starting material (as-received Arnot fly ash and clear FFA extract). The characteristics of zeolites such as total surface area, pore volume and acidity play significant roles in the application of zeolites. Therefore, it is vital to have a good understanding of the properties of zeolites.

3.4.1 Elemental analysis

The elemental analysis of as-received Arnot coal fly ash and solid products was carried out using a qualitative analytical technique such as Energy dispersive spectroscopy (EDS) and quantitative analytical techniques such as X-ray fluorescence (XRF) spectroscopy and/or Laser ablation- inductively-coupled plasma-mass spectrometry (LA-ICP-MS). The quantitative elemental analysis of synthesis solutions (clear FFA extract) was carried out by Inductively-coupled plasma-optical emission spectrometry (ICP-OES).

Qualitative elemental analysis of synthesised zeolites was carried out by Energy dispersive spectroscopy (EDS) analysis. Samples were prepared for EDS analysis by placing a small amount of powdered material onto a conductive carbon layer mounted on a metal stub. The sample was then coated with a gold-palladium layer in a Quorum Q150T ES sputter coater. Energy dispersive spectroscopy (coupled to a scanning emission microscope) was used to determine the qualitative elemental composition of synthesised zeolites. EDS analysis was carried out by spot analysis of a number of different spots (10) for a given sample and the average composition (Si/Al molar ratio) was calculated for each sample.

X-Ray fluorescence (XRF) spectroscopy was carried out to determine the quantitative elemental composition of as-received Arnot coal fly ash and selected synthesised products (D2 and E2). The analysis of Arnot coal fly ash was carried out in triplicate (on three different samples) to determine the degree of homogeneity in the sample. In the case of synthesised products, the analysis was carried out in triplicate (on the same sample) to determine the precision of the analytical technique. Samples were prepared for XRF analysis by crushing the material using a jaw crusher until a fine powder less than 70 μm (particle size) was formed. The crushed material was then milled using a tungsten-carbide Zibb mill. A fused disc of the sample was prepared for major elemental analysis by mixing 0.7 g of powdered sample and 7 g of a mixture of high purity trace element and Rare Earth element-

Chapter 3 - Research Design and Methodology

free flux. Elemental analysis was carried out on a PANalytical Axios Wavelength Dispersive spectrometer coupled to SuperQ PANalytical software. The XRF spectrometer used is fitted with a rhodium tube, a scintillation detector and gas-flow proportional counter, which uses an Argon-Methane (90:10) gas mixture. The analysis of major elements was carried out under tube conditions of 50 kV and 50 mA. External standards (such as Basalt JB-1 and BE-N) were used to determine the standard deviation for elemental analysis by the XRF spectrometer. Correction of matrix effects in samples was carried out by application of theoretical alpha factors and the measurement of line-overlap factors compared to the raw intensities using the SuperQ PANalytical software.

The quantitative trace elemental analysis of selected hierarchical zeolites (D2 and E2) was determined by Laser ablation-inductively-coupled plasma-mass spectrometry (LA-ICP-MS). Trace elemental analysis of samples is carried out on polished mounts of XRF fused discs. Trace elemental analysis by LA-ICP-MS was carried out on an Agilent 7500ce ICP-MS instrument equipped with a Resonetics 193 nm Excimer laser. The ablation process was performed under helium gas flow at a flow rate of 350 mL/min, which was mixed with nitrogen (4 mL/min) and argon (900 mL/min) prior to analysis by ICP. The quantification of trace elements was carried out using Traceable NIST 612 standards for calibration of the instrument and the %SiO₂ (from the XRF measurement) was used as an internal standard.

The quantitative elemental composition of synthesis solutions (clear FFA extract) was determined by Inductively-coupled plasma-optical emission spectrometry (ICP-OES). The molar composition of synthesis solutions used for the preparation of zeolites was calculated from ICP-OES data. Liquid samples were prepared (in triplicate) by diluting 1 mL of the clear FFA extract sample with 9 mL of 2% nitric acid solution to form a 10X diluted solution. The 10X diluted solution then served as the stock solution to prepare a 100X diluted solution; 1 mL of 10X solution was mixed with 9 mL of 2% nitric acid solution to form a 100X diluted solution. The same procedure was followed to prepare 1000X and 10000X dilutions of the initial synthesis solution. The 10000X diluted solution was used to determine the elemental composition of the synthesis solutions. ICP-OES analysis was carried out on a Varian710ES Axial ICP spectrometer. The instrument was calibrated weekly using external standards and matrix effects were corrected after each analysis.

3.4.2 Mineralogical analysis by X-ray diffraction spectroscopy

The type of mineral phases present in as-received Arnot coal fly ash, fused fly ash and synthesised products was characterised by powder X-ray diffraction (XRD) spectroscopy. The powdered sample was placed into a clear, Perspex holder and smoothed until level with the top of the disk. The Perspex holder was then placed inside a PANalytical PW3830 X-Ray generator that was used for XRD analysis. Measurements were carried out at 40 kV and 25 mA using Cu $K\alpha_1$ radiation ($\lambda = 0.154$ nm), over a 2θ range of 4 to 60° at an exposure time of 10 minutes. The mineral phases present in sample materials were identified using Philips X'Pert Graphics and Identification software and JCPDS International Centre for Diffraction Data (1997) database.

3.4.3 Morphological analysis by Scanning emission microscopy and Transmission electron microscopy

The morphology of as-received Arnot coal fly ash, fused fly ash and synthesised products was determined by Scanning emission microscopy (SEM). Selected hierarchical zeolites (D2 and E2) were further characterised by High resolution-Transmission electron microscopy (HRTEM) to determine the fine structure of hierarchical zeolite X.

Scanning emission microscopy (SEM) was used to determine the morphology of as-received Arnot coal fly ash, fused fly ash and synthesised zeolites. Powdered samples were prepared for SEM analysis as described in Section 3.4.1 for EDS sample preparation. SEM analysis was then carried out by a Zeiss Auriga field emission gun (FEG)-scanning emission microscope at 5.0 kV. SEM micrographs were processed using Image J software.

High resolution-transmission electron microscopy (HRTEM) was used to determine the fine structure of selected synthesised zeolites (D2 and E2). Samples were prepared for HRTEM analysis by dispersion of a small amount of powdered sample in ethanol using an ultrasonic bath (for 10-15 minutes). A small amount of the dispersed sample was then placed (drop-wise) onto a nickel grid and allowed to dry. Once dry, the grid was placed into the Tecnai TF20 HRTEM instrument and analysis was carried out at 200 kV.

3.4.4 Structural analysis by Fourier transform infrared spectroscopy

Structural properties of pre-synthesis materials (as-received Arnot coal fly ash, fused fly ash and clear FFA extract) and synthesis products (unwashed and washed synthesised zeolites as well as supernatant samples) were characterised by Attenuated total reflectance (ATR)-Fourier transform infrared (FTIR) spectroscopy, this sampling technique provided fast and simple means for measuring FTIR spectra. Selected hierarchical zeolites (D2 and E2) were also analysed by (ATR) FTIR.

FTIR analysis of pre-synthesis materials was carried out to determine the type of bonds present in coal fly ash and the type of precursor species present in the fused fly ash powder and the synthesis solution (clear FFA extract). The clear FFA extract (0.12 Al·14.6 Na·1.00 Si·163 H₂O) was then subjected to hydrothermal treatment at 90 °C for different time periods. Synthesis products (solid and supernatant samples) were collected at time periods to study the transformation of the starting material to zeolites with time by FTIR. On the other hand, FTIR analysis of synthesised zeolites (unwashed and washed) and supernatant samples was carried out to determine the type of structural building units present in zeolites and the type of soluble species which remained in solution after zeolite synthesis.

Solid samples (such as Arnot coal fly ash, fused fly ash and selected synthesised zeolites, D2 and E2) were used as is, in a powdered form. On the other hand, samples collected at different time periods during hydrothermal synthesis such as the clear FFA extract, supernatant samples and solid samples (unwashed and washed zeolites) were freeze-dried prior to FTIR analysis. Liquid samples were freeze-dried using a Telstar LyoQuest freeze dryer instrument, by allowing the samples to be frozen at a temperature of -55 °C at 0.2 mbar for 3 hours prior to drying. The drying process was carried out at 25 °C at 0.2 mbar for 160 hours, until liquid samples were completely dried. Similarly, solid products were freeze-dried using the same instrument by allowing the samples to be frozen at a temperature of -55 °C at 0.2 mbar for 3 hours and subsequently drying the samples at 25 °C at 0.2 mbar for 20 hours, until the solid products were completely dried. Freeze-dried samples were then ground into a fine powder which was used for FTIR analysis. Prior to each FTIR analysis, a background spectrum was measured. FTIR analysis of powdered samples was then carried out by placing a small amount of powdered sample in the ATR sample slot of the Perkin Elmer FTIR Spectrum Two instrument and applying a force to the sample before the spectrum was

collected. A wavelength range of 400-4000 cm^{-1} was measured and collected by Spectrum software.

3.4.5 Textural analysis by Nitrogen physisorption

Textural properties (such as specific surface area, total pore volume, micropore volume and pore size distribution) of as-received Arnot coal fly ash and selected hierarchical zeolites (D2 and E2) were characterised by nitrogen (N_2) physisorption. As-received Arnot coal fly ash and synthesised zeolite samples, of known mass (0.2 g) were degassed at 90 °C for 2 hours under helium flow, after which degassing was carried out at 250 °C for 24 hours under helium flow. The degassing profile used for synthesised zeolite samples in this study was a modified method of the degassing procedure for hierarchical zeolite X reported by Musyoka, (2012).

Nitrogen physisorption was then carried out at -196 °C using a Micromeritics ASAP 2020 instrument, equipped with a thermal conductivity detector (TCD). The Brunauer–Emmett–Teller (BET) method was employed to determine the specific surface area in the relative pressure range of 0.0002 to 0.03. The total pore volume was determined using single-point adsorption at a relative pressure of 0.99. The micropore volume was determined using the t-plot method, while the Barrett-Joyner-Halenda (BJH) method was used to determine the pore size distribution of samples, using the adsorption branch of the isotherm.

3.4.6 Acidity determination by titrimetric analysis

The Brønsted acidity of selected, ion-exchanged H-zeolites (D2 and E2) was determined by titrimetric method by exchanging proton (H) and deuterium (D) in the hydroxyl groups of zeolites, using H_2O and D_2O molecules, as reported by Louis et al., (2004).

Samples of known mass (0.2 g) were placed in a glass sample tube and dried under nitrogen flow of 60 mL/min at 450 °C for 1 hour (using a heating rate of 15 °C/min) to desorb any water present in the zeolite framework. The temperature was then reduced to 200 °C and D_2O was allowed to pass through the sample tube under N_2 flow for 1 hour, allowing the zeolite sample to adsorb D_2O molecules. Excess D_2O molecules were removed from the sample by sweeping dry N_2 through the sample tube for 1 hour. Titration of Brønsted sites was carried out by the back-exchange of D atoms present on surface Brønsted acid sites with H atoms. This was achieved by passing H_2O saturated N_2 flow through the sample tube, allowing the exchange to take place. A sample of the exchange-water was collected in a cooled U-tube

Chapter 3 - Research Design and Methodology

trap (-78 °C) and the mass of the sample was recorded. This sample was transferred to an NMR tube under Argon flow and mixed with trifluoroacetic anhydride, to which CHCl_3 (10 wt%)/ CDCl_3 was added as a reference.

^1H and ^2D liquid NMR analysis was carried out using a Bruker UltraShield 300 MHz/54 mm spectrometer to determine the quantity of protonated and deuterated acids in the exchange-water sample. The Brönsted acidity was then measured based on the ratio of H to D and the mass of the exchange-water sample, as reported by Louis et al., (2004). In this way, the number of Brönsted acid sites in selected, ion-exchanged H-zeolites (D2 and E2) was determined.



3.5 Chapter Summary

South African coal fly ash, from the Arnot coal-fired power plant in Mpumalanga, was activated in the presence of an alkali (such as sodium hydroxide) by the fusion method to produce powdered fused fly ash (FFA). The powdered FFA was then mixed with deionised water (at a fixed solid to liquid ratio) and filtered to yield the clear FFA extract which was used as the synthesis solution for the preparation of zeolites by hydrothermal treatment.

In this study, the effect of pre-synthesis parameters such as Si/Al ratio and aluminium source were investigated by varying the molar regime of the synthesis solution by addition of an extra source of aluminium (either aluminium hydroxide or sodium aluminate) to the clear FFA extract. These pre-synthesis parameters were investigated to determine the influence of additional aluminium and counter-ions present in the source reagent on the morphology of zeolite X. Hydrothermal synthesis parameters such as hydrothermal temperature and static synthesis were investigated to probe the formation of zeolite X from a clear FFA extract, while the influence of hydrothermal time on zeolite crystallinity was monitored. A structural study was carried out by FTIR to monitor the structural species present in a clear FFA extract, synthesised products and supernatant samples at different hydrothermal time periods under fixed hydrothermal conditions.

Synthesised products were characterised by XRD and SEM-EDS. Selected synthesised zeolites (D2 and E2) were characterised by HR-TEM, FTIR, LA-ICP-MS and nitrogen physisorption. The selected zeolites were then ion-exchanged (to the H-form) prior to acidity determination by titrimetric method.

Characterisation of Fly Ash and the Alkali Fusion Process

4 Introduction

In this chapter the characterisation of as-received Arnot coal fly ash and fused fly ash by various analytical techniques such as SEM, XRD, FTIR, XRF and by nitrogen physisorption will be presented. Coal fly ash may serve as a potential starting material for zeolite synthesis due to high silicon and aluminium content; which are the main constituents of the zeolite framework. The characterisation of Arnot coal fly ash was carried out to determine the chemical and physical properties of the material and establish feedstock quality for tailoring the molar regime prior to zeolite synthesis.

Once the Arnot coal fly ash was deemed a suitable starting material, activation of the constituents of coal fly ash to more reactive aluminium and silicon species was required (Fernandez-Jimenez and Palomo, 2005). Alkali activation was carried out, as described in Section 3.3.1.1, by the fusion method. Coal fly ash was mixed with NaOH at a mass ratio of 1:1.2, respectively (fly ash:NaOH). The fly ash-NaOH mixture was agitated to form a homogeneous mixture which was fused at 550°C for 1.5 hours (Musyoka, 2012; Shigemoto et al., 1993). The fusion process involves the dissolution of silicon and aluminium species catalysed by an alkali (Fernandez-Jimenez and Palomo, 2005). The resultant material, powdered fused fly ash (FFA), was characterised by SEM, XRD and FTIR to determine changes in the morphological, mineralogical and structural properties of FFA compared to as-received Arnot coal fly ash.

4.1 Elemental Analysis of Arnot Fly Ash by X-Ray Fluorescence Spectroscopy

The elemental composition of coal fly ash is an important property to monitor. Coal fly ash contains the most important elements for zeolite synthesis; silicon and aluminium. The elemental composition of as-received Arnot fly ash was therefore analysed by X-ray fluorescence (XRF) spectroscopy, as described in Section 3.4.1. Three different Arnot coal fly ash samples were collected and major and trace XRF analysis of Arnot coal fly ash was carried out on these three different samples to determine the homogeneity of the Arnot coal fly ash feedstock. The major elemental composition of as-received Arnot coal fly ash is listed in Table 4.1, while trace elemental composition is listed in Table 4.2. Average elemental composition values and relative standard deviation were calculated for both the major and trace elements in Arnot coal fly ash; as shown in Table 4.1 and Table 4.2.

Table 4.1: The elemental composition of as-received Arnot coal fly ash and loss on ignition (L.O.I), determined by XRF (n= 3).

Major Elements (oxide form)	Sample A (mass %)	Sample B (mass %)	Sample C (mass %)	Average (mass %)	Relative Standard Deviation (%)
SiO ₂	51.55	51.4	51.58	51.51	0.19
Al ₂ O ₃	24.65	24.74	24.79	24.73	0.29
Fe ₂ O ₃	5.61	5.36	5.49	5.49	2.28
CaO	5.24	5.18	5.21	5.21	0.58
TiO ₂	1.44	1.45	1.45	1.45	0.40
MgO	1.42	1.37	1.41	1.40	1.89
K ₂ O	0.54	0.53	0.54	0.54	1.08
P ₂ O ₅	0.32	0.33	0.32	0.32	1.79
Na ₂ O	0.07	0.07	0.06	0.07	8.66
MnO	0.05	0.05	0.05	0.05	0.00
Cr ₂ O ₃	0.02	0.02	0.02	0.02	0.00
L.O.I.	7.8	7.91	7.74	7.82	1.10
Sum	98.71	98.43	98.66	98.60	

Table 4.2: The elemental composition of as-received Arnot coal fly ash (trace elements), as determined by XRF (n= 3).

Trace Elements	Sample A (ppm)	Sample B (ppm)	Sample C (ppm)	Average (ppm)	Relative Standard Deviation (%)
S	1 375	1 341	1 338	1351	2
Ba	934	891	894	906	3
Sr	824	799	804	809	2
Zr	410	397	400	402	2
Ce	234	211	226	224	5
V	128	148	134	137	8
La	114	109	111	111	2
Nd	81	73	78	77	5
Y	73	73	72	73	1
Ni	71	67	68	69	3
Zn	59	58	60	59	2
Pb	57	51	56	55	6
Cl	66	74	19	53	56
Cu	42	44	42	43	3
Th	38	38	41	39	4
Ga	39	37	38	38	3
Rb	29	29	34	31	9
Co	20	30	26	25	20
Nb	20	23	21	21	7
U	6	14	10	10	40

Variation within the three different samples was minimal for the major elements, as the relative standard deviation for major elements were below 5 %, as listed in Table 5.1. Due to the low concentration of minor and trace elements in coal fly ash, variation in the minor and trace elemental composition between coal fly ash samples was more pronounced, as shown in Table 4.2. However, the majority of trace elements exhibited good relative standard deviation which indicated that the sampling procedure for the feedstock (Arnot coal fly ash) was relatively homogeneous.

Coal fly ash is typically composed of metal oxides (silica, alumina, iron oxide and calcium oxide) as well as moisture and unburned carbon which may be quantified by the Loss on Ignition (L.O.I) value (Blissett and Rowson, 2012; Mishra and Das, 2010). Arnot coal fly ash contained an average of 24.73 mass % aluminium oxide, 51.51 mass % silicon oxide and 5.49 mass % iron oxide; in total these oxides made up 81.73 mass % of Arnot coal fly ash. According to the ASTM C618-84 classification of types of coal fly ash, the Arnot coal fly ash used in this study may be classified as Class F type coal fly ash since the sum of aluminium, iron and silicon oxides is > 70 mass % (Blissett and Rowson, 2012; Kruger, 1997). Class F type fly ash is typically formed from the combustion of bituminous and anthracite coal and is known as siliceous ash (Blissett and Rowson, 2012; Heidrich et al., 2013; Mishra and Das, 2010). Other metal oxides commonly found in coal fly ash (such as CaO, K₂O, MgO, Na₂O and TiO₂) were also present in Arnot coal fly ash in relatively minor quantities, as shown in Table 4.1. The average LOI value for Arnot coal fly ash was 7.82 mass %, which may correspond to carbon content or moisture in the material (Blissett and Rowson, 2012; Mishra and Das, 2010). The L.O.I value for Arnot coal fly ash is well within the range for bituminous coal (0-15), as reported by Heidrich et al., (2013). The high silicon and aluminium content in Arnot coal fly ash makes it a suitable starting material for zeolite synthesis. Arnot coal fly ash exhibited a SiO₂/Al₂O₃ ratio of 2.1, which is suitable for the synthesis of low-silica zeolites (such as zeolite X).

The trace elemental analysis of as-received coal fly ash was carried out by XRF spectroscopy; results were summarised in Table 4.2. Trace quantities of elements Ba, Ce, Cl, Co, Cu, Ga, La, Nb, Nd, Ni, Pb, Rb, S, Sr, Th, U, V, Y, Zn and Zr were present in coal fly ash. Some of these trace elements (such as strontium, nickel, zirconium and lead) are toxic (Shaheen et al., 2014). Arnot coal fly ash also contains radioactive elements such uranium (U) and thorium (Th). Vassilev et al., (2003) investigated the elemental composition of different Spanish coal fly ash samples and reported that the uranium content was between 6.5-10 ppm, which was similar to the level of U detected in Arnot coal fly ash. The presence of these toxic and radioactive components in coal fly ash is one of the environmental issues linked to the material. These elements may leach into surface- and ground-water at large landfills and storage areas (Heidrich et al., 2013; Shoumkova and Stoyanova, 2013). The utilisation of waste coal fly ash for the synthesis of zeolites may therefore alleviate some of the environment burdens associated with the storage and disposal of large quantities of coal fly ash.

4.2 Textural analysis of Arnot Fly Ash by nitrogen physisorption

The textural analysis of the as-received Arnot coal fly ash sample was determined by nitrogen physisorption, as described in Section 3.4.5. The nitrogen adsorption/desorption isotherm for as-received Arnot coal fly ash is depicted in Figure 4.1.

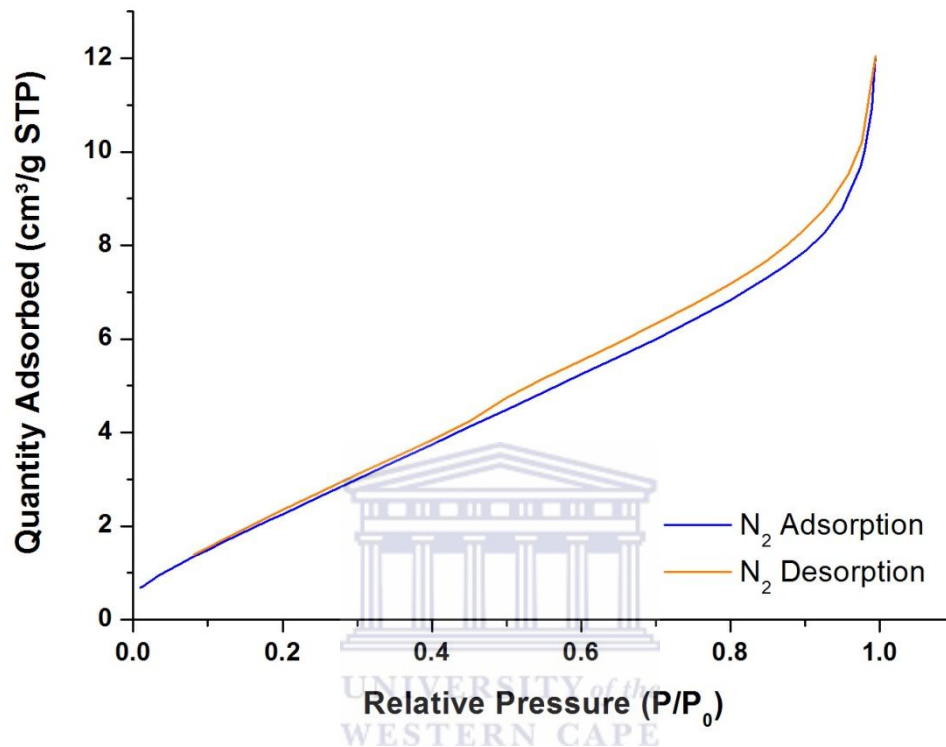


Figure 4.1: Nitrogen adsorption/desorption isotherm for as-received Arnot coal fly ash.

The adsorption/desorption isotherm for Arnot coal fly ash, depicted in Figure 4.1, corresponds to the type II isotherm according to the IUPAC classification of nitrogen adsorption/desorption isotherms (Sing, 1982). The type II isotherm usually represents macroporous materials and a situation in which a monolayer of nitrogen is formed at relatively low pressure while at relative higher pressure, multilayer adsorption of nitrogen may occur (Franus, 2012; Sing, 1982). The specific surface area of as-received Arnot coal fly ash was determined using the Brunauer–Emmett–Teller (BET) method in the relative pressure range of 0.01 to 0.3. The total pore volume was calculated by single point adsorption at a relative pressure of 0.99. The BET specific surface area, total pore volume and micropore volume are listed in Table 4.3.

Table 4.3: Textural properties of as-received Arnot coal fly ash determined by nitrogen physisorption.

BET specific surface area (m ² /g)	Total Pore Volume (x10 ⁻³ cm ³ /g)	Micropore Volume (cm ³ /g)
9.88	18.67	0

The BET specific surface area of Arnot coal fly ash was found to be relatively low, 9.88 m²/g. Wdowin et al., (2014) reported similar results; low specific surface area for a class F type Polish coal fly ash. The total pore volume was found to be 18.67 x 10⁻³ cm³/g while no micropore volume was observed, as listed in Table 4.3. This indicates that as-received Arnot coal fly ash is a macroporous material of low porosity, which is consistent with this isotherm (type II). Similar results were reported in literature for class F type Polish coal fly ash by Franus, (2012) and Wdowin et al., (2014). However, the specific surface area and total pore volume of as-received Arnot coal fly ash was relatively low in comparison with values reported for materials such as zeolites in literature (Franus, 2012; Tao et al., 2006; Wdowin et al., 2014).

Arnot coal fly ash is therefore classified as a macroporous material with relatively low specific surface area and low porosity. Arnot coal fly ash may however be converted to materials with relatively larger specific surface areas and porosity such as zeolites which have interesting applications (i.e. adsorption and shape-selective catalysis) due to the microporous nature of these materials (Chang and Shih, 2000; Tao et al., 2006).

4.3 Morphological Analysis of Arnot Fly Ash and Fused Fly Ash by Scanning Electron Microscopy

The morphology of Arnot coal fly ash and fused fly ash was determined by scanning electron microscopy (SEM), as described in Section 3.4.3. SEM micrographs of as-received Arnot coal fly ash and fused fly ash are depicted in Figure 4.2.

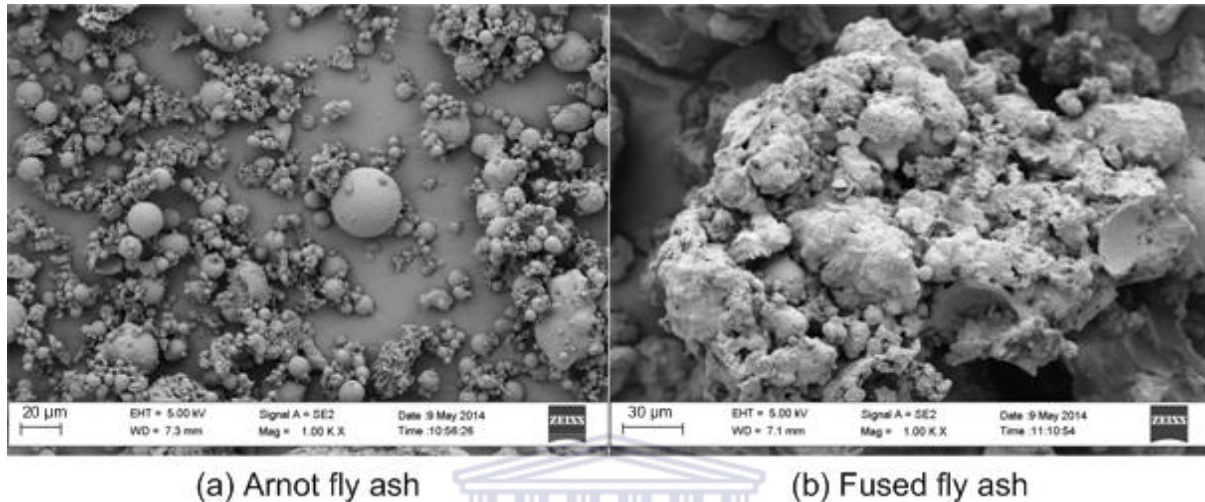


Figure 4.2: SEM micrographs of (a) as-received Arnot coal fly ash and (b) fused fly ash (1000 X magnification).

Coal fly ash morphology is largely determined by the thermal processes which occur during coal combustion, such as the temperature of combustion and the subsequent rate of cooling (Blissett and Rowson, 2012). Arnot coal fly ash, depicted in the SEM micrograph in Figure 4.2 (a), was composed of spherical particles and irregularly shaped particles. Spherical particles had a smooth surface which was attributed to an aluminosilicate glass coating (Franus, 2012). The size of spherical particles ranged from 0.2-35 µm in diameter. The alkali-activation of Arnot fly ash by fusion resulted in a complete change in the morphology of Arnot fly ash, as depicted in Figure 4.2 (b). Spherical particles are covered by an amorphous species which may be attributed to the aluminosilicate species formed during fusion. Some broken, hollow spheres were also observed in Figure 4.2 (b). This illustrates that the solid-state transformation of the mineral phases in Arnot fly ash to more reactive aluminosilicate precursor species by fusion with sodium hydroxide was achieved.

4.4 Qualitative Mineralogical Analysis of Arnot Fly Ash and Fused Fly Ash by X-Ray Diffraction Spectroscopy

The qualitative mineralogical content of as-received Arnot coal fly ash and fused fly ash was determined by powder X-ray diffraction (XRD) spectroscopy, as described in Section 3.4.2. Arnot coal fly ash was activated by the fusion method, as described in Section 3.3.1.1. Arnot coal fly ash was mixed with sodium hydroxide at a mass ratio of 1:1.2, respectively, and the mixture was fused at a temperature of 550 °C for 1.5 hours. XRD diffractograms of as-received Arnot coal fly ash and fused fly ash are depicted in Figure 4.3.

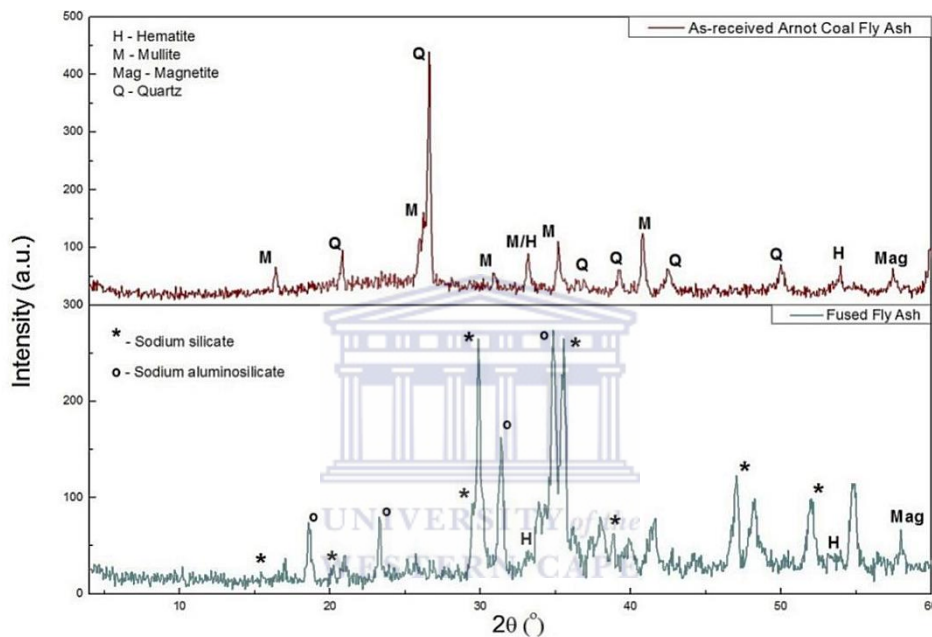


Figure 4.3: XRD diffractograms of as-received Arnot coal fly ash and fused fly ash, where Q denotes Quartz, M-Mullite, H-Hematite, Mag-Magnetite, *-Sodium silicate species and o-Sodium aluminosilicate species.

As-received Arnot coal fly ash was composed of crystalline mineral phases such as quartz (Q), mullite (M), hematite (H) and magnetite (Mag), as depicted in Figure 4.3. Although quantitative mineralogical analysis was not carried in this study, it is reported elsewhere that Arnot coal fly ash contained 62 wt% amorphous material (Musyoka, 2012). These mineral phases are typically observed in coal fly ash, as reported by Chang and Shih (1998) and Franus, (2012). The crystalline mineral phase quartz is made up of silicon oxide, while mullite is composed of both silicon and aluminium oxides (Chang and Shih, 2000). Hematite and magnetite are iron oxide mineral phases (Franus, 2012; Shoumkova and Stoyanova, 2013).

The solid-state interaction of sodium hydroxide (NaOH) with Arnot coal fly ash at 550 °C resulted in the complete transformation of silicon- and aluminium-containing mineral phases, such as quartz and mullite, into more soluble and reactive sodium silicate and sodium aluminosilicate species (Chang and Shih, 1998; Yaping et al., 2008). The absence of quartz and mullite diffraction peaks in the fused fly ash diffractogram, depicted in Figure 4.3, further confirms the reaction of these crystalline mineral phases with NaOH to yield sodium silicate as well as sodium aluminosilicate species. Chang and Shih, (2000) reported that the conversion of coal fly ash to more soluble aluminosilicate and silicate species by the fusion method increased the quantity of dissolved aluminosilicate and silicate species in aqueous solutions and thereby improved the yield of zeolites. The fusion step is therefore vital for the successful and efficient conversion of the refractive mineral phases in coal fly ash (such as quartz and mullite) to more suitable precursors, by liberating silicon and aluminium species for participation in further reactions such as hydrolysis and condensation, which lead to zeolite formation.

4.5 Structural Analysis of Arnot Fly Ash and Fused Fly Ash by Fourier Transform Infrared Spectroscopy

The structural configuration and nature of chemical bonds in as-received Arnot coal fly ash and fused fly ash were determined by Fourier Transform Infrared (FTIR) spectroscopy, as described in Section 3.4.4, and compared. Vibrational spectra obtained from FTIR analysis provide valuable information about the sample material (Criado et al., 2007). FTIR vibrational spectra for Arnot coal fly ash and fused fly ash in the wavenumber range 400-1600 cm^{-1} are depicted in Figure 4.4, with significant vibrational bands annotated. No significant vibrational bands were observed between 1600 and 4000 cm^{-1} other than a band present in both Arnot fly ash and fused fly ash at 3240 cm^{-1} (assigned to OH stretching in water molecules), hence this region was not reported.

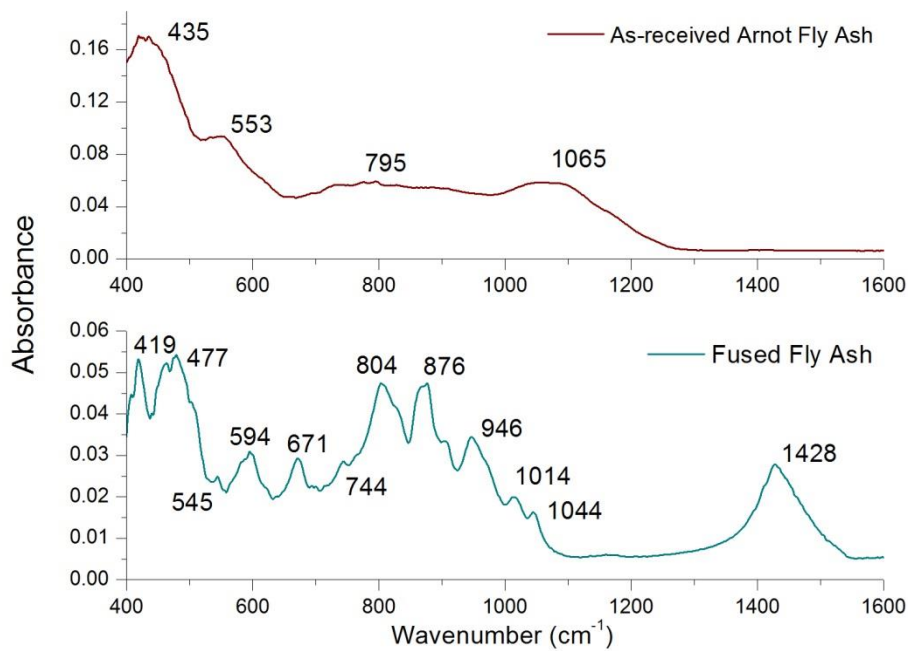


Figure 4.4: FTIR vibrational spectra of as-received Arnot coal fly ash and fused fly ash.

The main crystalline components of Arnot fly ash (such as mullite and quartz) are made up of silica and alumina tetrahedra of varying structural order. Vibrational bands observed in FTIR spectra, illustrated in Figure 4.4, are therefore assigned to the vibrational modes of T-O bonds, where T refers to either silicon or aluminium atoms. The vibrational spectrum of as-received Arnot fly ash contained four main bands at 435, 553, 795 and 1065 cm^{-1} .

Vibrational bands observed for as-received Arnot fly ash were broad, which is typical for silicate materials (Fernandez-Jimenez and Palomo, 2005). These bands were assigned to the vibrational modes of T-O (T= Si, Al) bonds present in Arnot fly ash. The internal bending vibrational band (at 435 cm^{-1}), symmetric stretching vibration (at 795 cm^{-1}) and internal asymmetric stretching vibrational band (at 1065 cm^{-1}) of T-O bonds were observed in the vibrational spectrum of as-received Arnot fly ash (Criado et al., 2007; Fernandez-Jimenez and Palomo, 2005). The asymmetric stretching band at 1065 cm^{-1} is associated with a silicon centre which is bonded to three other T atoms through oxo-bridges (Böke et al., 2015; Livage, 1994). The vibrational band observed at 553 cm^{-1} corresponded to vibrations of octahedrally coordinated aluminium atoms present in mullite (Criado et al., 2007). Typically, vibrational bands corresponding to bonds in quartz occur at 460, 522, 668, 697, 778-796,

1084 and 1150 cm^{-1} , as reported by Criado et al., (2007). Mullite is reported to commonly result in vibrational bands at 550-560 cm^{-1} and 1130-1180 cm^{-1} (Criado et al., 2007). The presence of the four broad vibrational bands in the FTIR spectrum in Figure 4.4 is attributed to the overlapping of vibrational bands of mullite, quartz and the amorphous components in Arnot fly ash.

After the fusion process, new bands were observed in the vibrational spectrum of fused fly ash, as depicted in Figure 4.4. The fusion of Arnot coal fly ash with sodium hydroxide (NaOH) converted the crystalline mineral components of fly ash (such as quartz and mullite) to more soluble phases (sodium silicate and sodium aluminosilicate species). These phases are composed of T-O bonds (in SiO_4 and AlO_4 tetrahedra) which give rise to the vibrational spectrum of fused fly ash, depicted in Figure 4.4. In addition to vibrational bands of silicate and aluminosilicate species, a broad vibrational band at 1428 cm^{-1} was also observed that may be attributed to calcium carbonate species formed during the high temperature fusion process which was carried out in air (Miller and Wilkins, 1952). Vibrational bands in the range 419-477 cm^{-1} were associated with the bending vibration of T-O bonds. Vibrational bands present in the wavenumber range of 800-500 cm^{-1} are characteristic of ring structures containing tetrahedrally coordinated T atoms. These vibrational bands therefore correspond to the building blocks of an aluminosilicate framework (Criado et al., 2007; Fernandez-Jimenez and Palomo, 2005). The vibrational band at 803 cm^{-1} was assigned to the symmetric stretching of Si-O-T bonds in silicate and aluminosilicate species (Mauritz and Warren, 1989).

Significant shifts in the stretching vibrational bands associated with T-O bonds to lower wavenumbers occurred in fused fly ash compared to as-received Arnot coal fly ash, similar to findings reported by Fernandez-Jimenez and Palomo (2005). The symmetric stretching band shifted to 744 cm^{-1} while the asymmetric stretching band shifted to 1044 cm^{-1} . The shift of stretching vibrations may be caused by the type of fly ash material used, as reported by Fernandez-Jimenez and Palomo (2005). Tetrahedrally-coordinated aluminium atoms were also thought to influence the wavenumber of T-O stretching vibrations. Fernandez-Jimenez and Palomo (2005) reported that a decrease in wavenumber for stretching vibrations occurred as the aluminium content in the system increased. The replacement of Si^{4+} with Al^{3+} resulted in a smaller bond angle and as a result, stretching vibrational bands appeared at lower wavenumbers due to the reduced bonding force (Fernandez-Jimenez and Palomo, 2005).

Upon closer examination, vibrational bands at 876 and 946 cm^{-1} were assigned to asymmetric stretching vibrations of terminal T-O bonds in relatively small aluminosilicate species, while vibrational bands at 1014 and 1044 cm^{-1} were assigned to asymmetric stretching vibrations of bridging T-O bonds in relatively large aluminosilicate species (Criado et al., 2007). Larger aluminosilicate species are formed by the condensation of relatively smaller aluminosilicate species. The condensation process may occur via two mechanisms; either the olation or oxolation reaction pathway as described in Section 2.2.2.1. More detailed assignments of the asymmetric stretching T-O bands to silicate species as well as the depolymerisation and condensation processes involving silicate species are illustrated in Figure 4.5.

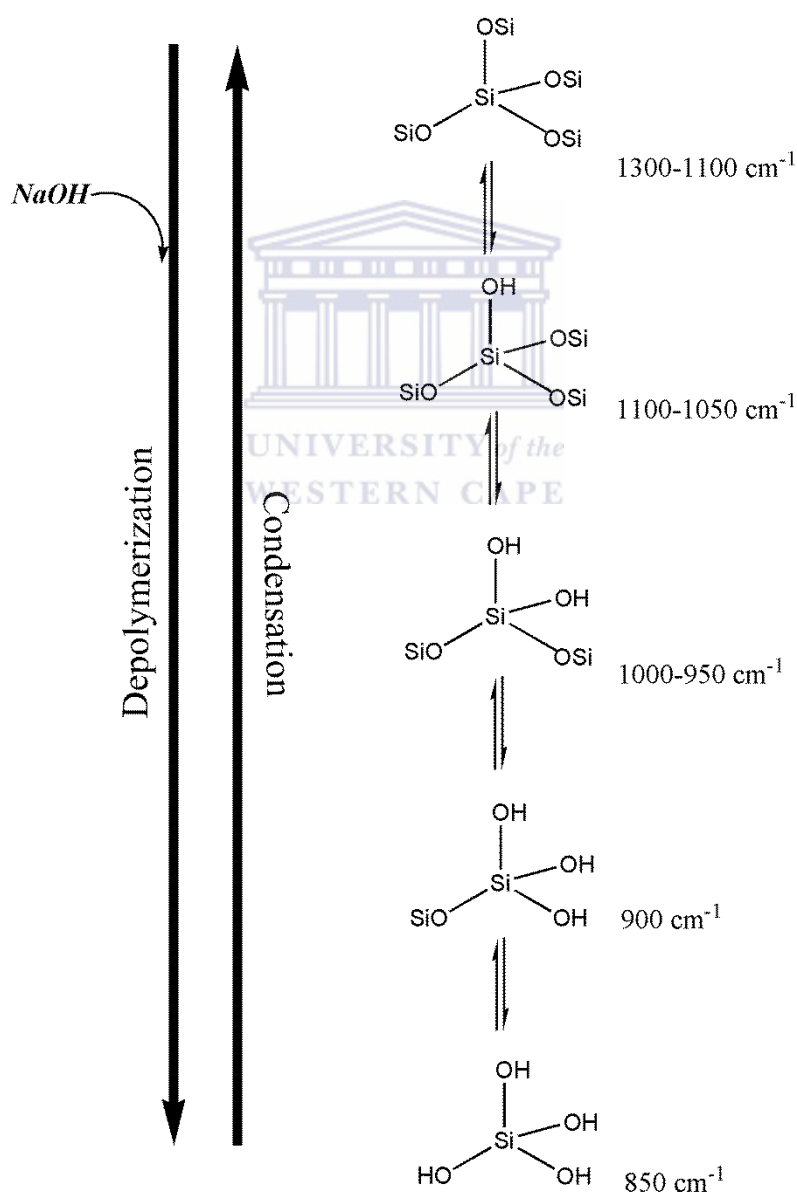


Figure 4.5: The depolymerisation and condensation process involving silicate species, including the corresponding wavenumbers for each species.

In Arnot coal fly ash the appearance of one asymmetric stretching vibrational band at 1065 cm^{-1} was attributed to silicon centres bonded to three other T atoms through an oxo-bridge. During the fusion process the depolymerisation of silicate (and aluminosilicate) species was catalysed by NaOH (a mineralising agent) in the solid-state, which resulted in the hydrolysis of Si-O-T bonds and yielded relatively smaller silicate (and aluminosilicate) species, as depicted in Figure 4.5. The asymmetric stretching vibrational bands for these smaller silicate (and aluminosilicate) species in fused fly ash were observed at lower wavenumbers compared to the asymmetric band observed for silicate species in Arnot coal fly ash.

Three additional asymmetric stretching vibrational bands were observed in the vibrational spectrum of fused fly ash at 876 , 946 and 1014 cm^{-1} . These bands may be associated with relatively smaller silicate (or aluminosilicate) species which are the products of the depolymerisation process depicted in Figure 4.5. The strong vibrational band at 876 cm^{-1} may be assigned to monomeric or dimeric silicate species, which is reported to appear at 850 cm^{-1} and 900 cm^{-1} by Böke et al., (2015). The vibrational band at 876 cm^{-1} may also be associated with OH bending vibration in Si-OH bonds. This band may therefore be associated with depolymerised silicate species that contain silanol (Si-OH) bonds (Criado et al., 2007; Lee and van Deventer, 2003). The vibrational bands at 946 cm^{-1} (strong) and 1014 cm^{-1} (weak) may be attributed to a silicon centre bonded to two other T atoms through an oxo-bridge, while the weak vibrational band at 1044 cm^{-1} may be associated with a silicon centre that is bonded to three other T atoms through oxo-bridges (Böke et al., 2015). The vibrational band at 946 and 1044 cm^{-1} may appear at lower wavenumbers compared to the values reported by Böke et al., (2015), due to the presence of aluminium atoms in these species.

Infrared results therefore indicated that the depolymerisation of the crystalline phases in Arnot coal fly ash by NaOH occurred to form relatively smaller silicate (and aluminosilicate) species containing one or more terminal OH bonds (silanol groups). These terminal OH groups may undergo condensation reactions to form larger silicate or aluminosilicate structures, as depicted in Figure 4.5, which may form part of a zeolite framework. The fusion of Arnot coal fly ash with sodium hydroxide in the solid-state was therefore achieved since quartz and mullite were transformed to new sodium aluminosilicate and sodium silicate species, as observed in Figure 4.4, which are more soluble and hence more reactive species are available after the fusion process that may serve as zeolite precursors. These results therefore served as further confirmation of results observed by SEM and XRD analysis.

4.6 Chapter Summary

The characterisation of Arnot coal fly ash and alkali-activation of this material by fusion was discussed in this chapter. As-received Arnot coal fly ash was determined, by XRF spectroscopy, to be rich in silica and alumina which are the main constituents of the zeolite framework. Arnot coal fly ash exhibited a $\text{SiO}_2/\text{Al}_2\text{O}_3$ ratio of 2.1, which was thought to be suitable for low-silica zeolite synthesis. Other elements included calcium, iron, magnesium and titanium oxides as well as toxic elements such as lead, nickel, strontium and zirconium. The predominant mineral phases present in Arnot coal fly ash were quartz and mullite, while iron oxides were present as hematite or magnetite, as determined by XRD spectroscopy. Morphological analysis, by SEM microscopy, revealed that Arnot coal fly ash contained spherical particles ranging from 0.2 to 35 μm in diameter, as well as irregularly shaped particles. Nitrogen physisorption revealed that as-received Arnot coal fly ash was a low surface area material with low total pore volume.

Once deemed a suitable starting material for zeolite synthesis, Arnot coal fly ash was alkali-activated by the fusion method using sodium hydroxide. Fusion was carried out at 550 °C for 1.5 hours after which SEM, XRD and FTIR analyses were carried out on powdered fused fly ash. Morphological analysis by SEM revealed that coal fly ash particles were transformed by NaOH during the solid-state fusion process and an amorphous aluminosilicate material covered the surface of coal fly ash particles after the fusion process. Mineralogical analysis by XRD revealed that the crystalline phases (quartz and mullite) of Arnot coal fly ash reacted with NaOH in the solid-state and were transformed into more soluble sodium silicate and sodium aluminosilicate species. Structural analysis by FTIR further confirmed these findings. The alkali-activation of Arnot coal fly ash by the fusion method therefore effectively transformed silicon and aluminium-containing crystalline phases (such as quartz and mullite) to more soluble and hence more reactive species, which may serve as zeolite precursors during hydrothermal treatment.

The influence of hydrothermal synthesis parameters on the formation of hierarchical zeolite X

5 Introduction

Once Arnot coal fly ash was deemed a suitable starting material for zeolite synthesis, the following step was the alkali activation of coal fly ash by the fusion method. The fused fly ash (FFA) was characterised prior to use for the synthesis of zeolites, as described in Chapter 4. In this chapter, the synthesis of hierarchical zeolite X from a clear FFA extract will be discussed. This chapter will focus on the effect of various hydrothermal synthesis parameters (such as hydrothermal temperature, static versus stirred hydrothermal synthesis) on the formation and morphology of hierarchical zeolite X. Characterisation of synthesised zeolites by SEM-EDS and XRD analysis will be presented. An FTIR structural study on the transformation of a clear FFA extract to zeolites with time will also be presented.

5.1 Hydrothermal synthesis of hierarchical zeolite X

Hierarchical zeolites are conventionally synthesised by either post-synthesis treatment of microporous zeolites or direct synthesis of hierarchical zeolites using structure-directing agents (Liu et al., 2009; Moller and Bein, 2011; Na et al., 2013). Typical structure-directing agents have included organosilane surfactants, silylated polymers and in some cases carbon nanoparticles and nanotubes in the synthesis of hierarchical zeolites (Na et al., 2013; Tao et al., 2006). Often these structure-directing agents require their own intricate synthesis procedure which adds further complexity and cost to the synthesis procedure for hierarchical zeolites.

In 2012, Musyoka reported a synthesis route for hierarchical zeolite X from a clear FFA extract of Arnot coal fly ash which was simple and effective compared to the conventional methods used for the synthesis of hierarchical zeolites. This synthesis route was therefore explored further in this study to determine the cause behind the formation of hierarchical zeolite X. In this study, the effect of different hydrothermal synthesis parameters (hydrothermal temperature, static/stirred synthesis) on the formation of hierarchical zeolite X from a clear FFA extract of Arnot coal fly ash was investigated. The effect of these parameters on the formation of hierarchical zeolite X will be discussed in this section.

5.1.1 The effect of hydrothermal temperature on hierarchical zeolite X formation

Zeolite crystallisation is greatly influenced by hydrothermal temperature, since a specific zeolite crystallises in a particular temperature range (Musyoka et al., 2014; Yu, 2007). The effect of hydrothermal temperature on hierarchical zeolite X formation was investigated as described in Section 3.3.2.1, Table 3.4. The synthesis solution used for hydrothermal experiments was a clear FFA extract generated, as described in Section 3.3.1.1 and 3.3.1.2. As-received Arnot coal fly ash was mixed with anhydrous sodium hydroxide pearls at a mass ratio of 1:1.2, respectively. The mixture was then fused at a temperature of 550 °C for 1.5 hours, after which the fused mass was allowed to cool and ground to form a homogeneous FFA powder. FFA powder and deionised water were then mixed together at a solid to liquid ratio of 1:2.5 for 2 hours at room temperature, followed by filtration to collect the extract.

Three different clear FFA extract samples were generated (without an additional Al source) and analysed by ICP-OES spectrometry. The major elemental composition of the three different clear FFA extract samples and relative standard deviation for each element is presented in Appendix A. The composition of clear FFA extract samples was similar in terms of K and Na which had a relative standard deviation of 1 and 3 %, respectively. The relatively higher deviation for Al, Ca and Si (8, 6 and 8 %, respectively) may be due to experimental errors during the preparation of fused fly ash and clear FFA extract samples, which may have resulted in slight variation in the composition of the clear FFA extract samples. The average molar composition of the clear FFA extract solution was calculated (as described in Appendix B) and summarised in Table 5.1.

Table 5.1: The average molar composition of a clear FFA extract, determined by ICP-OES (n= 3).

	Al	Ca	K	Na	Si	H ₂ O	Si/Al molar ratio	Na/Al molar ratio
Average Molar Composition	0.12	0.03	0.05	14.6	1.00	163	8.6	122

Zeolite synthesis from a clear FFA extract (with molar composition: 0.12 Al·14.6 Na·1.00 Si·163 H₂O) was carried out under stirred hydrothermal conditions at temperatures of 70, 80, 85, 90 and 94 °C for a fixed hydrothermal time period of 24 hours, while keeping all other synthesis parameters constant. In this case, no additional reagents (such as an additional

aluminium or silicon source) were used in the preparation of the synthesis solution. These experimental conditions were chosen based on results reported by Musyoka, (2012) for hierarchical zeolite X synthesis.

Solid products obtained after hydrothermal synthesis were white in colour. The yield of zeolite product, without any additional source of silicon or aluminium, was very low (~5.2 mass %), as presented in Table 6.2 for sample C6. The yield (mass %) of zeolite product was calculated based on the amount of silicon and aluminium available in the fly ash (determined by XRF, listed in Table 4.1) which was extracted to yield the clear FFA extract that was subsequently used in the synthesis of zeolites.

For every 1 g of aluminium in Arnot coal fly ash there was 2 g of silicon available in Arnot coal fly ash, as determined by XRF, listed in Table 4.1. Zeolite X (the target phase) and P are Al rich zeolites with framework Si/Al ratios of 1.1-1.5 and 2-8, respectively. The relatively low aluminium content in Arnot coal fly ash resulted in low aluminium content in the clear FFA extract. Consequently, the clear FFA extract had a high Si/Al molar ratio, as listed in Table 5.1. Therefore, the conversion of fly ash to zeolite products was limited by the low availability of soluble aluminium species, which resulted in the low yield of the zeolite product. This was further investigated by the addition of set amounts of an aluminium source, which will be presented in Chapter 6.

Solid products obtained by stirred hydrothermal synthesis of a clear FFA extract (0.12 Al·14.6 Na·1.00 Si·163 H₂O) at different hydrothermal temperatures for 24 hours were characterised by SEM-EDS and XRD analysis. The effect of hydrothermal temperature on the morphology of solid products was determined by SEM. SEM micrographs depicting solid products synthesised at different hydrothermal temperatures, at a fixed hydrothermal time of 24 hours, are illustrated in Figure 5.1.



Figure 5.1: SEM micrographs of Na-zeolites synthesised under stirred conditions from a clear FFA extract (without an additional Al source) at hydrothermal temperatures between 70-94 °C and a fixed hydrothermal time of 24 hours. Images were obtained at 10 000 X magnification (left) and 50 000 X magnification (right).

Zeolite Na-P1 crystals exhibited a granular pseudo-spherical morphology (typical of zeolite Na-P1), as depicted in Figure 5.1. Intergrown disc-like platelets were also observed in some cases, as depicted in Figure 5.1. The presence of disc-like zeolite crystals were observed at relatively higher hydrothermal temperatures (> 85 °C), together with the typical Na-P1 morphology. However, hydrothermal treatment at 70 °C also resulted in the formation of intergrown disc-like crystals that had much narrower platelets than the platelets formed at slightly higher temperatures (85 - 94 °C).

SEM micrographs were also used to determine the average particle size of Na-zeolites. Image J software was used to measure the dimensions of several hierarchical zeolite particles; results were used to calculate the average particle size in terms of length (l) and width (w). The calculated results are reported in Table 5.2 along with the Si/Al and Na/Al (wt %) ratio of Na-zeolites, as determined by EDS analysis.

Table 5.2: Summary of properties of Na-zeolites synthesised from a clear FFA extract (without an additional Al source) at different hydrothermal temperatures, for a fixed hydrothermal time period of 24 hours.

Code	Parameter: Temperature (°C)	Si/Al wt % ratio of Na- zeolite product	Na/Al wt % ratio of Na- zeolite product	Other cations in Na-zeolite product	Average Particle Size l, w (nm)
A1	70	1.3	0.6	Ca, K	N.D
A2	80	1.2	0.7	-	N.D
A3	85	1.3	0.6	-	1960, 86
A4	90	1.2	0.7	-	1200, 126
A5	94	1.3	0.8	-	2100, 260

l-length, w-width, N.D-not detected

There was no direct correlation between temperature and average particle size (length). However, the average particle width increased as the hydrothermal temperature was increased. The increase in hydrothermal temperature from 70 to 94 °C did not have a significant effect on the Si/Al molar ratio of Na-zeolites. The Si/Al ratio of synthesised zeolites were in the range of 1.2 - 1.3 which is characteristic of zeolite Na-X (Payra and Dutta, 2003; Yu, 2007). The Na/Al ratio of synthesised Na-zeolites ranged from 0.6 to 0.8 . Typically, Na-zeolites exhibit a Na/Al ratio of 1 which signifies that each aluminium atom in

the zeolite framework is counter-balanced by a sodium cation. The lower Na/Al ratio of Na-zeolites may suggest that other cations (such as Ca and/or K detected by EDS) may also serve as counter-ions in the zeolite framework together with sodium.

XRD diffractograms of Na-zeolites synthesised under stirred hydrothermal conditions at different hydrothermal temperatures, for a fixed time period of 24 hours, are depicted in Figure 5.2. In Figure 5.2, peaks annotated by P represent zeolite Na-P1 and peaks along the dotted line represent zeolite Na-X.

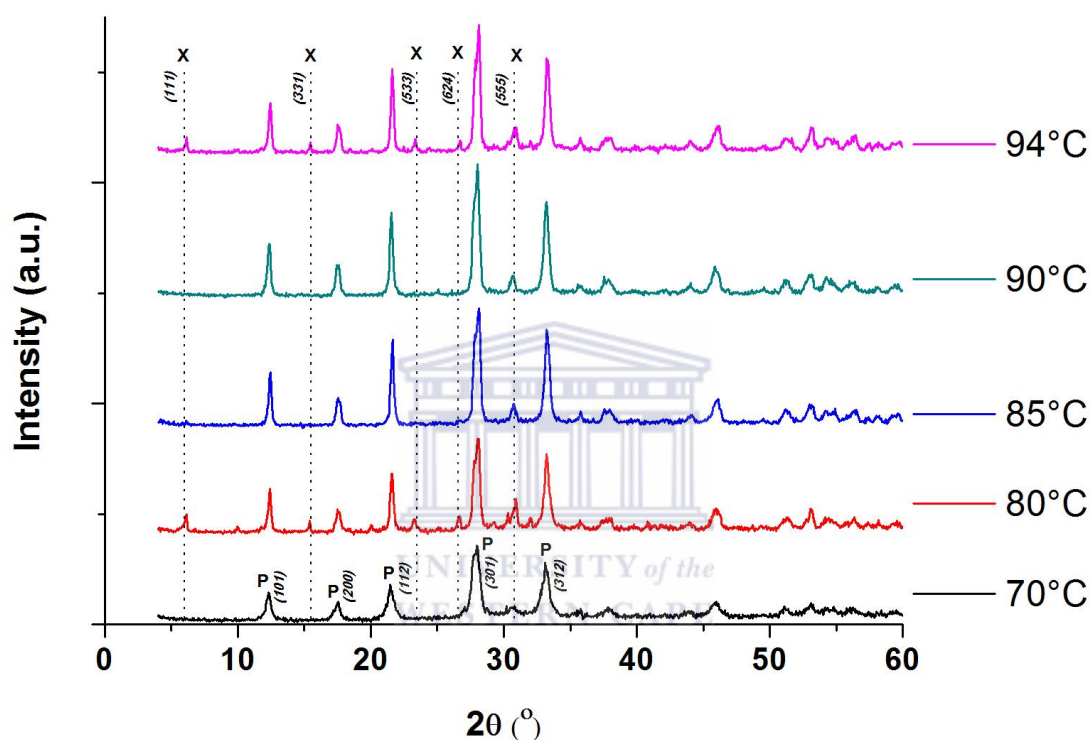


Figure 5.2: XRD diffractograms of Na-zeolites synthesised under stirred conditions from a clear FFA extract (without an additional Al source) at hydrothermal temperatures between 70 and 94 °C, at a fixed hydrothermal time of 24 hours.

The major zeolite phase that crystallised using the applied molar regime and under the stirred hydrothermal conditions studied was zeolite Na-P1. Minor zeolite Na-X peaks were observed, particularly at hydrothermal temperatures of 80 and 94 °C. Therefore, no clear correlation between temperature and zeolite Na-X could be drawn under these hydrothermal conditions. However, the crystallinity of zeolite Na-P1 improved dramatically as the hydrothermal temperature was increased from 70 to 94 °C. Hydrothermal temperature is known to enhance the processes of nucleation and crystal growth in zeolite crystallisation

(Yu, 2007). The improved crystallinity of Na-P1 may therefore be attributed to enhanced crystallisation processes during hydrothermal treatment at relatively higher temperatures.

The transformation of metastable Na-X to thermodynamically more stable Na-P1 is known to occur for prolonged hydrothermal time periods or at relatively higher hydrothermal temperatures (Feijen et al., 1994; Yu, 2007). This transformation is due to Ostwald's law of successive transformations, which states that metastable zeolite phases (such as zeolite X) will transform into more stable phases (such as zeolite P) with time (Davis and Lobo, 1992; Feijen et al., 1994; Yu, 2007). The transformation of zeolite Na-X to zeolite Na-P1 was confirmed by the low Si/Al ratio of solid products between 1.2 and 1.3, as listed in Table 5.2. The Si/Al ratio of zeolite Na-P1 is usually ~ 2 (Payra and Dutta, 2003). The deviation of Si/Al ratio of Na-P1 synthesised in this study from literature values may be as a result of transformation of zeolite X to zeolite P1 with time. It is proposed that the hydrothermal time of 24 hours is too long for the preferential formation of zeolite X, under the hydrothermal conditions studied.

The synthesis of hierarchical zeolite X from a clear FFA extract (with Si/Al molar ratio of 8.3) under the same stirred synthesis conditions, at hydrothermal temperatures of 80, 90 and 94 °C for 24 hours, was reported by Musyoka, (2012). Musyoka, (2012) reported that the crystallisation of zeolite Na-P1 was favoured at lower hydrothermal temperatures of 60 and 70 °C. However, in this study the hydrothermal treatment of a clear FFA extract under the investigated stirred hydrothermal conditions resulted in the preferential formation of Na-P1 instead of Na-X. The observed difference in zeolite crystallisation may be due to the higher Si/Al ratio of clear FFA extract samples used as synthesis solutions and/or the hydrothermal period employed (Feijen et al., 1994; Yu, 2007). In another study, Musyoka et al., (2012) reported the synthesis of Na-P1 from three different South African coal fly ash sources under static hydrothermal conditions of 140 °C for 48 hours. Musyoka et al., (2012) mixed coal fly ash with a sodium hydroxide solution and aged the synthesis mixture (Si/Al molar ratio of 1.4) at 47 °C for 48 hours under stirred conditions (800 rpm), prior to hydrothermal synthesis. The synthesis conditions used by Musyoka et al., (2012) avoided the fusion step (used in this study) by using the ageing process prior to hydrothermal treatment. Therefore, observed differences may be due to the method of fly ash activation and/or variation in the Si/Al molar ratio of synthesis solutions.

The morphology of the zeolite crystals, depicted in Figure 5.1, was similar to zeolite Na-P1 and zeolite Na-X crystals reported in literature (Franus, 2012; Inayat et al., 2012; Musyoka,

2012; Wdowin et al., 2014). Wdowin et al., (2014) reported a similar agglomerated granular morphology of zeolite Na-P1 crystals which was synthesised from Polish coal fly ash. On the other hand, Musyoka, (2012) reported that zeolite X crystals (synthesised using the same procedure reported in this study) exhibited intergrown disc-like platelet morphology. The formation of zeolite X with intergrown disc-like platelet morphology has been reported by other researchers as well (Franus, 2012; Inayat et al., 2012). Franus, (2012) synthesised zeolite X from coal fly ash which exhibited “ball of wool” morphology similar to the hierarchical zeolite X crystals synthesised by Musyoka, (2012), however these zeolite crystals were not well-defined. Inayat et al., (2012) however, synthesised hierarchical zeolite X with “house of card” morphology similar to the disc-like zeolite crystals formed in this study, using a mesopore-directing organic agent such as 3-(trimethoxysilyl) propyl hexadecyl dimethyl ammonium chloride (TPHAC). The disc-like morphology of Na-zeolites formed in this study was however synthesised in the absence of any additional structure-directing agents.

In this study, the hierarchical morphology of Na-zeolites was observed, as depicted in SEM micrographs, in the hydrothermal temperature range of 80 to 94 °C, an intermediate hydrothermal temperature of 90 °C was therefore set for subsequent experiments.

5.1.2 The effect of static synthesis on hierarchical zeolite X formation

Zeolite morphology is reportedly influenced by stirring the synthesis solution during hydrothermal treatment (Hanif et al., 2000; Yu, 2007), as carried out for samples discussed in section 5.1.1. The degree of crystal intergrowth may also be influenced by stirring the synthesis mixture during hydrothermal treatment (Hanif et al., 2000). The influence of stirring on the formation of hierarchical zeolite X is therefore an important factor to investigate to gain insight into the formation of this particular zeolite. As described in Section 3.3.2.2, the hydrothermal treatment of a clear FFA extract (with molar composition: 0.12 Al·14.6 Na·1.00 Si·163 H₂O) was therefore carried out under static synthesis conditions (90 °C for 24 hours), for comparison with the stirred (300 rpm) hydrothermal synthesis system used in this study. No additional aluminium or silicon sources were used in the preparation of the synthesis solution.

Synthesised Na-zeolites were characterised by SEM-EDS and XRD analysis. The effect of static synthesis on the morphology of Na-zeolites was determined by SEM. SEM micrographs of Na-zeolites synthesised under static hydrothermal conditions are compared with products synthesised under stirred hydrothermal conditions, as depicted in Figure 5.3.

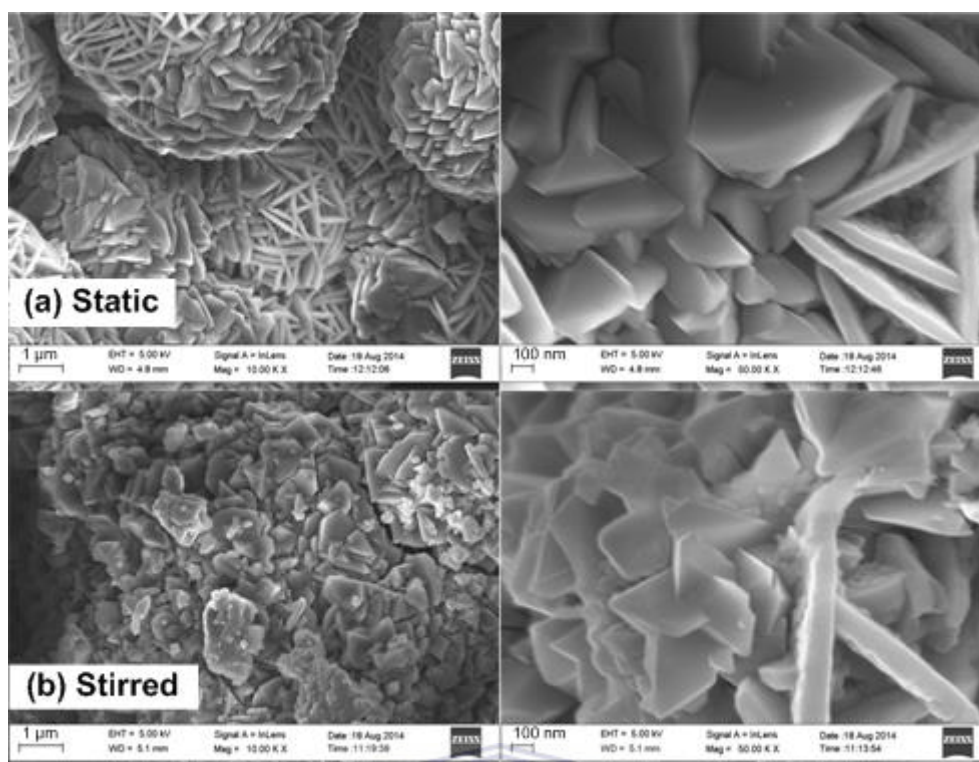


Figure 5.3: SEM micrographs of Na-zeolites synthesised from a clear FFA extract (without an additional Al source) under (a) static and (b) stirred hydrothermal conditions, at 90 °C for 24 hours. Images were measured at 10 000 X magnification (left) and 50 000 X magnification (right).

Under static conditions intergrown disc-like platelets were formed in an agglomerated ball-like manner, as depicted in Figure 5.3 (a). Under stirred conditions highly agglomerated crystals were formed together with disc-like platelet crystals, as depicted in Figure 5.3 (b). The average particle size in terms of length and width (determined using SEM microscopy) and the Si/Al and Na/Al (wt %) ratio (determined by EDS analysis) of Na-zeolites synthesised under static and stirred hydrothermal conditions of 90 °C for 24 hours is summarised in Table 5.3.

Chapter 5

Table 5.3: Summary of properties of Na-zeolites synthesised from a clear FFA extract (without an additional Al source) under static or stirred hydrothermal conditions, at 90 °C for 24 hours.

Code	Parameter investigated: Static/stirred synthesis	Si/Al wt % ratio of Na-zeolite product	Na/Al wt % ratio of Na-zeolite product	Other cations in Na-zeolite product	Average Particle Size l, w (nm)
B1	Static	1.2	0.7	Ca, Ti	1800, 67
A4	Stirred (300 rpm)	1.2	0.7	-	1200, 126

l-length, w-width

In both cases, the crystallised product had a Si/Al ratio of 1.2 which is in the range of zeolite X (1.1-1.5). The Na/Al ratio of both Na-zeolites was 0.7, which suggests that Ca detected by EDS, may serve as counter-ions in the zeolite framework together with sodium. Under static hydrothermal conditions, the average particle size (1800 nm) was greater compared to stirred hydrothermal synthesis (1200 nm) while the average particle thickness was relatively smaller (67 nm) compared to stirred hydrothermal conditions (126 nm). Therefore, relatively longer and thinner crystals were formed under the static hydrothermal conditions applied in this study.

XRD diffractograms of Na-zeolites synthesised under static and stirred hydrothermal conditions are depicted in Figure 5.4. In Figure 5.4, peaks annotated by S represent hydroxysodalite while peaks annotated by P represent zeolite Na-P1 and peaks along the dotted line represent zeolite Na-X.

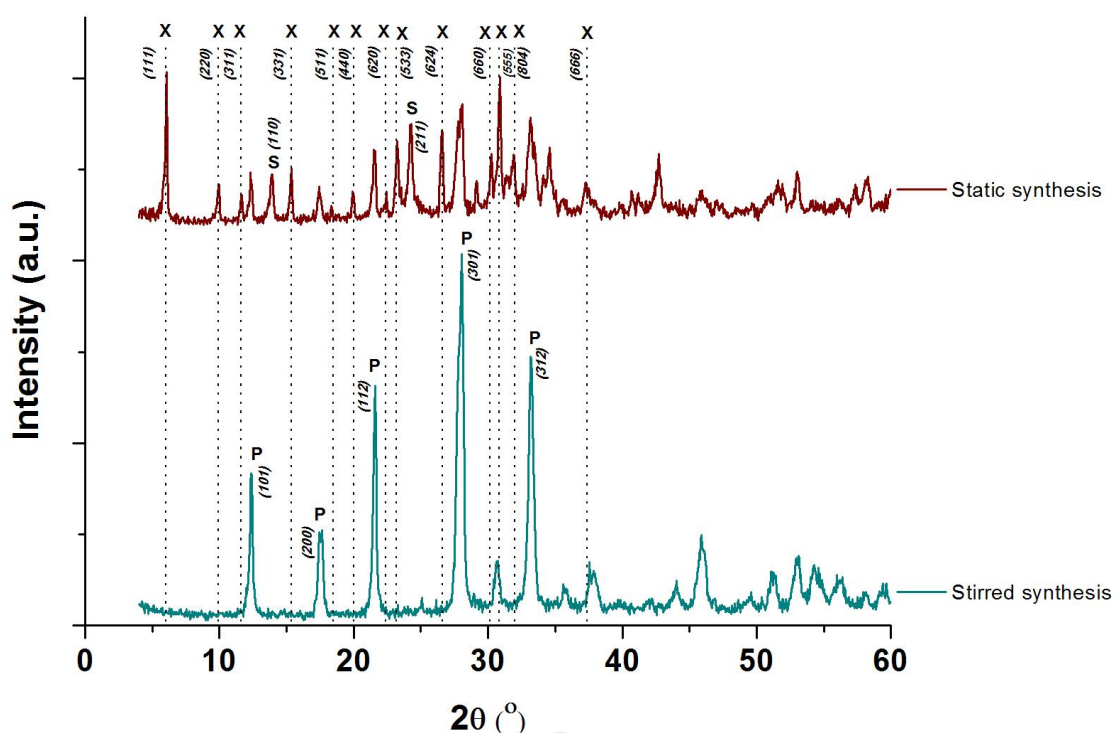


Figure 5.4: XRD diffractograms of Na-zeolites synthesised from a clear FFA extract (without an additional Al source) under static and stirred hydrothermal conditions, at 90 °C for 24 hours.

Under the hydrothermal conditions investigated (90 °C, 24 hours), zeolite Na-X crystallised as the major phase under static conditions, while under stirred conditions zeolite Na-P1 crystallised preferentially. This was attributed to differences between the crystallisation kinetics for the synthesis system under static and stirred conditions; improved crystallisation kinetics may occur under stirred hydrothermal conditions compared to static conditions (Yu, 2007).

Stirring the synthesis solution during hydrothermal treatment may have caused supersaturation to be achieved relatively faster compared to static conditions, thereby speeding up the crystallisation process. The study on the influence of stirring on hierarchical zeolite X formation revealed that zeolite Na-X was formed under static hydrothermal conditions while relatively high purity zeolite Na-P1 was formed under stirred hydrothermal conditions using the same molar formulation. By stirring the synthesis solution, crystallisation processes were enhanced by the improved mass transfer of nutrients to the growing crystal surface. In this way, improved crystallisation kinetics under stirred hydrothermal conditions (90 °C for 24 hours) resulted in the formation of the thermodynamically more stable phase (zeolite Na-P1) while static synthesis resulted in the

crystallisation of relatively less stable zeolite Na-X. It has been reported elsewhere that stirring a fused fly ash solution during hydrothermal treatment reduced the time required for the crystallisation of zeolite Na-P1 compared to static hydrothermal synthesis (Chang and Shih, 1998).

The morphology of zeolites crystallised under static and stirred hydrothermal conditions were similar to the morphology of zeolite Na-X and Na-P1 reported in literature (Inayat et al., 2012; Musyoka, 2012; Wdowin et al., 2014). The intergrown disc-like platelets resembled the zeolite X crystals with hierarchical morphology reported by Inayat et al., (2012) and Musyoka, (2012). However, zeolite X crystals typically exhibit an octahedral morphology. The crystal morphology observed under stirred hydrothermal conditions was similar to the typical morphology of Na-P1 crystals, as reported by Wdowin et al., (2014). Stirred hydrothermal conditions were used for subsequent experiments and the effect of hydrothermal time on the crystallinity of hierarchical zeolite X was then monitored.

5.1.3 The effect of hydrothermal time on hierarchical X crystallisation

Hydrothermal time is an important factor to monitor during zeolite synthesis, since zeolites are thermodynamically metastable crystalline phases (Davis and Lobo, 1992; Yu, 2007). The earlier study on the effect of temperature revealed that the hydrothermal period of 24 hours was too long for the crystallisation of Na-X and instead, Na-P1 crystallised in the temperature range investigated at a crystallisation time of 24 hours. The effect of hydrothermal time on zeolite X crystallisation from a clear FFA extract (molar composition: $0.12 \text{ Al} \cdot 14.6 \text{ Na} \cdot 1.00 \text{ Si} \cdot 163 \text{ H}_2\text{O}$) was therefore monitored at a fixed hydrothermal temperature of 90°C , keeping all other synthesis parameters constant. No additional sources of silicon or aluminium were used in the preparation of the synthesis solution. Synthesised Na-zeolites were characterised by SEM-EDS and XRD analysis.

The effect of hydrothermal time on the morphology of Na-zeolites was determined by SEM analysis. SEM micrographs of Na-zeolites synthesised from a clear FFA extract at a fixed hydrothermal temperature of 90°C for different time periods are depicted in Figure 5.5.

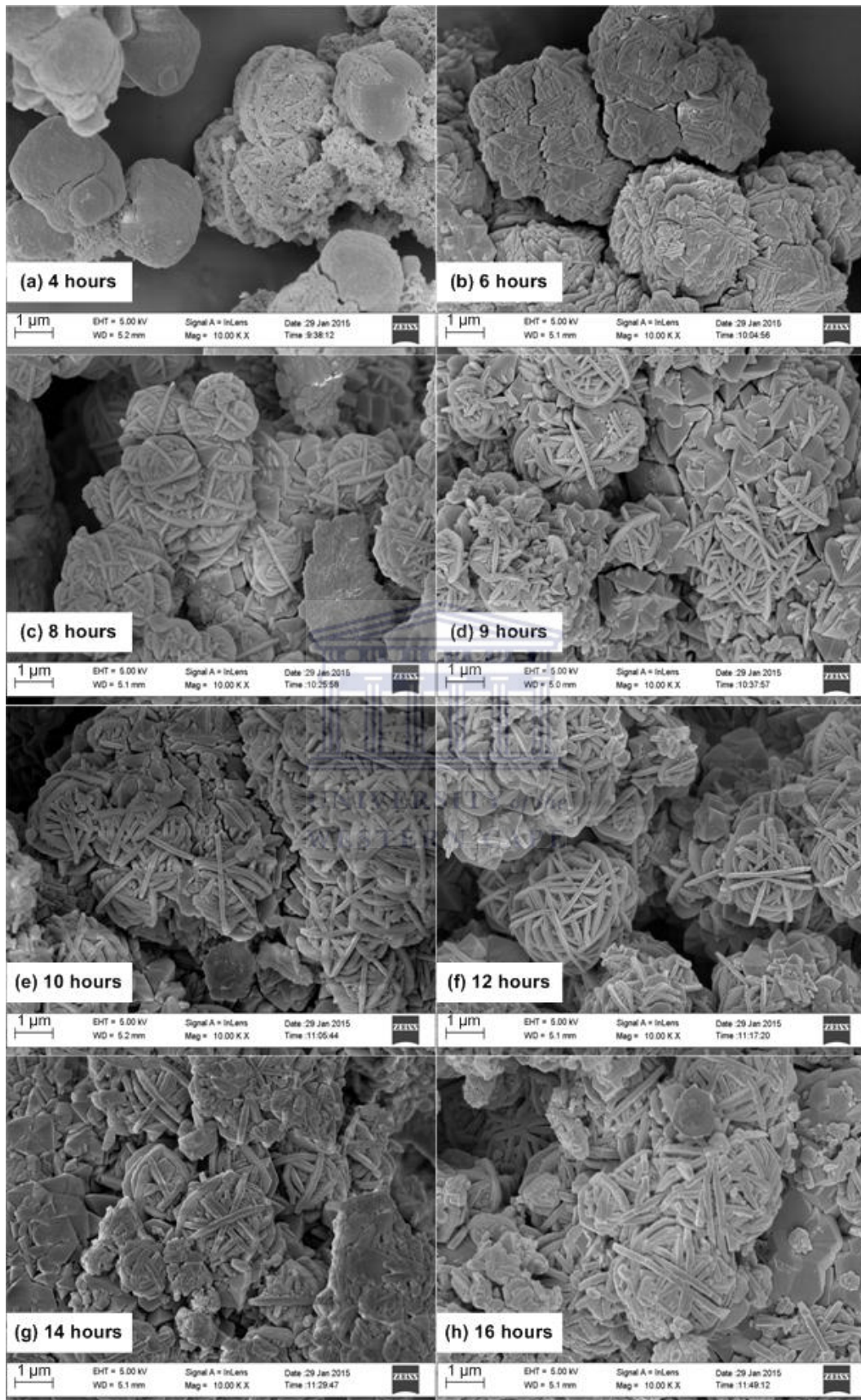


Figure 5.5: SEM micrographs (10 000X magnification) of Na-zeolites synthesised from a clear FFA extract (without an additional Al source) for different hydrothermal time periods, at a fixed hydrothermal temperature of 90°C.

Chapter 5

The morphology of solid products was affected by hydrothermal time. Intergrown disc-like crystals resembling the hierarchical morphology of zeolite X was observed between 8 and 20 hours of hydrothermal treatment, as illustrated in Figure 5.5. Well-defined ball-like aggregates of these disc-like crystals were observed between 12 and 16 hours of hydrothermal treatment at 90 °C. However, after 20 hours the formation of agglomerated crystals was favoured over the disc-like platelet morphology. After 24 hours of hydrothermal treatment the morphology of the solid product resembled that of typical Na-P1 crystals. The change in morphology may correspond to the transformation of zeolite phases from X to P which occurs according to Ostwald's law of successive transformations. The average particle size, Si/Al and Na/Al (wt %) ratio of Na-zeolites synthesised for different hydrothermal time periods (at a fixed hydrothermal temperature of 90°C) is summarised in Table 5.4.

Table 5.4: Summary of properties of Na-zeolites synthesised from a clear FFA extract (without additional reagents) for different hydrothermal time periods, at a hydrothermal temperature of 90°C.

Code	Parameter investigated: Time (hours)	Si/Al wt % ratio of Na- zeolite product	Na/Al wt % ratio of Na- zeolite product	Other cations present in Na- zeolite product	Average Particle Size l, w (nm)
C1	6	1.3	0.6	Ca	555, 43
C2	8	1.3	0.7	Ca	1330, 65
C3	10	1.3	0.6	Ca	1542, 104
C4	12	1.3	0.7	Ca	1517, 87
C5	14	1.3	0.7	Ca	1137, 140
C6	16	1.3	0.8	Ca	1129, 162
C7	20	1.2	0.7	-	2100, 130
C8	24	1.2	0.7	-	1200, 126

l-length, w-width

The hydrothermal time period did not have a significant effect on the Si/Al ratio of synthesised zeolites. As observed previously, synthesised zeolites all exhibited Si/Al ratios between 1.2 and 1.3, which is in the expected range for zeolite X. The Na/Al ratio of Na-zeolites ranged from 0.6 to 0.8 which indicates that other cations (such as Ca detected by EDS) may also serve as counter-ions in the zeolite framework. There was no direct correlation between hydrothermal time and the average particle size of the zeolite crystals. The average particle size of disc-like platelets ranged from 555 to 2100 nm in length and 43 to 162 nm in width, as shown in Table 5.4.

XRD diffractograms of Na-zeolites synthesised from a clear FFA extract (molar composition: 0.12 Al·14.6 Na·1.00 Si·163 H₂O) under stirred hydrothermal conditions at 90°C for different time periods are illustrated in Figure 5.6. In Figure 5.6, peaks annotated by S represent hydroxysodalite, while peaks annotated by P represent zeolite Na-P1 and peaks along the dotted line represent zeolite Na-X.

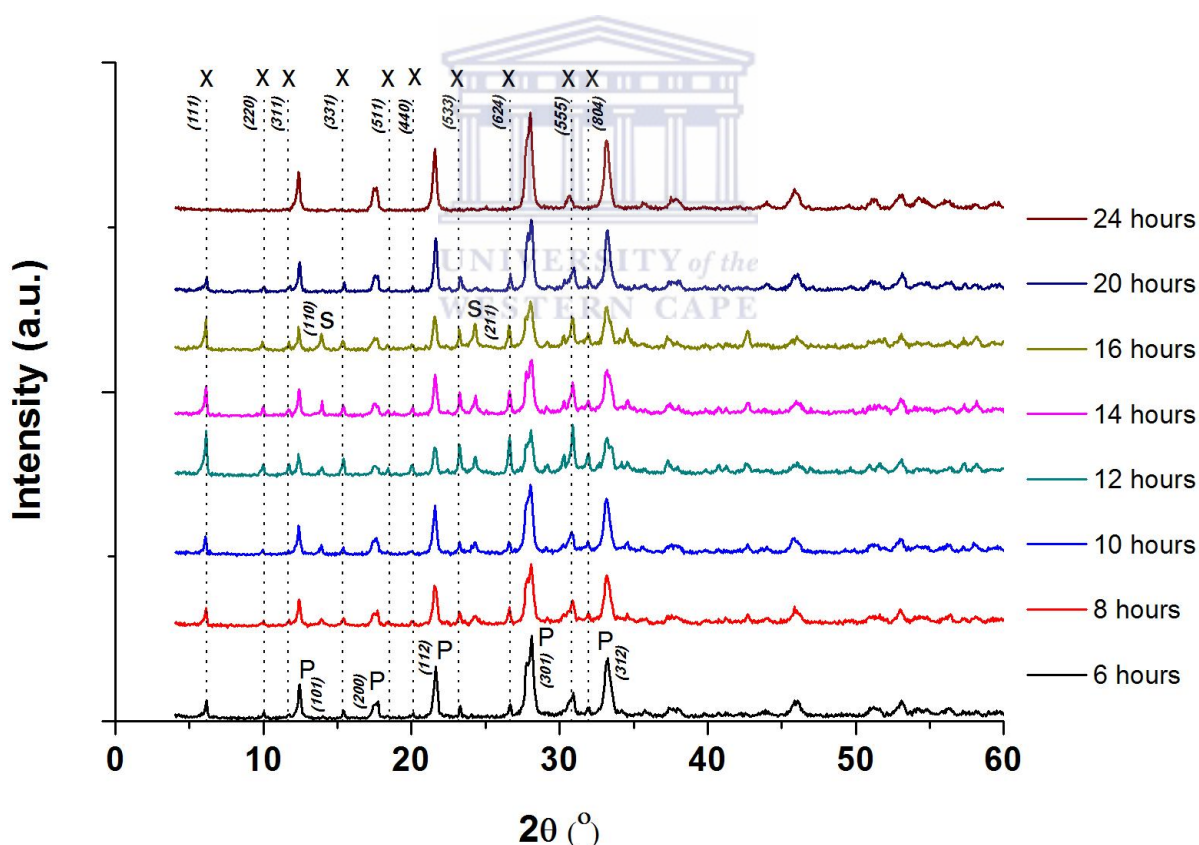


Figure 5.6: XRD diffractograms of Na-zeolites synthesised from a clear FFA extract (without an additional Al source) for different hydrothermal time periods, at a fixed hydrothermal temperature of 90°C.

The crystallisation of zeolite Na-P1 as the major phase occurred up to 10 hours of hydrothermal treatment, while zeolite Na-X crystallised as the major phase between 12 and 16 hours of hydrothermal treatment. The appearance of minor hydroxysodalite peaks were observed between 8 and 16 hours of crystallisation. Prolonging the hydrothermal treatment to 20-24 hours resulted in the formation of Na-P1 as the major phase. The formation of Na-P after 20 hours of hydrothermal treatment was expected since it follows Ostwald's law of successive transformations (Davis and Lobo, 1992; Feijen et al., 1994; Yu, 2007). The morphology of synthesised Na-zeolites resembled the hierarchical morphology of zeolite X reported by Inayat et al., (2012) and Musyoka, (2012) between 8 and 20 hours of crystallisation. On the other hand, the synthesised Na-zeolite that crystallised after 24 hours exhibited the typical morphology of zeolite Na-P1, as reported by Wdowin et al., (2014).

The study on the effect of hydrothermal time on the crystallisation of zeolite X illustrated that this zeolite was most favourably formed between 12 and 16 hours of hydrothermal treatment at 90 °C under the applied synthesis conditions. However, zeolite Na-X crystallised together with traces of Na-P1 and hydroxysodalite. The highest crystallinity of zeolite Na-X was achieved after 12 hours of hydrothermal treatment. Zeolite X is known to exhibit a framework Si/Al ratio of 1-1.5, while zeolite P1 typically exhibits a framework Si/Al ratio of 2-8 (Eulenberger et al., 1967; Payra and Dutta, 2003). As mentioned in Chapter 2, these low-silica zeolites are synthesised under similar hydrothermal conditions (i.e. high alkalinity and low Si/Al molar ratio of the synthesis solution). Boundary regions exist where a certain molar composition gives rise to two different zeolite phases; this effect was observed in this study. The crystallisation of zeolite Na-X in the presence of zeolite Na-P1 indicated that the molar composition of the synthesis solution used in this study lies on or close to the boundary region for the formation of zeolite Na-X and Na-P1, under the hydrothermal conditions investigated. The crystallisation of zeolite Na-P1 together with zeolite Na-X may have been as a result of the relatively high Si/Al molar ratio (8.6) of the synthesis solution.

The influence of synthesis conditions (such as hydrothermal temperature and time, static versus stirred hydrothermal synthesis presented in Section 5.1) on the formation and morphology of hierarchical zeolite X illustrated that the crystallisation of this particular zeolite with hierarchical morphology is dependent on hydrothermal temperature and time. However, zeolite X with hierarchical morphology was able to crystallise in both stirred and static hydrothermal synthesis systems. Hierarchical zeolite X formation and morphology was therefore relatively more sensitive to crystallisation temperature and time than static/stirred

Chapter 5

hydrothermal synthesis conditions. The following step in this study was to carry out FTIR structural analysis on the clear FFA extract, Na-zeolites synthesised for different hydrothermal times as well as supernatant samples (collected at different time intervals) to better understand the transformation of a clear FFA extract into zeolites.



5.2 Structural study of the transformation of the clear FFA extract to zeolites with time

The transformation of a clear FFA extract to zeolites with time was investigated under stirred hydrothermal conditions (90 °C, 300 rpm), as described in Section 3.3.2.3. As reported previously, fly ash based zeolites prepared from a clear fused fly ash extract (0.12 Al·14.6 Na·1.00 Si·163 H₂O), without additional reagents, were observed to transform between phases, Na-P1 and Na-X, with time. In this study, the transformation of a clear fused fly ash extract (molar composition: 0.12 Al·14.6 Na·1.00 Si·163 H₂O) to zeolites with time (2-16 hours) was therefore studied by Fourier transform infrared (FTIR) spectroscopy, as described in Section 3.4.4. FTIR spectroscopy was used to determine the type of bonds and configurations present in the clear FFA extract, solid product (unwashed and washed) and supernatant samples collected at set time intervals.

Zeolites are microporous aluminosilicate materials composed of silica (SiO₄) and alumina (AlO₄) tetrahedra connected by common oxygen atoms (Granda Valdes et al., 2006; Weitkamp, 2000). These SiO₄ and AlO₄ tetrahedra are known as the primary building units (PBUs) of zeolites (Mozgawa et al., 2011). Primary building units join together in various ways to form different secondary building units (SBUs) such as S4R, S6R, D4R and D6R units (McCusker and Baerlocher, 2007; Mozgawa et al., 2011). Zeolites are often characterised by a specific SBU, although more than one SBU may be found in a particular zeolite framework (Mozgawa et al., 2011). For example, zeolite P is typically associated with S4R structural units while zeolite A is characterised by the presence of D4R units and zeolite X by D6R units (Criado et al., 2007; Mozgawa et al., 2011). On the other hand, hydroxysodalite is composed of sodalite units (made up of S6R and S4R units) joined together by shared S4R units (Fernandez-Jimenez and Palomo, 2005).

Vibrational spectroscopy, such as FTIR spectroscopy, enables the detection of the secondary building units (SBUs) of zeolites (Criado et al., 2007). Secondary building units are typically observed in the 800-500 cm⁻¹ wavenumber range, in infrared spectroscopy, due to the vibrations of tetrahedral units in two- or three-dimensional aluminosilicate structures (Criado et al., 2007; Fernandez-Jimenez and Palomo, 2005). Vibrational bands in this region of the infrared (IR) spectrum provide information about the environment of framework tetrahedra which includes; the amount of units in ring structures and the type of ring structure involved (Criado et al., 2007). FTIR spectroscopy is therefore a useful tool for identifying specific zeolites by their characteristic secondary building units.

Aluminosilicate materials, such as zeolites, typically exhibit vibrations of alumina and silica tetrahedra (TO_4 , $T = \text{Al}$ or Si) in the IR range of $1200\text{-}400\text{ cm}^{-1}$ (Criado et al., 2007; Mozgawa et al., 2011). FTIR spectra presented in this study will therefore be presented in the mid-IR range, applicable to aluminosilicate materials. In this study, zeolites were synthesised from a clear FFA extract (molar composition: $0.12\text{ Al}\cdot 14.6\text{ Na}\cdot 1.00\text{ Si}\cdot 163\text{ H}_2\text{O}$) under stirred hydrothermal conditions. The clear FFA extract was freeze-dried and analysed by FTIR spectroscopy to determine the type of bonds and soluble precursor species present in the synthesis solution, as depicted in Figure 5.7.

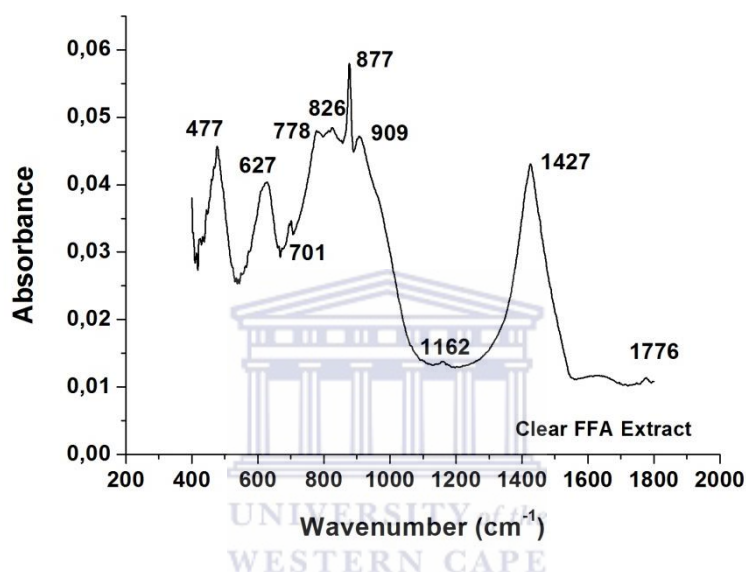


Figure 5.7: FTIR spectrum of the freeze-dried clear FFA extract without an additional Al source (molar composition: $0.12\text{ Al}\cdot 14.6\text{ Na}\cdot 1.00\text{ Si}\cdot 163\text{ H}_2\text{O}$) used for hydrothermal synthesis of zeolites.

The FTIR spectrum of the clear FFA extract was composed of bands associated with aluminosilicates ($1162\text{-}400\text{ cm}^{-1}$) and calcium carbonate species (1427 and 1776 cm^{-1}) (Criado et al., 2007; Lee and van Deventer., 2003; Miller and Wilkins, 1952; Mozgawa et al., 2011). Bending vibrations of aluminosilicate tetrahedra were present at 477 cm^{-1} , while asymmetric stretching vibrations were observed at $909\text{-}877\text{ cm}^{-1}$ (terminal T-OH bonds) and 1162 cm^{-1} (bridging T-O bonds) (Criado et al., 2007; Lee and van Deventer, 2003; Mozgawa et al., 2011). More detailed assignments of asymmetric stretching vibrations are listed in Table 5.5, together with the vibrational bands for SBU units (such as D4R and D6R rings) as reported by Mozgawa et al., (2011).

Chapter 5

Table 5.5: Vibrational band assignments for aluminosilicates present in the clear FFA extract.

Vibrational band (cm ⁻¹)	Assignment (T = Al, Si)
477	Bending vibration of Si-O-T bonds
574, 502	Double 6-membered rings (D6R units)*
555	Double 4-membered rings (D4R units)*
627	Single 6-membered rings (S6R units)
701, 778	Single 4-membered rings (S4R units)
826	Symmetric stretching (Si-O-Si bonds)
877	SiO ₄ ⁻⁴ or bending vibrations of T-OH bonds
909	-SiO ₃
1162	≡SiO

*Mozgawa et al., (2011)

The vibrational band at 1162 cm⁻¹ is usually associated with highly condensed aluminosilicate materials. On the other hand, the strong band observed at 877 cm⁻¹ is associated with small silicate anions and may also be attributed to bending vibrations of T-OH bonds (Bass and Turner, 1997; Lee and van Deventer., 2003; Shigemoto et al., 1995). The vibrational band at 826 cm⁻¹ was attributed to symmetric stretching of Si-O-Si bonds in aluminosilicate materials (Mauritz and Warren, 2003). Vibrational bands were also observed in the SBU wavenumber region between 800 and 500 cm⁻¹, as depicted in Figure 5.7. The presence of a vibrational band at 627 cm⁻¹ was attributed to single 6-membered ring (S6R) structures, which may serve as precursors for zeolite X, P1 or hydroxysodalite during hydrothermal synthesis (Mozgawa et al., 2011). Vibrational bands at 701 and 778 cm⁻¹ were associated with single 4-membered ring (S4R) structures. These bands may also serve as precursors for zeolite X, P1 or hydroxysodalite (Mozgawa et al., 2011). Compared to the

vibrational spectrum of fused fly ash, depicted in Figure 4.4, the disappearance of bands associated with relatively larger aluminosilicate species was observed in the vibrational spectrum of the freeze-dried clear FFA extract. This is due to the dissolution of relatively small, soluble silicate and/or aluminosilicate species during the preparation of the clear FFA extract solution.

Depending on the hydrothermal conditions applied to the clear FFA extract, a variety of zeolites may crystallise (Feijen et al., 1994; Yu, 2007). At relatively low temperatures, the crystallisation of zeolites such as Na-A, Na-X and Na-P1 has been reported (Chang and Shih, 1998; Musyoka, 2012; Shigemoto et al., 1995; Wdowin et al., 2014). The presence of secondary building blocks, S4R and S6R in the clear FFA extract, may favour the formation of zeolite P which is composed of S4R units linked together (Mozgawa et al., 2011). On the other hand, S4R units may link together (by condensation reactions of T-OH bonds as depicted in Section 4.5, Figure 4.5) to form D4R units which are the secondary building blocks of zeolite A (Shigemoto et al., 1995). Similarly, S6R units may link together through dehydration of T-OH bonds to form D6R linkages and larger secondary building blocks, such as the β (sodalite) cages, of the zeolite X framework. Sodalite cages may also join together by common S4R faces to form hydroxysodalite (Mozgawa et al., 2011; Shigemoto et al., 1995). The hydrothermal synthesis conditions applied to the clear FFA extract therefore plays an important role in the type of zeolite that is formed.

Clear FFA extract samples (0.12 Al·14.6 Na·1.00 Si·163 H₂O) without an additional Al source were subjected to stirred hydrothermal treatment at 90 °C (300 rpm), for time periods varying from 2 to 16 hours as described in Section 3.3.2.3 (Codes C1 to C6). As reported previously, prolonged hydrothermal times (> 20 hours) resulted in the preferential formation of Na-P1, instead of Na-X, and therefore the structural study was carried out up to 16 hours of synthesis time. After hydrothermal synthesis, unwashed solid products (Na-zeolites) were collected and freeze-dried prior to analysis by FTIR. FTIR vibrational spectra of unwashed Na-zeolites synthesised under stirred hydrothermal treatment at 90 °C for different time periods are illustrated in Figure 5.8.

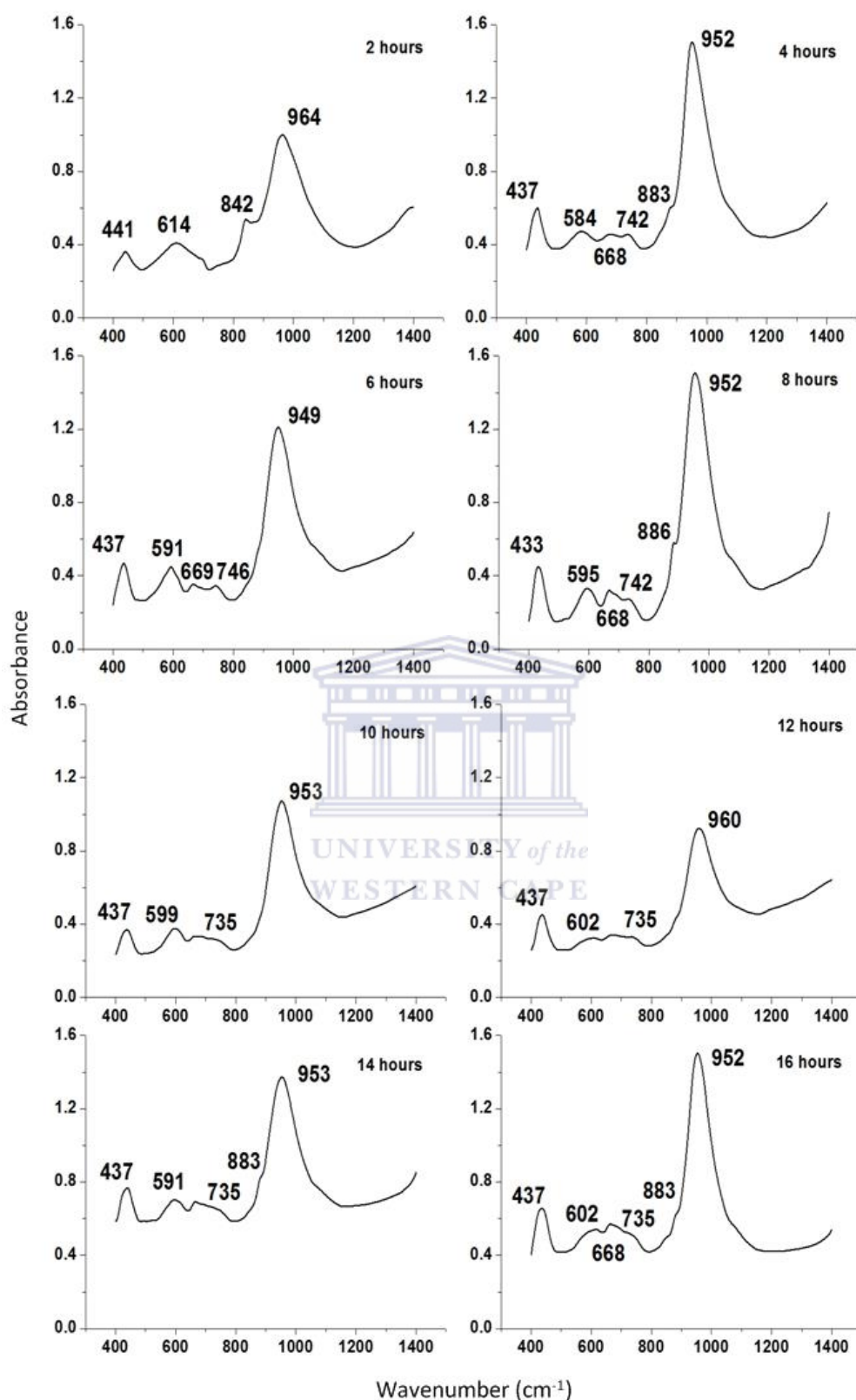


Figure 5.8: FTIR spectra of freeze-dried, **unwashed** Na-zeolites synthesised from a clear FFA extract without an additional Al source (molar composition: 0.12 Al·14.6 Na·1.00 Si·163 H₂O) for different time periods, under stirred hydrothermal conditions of 90 °C.

Chapter 5

FTIR spectra of unwashed Na-zeolites exhibited typical aluminosilicate vibrations, as depicted in Figure 5.8. The bending T-O vibration ($441\text{-}433\text{ cm}^{-1}$), symmetric stretching band of Si-O-T bonds ($669\text{-}668\text{ cm}^{-1}$), asymmetric stretching vibration of T-OH bonds ($886\text{-}883\text{ cm}^{-1}$ and $985\text{-}962\text{ cm}^{-1}$) and vibrations corresponding to SBUs in the wavenumber range from 800 to 500 cm^{-1} were observed in the vibrational spectra of unwashed Na-zeolites. More detailed assignments of vibrational bands are listed in Table 5.6.

Table 5.6: Vibrational band assignments for aluminosilicate species present in **unwashed** Na-zeolites.

Vibrational band (cm^{-1})	Assignment (T = Al, Si)
441-433	Bending vibration of Si-O-T bonds
584	D6R unit (characteristic of zeolite X)
614-591	S6R unit (found in zeolite X, P or hydroxysodalite)
669-668	Symmetric stretching (Si-O-T bonds)
746-735	S4R unit (characteristic of zeolite P, found in zeolite X and hydroxysodalite)
886-883	SiO_4^{4-}
964-949	$=\text{SiO}_2$

As listed in Table 5.6, the asymmetric stretching band at $886\text{-}883\text{ cm}^{-1}$ was assigned to small silicate anions which are soluble, reactive species. The asymmetric stretching vibrational band at $964\text{-}949\text{ cm}^{-1}$ is associated with a silicon centre that is connected to two other T atoms through a common oxygen atom (Böke et al., 2015). The asymmetric stretching band at $964\text{-}949\text{ cm}^{-1}$ was therefore attributed to zeolite framework species. In the case of unwashed Na-zeolites, vibrational bands appearing in the SBU range were broad as depicted in Figure 5.8. The vibrational band observed at 584 cm^{-1} was assigned to vibrations of the D6R unit (characteristic of zeolite X), while the band at $614\text{-}591\text{ cm}^{-1}$ was assigned to S6R units. The vibrational band corresponding to the S4R unit (characteristic of zeolite P1) was observed at $746\text{-}735\text{ cm}^{-1}$ (Criado et al., 2007). It is noteworthy that the S4R and S6R bands may be associated with either zeolite X, P1 or hydroxysodalite. The solid product was then washed with deionised water, as described in Section 3.3.3, and freeze-dried prior to analysis

Chapter 5

by FTIR. FTIR vibrational spectra of washed Na-zeolites synthesised under stirred hydrothermal treatment (90 °C) are illustrated in Figure 5.9.



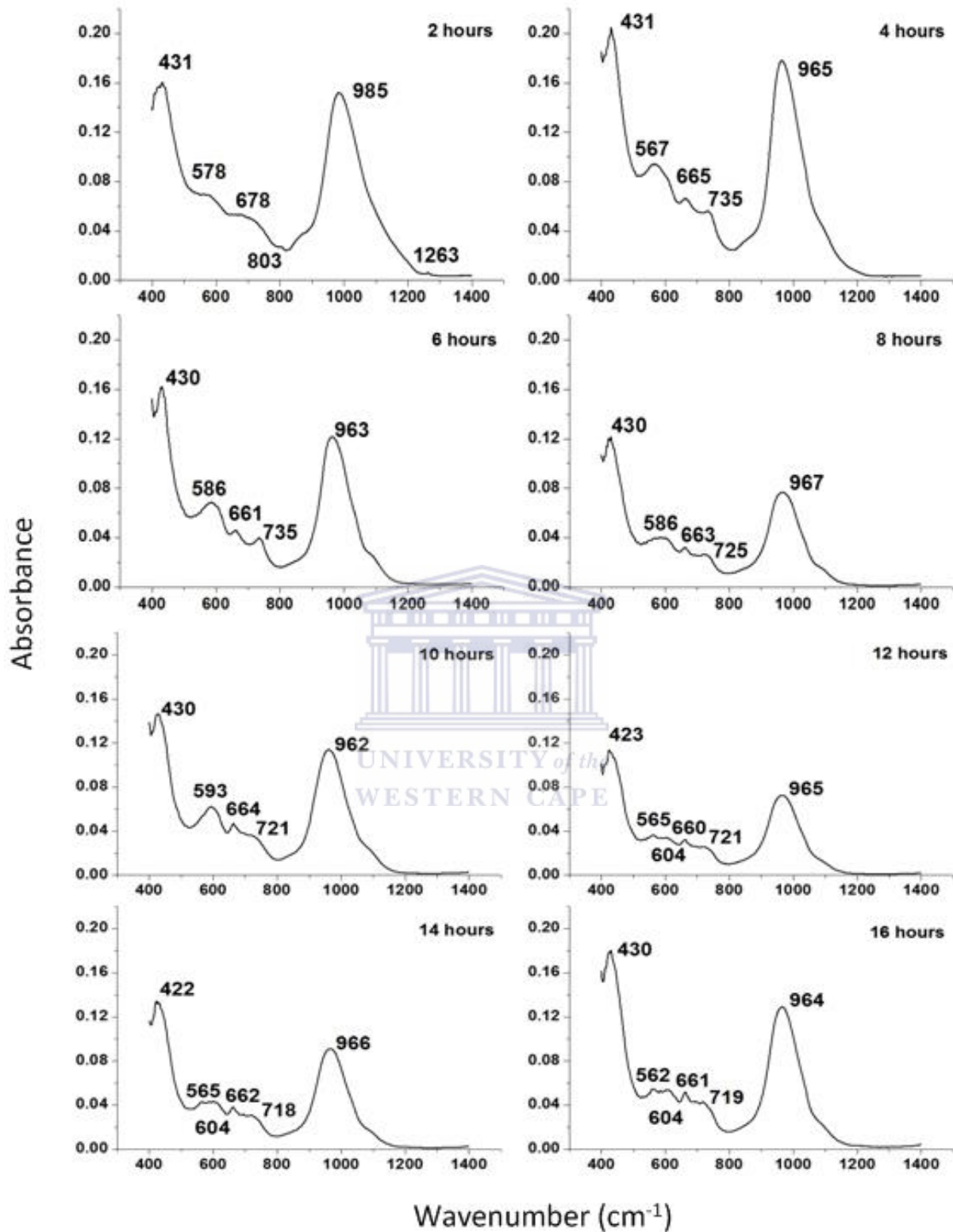


Figure 5.9: FTIR spectra of freeze-dried, **washed** Na-zeolites synthesised from a clear FFA extract without an additional Al source (molar composition: 0.12 Al·14.6 Na·1.00 Si·163 H₂O) for different time periods, under stirred hydrothermal conditions of 90 °C.

The typical aluminosilicate vibrations were observed for washed Na-zeolites, as depicted in Figure 5.9. The bending T-O vibrational band ($431\text{-}422\text{ cm}^{-1}$), symmetric stretching band of Si-O-T bonds ($678\text{-}660\text{ cm}^{-1}$), asymmetric stretching vibration of terminal T-OH bonds ($985\text{-}962\text{ cm}^{-1}$) and asymmetric stretching vibration of bridging T-O bonds (1263 cm^{-1}) were observed in Figure 5.9. In the case of washed Na-zeolites, the asymmetric stretching vibration of bridging T-O bonds was not well resolved as depicted in Figure 5.9, which may be due to overlapping of the band associated with asymmetric stretching vibrations of terminal T-OH bonds. Vibrational bands corresponding to SBUs in the wavenumber range from 800 to 500 cm^{-1} were also observed in washed Na-zeolites, as expected (Criado et al., 2007; Mozgawa et al., 2011). More detailed assignments of vibrational bands are listed in Table 5.7.

Table 5.7: Vibrational band assignments for aluminosilicate species present in **washed** Na-zeolites.

Vibrational band (cm^{-1})	Assignment (T = Al, Si)
431-422	Bending vibration of Si-O-T bonds
586-562	D6R unit (characteristic of zeolite X)
608-593	S6R unit (found in zeolite X, P or hydroxysodalite)
678-660	Symmetric stretching (Si-O-T bonds)
735-718	S4R unit (characteristic of zeolite P, found in zeolite X and hydroxysodalite)
985-962	$=\text{SiO}_2$
1076-1073, 1263	$\equiv\text{SiO}$

The bridging T-O asymmetric stretching vibration appeared at $1076\text{-}1073\text{ cm}^{-1}$ as a weak (shoulder) band after 6 hours of hydrothermal treatment. This band is typically associated with relatively larger polymeric aluminosilicate species and three-dimensional aluminosilicate ring structures (Bass and Turner, 1997). According to Böke et al., (2015), this band is associated with aluminosilicate species that contain a silicon centre with three bridging bonds with other T atoms. The lower frequency of the bridging T-O asymmetric stretching vibration ($1076\text{-}1073\text{ cm}^{-1}$) observed after 4 hours of hydrothermal treatment compared to the T-O asymmetric stretching vibrational band (at 1263 cm^{-1}) observed after 2

hours of hydrothermal treatment is typically associated with the incorporation of aluminium atoms into the zeolite framework, as reported elsewhere (Criado et al., 2007; Mosgawa et al., 2004).

On the other hand, vibrational bands at 985-962 cm^{-1} were attributed to aluminosilicate species containing a silicon centre with two terminal T-OH bonds and two bridging bonds with other T atoms (Böke et al., 2015). These partially condensed aluminosilicate species may be due to the formation of polymeric aluminosilicate species such as secondary building units, which contain both bridging (Si-O-T) and terminal (T-OH) bonds. As hydrothermal treatment time increased the intensity of the terminal T-O asymmetric stretching band (at 985-962 cm^{-1}) decreased and the bridging T-O vibration appeared as a shoulder. This indicated the transformation of relatively small, soluble aluminosilicate species into larger aluminosilicates (such as SBUs) through condensation reactions, as depicted in Section 4.5, Figure 4.5. These larger aluminosilicate species then served as precursors for the formation of zeolites. The asymmetric stretching band at 985-962 cm^{-1} therefore serves as an indication of the degree of polymerisation in the zeolite material as hydrothermal time increased.

Compared to the vibrational spectrum of the freeze-dried clear FFA extract depicted in Figure 5.7, the bending vibration of T-O bonds appeared at a lower vibration (431-422 cm^{-1}) in washed Na-zeolite products while the band at 477 cm^{-1} (observed in Figure 5.7) was not observed in Figure 5.9. This indicates that the band observed at 431-422 cm^{-1} is a zeolite framework-specific band. The bending vibrational band of T-O bonds which appeared at 477 cm^{-1} in the clear FFA extract may therefore be attributed to non-framework species (such as soluble silicate and/or aluminosilicate species).

The symmetric stretching band of Si-O-T bonds at 678-660 cm^{-1} observed in washed Na-zeolites is thought to be a zeolite framework-specific band since it did not appear in the vibrational spectrum of the clear FFA extract. However, a vibrational band appeared at 826 cm^{-1} , in the vibrational spectra of clear FFA extract, which was attributed to the symmetric stretching of Si-O-Si bonds. The band at 826 cm^{-1} is therefore thought to be associated with soluble silicate and/or aluminosilicate species in the clear FFA extract. Furthermore, the asymmetric stretching vibrational band observed at 985-962 cm^{-1} in washed Na-zeolites, attributed to relatively more condensed silicate and/or aluminosilicate species, was not observed in the clear FFA extract. This was as expected since the band at 985-962 cm^{-1} is related to the aluminosilicate species in the zeolite framework and is therefore thought to be a zeolite framework-specific band.

On the other hand, vibrational spectra of washed Na-zeolites (depicted in Figure 5.9) were very similar to that of unwashed Na-zeolites depicted in Figure 5.8, with a few notable differences. Firstly, the vibrational band corresponding to the Si-O-T bending mode ($431\text{-}422\text{ cm}^{-1}$) in the spectra of washed Na-zeolites (observed in Figure 5.9) was relatively more intense compared to the bending Si-O-T band in the spectra of unwashed Na-zeolites (observed in Figure 5.8). In the vibrational spectra of unwashed Na-zeolites, a vibrational band attributed to symmetric stretching of Si-O-Si bonds was observed at $886\text{-}883\text{ cm}^{-1}$ which was absent in the vibrational spectra of washed Na-zeolites, as depicted in Figure 5.9. This band was also present in the vibrational spectra of the clear FFA extract at 877 cm^{-1} , as depicted in Figure 5.7. This confirms that the band observed at $886\text{-}883\text{ cm}^{-1}$ is due to small, soluble silicate anions present in the synthesis solution during hydrothermal treatment. The presence of the shoulder band at $1076\text{-}1073\text{ cm}^{-1}$ in washed Na-zeolites, attributed to highly condensed silicate and/or aluminosilicate species, was not observed in the vibrational spectra of unwashed Na-zeolites, which may be due to overlapping of asymmetric stretching vibrational bands in this region.

The presence of zeolite SBUs was also observed between 800 and 500 cm^{-1} in the spectra of washed Na-zeolites, as depicted in Figure 5.9 (Criado et al., 2007; Mozgawa et al., 2011). SBU composition of Na-zeolites varied as hydrothermal time was increased. Assignment of SBU vibrational bands in Na-zeolites, observed at different time periods during stirred hydrothermal treatment at $90\text{ }^{\circ}\text{C}$, were summarised in Table 5.8.

Table 5.8: Type of secondary building units observed by FTIR at different time periods during stirred hydrothermal treatment at $90\text{ }^{\circ}\text{C}$.

Hydrothermal time (hours)	4-8	10-16
Secondary Building Unit (SBUs observed by FTIR)	<p>D6R (characteristic of zeolite X)</p> <p>S4R (characteristic of zeolite P, found in zeolite X and hydroxysodalite)</p>	<p>D6R (characteristic of zeolite X)</p> <p>S4R (characteristic of zeolite P, found in zeolite X and hydroxysodalite)</p> <p>S6R (found in zeolite X, P and hydroxysodalite)</p>

The vibrational band observed at 586-562 cm^{-1} was attributed to vibrations of the D6R structural unit (Criado et al., 2007; Mozgawa et al., 2011). D6R units, which are characteristic of zeolite X, were observed for the entire hydrothermal time range (2-16 hours) investigated. Other vibrational bands, corresponding to the S4R (735-718 cm^{-1}) and S6R (608-593 cm^{-1}) structural units, were also observed for washed Na-zeolites, as illustrated in Figure 5.9, indicating the formation of other zeolites phases such as zeolite P1 and/or hydroxysodalite. The characteristic vibrational band of zeolite P1 (S4R band) was observed after 4 hours of hydrothermal synthesis while the vibrational band of the S6R unit was observed after 10 hours. While the S4R unit is associated with zeolite P1, both S4R and S6R units may also be assigned to the zeolite X or hydroxysodalite framework (Mozgawa et al., 2011). S4R and S6R units observed in the vibrational spectra of Na-zeolites indicated the crystallisation of zeolite X occurred together with zeolite P1 and/or hydroxysodalite. It should be noted that the S4R band became weaker (appeared as a shoulder band) as hydrothermal time increased, indicating the preferential formation of Na-X between 10 and 16 hours of hydrothermal treatment.

Zeolite X is a metastable aluminosilicate which may transform into more dense phases with time. Zeolite X is composed of D6R units and β -cages (Criado et al., 2007; Mozgawa et al., 2011) which recrystallises with time to form the thermodynamically more stable and dense P1, according to Ostwald's law of successive transformations (Davis and Lobo, 1992). The transformation of clear FFA extract samples under stirred hydrothermal conditions (at 90 °C) resulted in the co-crystallisation of zeolite X and P1, while preferential formation of zeolite X was observed between 10-16 hours of hydrothermal treatment. FTIR results were in good agreement with XRD data depicted in Figure 5.6. It is therefore proposed that the formation of crystalline zeolite X with hierarchical morphology, between 10 and 16 hours of hydrothermal treatment, is linked to the presence of zeolite P1 building units intergrown with the zeolite X framework.

FTIR analysis of freeze-dried supernatant samples was then carried out to determine the type of species present in solution after different periods of hydrothermal treatment. Supernatant samples were freeze-dried prior to FTIR analysis as described in Section 3.4.4. Vibrational spectra of freeze-dried supernatant samples are depicted in Figure 5.10.

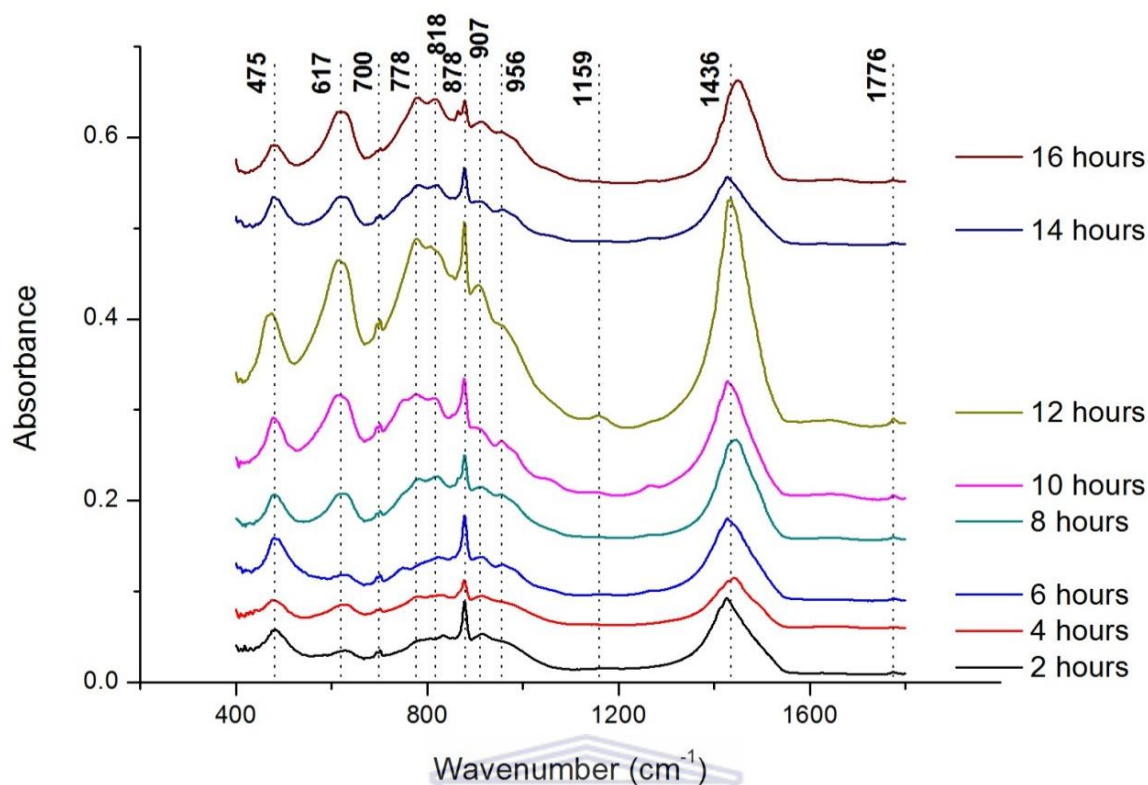


Figure 5.10: FTIR spectra (wavenumber range 2000-400 cm^{-1}) of freeze-dried supernatant samples collected at different hydrothermal time periods.

As observed in Figure 5.10, FTIR vibrational spectra of freeze-dried supernatant samples are similar to the vibrational spectrum of the freeze-dried clear FFA extract depicted in Figure 5.7. Vibrational spectra of freeze-dried supernatant samples contained vibrations of aluminosilicate species (1159-475 cm^{-1}) as well as calcium carbonate species (1436 and 1776 cm^{-1}). The vibrational band observed at 475 cm^{-1} was associated with bending vibrations of T-O bonds. Asymmetric stretching vibrations were observed at 907-878 cm^{-1} (relatively less condensed aluminosilicate species), 956 cm^{-1} and 1159 cm^{-1} (relatively more condensed aluminosilicate species). As reported previously, the band at 878 cm^{-1} may also be associated with the bending T-OH vibrations.

Vibrational bands were also observed in the IR range corresponding to secondary building units of zeolites. FTIR spectra of freeze-dried supernatant samples in the wavenumber range of 800-400 cm^{-1} are depicted in Figure 5.11, to illustrate vibrations corresponding to SBUs more clearly.

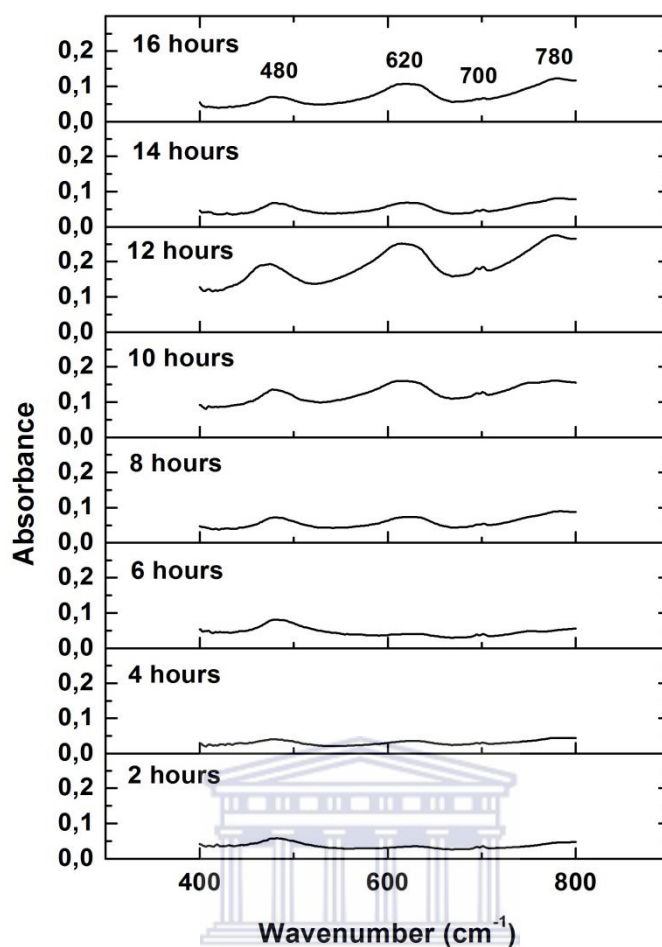


Figure 5.11: FTIR spectra (wavenumber range 800-400 cm^{-1}) of freeze-dried supernatant samples collected at different hydrothermal time periods.

The band associated with vibrations of S6R units was observed at 620 cm^{-1} , while the vibrational band characteristic of zeolite P1 (S4R band) was observed at 702 and 780 cm^{-1} , as depicted in Figure 5.11. The band associated with vibrations of S6R units was present throughout the investigated hydrothermal period. The intensity of the S6R band varied with hydrothermal time; increased intensity was observed between 8 and 16 hours of hydrothermal period. However, in the initial stages of hydrothermal treatment this peak was very weak. This may be due to the linkage of two S6R units through condensation reactions of terminal T-OH bonds to form D6R linkages in the initial stages of hydrothermal treatment. These D6R linkages connect β -cages together to form the zeolite X framework (Balkus and Ly, 1991; Shigemoto et al., 1995). These results correspond to the FTIR results of washed Na-zeolites, depicted in Figure 5.9, which indicated that zeolite X was preferentially formed between 10 and 16 hours of hydrothermal treatment.

On the other hand, the S4R vibration was present as a weak band in supernatant samples, indicating its availability to be incorporated into the zeolite framework either as part of β -cages for the zeolite X framework or as building units for the zeolite P1 framework. This further confirms the crystallisation of zeolite P1 together with zeolite X, as was observed by XRD illustrated in Figure 5.6.

Compared to the vibrational spectrum of the freeze-dried clear FFA extract depicted in Figure 5.7, the vibrational spectra of freeze-dried supernatant samples was the same with the exception of a very weak band at 956 cm^{-1} observed after 10 hours of hydrothermal treatment. Typically, this band is associated with silicate/aluminosilicate species containing a silicon centre connected to two other T atoms via an oxo-bridge. These silicate/aluminosilicate species are typically present as three-dimensional ring structures as reported by Bass and Turner, (1997) that serve as precursors for zeolite synthesis. The relatively weak intensity (or absence) of this band in the freeze-dried supernatant samples during the hydrothermal period investigated is thought to be due to the incorporation of these species into the solid zeolite framework. Furthermore, the presence of SBUs in the freeze-dried supernatant samples (such as S4R and S6R units) indicates that aluminosilicate species initially present in the clear FFA extract were not completely converted to solid zeolite products.

Compared to the vibrational spectra of the washed Na-zeolites depicted in Figure 5.9, the main difference in the vibrational spectra of supernatant samples was the presence of the bending T-O vibrational band at a relatively higher wavenumber (475 cm^{-1}), the symmetric stretching T-O vibrational band at 818 cm^{-1} and the asymmetric stretching T-OH band of small, soluble silicate species at 878 and 907 cm^{-1} . These bands were not present in the vibrational spectra of Na-zeolite products. The vibrational spectra of freeze-dried supernatant samples therefore exhibited vibrational bands of the soluble species present in the synthesis solution during the hydrothermal treatment.

Typically, the transformation of coal fly ash to zeolites occurs as follows; (1) the depolymerisation and dissolution of silicon and aluminium from coal fly ash, (2) condensation reactions involving silicate and aluminate ions which yield an amorphous aluminosilicate gel and (3) crystallisation from an amorphous aluminosilicate gel which results in the formation of a crystalline zeolite product (Murayama et al., 2002). In the transformation of a clear FFA extract to zeolites, the depolymerisation and dissolution step occurred during the alkali-activated fusion and extraction processes. The clear FFA extract

therefore contained small, soluble silicate and aluminosilicate species as well as small SBUs, as depicted in Figure 5.7, which served as precursor species for zeolite synthesis. Further condensation reactions between these small, soluble precursor species yielded the relatively larger, aluminosilicate precursor species. The crystallisation of aluminosilicate precursor species during hydrothermal treatment resulted in a crystalline zeolite product. Hydrothermal treatment of clear FFA extract samples at 90 °C resulted in solid products composed of both zeolite X and P1.

The vibrational spectra of Na-zeolite products contained bands corresponding to zeolite framework-specific species, while supernatant samples contained vibrational bands of the soluble species present in the synthesis solution after hydrothermal treatment. The crystallisation of zeolite X with hierarchical morphology was observed between 10 and 16 hours of hydrothermal treatment, in the presence of zeolite P1. When similar synthesis conditions give rise to two different zeolite phases, structural defects may occur which result in crystal intergrowth or stacking faults (McCusker and Baerlocher, 2007). In this study, the crystallisation of zeolite X with hierarchical morphology was observed in the presence of zeolite P1 building units (SBUs such as S4R and S6R units). These secondary building units may have been incorporated into the zeolite X framework causing either stacking faults or crystal intergrowth to occur, which may have resulted in the formation of the intergrown, platelet-like crystals described as hierarchical zeolite X. The hierarchical morphology of zeolite X is therefore proposed to be linked to the presence of zeolite P1 building units intergrown into the zeolite X framework.

Although this study provided valuable information regarding the transformation of a clear FFA extract to zeolite products with time, further characterisation of hierarchical zeolite X was required to gain more insight into the formation of this particular zeolite from a clear FFA extract.

5.3 Chapter Summary

The effect of hydrothermal synthesis parameters (such as hydrothermal temperature and time, agitation) on hierarchical zeolite X formation were investigated in this chapter. The effect of hydrothermal temperature, time and static synthesis was carried out using a molar formulation $0.12 \text{ Al} \cdot 14.6 \text{ Na} \cdot 1.00 \text{ Si} \cdot 163 \text{ H}_2\text{O}$, without additional sources of silicon or aluminium. Hydrothermal temperature, investigated in the range from 70 to 94 °C for 24 hours, was found to influence both the crystallinity and morphology of synthesised zeolites. As the hydrothermal temperature increased, the zeolite X hierarchical morphology changed (i.e. platelet thickness increased). Hydrothermal treatment was then carried out under static conditions (90°C, 24 hours) to determine the effect of stirring on the formation of hierarchical zeolite X. Zeolite Na-X was favourably formed under static conditions, while zeolite Na-P1 was formed under stirred conditions. This was attributed to enhanced crystallisation kinetics under stirred hydrothermal conditions, which caused the rapid transformation of zeolite Na-X to Na-P1 according to Ostwald's law of successive transformations.

The effect of hydrothermal time on hierarchical zeolite X crystallinity was therefore investigated under stirred conditions at a 90 °C. This study revealed that zeolite Na-X with hierarchical morphology was most favourably formed between 12 and 16 hours of stirred hydrothermal treatment at 90 °C. However, zeolite Na-X crystallised together with Na-P1 as a minor phase. This was proposed to be due to molar composition of the synthesis solution used in this study that was on or close to the boundary region for zeolite Na-X and Na-P1, under the hydrothermal conditions investigated. The transformation of a clear FFA extract ($0.12 \text{ Al} \cdot 14.6 \text{ Na} \cdot 1.00 \text{ Si} \cdot 163 \text{ H}_2\text{O}$) under stirred hydrothermal conditions (at 90 °C) was therefore monitored by FTIR analysis for the hydrothermal time range of 2 to 16 hours. The presence of small, soluble silicate and aluminosilicate species was observed in the spectra of freeze-dried clear FFA extract and supernatant samples, while framework-specific species were observed in the spectra of solid zeolite products. The soluble silicate and aluminosilicate species in solution were thought to undergo condensation reactions which yielded aluminosilicate precursors (D6R units) for incorporation into the zeolite X framework, most favourably between 10 and 16 hours of hydrothermal treatment. The formation of zeolite X with hierarchical morphology was linked to the presence of zeolite P1 structural units intergrown into the framework of zeolite X. The crystallisation of zeolite Na-P1 as a minor phase together with zeolite Na-X was thought to be due to the Si/Al ratio of the synthesis solution.

The influence of molar regime adjustment on the formation of hierarchical zeolite X

6 Introduction

The study on the effect of hydrothermal time on the crystallisation of zeolite X illustrated that this zeolite was most favourably formed between 12 and 16 hours of hydrothermal treatment at 90 °C under the applied synthesis conditions. However, zeolite Na-X crystallised together with traces of Na-P1 and hydroxysodalite. The crystallisation of zeolite Na-P1 together with zeolite Na-X may have been as a result of the relatively high Si/Al molar ratio (8.6) of the synthesis solution. The effect of Si/Al ratio on the formation of hierarchical zeolite X was therefore the next synthesis parameter investigated. This chapter will focus on the effect of Si/Al ratio and Al source on the yield, formation and morphology of hierarchical zeolite X. The effect of Si/Al molar ratio on the formation of hierarchical zeolite X was investigated using aluminium hydroxide (or sodium aluminate) as an additional source of aluminium under stirred hydrothermal conditions (90 °C, 16 hours). Characterisation of synthesised zeolites by SEM-EDS and XRD analysis will be presented. The characterisation of selected hierarchical zeolites by analytical techniques such as XRF, LA-ICP-MS, HR-TEM, FTIR, nitrogen physisorption and titrimetric acidity determination will also be discussed.

6.1 The effect of Si/Al ratio on hierarchical zeolite X formation

The process of zeolite formation is influenced by many factors such as molar composition of the synthesis mixture, sources of reactants, Si/Al ratio, system alkalinity, and water content (Feijen et al., 1994; Shoumkova and Stoyanova, 2013; Yu, 2007). Zeolite composition and morphology are influenced by the Si/Al ratio of the initial synthesis solution. The influence of Si/Al ratio on the formation of zeolite Na-X from coal fly ash has been reported in literature (Chang and Shih, 2000; Shigemoto et al., 1993). Musyoka, (2012) synthesised hierarchical zeolite X from a clear fused fly ash extract and investigated the effect of hydrothermal temperature and ageing on the formation of hierarchical zeolite X. However, Musyoka, (2012) did not report the effect of Si/Al ratio on the formation of this zeolite. Therefore, the effect of Si/Al molar ratio (of the synthesis solution) on the formation of hierarchical zeolite X was investigated in this study. The Si/Al molar ratio of the synthesis solution was varied by the addition of different amounts of anhydrous aluminium hydroxide to clear FFA extract solutions, as described in Section 3.3.1.3 and Table 3.3. The elemental composition of resultant solutions were analysed by ICP-OES and normalised by setting the

Chapter 6

moles of Si = 1, as described in Appendix B. The calculated and measured Si/Al molar ratios of synthesis solutions are summarised in Table 6.1.

Table 6.1: Variation of Si/Al molar ratio of synthesis solution by addition of different quantities of aluminium hydroxide to clear FFA extract solutions.

Code	Synthesis solution						
	Initial Si (mol)	Initial Al (mol)	Additional Al (mol)	Total Al (mol)	Si/Al molar ratio (calculated)	Si/Al molar ratio	Total Na (mol)
							Determined by ICP-OES (n=3)
C6	1	0.116	0	0.116	8.6	8.6	14.6
D1	1	0.116	0.006	0.122	8.2	8.4	16.2
D2	1	0.116	0.021	0.137	7.3	7.6	18.8
D3	1	0.116	0.044	0.160	6.2	6.7	19.2
D4	1	0.116	0.070	0.186	5.4	5.8	20.1
D5	1	0.116	0.197	0.313	3.2	3.4	20.3

The Si/Al molar ratio of the synthesis solutions, determined by ICP-OES, was similar to the calculated Si/Al molar ratio values (listed in Table 6.1). The percentage standard deviation was calculated, as shown in Appendix A, for aluminium and silicon. The percentage standard deviation ranged between 0.1 and 5.0% for aluminium and 0.2 and 3.1% for silicon; which was relatively low. However, samples D3 and D4 had a slightly higher Si/Al molar ratio (as determined by ICP-OES) than the calculated value. This may have been due to experimental errors during the addition of aluminium source to the clear FFA extract samples or during the preparation of the ICP-OES sample and/or due to instrument errors. The apparent increase in the Na content was unexpected and may have been due to experimental errors (during the preparation of ICP-OES samples), instrumental errors and/or errors arising due to the normalisation of the molar composition by setting Si=1.

Resultant synthesis solutions were then subjected to magnetically stirred hydrothermal conditions of 90°C for 16 hours (at 300 rpm). Zeolite synthesis experiments were carried out at a hydrothermal time of 16 hours due to the relatively high crystallinity of zeolite X. Solid products obtained after hydrothermal synthesis were white in colour. The mass of solid products were measured and the yield (mass %) of selected zeolite products (see XRD for

Chapter 6

confirmed phase) were calculated based on the amount of fly ash used and the total Si and Al content available in the fly ash feedstock (determined by XRF spectroscopy, presented in Table 4.1) to be converted to a zeolite product. In cases when an additional reagent was used (such as aluminium hydroxide in the calculated example below), this was incorporated into the total of Si and Al available. The yield of zeolite product for samples C6 and D1-D5 are presented in Table 6.2.



Chapter 6

Table 6.2: The calculation of zeolite yield (mass %) from coal fly ash, using aluminium hydroxide as an additional Al source

Code	Total SiO ₂ available in feedstock (determined by XRF)	Total Al ₂ O ₃ available in feedstock (determined by XRF)	Mass of Fly ash used	Mass of SiO ₂ in feedstock	Mass of Al ₂ O ₃ in feedstock	Mass of Si in feedstock	Mass of Al in feedstock	Total Si and Al in feedstock	Mass of additional Al source	Mass of zeolite	Yield of zeolite
	mass %		grams								mass %
C6									0	0.705	5.2
D1									0.008	0.745	5.5
D2	51.51	24.73	36.36	18.73	8.99	8.76	4.77	13.52	0.027	0.827	6.1
D3									0.059	1.070	7.9
D4									0.093	1.158	8.5
D5									0.263	1.750	12.7



The yield of zeolite product without any additional aluminium source was very low (5.2 mass %), as discussed previously in Section 5.1.1. As presented in Table 6.2, the yield (mass %) of zeolite product (sample D5) increased from 5.2 mass % to 12.7 mass %, by adding 0.263 g of Al (in the form of aluminium hydroxide) to the clear FFA extract prior to hydrothermal synthesis. The increased yield of zeolite product was attributed to the increased utilisation of silicon in the feedstock, in the presence of additional aluminium, to form the zeolite framework. The yield of zeolite product increased as the amount of additional aluminium into the system was increased (for samples D1 to D5), as listed in Table 6.2. This further confirms that the initially low aluminium content used in the clear FFA extract limited the conversion of fly ash to zeolites and resulted in the low yield of zeolite product.

According to the principles of green chemistry outlined in Chapter 2, the use of an efficient atom economy was not fully achieved in the conversion of a clear FFA extract (without additional reagents) to hierarchical zeolite X. However, the addition of small quantities of an extra aluminium source was proven to enhance the yield of zeolite product (almost three-fold) in this study. Furthermore, the use of secondary substances (such as structure-directing agents) for the formation of a hierarchical zeolite material was avoided using this simple synthesis route.

Synthesised Na-zeolites were characterised by SEM-EDS and XRD analysis. The effect of Si/Al molar ratio on the morphology of hierarchical zeolite X was determined by SEM analysis. SEM micrographs of Na-zeolites prepared from synthesis solutions with different Si/Al molar ratios (achieved by the addition of anhydrous aluminium hydroxide to the clear FFA extract) are depicted in Figure 6.1.

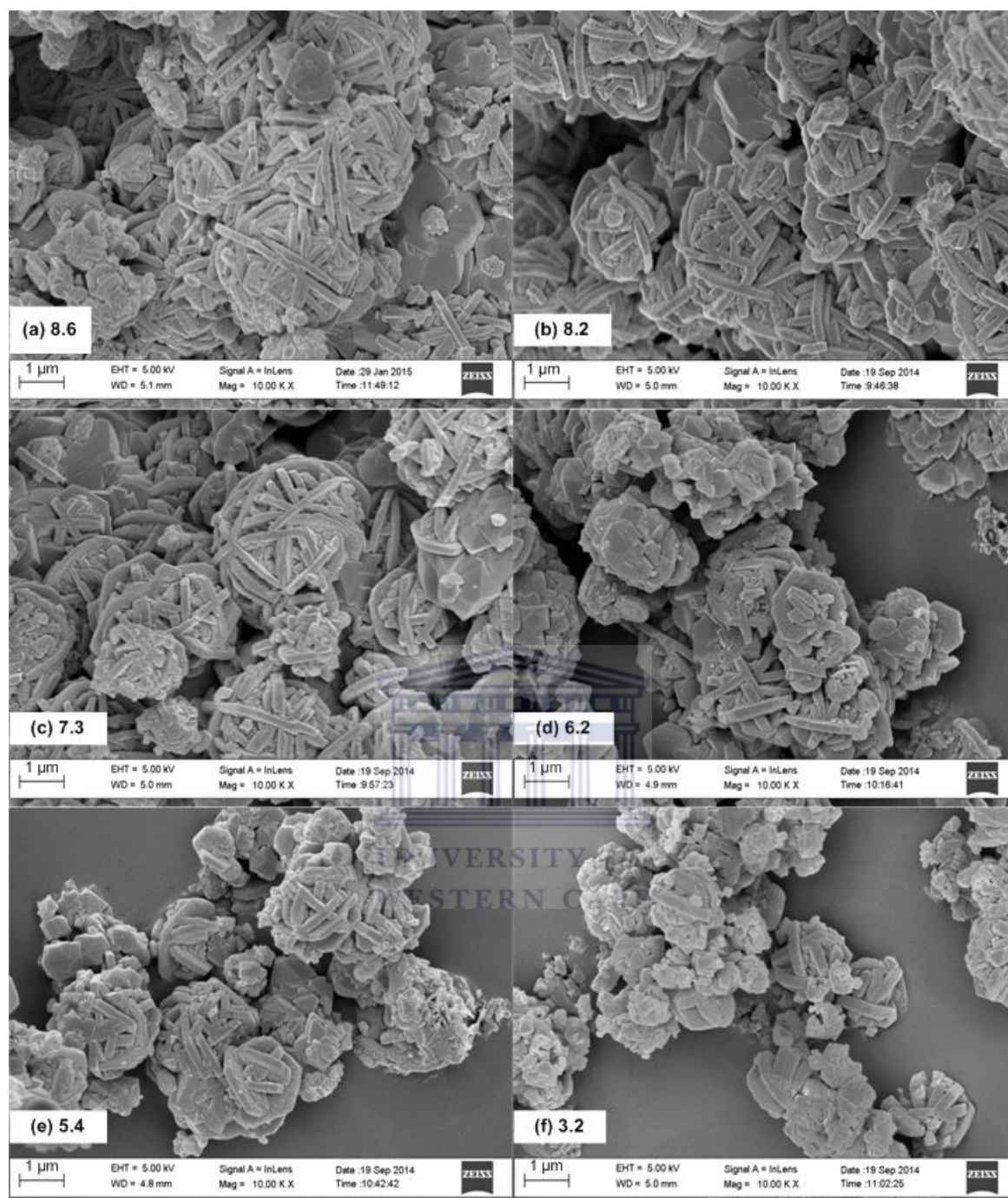


Figure 6.1: SEM micrographs (10 000X magnification) of Na-zeolites synthesised under stirred hydrothermal conditions at a temperature of 90 °C for 16 hours at different Si/Al molar ratios (achieved by addition of aluminium hydroxide to the synthesis mixture).

The disc-like crystal morphology of zeolite X was observed as ball-like aggregates at relatively high Si/Al molar ratios, as depicted in Figure 6.1 (a)-(c). These disc-like platelets are formed due to the preferential growth of the crystal in a particular direction or the suppression of growth of particular crystal faces. Small quantities of agglomerated octahedral crystals, characteristic of zeolite X, were also observed. At relatively low Si/Al molar ratios,

Chapter 6

agglomerated octahedral crystals were observed together with fewer disc-like crystals, as depicted in Figure 6.1 (d)-(f). It is noteworthy that at relatively low Si/Al molar ratios, disc-like crystals were not formed in the ball-like aggregated manner, which is characteristic of zeolite X with hierarchical morphology. The formation of hierarchical zeolite crystals was therefore suppressed at relatively low Si/Al molar ratios.

The average particle size of Na-zeolites was determined using SEM micrographs. The dimensions of several particles were measured using Image J software and results were used to calculate the average particle size in terms of length (l) and width (w). The average particle size, Si/Al and Na/Al (wt %) ratio of Na-zeolites synthesised at different Si/Al molar ratios, under stirred hydrothermal conditions of 90°C for 16 hours, is summarised in Table 6.3. The Si/Al and Na/Al (wt %) ratio of synthesised Na-zeolites were determined using EDS analysis. The calculated Si/Al molar ratio of the synthesis solutions and zeolite phases determined by XRD is also presented in Table 6.3.

Table 6.3: Summary of properties of Na-zeolites synthesised at different Si/Al molar ratios (achieved by addition of aluminium hydroxide to the synthesis mixture), under stirred hydrothermal conditions at 90 °C for 16 hours.

Code	Parameter investigated: Si/Al molar ratio of synthesis solution	Zeolite phases (determined from XRD)	Si/Al wt % ratio of Na-zeolite product	Na/Al wt % ratio of Na-zeolite product	Other cations present in Na-zeolite product	Average Particle Size l, w (nm)
C6	8.6	X, S, P	1.3	0.8	Ca	1129, 162
D1	8.2	X, S, P	1.2	0.8	-	1332, 170
D2	7.3	X, S	1.3	0.7	-	1512, 153
D3	6.2	X, S	1.2	0.8	-	1219, 168
D4	5.4	X, S	1.3	0.7	-	1394, 170
D5	3.2	X, S	1.2	0.8	-	1242, 220

X-zeolite X, P-zeolite P1, S-hydroxysodalite; l-length, w-width

The Si/Al ratio of synthesised Na-zeolites was between 1.2 and 1.3 as determined by EDS, which falls in the Si/Al range characteristic of zeolite X (1.0-1.5) (Payra and Dutta, 2003; Yu, 2007). The Si/Al molar ratio of the synthesis solution did not have a significant effect on the

Si/Al ratio of synthesised Na-zeolites. The Na/Al ratio of Na-zeolites ranged from 0.7 to 0.8 which suggests that other cations (such as Ca detected by EDS) may serve as counter-ions in the zeolite framework. Although, the addition of aluminium to the synthesis solution did not have an effect on the Si/Al ratio of the zeolite product, the Si/Al molar ratio of the synthesis solution influenced the morphology of zeolite crystals, as depicted in Figure 6.1 and shown in Table 6.3. A decrease in Si/Al molar ratio in the synthesis solution did not have a significant effect on the average particle size of zeolite X crystals. Therefore, decreasing the Si/Al molar ratio (by addition of an aluminium source) did not cause a significant change in zeolite properties such as Si/Al framework ratio or particle size. However, an increase in the width of the hierarchical zeolite X crystals from 162 nm to 220 nm was observed as the Si/Al molar ratio of the synthesis solution was decreased. Platelet broadening was observed in relatively low Si/Al molar ratio synthesis environments, which may be due to enhanced crystal growth along the crystal face responsible for crystal broadening.

XRD diffractograms depicted in Figure 6.2 represent Na-zeolites prepared from synthesis solutions with different Si/Al molar ratios; peaks annotated by S represent hydroxysodalite, P represents zeolite Na-P1 and dotted lines annotated by X represents zeolite Na-X.

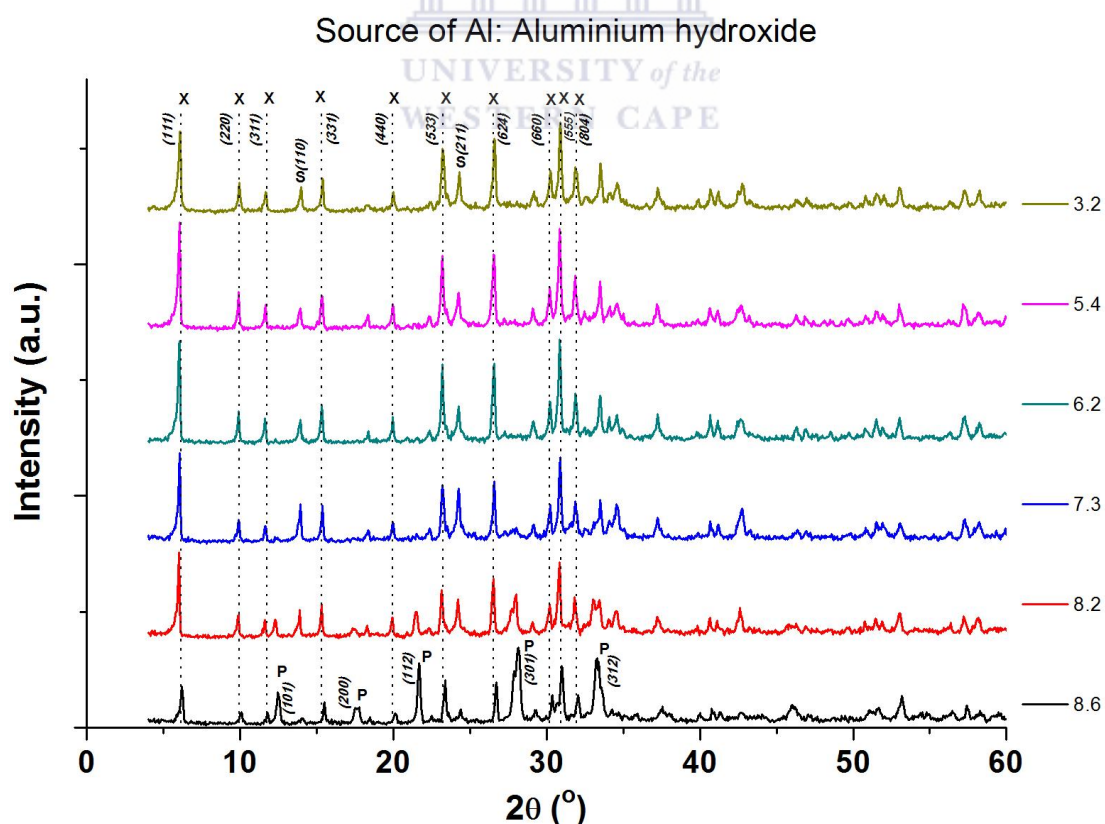


Figure 6.2: XRD diffractograms of Na-zeolites synthesised under stirred hydrothermal conditions at a temperature of 90 °C for 16 hours at different Si/Al molar ratios (achieved by addition of aluminium hydroxide to the synthesis mixture).

Zeolite X crystallised as the major phase when the Si/Al molar ratio of the synthesis solution was between 8.2 and 3.2. The crystallinity of zeolite Na-X increased as the Si/Al molar ratio decreased, up to 5.4. A decrease in Si/Al molar ratio of the synthesis solution also resulted in a decrease in the peak intensity of zeolite Na-P1 reflections up to 7.3, at which point major zeolite Na-P1 reflections were no longer observed by XRD. Two other peaks, associated with hydroxysodalite, were observed in the diffractograms of zeolite Na-X at 2θ values of 14° and 24° , as depicted Figure 6.2. In the absence of additional aluminium, as for sample C6 with Si/Al molar ratio 8.6, both zeolite Na-X and Na-P1 crystallised together; hydroxysodalite reflections were also observed.

Under the synthesis conditions investigated in this study, the crystallisation of a particular zeolite phase was found to be dependent on the Si/Al molar ratio of the synthesis solution. The presence of additional aluminium caused an increase in the crystallinity of zeolite X and stimulated the growth of zeolite X crystals in the direction that caused platelet broadening. At relatively high Si/Al molar ratios (~ 8.6), zeolite Na-P1 formed as a major phase together with zeolite Na-X while at relatively lower Si/Al molar ratios (≤ 8.2) zeolite Na-X crystallised as the major phase. However, no pure zeolite Na-X phase was synthesised. Comparing the morphology of synthesised Na-zeolites (presented in Figure 6.1) to the XRD diffraction patterns of the Na-zeolites (presented in Figure 6.2), it is noteworthy that zeolites with hierarchical morphology were observed in the presence of mixed phase zeolites containing the mineral phases X, P1 and hydroxysodalite. On the other hand, the zeolite with the least hierarchical morphology contained the mineral phases X and hydroxysodalite. This illustrates that the hierarchical morphology observed was due to the intergrowth of zeolite X with other mineral phases such as zeolite P1.

Based on this study, it may therefore be concluded that the hierarchical zeolite X morphology is favourably formed in relatively high Si/Al (aluminium-deficient) synthesis environments due to the presence of zeolite P1, while the typical octahedral morphology of zeolite X is preferentially formed in relatively low Si/Al (aluminium-enriched) environments. The Si/Al molar ratio of the synthesis solution therefore not only influenced the type of zeolite phase which crystallised but also played a crucial role in determining the morphology of zeolite crystals, particularly in the case of hierarchical zeolite X. This study therefore revealed that hierarchical zeolite X crystallises under a defined set of conditions (in terms of Si/Al molar ratio of the synthesis solution). The adjustment of the Si/Al molar ratio of the synthesis solution illustrated two other important factors. Firstly, the additional of a small amount of

extra aluminium source enhanced zeolite X crystallisation and zeolite yield increased almost three-fold. Secondly, the degree of mesoporosity of the zeolite material was varied by adjusting the Si/Al ratio of the synthesis solution.

Other researchers have reported that Si/Al ratio of the synthesis solution influenced the type of zeolite phase that crystallised (Chang and Shih, 2000; Shigemoto et al., 1993). In these studies, zeolite X with typical octahedral morphology crystallised from a slurry of fused fly ash without the addition of extra reagents (Chang and Shih, 2000; Shigemoto et al., 1993). Shigemoto et al., (1993) reported that, under the synthesis conditions studied, decreasing the Si/Al ratio resulted in the preferential formation of zeolite A over zeolite X. Chang and Shih, (2000) studied the effect of Si/Al ratio on zeolite A formation by the addition of aluminium hydroxide to a slurry of fused fly ash and reported similar findings as Shigemoto et al., (1993). Under the hydrothermal conditions studied by Chang and Shih, (2000) and Shigemoto et al., (1993), either zeolite A or X crystallised depending on the Si/Al ratio of the synthesis solution. In this study, the presence of additional aluminium was found to enhance the crystallisation of octahedral zeolite X from a clear FFA extract. Musyoka, (2012) reported the synthesis of hierarchical zeolite X from the clear FFA extract with a Si/Al molar ratio of 8.3. The correlation between Si/Al molar ratio of the synthesis solution and the hierarchical morphology of zeolite X was however not reported in the study by Musyoka, (2012).

6.2 The effect of aluminium source on hierarchical zeolite X formation

Zeolite synthesis is known to be influenced by many factors, one such factor being the source of reactants (Feijen et al., 1994; Shoumkova and Stoyanova, 2013). The main constituents of zeolites are aluminium and silicon, the sources of these reactants play an important role in zeolite synthesis (Shigemoto et al., 1993; Yu, 2007). The level of solubility and reactivity varies between different reactant sources. In the case of zeolite synthesis, the availability and nature of polysilicate and aluminosilicate species plays a vital role in the processes of nucleation and crystal growth (Yu, 2007). Shigemoto et al., (1993) studied the effect of different silicon and aluminium sources on zeolite formation and reported that reactant sources significantly affected zeolite formation and crystallinity. Musyoka, (2012) synthesised hierarchical zeolite X from a clear fused fly ash extract. However, Musyoka, (2012) did not report the effect of the aluminium source (or Si/Al molar ratio) on the formation of hierarchical zeolite X. Therefore, the effect of aluminium source on hierarchical zeolite X formation was investigated in this study. The influence of aluminium source on the

formation of hierarchical zeolite X was carried out by addition of anhydrous sodium aluminate (instead of aluminium hydroxide) to the clear FFA extract, at different Si/Al molar ratios, as described in Section 3.3.1.3 and Table 3.3. The elemental composition of resultant solutions were analysed by ICP-OES and normalised by setting the moles of Si = 1, as described in Appendix B. The calculated and measured Si/Al molar ratios as well as the sodium (Na) content of synthesis solutions are summarised in Table 6.4.

Table 6.4: Variation of Si/Al molar ratio of synthesis solution by addition of sodium aluminate.

Synthesis solution							
Code	Initial Si (mol)	Initial Al (mol)	Additional Al (mol)	Total Al (mol)	Si/Al (calculated)	Si/Al	Total Na (mol)
						Determined by ICP-OES (n=3)	
C6	1	0.116	0	0.116	8.6	8.6	14.6
E1	1	0.116	0.006	0.122	8.2	8.6	21.1
E2	1	0.116	0.021	0.137	7.3	7.7	22.3
E3	1	0.116	0.044	0.160	6.2	6.5	22.3
E4	1	0.116	0.070	0.186	5.4	5.9	20.2
E5	1	0.116	0.197	0.313	3.2	3.3	23.4

The actual Si/Al molar ratio of the synthesis solutions, determined by ICP-OES, was similar to the calculated Si/Al molar ratio values (presented in Table 6.4). The percentage standard deviation was calculated for aluminium and silicon, as shown in Appendix A. The percentage standard deviation ranged between 1.2 and 6.4% for aluminium and 0.1 and 8.1% for silicon; which was relatively low. The elemental composition of synthesis solutions prepared using aluminium hydroxide (presented in Table 6.1) and the Si/Al ratios of synthesis solutions prepared using sodium aluminate (presented in Table 6.4) were comparable. Furthermore in the case of sodium aluminate addition, a significant increase in sodium content was observed as the amount of sodium aluminate added increased which was as expected. However, the Na content in sample E4 did not follow the trend which may be due to instrumental errors. The increase observed in this case was much higher than that observed when aluminium hydroxide was used (as listed in Table 6.1).

Chapter 6

Resultant synthesis solutions were subjected to stirred hydrothermal conditions of 90 °C for 16 hours. Synthesised Na-zeolites were characterised by SEM-EDS and XRD analysis. Solid products obtained after hydrothermal synthesis were white in colour. The mass of solid products were measured and the yield (mass %) of selected zeolite products (see XRD for confirmed phase) were as described in Section 6.1. In cases when an additional reagent was used (such as sodium aluminate in this case), the mass of additional aluminium was incorporated into the total of Si and Al available. The yield of zeolite product for samples C6 and E1-E5 are presented in Table 6.5.



Chapter 6

Table 6.5: The calculation of zeolite yield (mass %) from coal fly ash, using sodium aluminate as an additional Al source

Code	Total SiO ₂ available in feedstock (determined by XRF)	Total Al ₂ O ₃ available in feedstock (determined by XRF)	Mass of Fly ash used	Mass of SiO ₂ in feedstock	Mass of Al ₂ O ₃ in feedstock	Mass of Si in feedstock	Mass of Al in feedstock	Total Si and Al in feedstock	Mass of additional Al source	Mass of zeolite	Yield
	mass %		grams								mass %
C6									0	0,705	5,2
E1									0,008	0,748	5,5
E2	51,51	24,73	36,36	18,73	8,99	8,76	4,77	13,52	0,027	0,838	6,2
E3									0,059	1,068	7,9
E4									0,093	1,318	9,7
E5									0,263	1,898	13,8



As presented in Table 6.5, the yield (mass %) of zeolite product increased from 5.2 mass % (C6, in the absence of an additional aluminium source) to 13.8 mass % (sample E5), by adding 0.263 g of Al (in the form of sodium aluminate) to the clear FFA extract prior to hydrothermal synthesis. The yield of solid zeolite product increased as the amount of additional aluminium into the system increased (samples E1 to E5), as listed in Table 6.5. As discussed in Section 6.1, the increased yield of zeolite product was attributed to the increased utilisation of silicon in the feedstock, in the presence of additional aluminium, to form the zeolite product. Compared to aluminium hydroxide addition presented in Table 6.2 (sample D5), a slightly higher yield (13.8 mass %) was observed in the case of sodium aluminate addition (sample E5).

The effect of aluminium source (and Si/Al molar ratio) on the morphology of hierarchical zeolite X was determined by SEM microscopy. SEM micrographs of Na-zeolites synthesised at different Si/Al molar ratios, achieved by the addition of anhydrous sodium aluminate to the synthesis solution, are depicted in Figure 6.3.



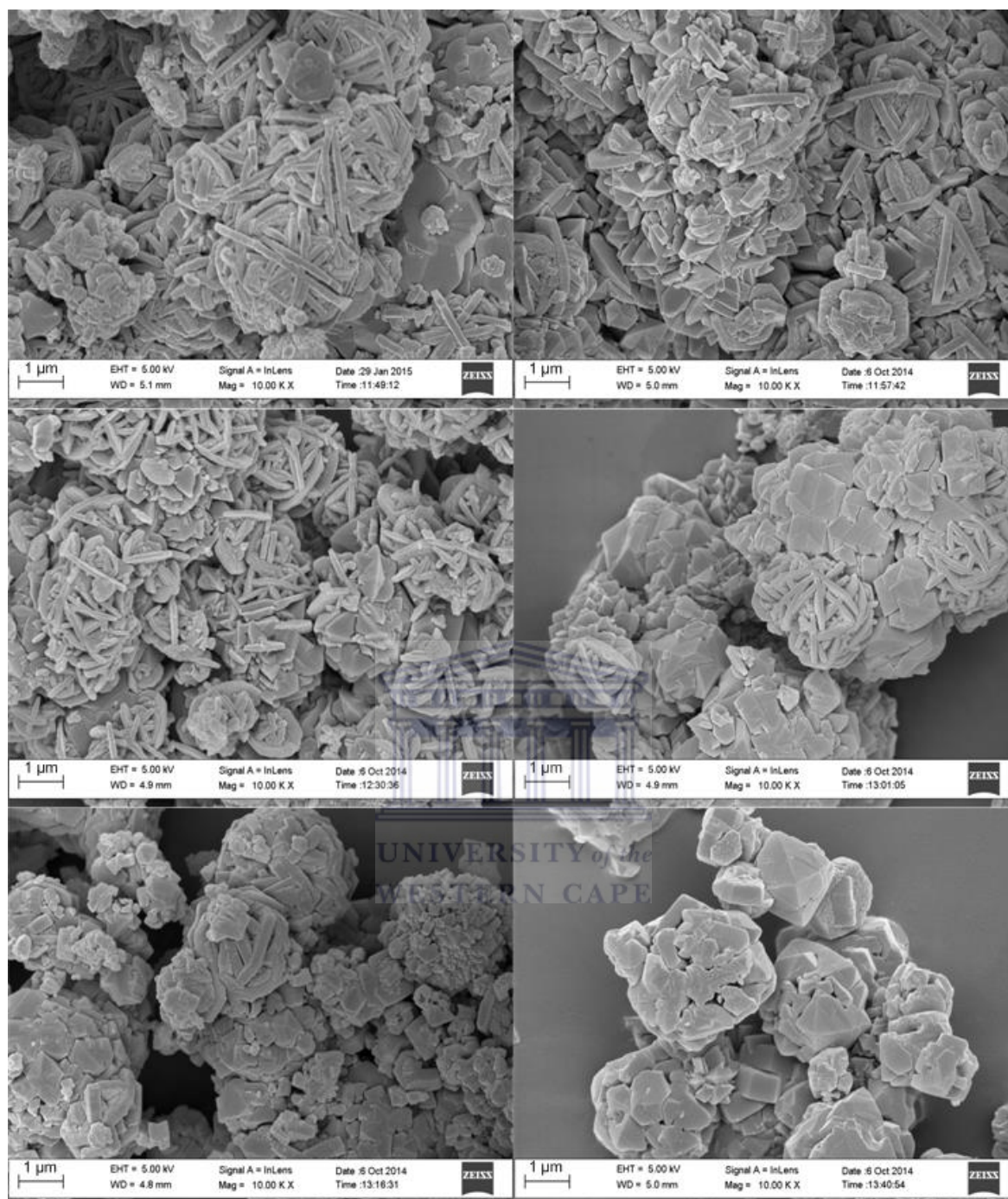


Figure 6.3: SEM micrographs (10 000X magnification) of Na-zeolites synthesised under stirred hydrothermal conditions at a temperature of 90 °C for 16 hours at different Si/Al molar ratios (achieved by addition of sodium aluminate to the synthesis mixture).

The addition of anhydrous sodium aluminate to the clear FFA extract significantly influenced the morphology of hierarchical zeolite X, as depicted in Figure 6.3. As the Si/Al molar ratio of the synthesis solution was decreased, the formation of hierarchical zeolite X platelets was suppressed. At relatively high Si/Al molar ratios aggregates of disc-like crystals were

observed, as depicted in Figure 6.3 (a)-(c), similar to the morphology of hierarchical zeolite X reported by Musyoka, (2012). At relatively low Si/Al molar ratios (>6.2), the formation of aggregated, disc-like crystals was not as prominent and agglomerated crystals with the typical zeolite X octahedral morphology was observed, as depicted in Figure 6.3 (d)-(f). Similar results were observed when aluminium hydroxide was used as the aluminium source, as depicted in Figure 6.1. Relatively low Si/Al molar ratios caused the suppression of disc-like zeolite X crystals with hierarchical morphology and resulted in the formation of octahedral shaped zeolite X crystals.

The average particle size, Si/Al and Na/Al (wt %) ratio of Na-zeolite products that had been synthesised at different Si/Al molar ratios, by adding anhydrous sodium aluminate, is summarised in Table 6.6. The calculated Si/Al molar ratio of synthesis solutions and zeolite phases determined by XRD is also presented in Table 6.6.

Table 6.6: Summary of properties of Na-zeolites synthesised at different Si/Al molar ratios (achieved by addition of sodium aluminate to the synthesis mixture), under stirred hydrothermal conditions at 90 °C for 16 hours.

Code	Parameter investigated: Aluminium source (at different Si/Al molar ratios of synthesis solution)	Zeolite phases (determined by XRD)	Si/Al wt % ratio of Na-zeolite product	Na/Al wt % ratio of Na-zeolite product	Other cations present in Na-zeolite product	Average Particle Size l, w (nm)
C6	8.6	X, S, P	1.3	0.8	Ca	1129, 162
E1	8.2	X, S, P	1.3	0.8	Ca	1237, 191
E2	7.3	X, S, P	1.3	0.8	Ca	972, 97
E3	6.2	X, S, P	1.3	0.7	K	1027, 102
E4	5.4	X, S	1.2	0.8	-	1072, 218
E5	3.2	X, S	1.1	0.8	K	1231, 467

X-zeolite X, P-zeolite P1, S-hydroxysodalite; l-length, w-width

The Si/Al ratio of synthesised Na-zeolites was between 1.1 and 1.3, as shown in Table 6.6, which was in the acceptable Si/Al range for zeolite X (Payra and Dutta, 2003; Yu, 2007).

Variation of the Si/Al molar ratio of the synthesis solution did not have a significant effect on the framework Si/Al ratio of synthesised Na-zeolite products. The Na/Al ratio of Na-zeolites was between 0.7 and 0.8, which suggests that other cations (such as Ca and/or K detected by EDS) may serve as counter-ions in the zeolite framework. With regard to the average particle size of synthesised Na-zeolites, decreasing the Si/Al molar ratio of the synthesis solution (by sodium aluminate addition) did not have a significant effect on the average particle size of the zeolite crystals. Therefore, varying the Si/Al molar ratio of the synthesis solution from 8.6 to 3.2 did not have a significant effect on zeolite properties (such as framework Si/Al ratio and particle size). However, the width of disc-like crystals was influenced by sodium aluminate addition as observed in the case of aluminium hydroxide addition. A decrease in Si/Al molar ratio from 8.6 to 3.2 resulted in a significant increase in the width of disc-like crystals from 162 nm to 467 nm. The change in particle dimensions may be as a result of the transformation of the morphology of zeolite crystals from the disc-like crystal morphology to the typical octahedral morphology, as depicted in Figure 6.3.

XRD diffractograms of Na-zeolites synthesised using different Si/Al molar ratios in the formulation (achieved by anhydrous sodium aluminate addition) are presented in Figure 6.4.

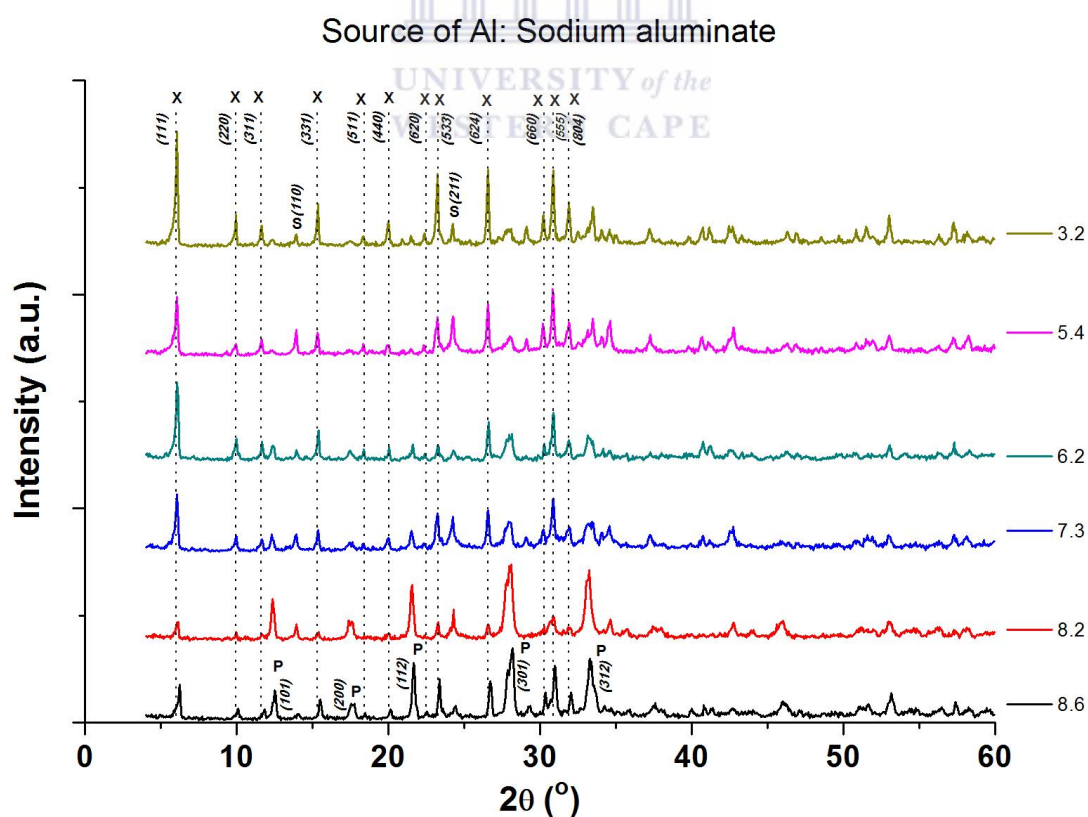


Figure 6.4: XRD diffractograms of Na-zeolites synthesised under stirred hydrothermal conditions at a temperature of 90 °C for 16 hours at different Si/Al molar ratios (achieved by addition of sodium aluminate to the synthesis mixture).

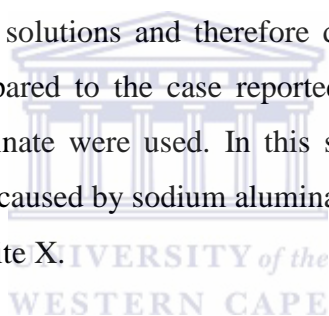
The most crystalline Na-X was formed at a relatively low Si/Al molar ratio of 3.2 using sodium aluminate as an additional Al source, as observed in Figure 6.4. However, zeolite hydroxysodalite was present as a minor phase under these conditions. At relatively high Si/Al molar ratios (8.6 and 8.2) zeolite Na-P1 crystallised as the major phase with zeolite Na-X and hydroxysodalite as minor phases. As the Si/Al molar ratio of the synthesis solution was decreased, the crystallinity of Na-X increased while Na-P1 crystallinity decreased. However, no clear trend was observed for hydroxysodalite crystallinity as Si/Al molar ratio of the synthesis solution was adjusted. The crystallisation of mixed phase zeolites (X and P1) resulted in the formation of hierarchical zeolite crystals, while crystalline zeolite X (with minor hydroxysodalite and Na-P1 peaks) resulted in the least hierarchical zeolite with octahedral morphology. The formation of hierarchical zeolite crystals is therefore proposed to be due to intergrowth of zeolite X with P1.

Although similar Si/Al molar ratios were investigated (in the case of aluminium hydroxide and sodium aluminate addition), a much lower Si/Al molar ratio (3.2) was required for the formation of relatively crystalline zeolite X in the case of sodium aluminate addition compared to aluminium hydroxide addition, as depicted in Figure 6.2 and 6.4. It is therefore proposed that aluminium hydroxide addition was more effective than sodium aluminate as an additional Al source for the crystallisation of zeolite Na-X under the hydrothermal conditions investigated. In this study, variation in Na-X crystallinity may be due to the differences in the solubility and reactivity of aluminium hydroxide compared to sodium aluminate. However, sodium aluminate and aluminium hydroxide are both soluble in basic solutions and aluminium species exist as $[\text{Al}(\text{OH})_4]^-$ anions which is a soluble, reactive ion that serves as a precursor for zeolite formation (Davis and Lobo, 1992). Therefore the difference in solubility and reactivity between these two aluminium sources is expected to be insignificant. It is noteworthy that the addition of sodium aluminate to the synthesis solutions significantly increased the amount of sodium cations available in solution (as listed in Table 6.4) to serve as charge-compensating cations, which may have influenced the crystallisation of pure zeolite Na-X. The extra sodium content may also be responsible for the enhanced formation of octahedral zeolite X crystals and inhibition of the formation of intergrown zeolite platelets, as observed in Figure 6.3.

In conclusion, aluminium hydroxide was more effective as a source of additional aluminium for the synthesis of crystalline zeolite X under the hydrothermal conditions investigated. However, the formation of hierarchical zeolite X crystals was most favourable in the presence

of other zeolite phases (such as zeolite P1) and crystallised from synthesis solutions with specific Si/Al molar ratios in the range of 8.6-7.3. The study on the influence of aluminium source on hierarchical zeolite X formation and morphology therefore revealed that the extra sodium cation content in the synthesis solution (caused by sodium aluminate addition) negatively influenced the formation of zeolite X with hierarchical morphology. The source of aluminium species therefore played an important role in the crystallisation and morphology zeolite X. However, the Si/Al molar ratio (aluminium content) of the synthesis solution had the greatest effect on the morphology of hierarchical zeolite X crystals.

Shigemoto et al., (1993) studied the effect of aluminium source (using sodium aluminate and mullite) on zeolite formation from coal fly ash. Shigemoto et al., (1993) reported that sodium aluminate improved the crystallinity of zeolite X compared to mullite. The poor crystallinity of zeolite X formed using mullite was attributed to the lower reactivity of mullite compared to sodium aluminate (Shigemoto et al., 1993). In this study however, the aluminium sources used were both soluble in basic solutions and therefore differences between sources were thought to be insignificant compared to the case reported by Shigemoto et al., (1993) in which mullite and sodium aluminate were used. In this study however, the additional Na content in the synthesis solution (caused by sodium aluminate addition) negatively influenced the formation of hierarchical zeolite X.



6.3 Further characterisation of selected hierarchical zeolite X

Selected synthesised zeolites (annotated by codes D2 and E2 as shown in Table 6.3 and 6.5, respectively) were chosen for further characterisation due to the relatively high crystallinity of zeolite X (particularly for D2) and the hierarchical morphology of the zeolite crystals. Zeolite D2 was prepared using aluminium hydroxide as an additional source of aluminium while zeolite E2 was prepared using sodium aluminate in equivalent conditions. Synthesised Na-zeolites (D2 and E2) were replicated for further characterisation by XRF, LA-ICP-MS, HR-TEM, FTIR and nitrogen physisorption. Na-zeolites (D2 and E2) were then protonated and characterised by titrimetric acidity determination.

6.3.1 Elemental Analysis by XRF and LA-ICP-MS

The elemental composition of synthesised zeolites, D2 and E2, were determined by XRF and LA-ICP-MS spectroscopy for major and trace elemental analysis, respectively, as described in Section 3.4.1. The major elemental composition of zeolites D2 and E2, determined by XRF, is listed in Table 6.7.

Table 6.7: Major elemental composition of zeolites D2 and E2 and loss on ignition (L.O.I), determined by XRF spectroscopy (n= 3).

Major Elements (oxide form)	D2 (mass %)	Relative Standard Deviation (%)	E2 (mass %)	Relative Standard Deviation (%)
SiO ₂	38.08	0.3	38.18	0.2
Al ₂ O ₃	29.17	0.2	29.17	0.1
Na ₂ O	17.89	0.7	18.08	0.2
K ₂ O	0.22	10.6	0.19	5.3
CaO	0.19	2.7	0.16	0.1
Fe ₂ O ₃	0.17	5.8	0.18	2.8
TiO ₂	0.04	13.2	0.04	13.4
L.O.I	13.37	0.7	13.19	0.5
Sum	99.12		99.19	

The major elemental composition of synthesised zeolites (D2 and E2) were analysed in triplicate (on the same sample) by XRF to determine the precision of the sample preparation procedure. As presented in Table 6.7, the relative standard deviation (RSD) of major elements (Si, Al, Na, Ca and Fe) were $\leq 5\%$ which indicated that the sample preparation

procedure was precise. In the case of elements (K and Ti), the RSD values were relatively high which may be due to the low concentration of these elements in the zeolite framework.

Synthesised zeolites (D2 and E2) were mainly composed of silicon, aluminium and sodium, as listed in Table 6.7, which was as expected. Typically, zeolites are hydrophilic materials and therefore the high L.O.I value of 13.37 and 13.19 (for D2 and E2, respectively) may be attributed to moisture in the zeolite framework since the presence of carbon in the zeolite framework is unlikely. The Si/Al molar ratio of the synthesised zeolites (D2 and E2) was calculated to be 1.1, which falls within the acceptable range for zeolite X (1.1-1.5). The Na/Al molar ratio of synthesised zeolites (D2 and E2) was calculated to be 1.0, which illustrates that sodium serves as a charge-compensating cation to all aluminium incorporated into the zeolite framework as expected. The slightly higher Na content in zeolite E2 may be due to the sodium aluminate source used during zeolite synthesis.

Other elements (such as Ca, Fe, K and Ti) were also detected by XRF spectroscopy as minor elements in the zeolite products. Cations such as calcium and potassium are also known to serve as charge-compensating cations in the zeolite framework. However, since the Na/Al molar ratio of zeolites was observed to be 1.0, these cations are therefore not present as charge-compensating cations for the zeolite framework but may be present in the framework as extra-framework species. Iron and titanium species are most likely present in the zeolite framework as extra-framework species. The trace elemental composition of zeolites D2 and E2, determined by LA-ICP-MS, is listed in Table 6.8.

Table 6.8: Trace elemental composition of zeolites D2 and E2, determined by LA-ICP-MS spectroscopy (n= 3).

Trace elements	D2 (ppm)	Relative Standard Deviation (%)	E2 (ppm)	Relative Standard Deviation (%)
Sr	27.9	0.2	26.2	1
Zn	26.4	12	31.9	18
Cu	14.4	27	17.7	6
V	12.9	1	13.0	0.2
Cr	8.1	10	8.7	6
Zr	7.4	8	6.8	4
Ba	6.8	7	7.4	2
Rb	6.7	16	5.8	12
Sc	5.8	1	5.7	2
Ni	4.7	43	4.9	23
Pb	3.6	12	4.8	5
Cs	2.4	12	2.6	9
Co	0.9	6	0.9	18
U	0.6	5	0.8	11
Mo	0.5	26	0.5	16
Hf	0.4	19	0.4	8

The trace elemental analysis of selected synthesised zeolites (D2 and E2) was carried out in triplicate (on the same sample) by LA-ICP-MS, to determine the precision of the sample preparation procedure. The relative standard deviation (RSD) for trace element analysis was calculated and listed in Table 6.8. Although the RSD of certain elements were below 5%, the majority of the elements exhibited relatively large RSDs. Since the RSDs of certain elements were at an acceptable level, the sample preparation procedure is thought to be precise. The high RSDs exhibited by other trace elements were therefore attributed to the relatively low concentrations of these elements in the zeolite product.

The trace elemental composition of selected synthesised zeolites (D2 and E2), listed in Table 6.8, revealed that most of the trace elements present in Arnot coal fly ash (listed in Table 4.2) were found in association with the solid zeolite product. Selected synthesised zeolites, D2 and E2, contained traces of the elements Ba, Co, Cr, Cs, Cu, Hf, Mo, Ni, Pb, Rb, Sc, Sr, U, V, Zn and Zr. The trace elements are thought to be present in the zeolite framework as extra-framework species. The presence of elements, such as Co, Cu, Mo, Ni, Sr and Zn, has been reported to enhance the catalytic activity of zeolites for specific reactions (Hölderich and van Bekkum, 1991). However, trace elements present in the zeolite framework such as Ni, Pb, Sr and Zr are toxic while U is a radioactive element (Shaheen et al., 2014). Although these elements are present in trace amounts, the effect of these elements should be considered before application of the zeolite, although they are not known to leach. The percentage of elements in fly ash transferred to the solid zeolite product was calculated using XRF and LA-ICP-MS spectroscopy data for Arnot coal fly ash and zeolite sample D2, as listed in Table 6.9.

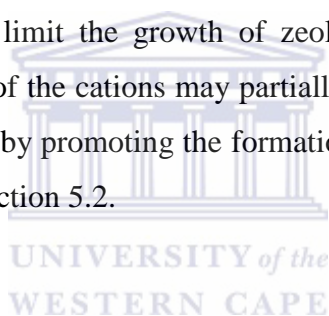
Table 6.9: The percentage of fly ash elements transferred to the solid zeolite product

Elements	Average (mass %)		Average (mass in grams used/produced)		Yield (mass %)
	Fly ash	Zeolite D2	Fly ash	Zeolite D2	
SiO ₂	56,74	44,40	20,63	0,37	1,8
Al ₂ O ₃	27,24	34,01	9,90	0,28	2,8
Fe ₂ O ₃	6,04	0,20	2,20	1,64E-03	0,1
CaO	5,74	0,23	2,09	1,87E-03	0,1
TiO ₂	1,59	0,04	0,58	3,62E-04	0,1
MgO	1,54	0	0,56	0	0,0
K ₂ O	0,59	0,25	0,21	2,09E-03	1,0
Na ₂ O	0,07	20,86	0,03	0,17	646,1
MnO	0,06	0	0,02	0	0
P	1,45E-01	0	5,29E-02	0	0
S	1,35E-01	0	4,91E-02	0	0
Ba	9,06E-02	6,78E-04	3,30E-02	5,61E-06	0,02
Sr	8,09E-02	2,79E-03	2,94E-02	2,31E-05	0,1
Zr	4,02E-02	7,44E-04	1,46E-02	6,15E-06	0,04
Ce	2,24E-02	0	8,13E-03	0	0
Cr	1,84E-02	8,07E-04	6,69E-03	6,67E-06	0,1
V	1,37E-02	1,29E-03	4,97E-03	1,07E-05	0,2
La	1,11E-02	0	4,05E-03	0	0
Nd	7,73E-03	0	2,81E-03	0	0
Y	7,27E-03	0	2,64E-03	0	0
Ni	6,87E-03	4,72E-04	2,50E-03	3,90E-06	0,2
Zn	5,90E-03	2,64E-03	2,15E-03	2,19E-05	1,0
Pb	5,47E-03	3,57E-04	1,99E-03	2,95E-06	0,1
Cu	4,27E-03	1,44E-03	1,55E-03	1,19E-05	0,8
Th	3,90E-03	0	1,42E-03	0	0
Ga	3,80E-03	0	1,38E-03	0	0
Rb	3,07E-03	6,74E-04	1,12E-03	5,57E-06	0,5
Co	2,53E-03	9,47E-05	9,21E-04	7,83E-07	0,1
Nb	2,13E-03	0	7,76E-04	0	0
U	1,00E-03	6,07E-05	3,64E-04	5,02E-07	0,1

As expected, the proportion of silicon and aluminium transformed into the zeolite framework was very low, as discussed in Section 6.1. The large Na content in the zeolite product (listed in Table 6.9, marked in red) was due to the additional sodium hydroxide added to the system during the activation of fly ash. The proportion of other elements transferred from fly ash to the solid zeolite product was $\leq 1\%$, which indicates that only a small percentage of the elements in Arnot coal fly ash form part of the solid product (zeolite). Some of the trace

elements were not transferred to the zeolite product at all. A large percentage of the elements in the fly ash source were therefore not utilised (and were present in the fused fly ash residue or supernatant). This may have contributed to the low yield of the solid zeolite product, as discussed in Section 5.1.1 and 6.1.

As discussed previously, the presence of additional cations (other than sodium) in the synthesis solution during zeolite synthesis may influence the hydrothermal process (Petrik, 2007; Yu, 2007). Cations in solution may serve as limited structure-directing agents that order water molecules around themselves. Water molecules are subsequently replaced by silica and alumina tetrahedra resulting in the formation of cage-like structures which serve as zeolite precursors (Feijen et al., 1994). Different cations order water molecules in different ways and therefore result in the formation of different SBUs (zeolite precursor species) which may be incorporated into the zeolite framework. Certain cations (such as potassium) are also known to inhibit the growth of zeolites (Petrik, 2007; Yu, 2007). The presence of these structure-inhibiting cations may limit the growth of zeolite crystals in certain directions. These structure-directing effects of the cations may partially be responsible for the formation of hierarchical zeolite X crystals, by promoting the formation of specific SBU units as shown in the FTIR study presented in Section 5.2.



6.3.2 Morphological (fine structure) analysis by HR-TEM

The fine structure of synthesised zeolites (D2 and E2) was analysed by HR-TEM microscopy. An HR-TEM micrograph of zeolite D2 (hierarchical Na-X prepared using aluminium hydroxide as an additional aluminium source) is presented in Figure 6.5 (a). A selected area electron diffraction (SAED) pattern for zeolite D2 was also measured, as depicted in Figure 6.5 (b).

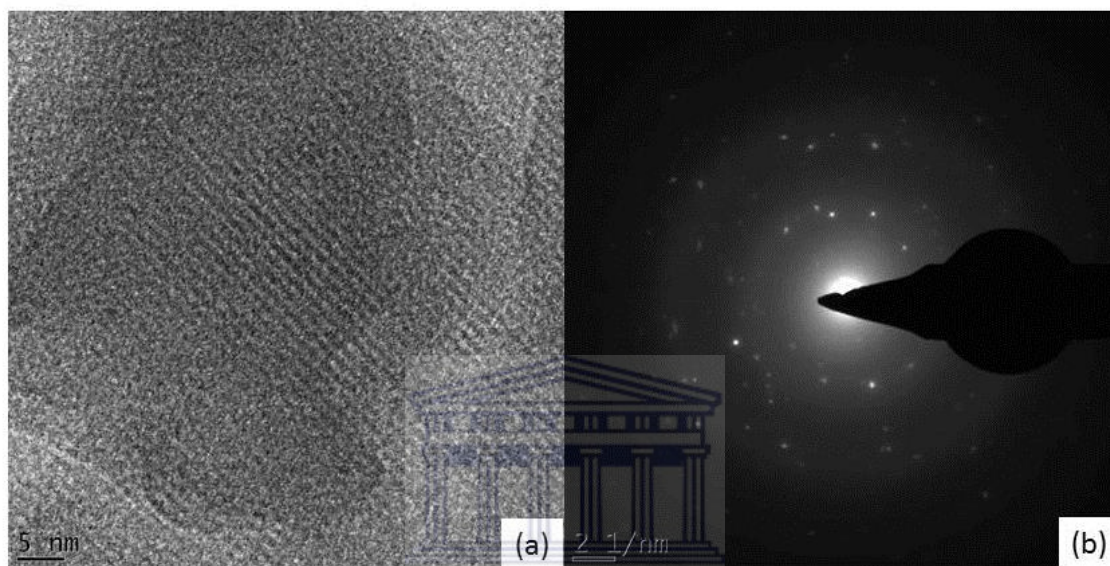


Figure 6.5: HR-TEM micrograph (a) and SAED diffraction pattern (b) of zeolite D2 (NA-X) synthesised from a clear FFA extract, using aluminium hydroxide as an additional aluminium source.

The lattice fringes of the zeolite material were observed in Figure 6.5 (a), illustrating that zeolite D2 is a crystalline material. The d-spacing of zeolite D2 was calculated to be 1.43 nm, which corresponds to crystal growth in the [111] direction. Hydrated zeolite Na-X is reported to exhibit a d-spacing of 1.45 nm for crystal growth in the [111] direction by Treacy and Higgins (2001). The SAED pattern for zeolite D2, depicted in Figure 6.5 (b), indicated that the zeolite material is polycrystalline in nature. The d-spacing value of 1.43 nm corresponded to the most intense diffraction peak observed by XRD at 2θ value of 6.1° , as depicted in Figure 6.2, which was attributed to zeolite Na-X.

An HR-TEM micrograph of zeolite E2 (hierarchical Na-X prepared using sodium aluminate as an additional aluminium source) is presented in Figure 6.6 (a). An SAED pattern for zeolite E2 was also measured, as depicted in Figure 6.6 (b).

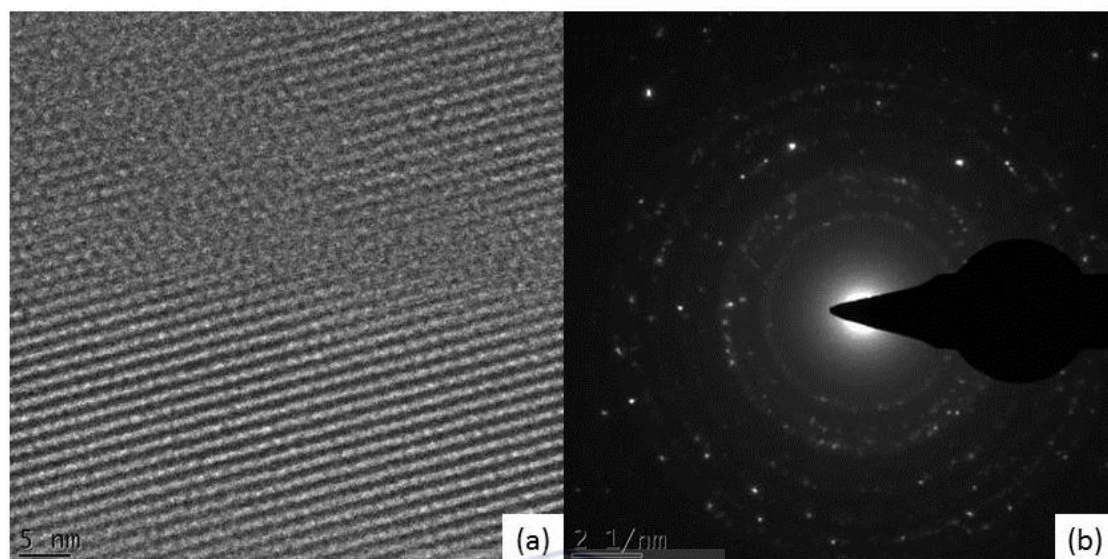


Figure 6.6: HR-TEM micrograph (a) and SAED diffraction pattern (b) of zeolite E2 (NA-X) synthesised from a clear FFA extract, using sodium aluminate as an additional aluminium source.

Zeolite lattice fringes were clearly observed in Figure 6.6 (a) with a d-spacing of 1.45 nm, which corresponded to crystal growth in the [111] direction (as was reported for zeolite D2). The well-defined diffraction pattern observed by SAED, depicted in Figure 6.6 (b), indicated that zeolite E2 is a polycrystalline material.

In both cases, the d-spacing was measured from HR-TEM microscopy data was ~ 1.45 nm, which corresponds to preferential crystal growth in the [111] direction. However, the supercage ring opening of 0.74 nm was not observed by HR-TEM microscopy. HR-TEM results were therefore in good agreement with XRD diffraction data, which indicated that highly crystalline zeolite Na-X (with polycrystalline morphology) was formed in the case of zeolite D2 and E2.

6.3.3 Structural Analysis by FTIR

Structural analysis of synthesised Na-X zeolites (D2 and E2) was carried out by FTIR spectroscopy. Vibrational spectra of zeolite D2 and E2 were similar, as depicted in Figure 6.7, indicating that zeolite D2 and E2 were composed of similar structural units. Typical aluminosilicate vibrations were observed for zeolite D2 and E2 namely; bending vibration at 428 cm^{-1} , symmetric stretching vibration at 662 cm^{-1} and asymmetric stretching vibration (960 cm^{-1}) of tetrahedrally coordinated silicon and aluminium atoms (i.e. Si-O-T bonds) in the zeolite framework (Criado et al., 2007; Mozgawa et al., 2011).

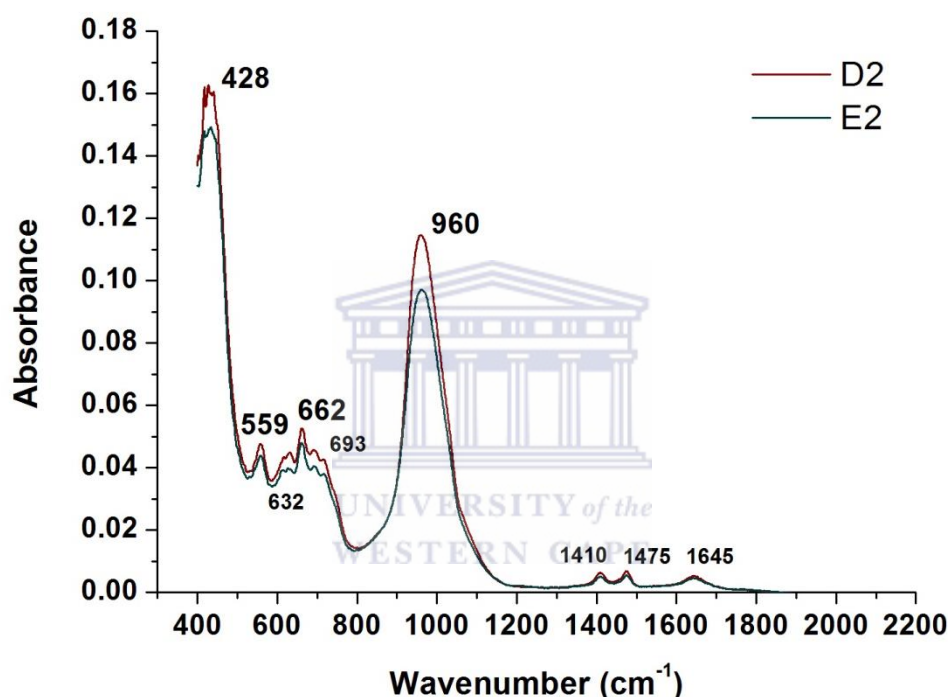


Figure 6.7: FTIR spectra of Na-zeolite D2 and E2 synthesised from a clear FFA extract at $90\text{ }^{\circ}\text{C}$ for 16 hours.

Vibrational bands were also observed in the IR region associated with secondary building units of zeolites; between 800 and 500 cm^{-1} . The main vibrational band present in this region, at 559 cm^{-1} , corresponds to the D6R structural unit (Mozgawa et al., 2011). This band is characteristic of zeolite Na-X. Weak bands at 632 cm^{-1} and 693 cm^{-1} were attributed to S6R and S4R units, respectively (Mozgawa et al., 2011). These bands may be attributed to either zeolite Na-X or Na-P1. As discussed in Section 5.2, the presence of these SBUs in the hierarchical zeolite product may be due to the intergrowth of other zeolites (such as zeolite P1) into the zeolite X framework or stacking faults in the zeolite X framework, which is the proposed cause of the observed hierarchical morphology of zeolite X crystals. These

structural defects often occur at the boundary region for two zeolite phases that crystallise under similar synthesis conditions. Synthesised zeolites, D2 and E2, were therefore further confirmed to be zeolite Na-X with minor intergrowth of zeolite P1.

Three weak bands were also observed between 1700 and 1400 cm^{-1} , as depicted in Figure 6.7. The vibrational band at 1645 cm^{-1} was attributed to the bending vibration of water molecules adsorbed to the zeolite surface (Galhotra et al., 2009; Li et al., 2005). The vibrational bands at 1410 and 1475 cm^{-1} are interesting since they do not appear in the vibrational spectra of conventional zeolites. These bands were attributed to carbonate species, either potassium or sodium bicarbonate (Miller and Wilkins, 1952). The presence of these cations in zeolite D2 and E2 were also detected by XRF spectroscopy (as listed in Table 6.6). The presence of calcium carbonate species was also detected by FTIR in the clear FFA extract used for zeolite synthesis, as depicted in Figure 5.7. The vibrational bands observed at 1410 and 1475 cm^{-1} may therefore also correspond to calcium carbonate species.

A typical FTIR spectrum of Na-X (Si/Al ratio = 1.5-2.5) was presented in Figure 2.8, as reported by Thuadaj and Nuntiya, (2012). The typical aluminosilicate vibrational bands for zeolites were observed at 460 cm^{-1} (bending vibration of Si-O-T bonds), 667 cm^{-1} (symmetric stretching vibration of Si-O-T bonds) as well as 980 and 1060 cm^{-1} (asymmetric stretching vibrations of Si-O-T bonds). The characteristic SBU of zeolite X (the D6R unit) was observed at 560 cm^{-1} . The presence of another SBU, namely the S4R unit, was observed at 674 and 751 cm^{-1} . Compared to the FTIR spectrum of zeolite Na-X in Figure 2.8, the FTIR spectra of synthesised zeolites D2 and E2 contained similar vibrational bands with the exception of bands at 751 cm^{-1} (which was not observed) and 632 cm^{-1} (which was attributed to the S6R unit typically found in zeolites X, P and hydroxysodalite). Vibrational bands in the FTIR spectra of synthesised zeolites appeared at slightly lower wavenumbers (428, 662 and 960 cm^{-1}), which typically indicates the increased incorporation of aluminium into the zeolite framework (Fernandez-Jimenez and Palomo, 2005). This is as expected since synthesised zeolites D2 and E2 exhibited a relatively lower Si/Al ratio (1.1) than zeolite Na-X reported by Thuadaj and Nuntiya, (2012).

6.3.4 Textural Properties by N₂ physisorption

Textural properties of selected synthesised Na-X zeolites D2 and E2, such as BET surface area, micropore area and volume and mesopore volume, were determined by nitrogen physisorption. The nitrogen adsorption/desorption isotherms of Na-X zeolites D2 and E2 are depicted in Figure 6.8.

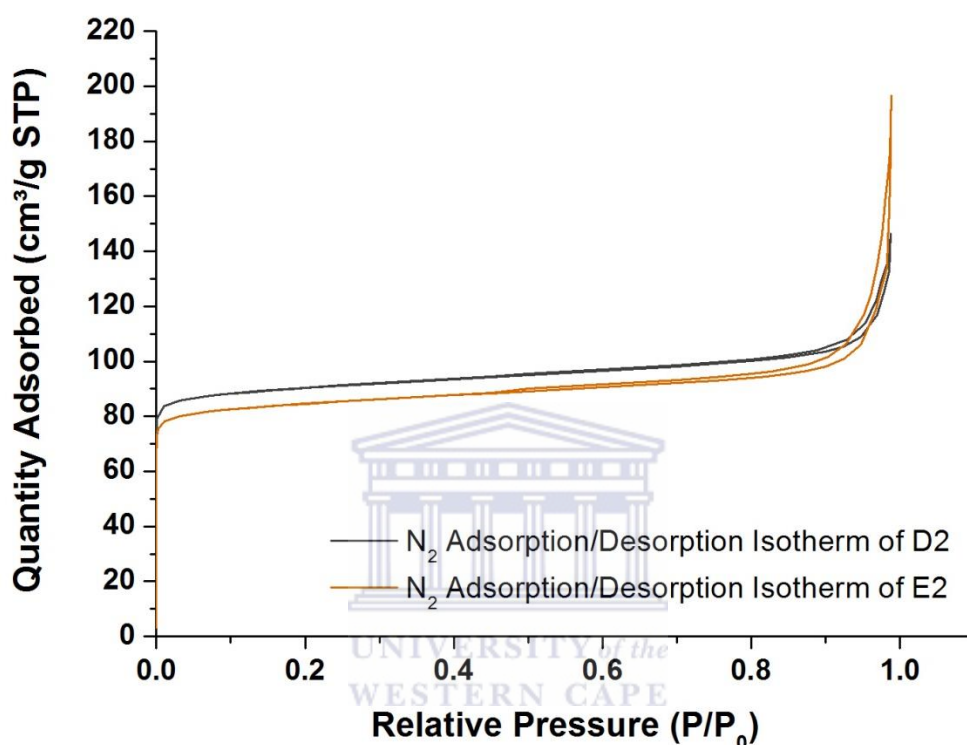


Figure 6.8: Nitrogen adsorption/desorption isotherm of Na-X zeolite D2 and E2.

The nitrogen isotherms exhibit type I behaviour, according to the classification by IUPAC, which is characteristic of microporous materials (Sing, 1982). At relatively higher partial pressures, a type H4 hysteresis loop was observed for sample D2 and E2. These materials therefore also exhibit some type IV behaviour which indicates the presence of mesopores in the zeolite structure as well as micropores (Thommes, 2007; Zhang et al., 2013). As observed from the N₂ adsorption/desorption isotherms in Figure 6.8, the offset of the isotherm is higher in the case of Na-zeolite D2 therefore Na-zeolite D2 is expected to exhibit relatively greater microporosity than Na-zeolite E2. On the other hand, the hysteresis loop of Na-zeolite E2 is relatively larger than that of Na-zeolite D2, therefore Na-zeolite E2 is expected to exhibit relatively higher mesoporosity than Na-zeolite D2.

The adsorption branch of the N₂ isotherm was used to determine the BJH pore size distribution of Na-zeolites (D2 and E2), as depicted in Figure 6.9, with an inset of the pore diameter range from 2-20 nm.

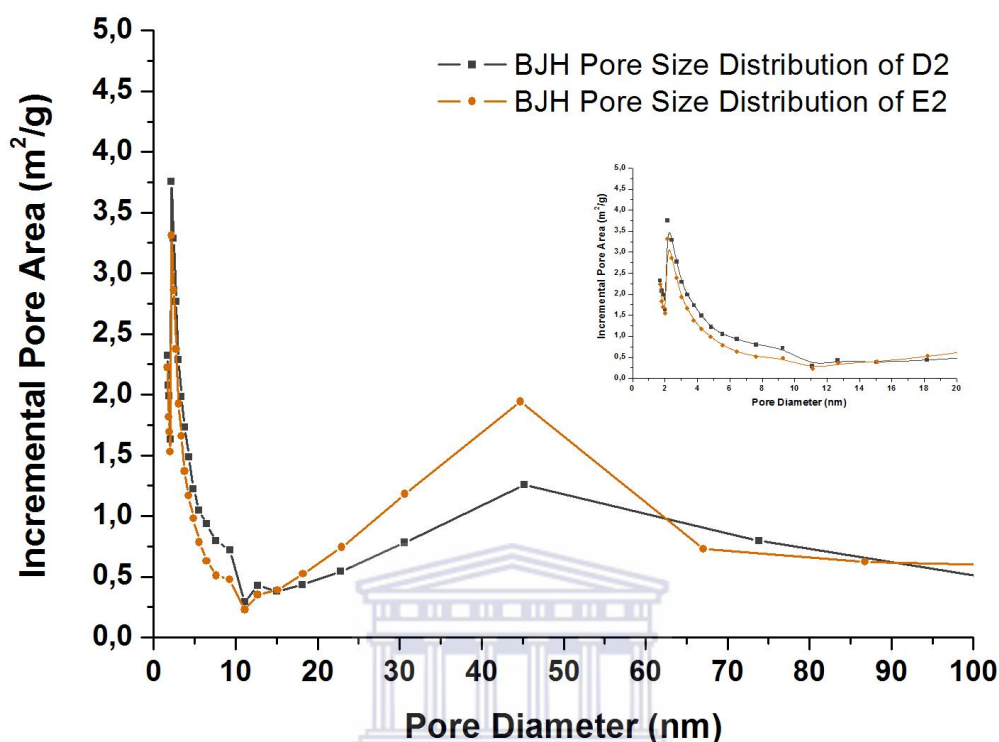


Figure 6.9: BJH pore size distribution of Na-X zeolite D2 and E2.

The BJH pore size distribution (PSD), depicted in Figure 6.9, illustrated that zeolite D2 and E2 contained a range of pore types. The mesopore PSD of zeolite D2 and E2 ranged from 2 to 75 nm. Two peak maxima were observed at ~2.3 and 44 nm for each zeolite. Synthesised Na-X zeolites D2 and E2 therefore contains interconnected micropores (with pore diameter ≤ 2 nm), mesopores (with pore diameters between 2 and 50 nm) and macropores (with pore diameters > 50 nm). The BJH pore size distribution of synthesised Na-X zeolites (D2 and E2) therefore confirms the hierarchical porous architecture of the material. Textural properties of Na-X zeolite D2 and E2 are summarised in Table 6.10, as well as the textural properties of a commercial Na-X zeolite reported by Kim and Ahn (2012).

Table 6.10: Textural properties of Na-X zeolite D2 and E2 determined by nitrogen physisorption.

Zeolite Code	Surface Area (m ² /g)			Pore Volume (cm ³ /g)		
	S _{BET}	S _{Micro}	S _{External}	V _{Total}	V _{Micro}	V _{Meso}
Commercial 13X*	582	-	-	0.215	0.199	0.086
D2	362	316	46	0.227	0.120	0.107
E2	338	294	44	0.305	0.112	0.193

*-from Kim and Ahn (2012)

The textural properties of synthesised zeolites were relatively similar. BET surface area of zeolite D2 and E2 was 362 and 338 m²/g, respectively, as listed in Table 6.10. However, significant differences were observed for the total pore volume and mesopore volume of the synthesised zeolites. Synthesised Na-zeolite D2 exhibited a total pore volume of 0.227 cm³/g and a mesopore volume of 0.107 cm³/g. Synthesised Na-zeolite E2 exhibited a relatively larger total pore volume of 0.305 cm³/g and a mesopore volume of 0.193 cm³/g. These differences may be attributed to the difference in the crystal morphology of zeolite D2 (listed in Table 6.3) compared to zeolite E2 (listed in Table 6.5). Zeolite crystals were much narrower in the case of E2 (97 nm), while the width of zeolite D2 crystals was 153 nm. The aggregated ball-like platelet morphology of synthesised hierarchical Na-X causes the formation of inter-crystal voids which results in the mesoporous nature of synthesised zeolites. The degree of mesoporosity may thus be tailored depending on the thickness of zeolite platelets, as illustrated in this study. Relatively narrower crystals (E2) resulted in a larger inter-crystal void volume and hence the mesopore volume of the material was greater compared to a zeolite with relatively thicker platelets (D2).

This study therefore illustrated that the degree of mesoporosity in zeolite X may be tailored by altering the platelet thickness of the material; using variation in the Si/Al molar ratio of the synthesis solution and aluminium source under the applied conditions. This property of hierarchical zeolite X is significant, especially in catalytic applications where the textural properties of the material have direct implications on the shape-selectivity for specific catalytic reactions. The porosity of hierarchical zeolite X makes it a favourable material for

application as a heterogeneous catalyst in various applications. Particularly, the presence of mesoporosity in the zeolite framework is an interesting property which may be applied in the transformation of large organic molecules. Compared to the conventional zeolite Na-X, reported to possess BET surface area of $582 \text{ m}^2/\text{g}$ by Kim and Ahn (2012), fly ash based zeolite D2 and E2 exhibited a relatively lower BET surface area. The lower BET surface area of synthesised zeolites is due to the enhanced mesopore void volume in the zeolite framework. The mesopore void volume of synthesised zeolites D2 and E2 was greater than the mesopore volume of commercial zeolite 13X, which was reported to be $0.086 \text{ cm}^3/\text{g}$ (Kim and Ahn, 2012). The enhanced mesoporosity of zeolite D2 and E2 was attributed to the hierarchical morphology of synthesised zeolites.

6.3.5 Acidity determination by titrimetric methods

Zeolite acidity was determined by titrimetric method using $\text{H}_2\text{O}/\text{D}_2\text{O}$ and NMR (as described in Section 3.4.6) to determine the Brönsted acidity of H-X zeolites, D2 and E2. H-zeolites were prepared by ion-exchange with a 1M ammonium chloride solution followed by calcination at an elevated temperature, as described in Section 3.3.3.2. The Brönsted acidity of zeolite D2 and E2 is summarised in Table 6.11, together with the Brönsted acidity of a commercial zeolite (13X) with Si/Al ratio of <1.5 which was determined by temperature-programmed desorption of ammonia as reported by Kim and Ahn (2012).

Table 6.11: Brönsted acidity of zeolite D2 and E2, determined by titrimetric method.

Zeolite code	Brönsted acidity (mmol H/g zeolite)
Commercial 13X	0.47
D2	1.12
E2	0.81

The Brönsted acidity of zeolite D2 was $1.12 \text{ mmol H/g zeolite}$, which was relatively higher than that of zeolite E2 at $0.81 \text{ mmol H/g zeolite}$, as listed in Table 6.11; both synthesised zeolites were more acidic than commercial zeolite 13X. Brönsted acidity is linked to the number of aluminium atoms in the zeolite framework. Zeolite D2 and E2 were expected to exhibit similar Brönsted acidity since XRF analysis revealed that the Si/Al molar ratio of D2

and E2 was 1.1. The observed difference in the Brönsted acidity of zeolite D2 and E2 may be due to differences in accessibility of acid sites between the two zeolites.

The Brönsted acidity of zeolite D2 and E2 was more than twice that of the commercial zeolite 13X. However, it should be noted that the Brönsted acidity reported by Kim and Ahn (2012) was determined by a different analytical technique (temperature-programmed desorption of ammonia). Nevertheless, hierarchical zeolite X (D2 and E2) synthesised in this study had appreciable Brönsted acid sites in the zeolite framework. Therefore, this material has potential as a solid acid in heterogeneous catalytic applications.



6.4 Chapter Summary

The effect of synthesis parameters (such as Si/Al ratio and aluminium source) on hierarchical zeolite X formation from a clear FFA extract were presented in this chapter. The crystallisation of zeolite Na-P1 as a minor phase together with zeolite Na-X was thought to be due to the Si/Al ratio of the synthesis solution. The effect of Si/Al molar ratio on the formation of hierarchical zeolite X under stirred hydrothermal conditions (90 °C, 16 hours) was therefore investigated by adding aluminium hydroxide (or sodium aluminate) as an additional source of aluminium. Variation in the Si/Al molar ratio (between 8.6 and 3.2) of the synthesis solution had a significant effect on the crystallinity and morphology of hierarchical zeolite X as well as zeolite mass yield.

As the Si/Al molar ratio of the synthesis solution (containing aluminium hydroxide as additional Al source) was decreased, the crystallinity of zeolite X increased. The crystallisation of hierarchical zeolite X was shown to occur under very specific conditions, from synthesis solutions with Si/Al molar ratios in the range of 7.3-8.6. Furthermore, as the Si/Al molar ratio of the synthesis solution decreased, zeolite platelet thickness increased and hence, the hierarchical morphology became less abundant. The adjustment of Si/Al molar ratio of the synthesis solution therefore allowed for the control of zeolite morphology and the degree of mesoporosity in the material. It was concluded that hierarchical zeolite X morphology was preferentially formed in relatively aluminium-deficient synthesis environments, while the typical octahedral morphology of zeolite X was favourably formed in relatively aluminium-enriched synthesis environments.

The increase in aluminium content in the synthesis solution did not result in the increased incorporation of aluminium into the zeolite framework, since the framework Si/Al ratio remained relatively constant. However, the additional aluminium content in the synthesis solution did translate into a higher yield of solid zeolite product. The zeolite mass yield increased from 5.2 % (C6) to 12.7 % (D5), almost three-fold, by slightly increasing the aluminium content in the synthesis solution using aluminium hydroxide. This further confirmed that the low availability of aluminium in the parent synthesis formulation (initially used for conversion to the zeolite product) was responsible for the low zeolite yield initially observed.

The type of aluminium source had an interesting effect on the crystallisation and morphology of zeolite X. Sodium aluminate addition resulted in the formation of thicker hierarchical zeolite X platelets compared to aluminium hydroxide addition. Furthermore, the formation of

octahedral zeolite X crystals was favoured in the presence of extra Na content (caused by sodium aluminate addition). Aluminium hydroxide was more effective as a source of additional aluminium in zeolite X crystallisation under the hydrothermal conditions investigated in this study. It was concluded that the source of aluminium played an important role in the crystallisation and morphology of zeolite X. However, adjusting the Si/Al molar ratio of the synthesis solution had the greatest effect on the crystallisation and morphology of hierarchical zeolite X.

Further characterisation of selected hierarchical zeolites (D2 and E2) by XRF, LA-ICP-MS, HR-TEM, FTIR, nitrogen physisorption and titrimetric acidity determination supported SEM and XRD results. The major and trace elemental analysis of zeolites (D2 and E2) by XRF and LA-ICP-MS spectroscopy revealed that zeolites D2 and E2 were mainly composed of Si, Al and Na. These zeolites exhibited a Si/Al molar ratio of 1.1 and a Na/Al molar ratio of 1.0. However, these zeolites also contained cations such as calcium, potassium and iron and titanium species as well as traces of other elements, which are assumed to be extra-framework species and not part of the zeolite X framework. HR-TEM microscopy confirmed that zeolite D2 and E2 both contained the fine structure of zeolite X with a d-spacing of ~1.45 nm. FTIR spectroscopy further confirmed that zeolite D2 and E2 exhibited the typical structural composition of zeolite X as well as secondary building units of zeolite P1 (S4R and S6R units), which were proposed to be intergrown into the zeolite X framework and responsible for the hierarchical morphology of this material. The textural analysis of zeolites D2 and E2 by nitrogen physisorption revealed that the material had a high BET surface area and contained micropores and exhibited enhanced mesoporosity. The Brønsted acidity of zeolite D2 and E2 (determined by titrimetric method) were 1.12 and 0.81 mmol H/g zeolite, respectively. The high BET surface area, micropore and mesopore volume of hierarchical zeolite X together with the appreciable solid acidity of the material gives it great potential as a heterogeneous solid acid catalyst in organic transformations.

Conclusions and Recommendations

7 Introduction

In this chapter a summary of the main findings will be presented together with recommendations for future work.

7.1 Main findings of this study

Hierarchical zeolite X was successfully synthesised from a clear FFA extract, under stirred hydrothermal conditions. The cause behind the formation of hierarchical zeolite X from a clear FFA extract was elucidated. Findings regarding the influence of synthesis parameters on hierarchical zeolite X formation and morphology were made, which will be summarised in this section.

7.1.1 The effect of synthesis parameters on hierarchical zeolite X formation

The baseline study involved stirred hydrothermal treatment of a clear FFA extract (with molar composition 0.12 Al·14.6 Na·1.00 Si·163 H₂O) in the hydrothermal temperature range of 70 to 94 °C for 24 hours. Zeolite Na-P1 crystallised as the major phase under the stirred synthesis conditions investigated, with the typical morphology of Na-P1. Improved crystallinity of Na-P1 was observed as the hydrothermal temperature increased. At relatively higher temperatures (>85 °C), zeolite crystals with hierarchical morphology was observed. Furthermore, platelet thickness was observed to increase from 86 to 260 nm as temperature increased.

The effect of static hydrothermal conditions on the formation of hierarchical zeolite X was investigated for comparison with the stirred hydrothermal synthesis system. Static hydrothermal treatment of a clear FFA extract (with molar composition 0.12 Al·14.6 Na·1.00 Si·163 H₂O) was carried out at 90 °C for 24 hours. Under static hydrothermal conditions hierarchical zeolite Na-X crystallised, while Na-P1 crystallised as the major phase under stirred conditions. The formation of Na-P1 under stirred conditions was attributed to Ostwald's law of successive transformations which states that a metastable phase will transform into a thermodynamically more stable phase with time. The hydrothermal time of 24 hours was therefore deemed too long under the stirred hydrothermal conditions investigated.

Chapter 7

The influence of hydrothermal synthesis time on hierarchical zeolite X quality was therefore investigated under stirred conditions. Stirred hydrothermal treatment (at 300 rpm) of a clear FFA extract (with the same molar formulation) was carried out at 90 °C for time periods ranging from 6 to 24 hours. The disc-like platelet morphology of hierarchical zeolite X was observed between 8 and 20 hours of hydrothermal treatment. While after 24 hours of crystallisation zeolite P1 formed, as noted previously. However, highly crystalline hierarchical zeolite Na-X was observed between 12 and 16 hours of hydrothermal treatment.

These findings illustrated that physical parameters such as hydrothermal temperature and time as well as agitation can alter the zeolite phase formed, even when the same molar formulation and source of feedstock was used, as illustrated by XRD data.

7.1.2 Structural study of the transformation of a clear FFA extract to hierarchical zeolite X with time monitored by Fourier transform infrared spectroscopy (FTIR)

The transformation of a clear FFA extract (with molar composition 0.12 Al·14.6 Na·1.00 Si·163 H₂O) to Na-zeolites, under stirred hydrothermal conditions of 90 °C for a time period of 2 to 16 hours, was monitored by FTIR spectroscopy. FTIR analysis revealed that small, soluble monomeric and polymeric silicate and aluminosilicate species were present in the clear FFA extract. Relatively larger, soluble secondary building units (SBUs), such as single 4-membered and single 6-membered rings, were also observed to be present in the clear FFA extract. These soluble silicate and aluminosilicate species served as precursors for zeolite synthesis.

During the hydrothermal treatment process (at 90 °C), soluble silicate and aluminosilicate precursor species joined together via condensation reactions to form secondary building units such as D6R units and/or D4R units. These secondary building units reacted further by condensation which resulted in the crystallisation of zeolite X (in the case of D6R units) and/or zeolite P1 (in the case of D4R units), depending on the hydrothermal time period (as well as the hydrothermal temperature and stirring). The vibrational spectra of these synthesised Na-zeolite products contained bands corresponding to zeolite framework-specific species. The crystallisation of a specific zeolite from a clear FFA extract was therefore reported to be strongly dependent on the hydrothermal synthesis conditions. Hierarchical zeolite X with high crystallinity was observed after 10 to 16 hours of stirred hydrothermal treatment at 90 °C, with zeolite P1 as a minor phase. The hierarchical morphology of zeolite

Chapter 7

X was linked to the incorporation of zeolite P1 building units (such as S4R and/or S6R units) intergrown into the zeolite X framework.

The vibrational spectra of supernatant samples contained soluble species present in the synthesis solution after the hydrothermal treatment step. These spectra further confirmed the incorporation of soluble building units such as S6R and S4R units into the zeolite framework, via condensation reactions. It is noteworthy that these soluble SBUs (S4R and S6R units) were also observed in the unwashed solid zeolite products, which indicated that part of the feedstock was wasted and not incorporated into the product (zeolite framework) resulting in the low yield observed.

7.1.3 The effect of molar regime adjustment on the formation of hierarchical zeolite X

Although highly crystalline hierarchical Na-X formed between 12 and 16 hours of hydrothermal treatment, traces of Na-P1 were detected by XRD and FTIR analysis. Therefore, the effect of Si/Al molar ratio of the synthesis solution on hierarchical zeolite X formation was investigated. The Si/Al molar ratio of the clear FFA extract was varied (between values 8.6 and 3.2) by addition of either aluminium hydroxide or sodium aluminate to the synthesis mixture. The resultant synthesis solution was subjected to stirred hydrothermal treatment at a temperature of 90 °C for 16 hours. Si/Al molar ratio of the synthesis solution greatly influenced the crystallisation, yield and morphology of zeolite X. As the Si/Al molar ratio of the synthesis solution increased, the crystallinity of zeolite X increased. However, the adjustment of the Si/Al molar ratio of the feedstock did not result in enhanced incorporation of aluminium into the zeolite framework since the Si/Al ratio of synthesised products remained relatively constant. The increased amount of aluminium in the synthesis solution did however result in an increase in the yield of zeolite product from 5.2 % (C6) to 12.7 % (D2) and 13.8 % (E2), which was almost three-fold. The increase in zeolite yield was attributed to the increased utilisation of silicon in the feedstock, in the presence of additional aluminium, to form the zeolite product.

At relatively high Si/Al molar ratios, the formation of ball-like aggregates of thin disc-like platelets was favoured. A decrease in the Si/Al molar ratio of the synthesis solution, by Al addition, resulted in broadening of zeolite platelets from 162 to 220 nm (in the case of aluminium hydroxide addition) and from 162 nm to 467 nm (in the case of sodium aluminate addition). In both cases, the presence of additional aluminium stimulated the growth of zeolite X crystals in the direction that caused platelet broadening. However, in the case of

Chapter 7

sodium aluminate addition platelet broadening was more enhanced. Furthermore, the formation of octahedral zeolite X crystals was observed (in the case of sodium aluminate addition) at a relatively low Si/Al molar ratio of 3.2, which was attributed to the presence of additional sodium cations (originating from the Al source) in the synthesis solution. The variation in zeolite Na-X crystallinity and morphology was therefore attributed to additional aluminium in the synthesis solution as well as the presence of excess sodium cations in the synthesis solution, in the case of sodium aluminate addition. This study therefore illustrated that the degree of mesoporosity of the zeolite material was varied by adjusting of Si/Al molar ratio of the synthesis solution, which is an important parameter to control in the application of these materials.

7.1.4 Further characterisation of selected hierarchical zeolite X

Further characterisation of selected hierarchical zeolites (D2 prepared using aluminium hydroxide and E2 prepared using sodium aluminate) was carried out by various analytical techniques such as XRF, LA-ICP-MS, HR-TEM, FTIR, nitrogen physisorption and titrimetric acidity determination. Major and trace elemental analysis of hierarchical zeolite X revealed that the material was mainly composed of silicon, aluminium and sodium cations and exhibited Si/Al molar ratios of 1.1, which is in the acceptable range for zeolite X. Hierarchical zeolite X exhibited the typical crystal lattice features for the faujasite phase as observed by HR-TEM microscopy and FTIR spectroscopy. Textural analysis of hierarchical zeolite X by nitrogen physisorption revealed that both materials had a high BET surface area of 338-362 m²/g and contained both micropores and mesopores. Titrimetric analysis was used to determine the Brönsted acidity of hierarchical zeolite X which ranged between 0.81-1.12 mmol H/g zeolite. The appreciable solid acidity and relatively high BET surface area as well as microporous and mesoporous nature of the material makes hierarchical zeolite X an interesting material for application as a heterogeneous solid acid catalyst in organic transformations.

This study illustrated that a specific set of conditions (in terms of molar composition and hydrothermal synthesis conditions) was required for the formation of hierarchical zeolite X. Hierarchical zeolite X was favourably formed in aluminium-deficient synthesis environments (i.e. relatively high Si/Al molar ratio of the synthesis solution) under the stirred hydrothermal conditions of 90 °C for 16 hours. The control of zeolite X morphology and mesoporosity was achieved by adjusting the Si/Al molar ratio of the synthesis solution in this study.

Chapter 7

Furthermore, the formation of hierarchical zeolite X was proved to be linked to the presence of zeolite P1 structural units (such as S4R and S6R units) intergrown into the framework of zeolite X.

7.2 Recommendations for future work

The study brought interesting findings to light regarding the effect of synthesis parameters (such as static synthesis, Si/Al ratio and aluminium source) on the hierarchical morphology of zeolite X. Further research into the formation hierarchical of zeolite X and characterisation of hierarchical zeolite X is required to probe the boundary conditions for the formation of this material.

1. In this study, it was observed that additional aluminium content resulted in platelet broadening. In the case of additional aluminium content in the form of sodium aluminate, the formation of octahedral zeolite X crystals was observed which was attributed to the additional aluminium content as well as the presence of additional sodium cations in the synthesis solution. The role of sodium and other cations in the formation of hierarchical zeolite X therefore needs to be investigated further. Cations are known to exhibit a limited structure-directing function in solution. In aqueous solution, water molecules are ordered around a cationic metal centre and replaced by silica and alumina tetrahedra. This results in the formation of cage-like aluminosilicate structures which serve as zeolite precursors. This structure-directing function of cations may influence the formation of hierarchical zeolite X from a clear FFA extract. The feedstock, coal fly ash (and the clear FFA extract), is composed of a variety of cations. Furthermore, synthesised products were observed to contain minor quantities of elements such as calcium, iron, potassium and titanium as well as a range of trace elements, which may play a role in the formation of hierarchical zeolite X. Therefore, the role of cations on the formation of hierarchical zeolite X needs to be investigated in more detail.
2. A range of minor and trace cations were detected in the zeolite product. However, the location of these elements in the zeolite framework is not known. These cations may be present in the pore system or on the surface of the zeolite. Surface characterisation of hierarchical zeolite X may be carried out by XPS spectroscopy to determine whether any elements are present on the surface of this material. Extra-framework species on the surface of zeolites may influence crystal growth by either enhancing growth in a

Chapter 7

particular direction or suppressing growth in a particular direction. This may influence the formation of hierarchical zeolite X. Surface characterisation of hierarchical zeolite X is therefore required.

3. The structural study of the transformation of a clear FFA extract to hierarchical zeolite X may be expanded by structural characterisation of synthesised products by solid-state ^{27}Al - and ^{29}Si -MAS-NMR spectroscopy. This technique could give more insight into the chemical environment of aluminium and silicon nuclei in the hierarchical zeolite X framework. Solid-state ^{27}Al -MAS-NMR may also be used to determine whether the additional aluminium content (for samples D1-5 and E1-5) was incorporated into the zeolite framework or present as extra-framework aluminium in the zeolite product.
4. The presence of soluble aluminosilicate species was observed by FTIR in the supernatant samples collected after zeolite synthesis. The supernatant samples of the zeolite synthesis process may therefore be recycled for further utilisation in zeolite or geopolymer synthesis.
5. A niche application for hierarchical zeolite X is yet to be identified. The application of hierarchical zeolite X as a green heterogeneous solid-acid catalyst in the transformation of organic molecules may be of interest due to the enhanced porosity of this material compared to conventional zeolites. The transformation of organic molecules over zeolites has been limited to small organic molecules due to the microporous nature of these materials. The presence of mesopores in the hierarchical zeolite framework may allow the transformation of relatively larger organic molecules.

References

References

- Adams, T.H. (2012). AACA 2012 CCP Survey Results. American Coal Ash Association. Accessed 10 July 2014. <<http://www.aaa-usa.org/Publications/ProductionUseReports.aspx>>.
- Aslam, W., Siddiqui, M.A.B., Jermy, B.R., Aitani, A., Cejka, J. & Al-Khattaf, S. (2014). Selective synthesis of linear alkylbenzene by alkylation of benzene with 1-dodecene over desilicated zeolites. *Catalysis Today*. 227, 187-197.
- Babajide, O., Musyoka, N., Petrik, L. & Ameer, F. (2012). Novel zeolite Na-X synthesized from fly ash as a heterogeneous catalyst in biodiesel production. *Catalysis Today*. 190, 54-60.
- Balkus, K.J. & Ly, K.T. (1991). The preparation and characterization of an X-type zeolite. *Journal of Chemical Education*. 68 (10), 875-877.
- Barman, S. (2010). The role of acid strength of modified NaX zeolites on gas phase ethylation of benzene. *Journal of Applied Sciences*. 10(21), 2602-2607.
- Bass, J.L. & Turner, G.L. (1997). Anion Distributions in Sodium Silicate Solutions. Characterization by ^{29}Si NMR and Infrared Spectroscopies, and Vapor Phase Osmometry. *Journal of Physical Chemistry*. 101, 10638-10644.
- Blissett, R.S. & Rowson, N.A. (2012). A review of the multi-component utilisation of coal fly ash. *Fuel*. 97, 1-23.
- Böke, N., Birch, G.D., Nyale, S.M. & Petrik, L. (2015). New synthesis method for the production of coal fly ash-based foamed geopolymers. *Construction and Building Materials*. 75, 189-199.
- Centi, G. & Perathoner, S. (2003). Catalysis and sustainable (green) chemistry. *Catalysis Today*. 77, 287-297.
- Chang, H. & Shih, W. (1998). A general method for the conversion of fly ash into zeolites as ion exchangers for cesium. *Industrial & Engineering Chemistry Research*. 37, 71-78.
- Chang, H. & Shih, W. (2000). Synthesis of zeolites A and X from fly ashes and their ion-exchange behaviour with cobalt ions. *Industrial & Engineering Chemistry Research*. 39, 4185-4191.

References

- Choi, M., Na, K., Kim, J., Sakamoto, Y., Terasaki, O. & Ryoo, R. (2009). Stable single-unit-cell nanosheets of zeolite MFI as active and long-lived catalysts. *Nature*. 461, 246-249.
- Corma, A., Rey, F., Rius, J., Sabater, M.J. & Valencia, S. (2004). Supramolecular self-assembled molecules as organic directing agent for synthesis of zeolites. *Nature*. 431, 287-290.
- Criado, M., Fernandez-Jimenez, A. & Palomo, A. (2007). Alkali activation of fly ash: Effect of SiO₂/Na₂O ratio. Part I: FTIR study. *Microporous and Mesoporous Materials*. 106, 180-191.
- Cubillas, P. & Anderson, M. W. (2010). Synthesis mechanism: Crystal growth and nucleation. In *Zeolites and Catalysis: Synthesis, Reactions and Applications*. Edited by Cejka, J., Corma, A. & Zones, S. Germany: Wiley-VCH Verlag GmbH & Co. KGaA.
- Cundy, C.S. & Cox, P.A. (2005). The hydrothermal synthesis of zeolites: Precursors, intermediates and reaction mechanism. *Microporous and Mesoporous Materials*. 82, 1-78.
- Davis, M.E. & Lobo, R.F. (1992). Zeolite and molecular sieve synthesis. *Chemistry of Materials*. 4, 756-768.
- Deng, Y., Flury, M., Harsh, J.B., Felmy, A.R. & Qafoku, O. (2006). Cancrinite and sodalite formation in the presence of cesium, potassium, magnesium, calcium and strontium in Hanford tank waste simulants. *Applied Geochemistry*. 21, 2049-2063.
- Deutschmann, O., Knözinger, H., Kochloefl, K. & Turek, T. (2009). Heterogeneous catalysis and solid catalysts. In *Ullmann's Encyclopedia of Industrial Chemistry*. Germany: Wiley-VCH Verlag GmbH & Co. KGaA.
- Di Renzo, F., Remoue, F., Massiani, P., Fajula, F., Figueras, F. & Des Courières, T. (1991). Crystallization kinetics of zeolite TON. *Zeolites*. 11(6), 539-548.
- Dumitriu, E. & Hulea, V. (2003). Effects of channel structures and acid properties of large-pore zeolites in the liquid-phase tert-butylation of phenol. *Journal of Catalysis*. 218, 249-257.
- Eskom, 2015. Integrated results for 2015, Facts sheet with additional information. Accessed 7 December 2015. <<http://www.eskom.co.za/IR2015/Pages/Default.aspx>>.

References

- Eulenberger, G.R., Shoemaker, D.P. & Keil, J.G. (1967). The crystal structures of hydrated and dehydrated synthetic zeolites with faujasite aluminosilicate frameworks. I. The dehydrated sodium, potassium, and silver forms. *The Journal of Physical Chemistry*. 71 (6), 1812-1819.
- Fadoni, M. & Lucarelli, L. (1999). Temperature programmed desorption, reduction, oxidation and flow chemisorption for the characterisation of heterogeneous catalysts. Theoretical aspects, instrumentation and applications. *Studies in Surface Science and Catalysis*. 120 (1), 177-225.
- Fernandez-Jimenez, A. & Palomo, A. (2005). Mid-infrared spectroscopic studies of alkali-activated fly ash structure. *Microporous and Mesoporous Materials*. 86, 207-214.
- Feijen, E.J.P., Martens, J.A. & Jacobs, P.A. (1994). Zeolites and their mechanism of synthesis. *Studies in Surface Science and Catalysis*. 84, 3-21.
- Franus, W. (2012). Characterization of X-type zeolite prepared from coal fly ash. *Polish Journal of Environmental Studies*. 21 (2), 337-343.
- Galhotra, P., Navea, J.G., Larsen, S.C. & Grassian, V.H. (2009). Carbon dioxide ($C_{16}O_2$ and $C_{18}O_2$) adsorption in zeolite Y materials: effect of cation, adsorbed water and particle size. *Energy and Environmental Science*. 2, 401-409.
- Granda Valdes, M., Perez-Cordoves, A.L. & Diaz-Garcia, M.E. (2006). Zeolites and zeolite-based materials in analytical chemistry. *Trends in Analytical Chemistry*. 25 (1), 24-30.
- Gupta, P. & Paul, S. (2014). Solid acids: Green alternatives for acid catalysis. *Catalysis Today*. 236, 153-170.
- Haber, J., Block, J.H. & Delmon, B. (1995). Manual of methods and procedures for catalyst characterisation. *Pure and Applied Chemistry*. 67, 1257-1306.
- Hagen, J. (2006). Industrial catalysis: A practical approach. 2nd Edition. Germany: WILEY-VCH Verlag GmbH & Co. KGaA.
- Hamilton, K.E., Coker, E.N., Sacco, A.Jr., Dixon, A.G. & Thompson, R.W. (1993). The effects of the silica source on the crystallization of zeolite NaX. *Zeolites*. 13(8), 645-653.

References

- Hanif, N., Anderson, M.W., Alfredsson, V. & Terasaki, O. (2000). The effect of stirring on the synthesis of intergrowths of zeolite Y polymorphs. *Physical Chemistry Chemical Physics*. 2, 3349-3357.
- Heidrich, C., Feuerborn, H. & Weir, A. (2013). Coal combustion products: a global perspective. World of Coal Ash Conference 2013. Kentucky, The United States of America. Accessed 7 December 2015. <<http://www.flyash.info/>>.
- Hölderich, W.F. & van Bekkum, H. (1991). Zeolites in Organic Syntheses. In Introduction to Zeolite Science and Practice. Edited by Flanigen, E.M., Jansen, J.C. & van Bekkum, H. The Netherlands: Elsevier B.V.
- Holm, M.S., Taarning, E., Egeblad, K. & Christensen, C.H. (2011). Catalysis with hierarchical zeolites. *Catalysis Today*. 168, 3-16.
- Hsu, H., Roselin, L.S., Selvin, R. & Bououdina, M. (2011). Enhanced activity of hierarchical zeolitic material with ZSM-5 structure for the tert-butylation of phenol. *Journal of Experimental Nanoscience*. 6(6), 612-621.
- Huang, Y., Wang, K., Dong, D., Li, D., Hill, M.R., Hill, A.J. & Wang, H. (2010). Synthesis of hierarchical porous zeolite NaY particles with controllable particle sizes. *Microporous and Mesoporous Materials*. 127, 167-175.
- Huang, Y., Yao, J., Zhang, X., Kong, C., Chen, H., Liu, D., Tsapatsis, M., Hill, M.R., Hill, A.J. & Wang, H. (2011) Role of ethanol in sodalite crystallization in an ethanol-Na₂O-Al₂O₃-SiO₂-H₂O system. *CrystEngComm*. 13, 4714-4722.
- Hunger, M. (2010). Catalytically active sites: Generation and characterization. In Zeolites and Catalysis: Synthesis, Reactions and Applications. Edited by Cejka, J., Corma, A. & Zones, S. Germany: Wiley-VCH Verlag GmbH & Co. KGaA.
- Huo, Q. (2011). Synthetic chemistry of the inorganic ordered porous materials. In Modern Inorganic Synthetic Chemistry. Edited by Xu, R., Pang, W. & Huo, Q. The Netherlands: Elsevier B.V.
- Hurgobin, S. (1998). The effect of synthesis and post-synthesis modifications on the activity of zeolite Beta for cumene synthesis. MSc Thesis. University of the Cape Town, South Africa.

References

- Inayat, A., Knoke, I., Spiecker, E. & Schwieger, W. (2012). Assemblies of mesoporous FAU-type zeolite nanosheets. *Angewandte Chemie International Edition*. 51, 1962-1965.
- Katsuki, K. & Hasewaga, M. (2007). Effect of anion species from Ca-sources on framework type of Na-Ca zeolites prepared at 80 °C. *Journal of Porous Materials*. 14(4), 401-407.
- Kim, K. & Ahn, H. (2012). The effect of pore structure of zeolite on the adsorption of VOCs and their desorption properties by microwave heating. *Microporous and Mesoporous Materials*. 152, 78-83.
- Koroglu, H.J., Sarioglan, A., Tatlier, M., Erdem-Senatalar, A. & Savasci, O.T. (2002). Effects of low-temperature gel aging on the synthesis of zeolite Y at different alkalinities. *Journal of Crystal Growth*. 241, 481-488.
- Kresge, C.T., Leonowicz, M.E., Roth, W.J., Vartuli, J.C. & Beck, J.S. (1992). Ordered mesoporous molecular sieves synthesized by a liquid-crystal template mechanism. *Nature*. 359, 710-712.
- Krishnan, A.V., Ojha, K. & Pradhan, N.C. (2002). Alkylation of phenol with tertiary butyl alcohol over zeolites. *Organic Process Research & Development*. 6, 132-137.
- Kruger, R.A. (1997). Fly ash beneficiation in South Africa: creating new opportunities in the market-place. *Fuel*. 76 (8), 777-779.
- Lalena, J.N., Cleary, D.A., Carpenter, E.E. & Dean, N.F. (2008). Solid-liquid reactions. In *Inorganic Materials Synthesis and Fabrication*. The United States of America: John Wiley & Sons, Inc.
- Lee, W.K.W. & van Deventer, J.S.J. (2003). Use of infrared spectroscopy to study geopolymerization of heterogeneous amorphous aluminosilicates. *Langmuir*. 19, 8726-8734.
- Lercher, J.A. & Jentys, A. (2007). Infrared and raman spectroscopy for characterizing zeolites. In *Introduction to Zeolite Science and Practice*. Edited by Cejka, J., van Bekkum, H., Corma, A. & Schuth, F. The Netherlands: Elsevier B.V.
- Li, G., Larsen, S.C. & Grassian, V.H. (2005). An FT-IR study of NO₂ reduction in nanocrystalline NaY zeolite: effect of zeolite crystal size and adsorbed water. *Catalysis Letters*. 103, 23-32.

References

- Liu, Y., Xu, J., Jin, L., Fang, Y. & Hu, H. (2009). Synthesis and modification of zeolite NaA adsorbents for separation of hydrogen and methane. *Asia-Pacific Journal of Chemical Engineering*. 4, 666-671.
- Livage, J. (1994). Sol-gel chemistry and molecular sieve synthesis. In *Advanced Zeolite Science and Applications*. Edited by Jansen, J.C., Stocker, M., Karge, H.G. & Weitkamp, J. The Netherlands: Elsevier B.V.
- Louis, B., Walspurger, S. & Sommer, J. (2004). Quantitative determination of Brønsted acid sites on zeolites: a new approach towards the chemical composition of zeolites. *Catalysis Letters*. 93, 81-84.
- Mauritz, K. A. & Warren, R.M. (1989). Microstructural evolution of a silicon oxide phase in a perfluorosulfonic acid ionomer by an in situ sol-gel reaction. *Macromolecules*. 22 (4), 1730-1734.
- McCusker, L.B. & Baerlocher, C. (2007). Zeolite Structures. In *Introduction to Zeolite Science and Practice*. Edited by Cejka, J., van Bekkum, H., Corma, A. & Schuth, F. The Netherlands: Elsevier B.V.
- Meier, W.M. & Baerlocher, C. (1999). Zeolite type frameworks: Connectivities, configurations and conformations. In *Structures and Structure Determination*. Edited by Baerlocher, C., Bennett, J.M., Depmeier, W., Fitch, A.N., Jobic, H., van Koningsveld, H., Meier, W.M., Pfenninger, A. & Terasaki, O. Germany: Springer-Verlag.
- Meise, W. & Schwochow, F.E. (1973). Kinetic studies on the formation of zeolite A. *Advances in Chemistry*. 121, 169-178.
- Miller, F.A. & Wilkins, C.H. (1952). Infrared spectra and characteristic frequencies of inorganic ions. *Analytical Chemistry*. 24 (8), 1253-1294.
- Mishra, D.P. & Das, S.K. (2010). A study of physico-chemical and mineralogical properties of Talcher coal fly ash for stowing in underground coal mines. *Materials Characterization*. 61, 1252-1259.
- Molina, A. & Poole, C. (2004). A comparative study using two methods to produce zeolites from fly ash. *Minerals Engineering*. 17, 167-173.

References

- Moller, K. & Bein, T. (2011). Pores within pores - How to craft ordered hierarchical zeolites. *Science*. 333, 297-298.
- Morris, R.E. & Wheatley, P.S. (2007). Diffraction techniques applied to zeolites. In *Introduction to Zeolite Science and Practice*. Edited by Cejka, J., van Bekkum, H., Corma, A. & Schuth, F. The Netherlands: Elsevier B.V.
- Mozgawa, W., Handke, M. & Jastrzebski, W. (2004). Vibrational spectra of aluminosilicate structural clusters. *Journal of Molecular Structure*. 704; 247-257.
- Mozgawa, W., Krol, M. & Barczyk, K. (2011). FT-IR studies of zeolites from different structural groups. *Chemik*. 65 (7), 667-674.
- Murayama, N., Yamamoto, H. & Shibata, J. (2002). Mechanism of zeolite synthesis from coal fly ash by alkali hydrothermal reaction. *International Journal of Mineral Processing*. 64, 1-17.
- Muriithi, G.N. (2012). Re-use of South African fly ash for CO₂ capture and brine remediation. PhD Thesis. University of the Western Cape, South Africa.
- Musyoka, N.M., Petrik, L.F., Gitari, W.M., Balfour, G. & Hums, H. (2012). Optimization of hydrothermal synthesis of pure phase zeolite Na-P1 from South African coal fly ashes. *Journal of Environmental Science and Health, Part A: Toxic/Hazardous Substances and Environmental Engineering*. 47 (3), 337-350.
- Musyoka, N. (2012). Zeolite A, X and Cancrinite from South African coal fly ash: mechanism of crystallization, routes to rapid synthesis and new morphology. PhD Thesis. University of the Western Cape, South Africa.
- Musyoka, N., Petrik, L. & Hums, E. (2013). PCT Patent WO 2013144865 A1, University of the Western Cape, South Africa.
- Musyoka, N., Petrik, L., Fatoba, O.O. & Hums, E. (2013). Synthesis of zeolites from coal fly ash using mine waters. *Minerals Engineering*. 53, 9-15.
- Musyoka, N.M., Petrik, L.F., Hums, E., Baser, H. & Schwieger, W. (2014). In-situ ultrasonic diagnostic of zeolite X crystallization with novel (hierarchical) morphology from coal fly ash. *Ultrasonics*. 54, 537-543.

References

- Myerson, A.S. (2002). Handbook of industrial crystallization. 2nd Edition. United Kingdom: Butterworth-Heinemann.
- Na, K., Jo, C., Kim, J., Cho, K., Jung, J., Seo, Y., Messinger, R.J., Chmelka, B.F. & Ryoo, R. (2011). Directing zeolite structures into hierarchical nanoporous architectures. *Science*. 333, 328-332.
- Na, K., Choi, M. & Ryoo. (2013). Recent advances in the synthesis of hierarchically nanoporous zeolites. *Microporous and Mesoporous Materials*. 166, 3-19.
- Ojha, K., Pradhan, N.C. & Samanta, A.N. (2003). Treated fly ash: A potential catalyst for alkylation of phenol with tert-butyl alcohol. *Indian Journal of Chemical Technology*. 10, 495-500.
- Payra, P. & Dutta, P.K. (2003). Zeolites: A primer. In Handbook of Zeolite Science and Technology. Edited by Auerbach, S.M., Carrado, K.A. & Dutta, P.K. The United States of America: Marcel Dekker, Inc.
- Petrik, L. (2009). The influence of cation, anion and water content on the rate of formation and pore size distribution of zeolite ZSM-5. *South African Journal of Science*. 105, 251-257.
- Querol, X., Moreno, N., Umana, J.C., Alastuey, A., Hernandez, E., Lopez-Soler, E. & Plana, F. (2002). Synthesis of zeolites from coal fly ash: an overview. *International Journal of Coal Geology*. 50, 413-423.
- Reyes, C.A.R., Williams, C., Alarcon, O.M.C. (2013). Nucleation and growth process of sodalite and cancrinite from kaolinite-rich clay under low-temperature hydrothermal conditions. *Materials Research*. 16(2), 424-438.
- Robson, H. (2001). Verified syntheses of zeolitic materials. 2nd Edition. The Netherlands: Elsevier B.V.
- Roth, W.J. & Cejka, J. (2011). Two-dimensional zeolite: dream or reality?. *Catalysis Science and Technology*. 1, 43-53.
- Rouessac, F. & Rouessac, A. (2007) Infrared spectroscopy. In Chemical Analysis. England: John Wiley & Sons, Inc.

References

- Shaheen, S.M., Hooda, P.S. & Tsadilas, C.D. (2014). Opportunities and challenges in the use of coal fly ash for soil improvements - A review. *Journal of Environmental Management*. 145, 249-267.
- Shigemoto, N., Hayashi, H. & Miyaura, K. (1993). Selective formation of Na-X zeolite from coal fly ash by fusion with sodium hydroxide prior to hydrothermal reaction. *Journal of Materials Science*. 28, 4781-4786.
- Shigemoto, N., Sugiyama, S., Hayashi, H. & Miyaura, K. (1995). Characterization of Na-X, Na-A, and coal fly ash zeolites and their amorphous precursors by IR, MAS NMR and XPS. *Journal of Materials Science*. 30, 5777-5783.
- Shoumkova, A. & Stoyanova, V. (2013). Zeolite formation by hydrothermal alkali activation of coal fly ash from power station “Maritsa 3”, Bulgaria. *Fuel*. 103, 533-541.
- Sing, K.S.W. (1982). Reporting physisorption data for gas/solid systems. *Pure and Applied Chemistry*. 54, 2201-2218.
- Tao, Y., Kanoh, H., Abrams, L. & Kaneko, K. (2006). Mesopore-modified zeolites: Preparation, characterization and applications. *Chemical Reviews*. 106, 896-910.
- Terasaki, O., Ohsuna, T., Liu, Z., Sakamoto, Y., Ruan, J. & She, S. (2007). Structural study of porous materials by electron microscopy. In *Introduction to Zeolite Science and Practice*. Edited by Cejka, J., van Bekkum, H., Corma, A. & Schuth, F. The Netherlands: Elsevier B.V.
- Tessonier, J., Louis, B., Walspurger, S., Sommer, J., Ledoux, M. & Pham-Huu, C. (2006). Quantitative measurement of the brönsted acid sites in solid acids: Toward a single-site design of Mo-modified ZSM-5 zeolite. *Journal of Physical Chemistry B*. 110, 10390-10395.
- Thommes, M. (2007). Textural characterization of zeolites and ordered mesoporous materials by physical adsorption. In *Introduction to Zeolite Science and Practice*. Edited by Cejka, J., van Bekkum, H., Corma, A. & Schuth, F. The Netherlands: Elsevier B.V.
- Thuadaj, P. & Nuntiya, A. (2012). Effect of the SiO₂/Al₂O₃ ratio on the synthesis of Na-X zeolite from Mae Moh fly ash. *Science Asia*. 38, 295-300.
- Treacy, M.M.J. & Higgins, J.B. (2001). *Collection of Simulated XRD Powder Patterns for Zeolites*. 4th Edition. The Netherlands: Elsevier B.V.

References

- van Hooff, J.H.C & Roelofsen, J.W. (1991). Techniques of zeolite characterization. In Introduction to Zeolite Science and Practice. Edited by Van Bekkum, H., Flanigen, E.M. & Jansen, J.C. The Netherlands: Elsevier B.V.
- Vassilev, S.V., Menendez, R., Alvarez, D., Diaz-Somoano, M. & Martinez-Tarazona, M.R. (2003). Phase-mineral and chemical composition of coal fly ashes as a basis for their multicomponent utilization. 1. Characterization of feed coals and fly ashes. *Fuel*. 82, 1793-1811.
- Wdowin, M., Franus, M., Panek, R., Badura, L. & Franus, W. (2014). The conversion technology of fly ash into zeolites. *Clean Technologies and Environmental Policy*. 16 (6), 1217-1223.
- Weitkamp, J. (2000). Zeolites and catalysis. *Solid State Ionics*. 131, 175-188.
- Weitkamp, J. & Hunger, M. (2007). Acid and base catalysis on zeolites. *Studies in Surface Science and Catalysis*. 168, 787-835.
- Wijnen, P.W.J.G., Beelen, T.P.M., de Haan, J.W., van de Ven, L.J.M. & van Santen, R.A. (1990). The structure directing effects of cations in aqueous silicate solutions. A ²⁹Si-NMR study. *Colloids and Surfaces*. 45, 255-268.
- Xavier, N.M., Lucas, S.D. & Rauter, A.P. (2009). Zeolites as efficient catalysts for key transformations in carbohydrate chemistry. *Journal of Molecular Catalysis A: Chemical*. 305, 84-89.
- Xie, J., Huang, M. & Kaliaguine, S. (1994). Base and acid sites in alkaline earth cation-exchanged X zeolites. *Catalysis Letters*. 29, 281-291.
- Xing-dong, L., Yi-pin, W., Xue-min, C., Yan, H. & Jin, M. (2013). Influence of synthesis parameters on NaA zeolite crystals. *Powder Technology*. 243, 184-193.
- Xu, L., Wu, L., Guan, J., Wang, H., Ma, Y., Song, K., Xu, H., Xing, H., Xu, C., Wang, Z. & Kan, Q. (2008). Synthesis, characterization of hierarchical ZSM-5 zeolite catalyst and its catalytic performance for phenol tert-butylation reaction. *Catalysis Communications*. 9, 1272-1276.

References

Yaping, Y., Xiaoqiang, Z., Weilan, Q. & Mingwen, W. (2008). Synthesis of pure zeolites from supersaturated silicon and aluminum alkali extracts from fused coal fly ash. *Fuel*. 87, 1880-1887.

Yu, J. (2007). Synthesis of zeolites. In *Introduction to Zeolite Science and Practice*. Edited by Cejka, J., van Bekkum, H., Corma, A. & Schuth, F. The Netherlands: Elsevier B.V.

Zhang, X., Tang, D., Zhang, M. & Yang, R. (2013). Synthesis of NaX zeolite: Influence of crystallization time, temperature and batch molar ratio $\text{SiO}_2/\text{Al}_2\text{O}_3$ on the particulate properties of zeolite crystals. *Powder Technology*. 235, 322-328.



Appendix

Appendix

Appendix A - The elemental composition of clear FFA extract samples determined by ICP-OES spectrometry.

Table A1: The average elemental composition of clear FFA extract (major elements), determined by ICP-OES, as well as calculated relative standard deviation (%) values.

Major elements	S1 (ppm)	S2 (ppm)	S3 (ppm)	Average S (1-3) (ppm)
Al	1089	1129	975	1064 ±8 %
Ca	351	383	395	376 ±6 %
K	688	669	673	676 ±1 %
Na	117755	111813	114177	114582 ±3 %
Si	8707	9808	10222	9579 ±8 %

Appendix

Appendix B - The calculation of molar composition of clear FFA extract from ICP-OES data

1. Calculation of moles of Al_2O_3 :

Mass conc. Al = 1064 ppm = 1.064 g/L

Volume of clear FFA extract (L) = 0.145 L

Mass of Al in clear FFA extract = 1.064 g/L \times 0.145 L = 0.1543 g

Molar mass of Al = 26.981 g/mol

$$\text{Moles of Al} = \frac{\text{mass}}{M_r} = \frac{0.1543 \text{ g}}{26.981 \text{ g/mol}} = 5.72 \times 10^{-3} \text{ mol}$$

2. Calculation of moles of CaO:

Mass conc. Ca = 376 ppm = 0.376 g/L

Volume of clear FFA extract (L) = 0.145 L

Mass of Ca in clear FFA extract = 0.376 g/L \times 0.145 L = 0.055 g

Molar mass of Ca = 40.078 g/mol

$$\text{Moles of Ca} = \frac{\text{mass}}{M_r} = \frac{0.055 \text{ g}}{40.078 \text{ g/mol}} = 1.36 \times 10^{-3} \text{ mol}$$

3. Calculation of moles of K_2O :

Mass conc. K = 676 ppm = 0.676 g/L

Volume of clear FFA extract (L) = 0.145 L

Mass of K in clear FFA extract = 0.676 g/L \times 0.145 L = 0.098 g

Molar mass of K = 39.098 g/mol

$$\text{Moles of K} = \frac{\text{mass}}{M_r} = \frac{0.098 \text{ g}}{39.098 \text{ g/mol}} = 2.51 \times 10^{-3} \text{ mol}$$

Appendix

4. Calculation of moles of Na₂O:

Mass conc. Na = 114582 ppm = 114.6 g/L

Volume of clear FFA extract (L) = 0.145 L

Mass of Na in clear FFA extract = 114.6 g/L × 0.145 L = 16.61 g

Molar mass of Na = 22.989 g/mol

$$\text{Moles of Na} = \frac{\text{mass}}{M_r} = \frac{16.61 \text{ g}}{22.989 \text{ g/mol}} = 7.15 \times 10^{-1} \text{ mol}$$

5. Calculation of moles of SiO₂:

Mass conc. Si = 9579 ppm = 9.579 g/L

Volume of clear FFA extract (L) = 0.145 L

Mass of Si in clear FFA extract = 9.579 g/L × 0.145 L = 1.389 g

Molar mass of Si = 28.085 g/mol

$$\text{Moles of Si} = \frac{\text{mass}}{M_r} = \frac{1.389 \text{ g}}{28.085 \text{ g/mol}} = 4.59 \times 10^{-2} \text{ mol}$$

6. Calculation of moles of H₂O:

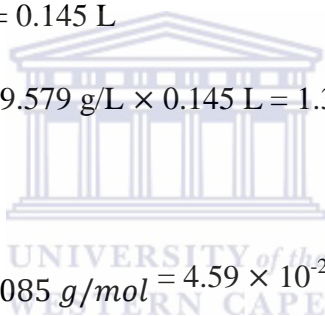
Volume of H₂O = 145 ml = 0.145 L

Density of H₂O = 1000 g/L

Molar mass of H₂O = 18

Mass of H₂O = density × volume = 1000 g/L × 0.145 L = 145 g

$$\text{Moles of H}_2\text{O} = \frac{\text{mass}}{M_r} = \frac{145 \text{ g}}{18 \text{ g/mol}} = 8.06 \text{ mol}$$



Appendix

7. Normalization of molar composition

The molar composition of the clear FFA extract was normalized by setting moles of Si = 1.

Table B1: Normalized molar composition of the clear FFA extract

Element	Moles of element	Normalization	Normalized moles of element
Al	5.72×10^{-3}	$\frac{5.72 \times 10^{-3}}{4.95 \times 10^{-2}}$	0.12
Ca	1.36×10^{-3}	$\frac{1.36 \times 10^{-3}}{4.95 \times 10^{-2}}$	0.03
K	2.51×10^{-3}	$\frac{2.51 \times 10^{-3}}{4.95 \times 10^{-2}}$	0.05
Na	7.23×10^{-1}	$\frac{7.23 \times 10^{-1}}{4.95 \times 10^{-2}}$	14.6
Si	4.95×10^{-2}	$\frac{4.95 \times 10^{-2}}{4.95 \times 10^{-2}}$	1.00
H ₂ O	8.06	$\frac{8.06}{4.95 \times 10^{-2}}$	163

